

DISSERTATION

PLASMA PROCESSING AND QUANTITATIVE CHARACTERIZATION OF  
3D POLYMERIC MATERIALS TO ENHANCE ANTIBACTERIAL PROPERTIES FOR  
BIOMEDICAL APPLICATIONS

Submitted by

Michelle N. Mann

Department of Chemistry

In partial fulfillment of the requirements

For the Degree of Doctor of Philosophy

Colorado State University

Fort Collins, Colorado

Summer 2018

Doctoral Committee:

Advisor: Ellen R. Fisher

Arun Kota

Melissa Reynolds

Martin McCullagh

Copyright by Michelle N. Mann 2018

All Rights Reserved

## ABSTRACT

### PLASMA PROCESSING AND QUANTITATIVE CHARACTERIZATION OF 3D POLYMERIC MATERIALS TO ENHANCE ANTIBACTERIAL PROPERTIES FOR BIOMEDICAL APPLICATIONS

Polymeric materials are used in numerous biomedical applications. Ultrafiltration blood dialysis membranes, polymeric tissue engineering scaffolds, drug-releasing composites, mesh wound dressings, and materials with anti-biofouling surfaces all rely on the desirable bulk properties of the polymer material (e.g., porosity, flexibility, mechanical strength). These materials, however, are prone to fouling by bacteria, proteins, and other macromolecules present in medical settings, ultimately decreasing material performance and lifetime. Moreover, with millions of biomedical devices deployed annually, hospital acquired infections are the cause of death for ~10% of American patients. To combat infection associated with biofouling, surface modification techniques are often employed to customize material surface properties yet retain the desired bulk characteristics.

Low-temperature plasmas (LTPs) are well suited for biomedical device processing, as they provide a sterile environment with a large parameter space that allows for tunable surface modification and the ability to retain the bulk properties of the polymer. Indeed, a large body of literature successfully describes the plasma processing of a variety of polymeric constructs for enhanced biocompatibility. More recently, plasmas have been investigated for the optimization of antibacterial polymeric materials. In this dissertation, plasma processing techniques, including  $\text{H}_2\text{O}_{(v)}$  plasma surface modification and plasma enhanced chemical vapor deposition

(PECVD), are used to (1) customize the surface properties of medically-relevant polymeric constructs towards improved wettability and biological outcomes and (2) enhance material antibacterial performance via tuning drug release or fabricating antifouling surfaces. Plasma processed materials are characterized with respect to changes in chemistry and wettability via X-ray photoelectron spectroscopy (XPS) and water contact angle goniometry, respectively. Biological evaluation strategies include the quantification of *Escherichia coli* (*E. coli*) and *Staphylococcus aureus* (*S. aureus*) population over time as well as numerous imaging techniques to assess bacteria after attachment and biofilm formation. More advanced biological performance testing has included static and dynamic protein fouling, water and protein flux studies, and thromboelastographic analysis of modified materials. Gas-phase spectroscopic techniques (e.g., optical emission spectroscopy), in combination with surface analysis and biological performance metrics, provide comprehensive insight into how plasma characteristics can be correlated to material properties, and, thus, interactions with bacteria and protein.

The dissertation begins with water vapor [ $\text{H}_2\text{O}_{(v)}$ ] plasma surface modification to create hydrophilic ultrafiltration polysulfone membranes. XPS revealed the permanency (>2 months) of the treatment arose from covalent incorporation of hydrophilic, oxygen-containing functional groups into the polymer backbone. Modified membranes demonstrated enhanced hydrodynamic characteristics and no longer required preconditioning, rendering them more practical for deployment in medical separations. Importantly, scanning electron microscopy (SEM) revealed no damage to the porous morphology from plasma treatment, thus, water vapor plasma modification provides a potential route to extend ultrafiltration membrane lifetime.

Chapter 4 highlights current fabrication and characterization methodologies for silver nanoparticle (AgNP)-loaded polymeric constructs, often researched for potential applications as

drug delivery systems, wound dressings, and anti-biofouling materials. Several methods were used to fabricate AgNP-loaded materials and their efficacy against *E. coli* was evaluated.  $\text{H}_2\text{O}_{(\text{v})}$  plasma surface modification was employed to enhance material surface wettability (explored by water contact angle goniometry) and nanoparticle incorporation. Compositional analyses reveal incorporation of AgNPs on the surface and bulk of the materials strongly depends on the fabrication methodology. More importantly, the nature of AgNP incorporation into the polymer has direct implications on the biocidal performance resulting from release of  $\text{Ag}^+$ . The materials fell significantly short of healthcare standards with respect to antimicrobial behavior, and, in comparing our results to numerous literature studies. Notably, we identified a glaring disparity in the way biological results are often described. Thus, Chapter 4 also contains a critical evaluation of the literature, highlighting select poor-performing materials to demonstrate several shortcomings in the quantitative analysis and reporting of the antibacterial efficacy of AgNP-loaded materials. Ultimately, we provide recommendations for best practices for better evaluation of these constructs towards improved antibacterial efficacy in medical settings.

Tygon® and other poly(vinyl chloride)-derived polymers are frequently used for tubing in blood transfusions, hemodialysis, and other extracorporeal circuit applications. These materials, however, tend to promote bacterial proliferation which contributes to the high risk of infection associated with device use. Antibacterial agents, such as nitric oxide (NO) donors, can be incorporated into these materials to eliminate bacteria before they can proliferate. The release of the antimicrobial agent from the device, however, is challenging to control and sustain on timescales relevant to blood transport procedures. Surface modification techniques can be employed to address challenges with controlled drug release. In Chapter 5, surface modification using  $\text{H}_2\text{O}_{(\text{v})}$  plasma is explored as a potential method to improve the biocompatibility of

biomedical polymers, namely to tune the NO-releasing capabilities from Tygon® films. Film properties are evaluated pre- and post-treatment by contact angle goniometry, XPS, and optical profilometry. H<sub>2</sub>O<sub>(v)</sub> plasma treatment significantly enhances the wettability of the nitric-oxide releasing films, doubles film oxygen content, and maintains surface roughness. Using the kill rate method, we determine both treated and untreated films cause an 8-log reduction in the population of both gram-negative *E. coli* and gram-positive *S. aureus*. Notably, however, H<sub>2</sub>O<sub>(v)</sub> plasma treatment delays the kill rate of treated films by 24 h, yet antibacterial efficacy is not diminished. NO release, measured via chemiluminescent detection, is also reported and correlated to the observed kill rate behavior. Overall, the delay in biocidal agent release caused by our treatment indicates plasma surface modification is an important route toward achieving controlled drug release from polymeric biomedical devices.

Chapter 6 describes the use of PECVD to deposit a film of 1,8-cineole, an antibacterial constituent of tea tree oil, on two-dimensional (2D) substrates. The resulting conformal, pinhole free films were highly customizable with respect to oxygen content and wettability. Notably, film wettability increased linearly with plasma pressure, yielding water contact angles ranging from ~50° to ~90°. XPS revealed less oxygen is incorporated at higher pressures, likely arising from the lower density of OH<sub>(g)</sub> species, as observed via optical emission spectroscopy. Further, we utilized H<sub>2</sub>O<sub>(v)</sub> plasma surface modification of the films to improve wettability and found this results in a substantial increase in surface oxygen content. To elucidate the role of film wettability and antibacterial properties, both as-deposited and H<sub>2</sub>O<sub>(v)</sub> plasma modified films were exposed to gram-negative *E. coli* and gram-positive *S. aureus*. In short, these essential oil-based films significantly reduced biofilm formation (4-7% coverage compared to ~40% for controls).

Chapter 7 expands on the essential oil work described in Chapter 6 by extending PECVD systems to two additional precursors as well as introducing three-dimensional (3D) porous polymeric substrates. Films from 1,8-cineole and terpinen-4-ol were deposited onto ultrafiltration membranes and porous scaffolds. Coated constructs were exposed to *E. coli* and bacterial attachment on the constructs was evaluated by colony counting and SEM techniques. Importantly, we demonstrate films from terpinen-4-ol can be deposited via plasma polymerization techniques. Using results from gas phase analyses and surface characterization, we make comparisons between films discussed in Chapter 6 and films deposited from similar essential-oil derived molecules.

This dissertation concludes with work expanding on that described in Chapter 3, exploring the H<sub>2</sub>O<sub>(v)</sub> plasma surface modification of ultrafiltration membranes. Specifically, we discuss setbacks often faced when working with industrial membranes and how these pose challenges to plasma processing and surface analysis. Chapter 8 concludes by providing insight into how changes in membrane composition may counteract desirable properties gained by plasma processing.

## TABLE OF CONTENTS

ABSTRACT.....	ii
LIST OF TABLES.....	x
LIST OF FIGURES .....	xii
CHAPTER 1 – INTRODUCTION .....	1
1.1 Motivation of research .....	1
1.2 Strategies to mitigate biofouling and enhance compatibility of biomaterials.....	3
1.2.1 Fundamentals of biofouling.....	3
1.2.2 Strategies for surface modification and enhanced antimicrobial performance.....	4
1.3 Fundamentals of plasma processing for polymeric materials.....	8
1.4 Plasma processing and characterization of polymeric materials for enhanced antibacterial properties .....	11
1.5 Overview of research .....	13
REFERENCES .....	15
CHAPTER 2 – EXPERIMENTAL METHODS .....	21
2.1 General information.....	21
2.1.1 Plasma reactor set-up.....	21
2.1.2 Precursor and substrate preparation.....	23
2.2 Plasma processing of polymeric materials.....	31
2.3 Gas-phase and material characterization techniques .....	35
2.4 Strategies for assessment of membrane performance.....	40
2.5 Bacterial assays.....	46
2.6 Analysis of blood coagulation dynamics .....	52
REFERENCES .....	54
CHAPTER 3 – HYDROPHILIC MODIFICATION OF ULTRAFILTRATION MEMBRANES BY LOW TEMPERATURE H <sub>2</sub> O <sub>(v)</sub> PLASMA TREATMENT TO ENHANCE PERFORMANCE.....	57
3.1 Introduction.....	57
3.2 Results .....	60
3.2.1 Surface chemistry.....	60
3.2.2 Changes in surface wettability and architecture .....	66
3.2.3 Ultrafiltration experiments.....	71
3.2.4 Fouling experiments.....	74
3.2.5 Control ultrafiltration experiments .....	74
3.3 Discussion.....	82
3.4 Summary and conclusions .....	88
REFERENCES .....	90



CHAPTER 4 – FABRICATION AND CHARACTERIZATION OF POLYMERIC CONSTRUCTS LOADED WITH ANTIBACTERIAL AG NANOPARTICLES .....	93
4.1 Introduction.....	93
4.2 Results .....	100
4.3 Discussion.....	113
4.4 Summary and conclusions .....	123
REFERENCES .....	124
CHAPTER 5 – H <sub>2</sub> O <sub>(v)</sub> PLASMA SURFACE MODIFICATION OF NITRIC OXIDE-RELEASING TYGON FILMS FOR CONTROL OF DRUG RELEASE KINETICS .....	127
5.1 Introduction.....	128
5.2 Results .....	132
5.2.1 Effect of plasma treatment on bactericidal activity of GSNO20 films.....	132
5.2.2 Effect of plasma treatment on NO release .....	138
5.2.3 Evaluation of film nitrogen content by XPS.....	141
5.3 Effect of plasma treatment on bactericidal activity and NO release kinetics .....	141
5.4 Summary and conclusions .....	145
REFERENCES .....	147
CHAPTER 6 –INVESTIGATION OF ANTIBACTERIAL ESSENTIAL OIL-DERIVED THIN FILMS FORMED VIA PLASMA-ENHANCED CHEMICAL VAPOR DEPOSITION.....	151
6.1 Introduction.....	151
6.2 Results .....	154
6.2.1 Gas-phase spectroscopy .....	154
6.2.2 Film morphology, roughness, and deposition rate.....	156
6.2.3 Film composition .....	159
6.2.4 Film wettability and aging .....	165
6.2.5 Bacterial interactions .....	168
6.3 Discussion.....	176
6.3.1 Understanding how plasma chemistry influences film deposition and functionality .....	176
6.3.2 Understanding how plasma chemistry influences film wettability and aging .....	179
6.3.3 Understanding how biological performance varies with film properties.....	181
6.4 Summary and conclusions .....	184
REFERENCES .....	185
CHAPTER 7 – FABRICATION OF ESSENTIAL OIL-DERIVED THIN FILMS FOR COMPLEX 3D BIOMEDICAL CONSTRUCTS.....	190
7.1 Introduction.....	191
7.2 Results .....	193
7.3 Discussion.....	206
7.4 Summary and conclusions .....	213
REFERENCES .....	214

CHAPTER 8 – INVESTIGATION OF THE EFFECT OF SOLVENT CLEANING AND H <sub>2</sub> O <sub>(v)</sub> PLASMA TREATMENT ON ULTRAFILTRATION MEMBRANE WETTABILITY AND PERFORMANCE .....	217
8.1 Introduction.....	217
8.2 Results .....	219
8.3 Discussion.....	231
8.4 Summary and conclusions .....	233
REFERENCES .....	235
CHAPTER 9 – RESEARCH SUMMARY AND PERSPECTIVES .....	236
9.1 Research summary .....	236
9.2 Future directions .....	238
REFERENCES .....	242
LIST OF ABBREVIATIONS.....	243

## LIST OF TABLES

2.1. Manufacturer provided details for ultrafiltration and microporous membranes.....	24
2.2. List of parameters for plasma systems described in this work .....	32
3.1. XPS composition of UPS membranes .....	62
3.2. Water and protein flux for UPS membranes.....	73
3.3. Control water and protein flux for UPS membranes .....	77
3.4. RFR, FRR, and protein adsorption for UPS membranes.....	78
3.5. Water and protein flux for UPS -0.....	81
4.1. Fabrication and analytical methods commonly employed for AgNP-loaded materials .....	97
4.2. Summary of <i>E. coli</i> kill rate results for AgNP-loaded materials .....	107
4.3. TEG metrics for AgNP-loaded scaffolds and electrospun fibers.....	112
5.1. Table of CFUs mL <sup>-1</sup> values for <i>E. coli</i> kill rate assays .....	134
5.2. Table of CFUs mL <sup>-1</sup> values for <i>S. aureus</i> kill rate assays.....	137
5.3. NO-release figures of merit for NO-releasing Tygon® films.....	139
6.1. Ratios of species in plasmas from OES spectra .....	157
6.2. Surface analysis data for ppCin films .....	160
6.3. WCA of aged ppCin films.....	167

7.1. Table of literature MIC values of essential oil components.....	194
7.2. XPS composition and binding environments for plasma polymerized coatings.....	203
7.3. Protein adsorption by mass per unit area for coating on PC-TE membranes.....	207
8.1. Average % mass loss of UF membranes following cleaning techniques .....	223
8.2. $\theta_{\text{static}}$ (°) for PVDF membrane tight sides after various cleaning techniques.....	225
8.3. WCA values for cleaned PES and PVDF membrane tight sides after modifications .....	226
8.4. Atomic compositions for PVDF membranes as-received and after cleaning treatments....	230

## LIST OF FIGURES

1.1. Flow diagram depicting routes towards achieving materials with antibacterial surfaces.....	7
1.2. Conceptual depiction of PECVD processes.....	9
2.1. General schematic of the ICP reactor used for the modifications described herein .....	22
2.2. Schematic of fabrication techniques used to create the polymeric constructs presented in this work .....	26
2.3. Schematic of holder for modification of commercial membranes.....	34
2.4. Calibration curve created for the analysis of Ag <sup>+</sup> content by flame AAS .....	41
2.5. Schematic of dead-end stirred cell setup for flux measurements .....	43
3.1. C <sub>1s</sub> XPS spectra for UPS membranes .....	63
3.2. FTIR spectra for UPS membranes .....	65
3.3. WCA for freshly treated and aged UPS membranes .....	67
3.4. SEM images for UPS membranes .....	69
3.5. Percent mass loss as a function of plasma treatment time for UPS membranes.....	70
3.6. Water and protein flux as a function of time for UPS membranes.....	72
3.7. Water flux for control filtration experiments.....	76
3.8. Water and protein flux for UPS membranes.....	80
3.9. PSf structure and positions for possible oxidation.....	84

4.1. Publications and citations for AgNP-loaded polymers since 1995.....	96
4.2. Schematic of fabrication techniques used to fabricate AgNP-loaded materials.....	99
4.3. Kill rate for AgNPs in <i>E. coli</i> culture .....	101
4.4. SEM images of AgNP-loaded materials.....	103
4.5. XPS and EDS data for AgNP-loaded materials.....	104
4.6. Ag <sub>3d</sub> XPS spectrum and SEM image for AgNP-loaded PCL films.....	106
4.7. Zone of inhibition data for AgNP-loaded materials .....	109
4.8. TEG traces for AgNP materials .....	111
5.1. GSNO structure and photographs of Tygon® films.....	130
5.2. <i>E. coli</i> kill rate for NO-releasing Tygon® films.....	133
5.3. <i>S. aureus</i> kill rate for NO-releasing Tygon® films .....	136
5.4. Photographs of films during kill rate assays and NO release over time.....	140
5.5. Conceptual cartoon of cross-linking upon plasma treatment.....	144
6.1. Representative OES spectra for 1,8-cineole plasmas .....	155
6.2. Deposition rate for ppCin films .....	158
6.3. SEM images of ppCin films.....	161
6.4. FTIR spectra for 1,8-cineole and 1,7-octadiene monomers and ppCin and ppOct films ....	162
6.5. C <sub>1s</sub> XPS spectra for deposited films.....	164
6.6. WCA for ppCin films as a function of power and pressure.....	166
6.7. Fluorescence microscopy images of <i>E.coli</i> attachment on deposited films.....	169
6.8. Fluorescence microscopy images of <i>S. aureus</i> attachment on deposited films .....	171

6.9. Bright field microscopy images of <i>E.coli</i> biofilm on deposited films .....	172
6.10. Bright field microscopy images of <i>S. aureus</i> biofilm on deposited films .....	173
6.11. Surface coverage of <i>E. coli</i> and <i>S. aureus</i> biofilm on untreated and treated ppCin .....	175
7.1. OES spectrum for a 100% terpinen-4-ol plasma .....	196
7.2. SEM images of films deposited on PC-TE membranes.....	197
7.3. SEM images of films deposited on PCL scaffolds .....	199
7.4. C <sub>1s</sub> XPS spectra for films deposited on flat substrates .....	200
7.5. C <sub>1s</sub> XPS spectra for films deposited on 3D constructs .....	201
7.6. Bright field images of <i>E. coli</i> biofilm on films deposited on glass.....	204
7.7. SEM images of <i>E. coli</i> attached on coated polymeric constructs .....	205
8.1. Flux for as-received, MeOH washed, and plasma treated PES membranes.....	221
8.2. SEM images of rinsed and plasma treated PES membranes .....	222
8.3. C <sub>1s</sub> XPS spectra for as-received, MeOH washed, and plasma treated PES membranes.....	228
8.4. Conceptual depiction of loss of wetting agent.....	234

# CHAPTER 1

## INTRODUCTION

This chapter contains an overview of the general principles pertaining to the research described in this dissertation. First, strategies to control biofouling of materials used in the biomedical industry are discussed. An argument is then made for the use of plasma processing to create improved antibacterial biomaterials. A discussion and detailed analysis of approaches for optimizing antibacterial properties using plasmas are also discussed. The chapter concludes with an overview of the research presented in the subsequent chapters of this dissertation.

### **1.1. Motivation of research**

The worldwide production of biomedical materials is a rapidly expanding, ~\$200 billion per year industry.<sup>1-2</sup> Polymeric biomaterials, like those used in wound healing, controlled drug delivery, artificial organs, and blood dialysis, are selected for their optimal bulk properties.<sup>2</sup> For example, membranes for hemodialysis or artificial kidneys rely on high permeability and selectivity for efficient and effective separations,<sup>3</sup> whereas Tygon® and similar thermoplastics are chosen for blood transport applications because of their excellent mechanical strength and flexibility.<sup>4</sup> Porous scaffolds for wound healing are designed to be bioresorbable and have porosity that mimics that of the extracellular matrix (ECM) for promotion of cell ingrowth and tissue repair.<sup>5</sup> Despite the ingenuity behind the design of such materials, all are prone to bacterial attachment and colonization, ultimately promoting biofilm formation and infection.<sup>1-2, 6</sup> Indeed, up to 70% of hospital acquired infections (HAIs) may be associated with implants or



devices.<sup>1, 7-8</sup> Such infections can increase risk of chronic, non-healing wounds, and patient mortality has been reported as high as 60%.<sup>2</sup>

As most biomedical devices are three-dimensional (3D) (e.g., catheters, wound dressings), bacteria can grow on both the inner and other surfaces of the material, meaning external hygiene measures are insufficient to control bacterial growth.<sup>9</sup> Polymer surfaces are particularly susceptible, as they are generally hydrophobic, limiting their biocompatibility and promoting bacterial attachment.<sup>5-6</sup> Attached bacteria very quickly colonize the surface, resulting in biofilm formation, or the emergence of strong, healthy, vigorously reproducing colonies of bacteria on a surface.<sup>1-2, 10</sup> For numerous reasons further discussed below (section 1.2.1), mature biofilms are notoriously difficult to eliminate compared to planktonic bacteria. Because biofilm formation commences with undesired interactions between bacteria and the material surface, it is typically agreed that mitigation tactics should involve an attempt to eliminate bacteria before biofilm maturation begins.<sup>11-12</sup> As such, antibiofouling strategies often take a materials-based approach, where materials are either incorporated with bactericidal agents (e.g., metal nanoparticles or antibiotics) that release to kill bacteria in the surrounding biological environment, or their surfaces are rendered non-fouling to discourage bacterial attachment. Each approach carries limitations; bactericidal agent release is difficult to control and sustain, whereas antifouling surfaces often contain no mechanisms by which to eradicate infection in surrounding tissue.

The ideal fabrication platform would utilize a dual approach to create biomaterials with both short-and long-term biocidal properties.<sup>12</sup> As such, this dissertation posits that exploiting the synergistic effect of both drug incorporation and surface modification can provide a reliable route to both control drug incorporation and release and permanently alter the material in favor of a low-fouling, antibacterial surface. Utilizing such a materials-based approach to address the

prevalence of HAIs can improve both patient healthcare outcomes and reduce the overuse and misuse of traditional antibiotic therapies that contribute to multi-drug resistance.

## **1.2. Strategies to mitigate biofouling and enhance compatibility of biomaterials**

### **1.2.1. Fundamentals of biofouling**

Biofilm formation is of particular concern in medical industries, where biofilms are associated with many chronic, recurrent infections and with numerous medical devices (e.g., cardiac pacemakers, stents, urinary catheters).<sup>1</sup> Many agree the hydrophobic surfaces of polymeric materials promote bacterial attachment compared to hydrophilic glass or metal,<sup>13-16</sup> leading to subsequent biofilm formation. Biofilm formation is a chemical, physical and biological process that occurs in four primary stages: reversible attachment, colonization, maturation, and dispersion.<sup>1,10</sup> It is important to note that another form of biofouling, protein adsorption, occurs almost immediately upon exposure of the material to the biological environment.<sup>2, 17-18</sup> This adsorptive protein fouling not only decreases material performance (i.e., decreased flux for dialysis membranes) but also conditions the material surface, rendering the native material surface more favorable for bacteria interactions.<sup>1-2, 6, 17-19</sup> As such, engineering such surfaces should also consider routes to minimize protein fouling.<sup>2</sup> The addition of a biocidal agent can then act as a second mechanism by which to prevent bacterial attachment should the surface be fouled by protein.

As biofilm maturation proceeds, infection remediation becomes significantly more difficult, as it can take 500-5000 times the concentration of biocidal agent to kill bacteria in a 7-day mature biofilm compared to the same planktonic organisms.<sup>20-21</sup> Its formation in wounds and semi-permanent implants significantly increase the risk of patient morbidity and mortality. For

example, the risk of developing catheter-related infections increases ~10% per day of use.<sup>9</sup> Biofilm resilience arises in part from their increased likelihood to develop antimicrobial resistance.<sup>1, 6, 22</sup> Perhaps the most widely recognized resistant strain plaguing clinical settings is the common “superbug”, methicillin-resistant *Staphylococcus aureus* (MRSA).<sup>23</sup> One reason for this is that biofilms secrete extracellular polysaccharide substances (EPS) that form a matrix around the maturing biofilm, rendering it particularly resistant to treatment.<sup>6, 10, 21-22</sup> The EPS serves as a barrier that may slow or impede the physical penetration of biocidal agents into the biofilm, resulting in recalcitrant bacterial infections.<sup>24-27</sup> Some propose another mechanism by which EPS may reduce the efficacy of antibiotics is through reacting, neutralizing or dilute the biocidal agent.<sup>24, 28</sup> A third reason for greater resistance to eradication may be the unique biological changes in bacteria growing on a surface. Interestingly, bacteria in biofilms are thought to shift phenotypes such that biofilm formation is favored, causing delayed wound healing and increasing infection likelihood.<sup>10, 29-30</sup> Indeed, Westgate and coworkers found that bacteria isolated from wounds have higher biofilm-forming potential than bacteria naturally found on human skin.<sup>31</sup> It is generally agreed that mature biofilms more closely resemble higher order tissue in that the structure of the complex biofilm matrix contains channels that facilitate nutrient transport.<sup>30</sup> Because of the numerous routes by which biofilms resist eradication, it is generally agreed mitigation strategies should strive to eliminate bacteria before or during the reversible attachment phase of the biofilm formation process.<sup>11-12</sup>

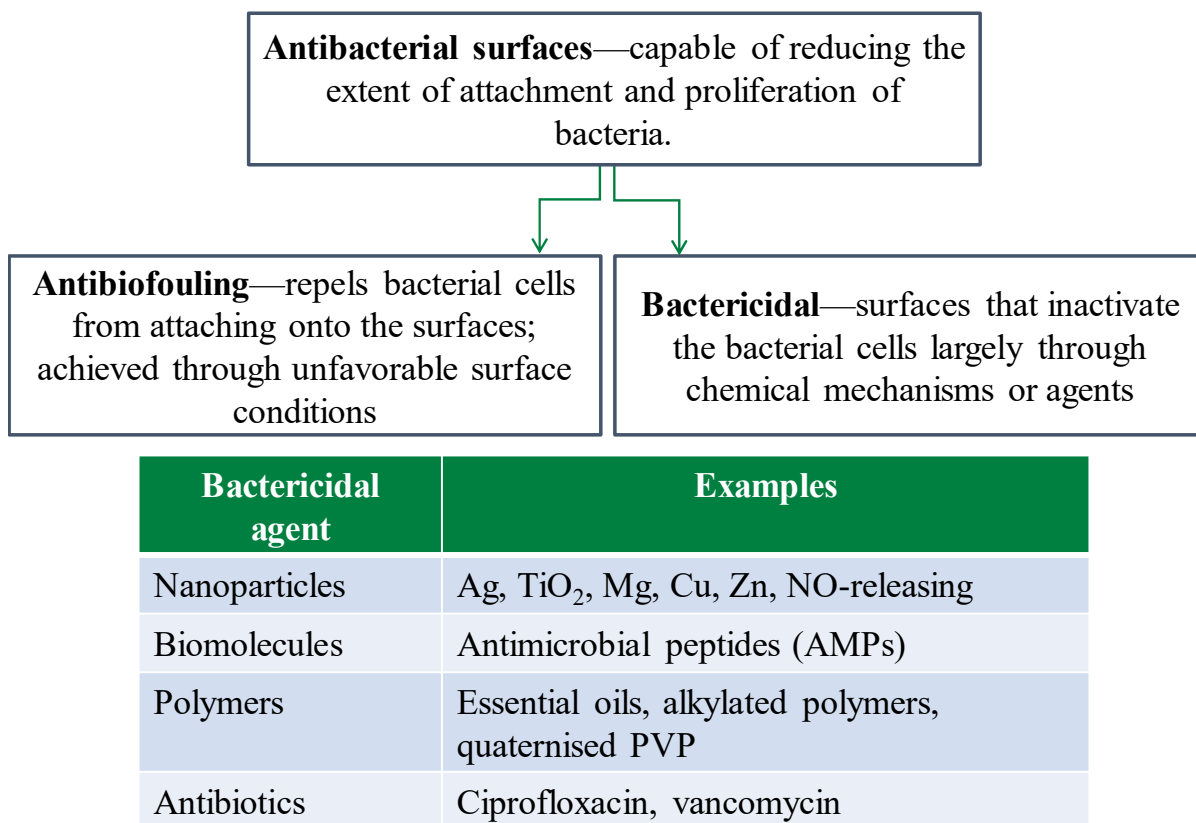
### **1.2.2. Strategies for surface modification and enhanced antimicrobial performance**

Ultimately, one key target of efforts to create biocompatible devices is the ability to tune the surface properties of the material, including hydrophilicity, surface charge, chemistry, and

roughness, with the goal of creating a material that will not only prevent a foreign body reaction, but also promote healing.<sup>32-37</sup> For example, we may wish to enhance the bioreactivity of the surface, creating functionalities (e.g., C–OH, O–C=O, NH<sub>2</sub>) that encourage the proliferation of mammalian cells,<sup>32, 36</sup> or introduce specific functionalities along a polymer chain to serve as signals to modulate the biological response.<sup>38</sup> This can be accomplished through chemical grafting,<sup>39</sup> chemical vapor deposition (CVD)<sup>39-42</sup>, or other wet chemical or photochemical strategies. Alternatively, we may design surfaces where interactions with cells are undesirable, discouraging non-specific interactions by adding low-fouling polymers (e.g., zwitterionic polymers,<sup>43-45</sup> polyethylene glycol (PEG)-based polymers,<sup>46-47</sup> dextran polysaccharides<sup>48</sup>), self-assembled monolayers (SAMs)<sup>49-51</sup>, or nanostructures.<sup>52-53</sup> These methods, however, often use excessive solvent or temperatures, carrying environmental implications, and such conditions are not ideal for these relatively delicate polymers. Moreover, these methodologies are often unable to conformally modify the interior and exterior of the 3D architectures of many biomaterials. Plasmas, however, can coat or selectively modify the material surface while maintaining critical bulk properties, such as pore size and bioresorbability.<sup>32, 54-55</sup> In addition, plasma treatments are rapid and can be low-temperature, often affording quick customization in a single step. Specifically, oxygen and nitrogen-containing precursors [e.g., H<sub>2</sub>O<sub>(v)</sub>, allylamine (allylNH), NH<sub>3</sub>] have been used to enhance the compatibility of biomaterials by increasing hydrophilicity via plasma surface modification.<sup>32, 36, 54, 56-58</sup>

Although these approaches have been shown to create biocompatible surfaces favorable for mammalian cell attachment and tissue growth, surface modification alone is typically insufficient to implement tunable and sustainable antibacterial properties. An ultimate goal would be to create plasma processing methodologies by which the material could be made biocompatible,

low-fouling, and antibacterial in a single step. Here, strategies to implement antibacterial properties into polymeric biomaterials are grouped into two broad categories, Figure 1.1. The first approach focuses on non-fouling surfaces to discourage bacterial attachment. This type of surface modification can be physical (e.g., surface texturing,<sup>2, 59</sup> nanopatterning<sup>53, 60-61</sup>) or chemical (e.g., tethering of quaternary ammonium,<sup>62-63</sup> coating with antimicrobial thin films<sup>64</sup>, heparin, or inorganic compounds<sup>65</sup>, grafting<sup>66</sup>, photochemical modification<sup>67-69</sup>). Low-fouling surfaces, however, do not systemically deliver therapeutic or antimicrobial agents to prevent infection in the surrounding tissue. Second, materials can be incorporated with bactericidal agents [e.g., metal nanoparticles,<sup>70-72</sup> synthetic antibiotics (ciprofloxacin, vancomycin, rifampicin, chlorhexidine),<sup>73</sup> antimicrobial peptides (AMPs)<sup>74-75</sup>] that release to kill bacteria in bulk solution. Biocidal agents can be incorporated into the polymer to actively eradicate bacteria, but it is difficult to control kinetics of their release. This approach, however, may fall short when used alone, as the therapeutic agent reservoir is limited, and its release is often difficult to control and predict.<sup>1</sup> Sub-inhibitory concentrations of a drug severely increase the risk of antibiotic resistance development.<sup>16</sup> Moreover, it is difficult to ensure that biocidal action occurs where intended (i.e., in surrounding tissue or localized at the material-biological interface). For example, a drug-releasing wound dressing may prevent external contamination of the wound and offer a “burst” release of antibiotics, yet the underside of a wound dressing can provide an environment ripe for colonization of common skin bacterial strains [e.g., *Staphylococcus epidermidis* (*S. epidermidis*), *Staphylococcus aureus* (*S. aureus*), and *Escherichia coli* (*E. coli*)].<sup>23</sup> As biofilms can form within 24 h, but can take 7-10 days to mature, a primary goal of this dissertation is to investigate platforms to conformally modify the surfaces of these complex, three-dimensional constructs, implementing surface properties that enhance



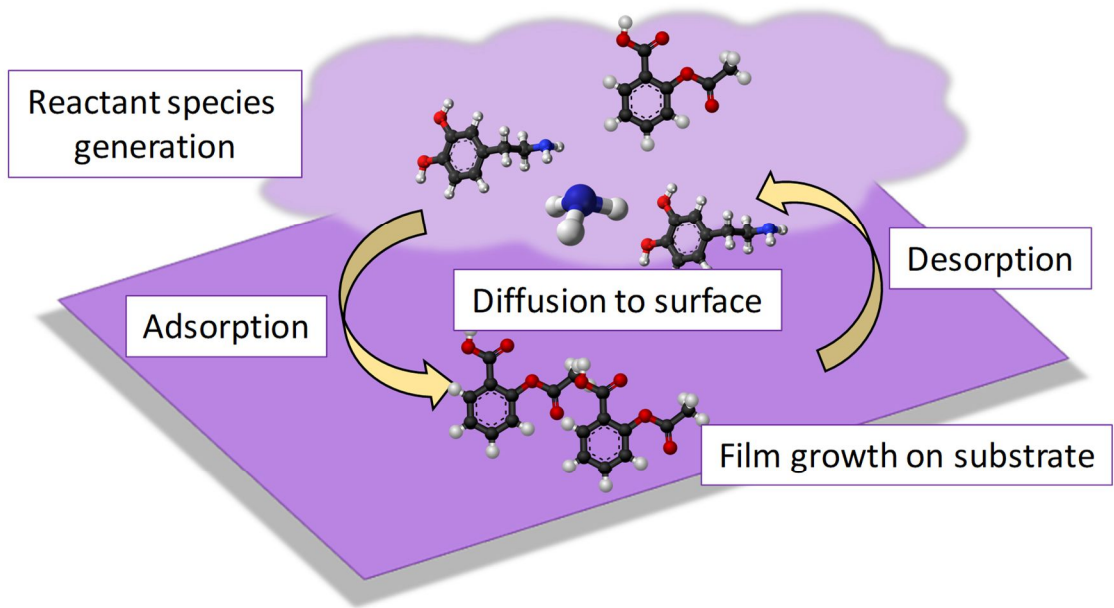
**Figure 1.1.** Diagram depicting routes towards achieving materials with antibacterial surfaces and common analytical techniques to evaluate their effectiveness.

the materials biocompatibility as well as implement tunable, short- and long-term effectiveness against bacteria.<sup>1, 76</sup>

### **1.3. Fundamentals of plasma processing for polymeric materials**

Plasma, the fourth state of matter, is a partially ionized gas comprising ions, electrons, photons, radicals, and neutral and excited state molecules.<sup>77-78</sup> Plasmas utilized within the context of this dissertation were inductively-coupled plasmas (ICPs), specifically those wherein the gas temperature is <1000 K, appropriately termed low-temperature plasmas (LTPs). LTPs can modify polymers via three primary techniques (1) etching the polymeric material; (2) plasma surface modification wherein the material is functionalized with a desired chemistry; and (3) plasma-enhanced CVD (PECVD) wherein a conformal film is deposited on the material.<sup>77-78</sup> PECVD and plasma surface modification have both been established as methodologies by which to enhance advantageous properties of a biomaterial, potentially providing routes to advanced high performing materials for a range of biological applications.<sup>32, 36, 58, 77, 79-80</sup>

PECVD, depicted conceptually in Figure 1.2, is a well-established technique that allows for the fabrication of soft matter thin films from solid, liquid, or gaseous precursors where conventional methods may fail (e.g., monomers with only C=C functionality or ring structures).<sup>16, 77-78</sup> Moreover, PECVD is ideal for coating biomedical devices, even those with morphologically complex architectures, as it provides a universal dry, single-step and sterile platform for device fabrication at low temperatures (~300 K), where the bulk mechanical properties and architecture of the underlying substrate are retained.<sup>78</sup> Furthermore, changing deposition parameters [e.g., power ( $P$ ), pressure ( $p$ )] alters the degree of monomer fragmentation



**Figure 1.2.** Conceptual depiction of PECVD processes.



and crosslinking in the film, thus potentially allowing for tailoring of film properties such as thickness, wettability, and surface chemistry for a desired application.<sup>77, 79</sup>

We have previously shown that PECVD can fabricate controllable material surfaces that lead to predictable interactions with biomolecules. In one example, the Fisher group developed an allylamine (allylNH) and allyl alcohol (allylOH) copolymerization PECVD system whereby 3D scaffolds could be rendered biologically-reactive.<sup>57</sup> The properties of the plasma polymerized coatings were tunable by adjusting the ratio of the two plasma precursors. Importantly, the nitrogen and oxygen content were predictable, resulting in customizable biological reactivity outcomes. Upon interfacing with human dermal fibroblasts (HDFs), copolymerized films enhanced cell viability, a promising result for our biologically-relevant scaffold materials.

In a related PECVD study, a variety of fluorocarbon (FC) precursors were used to achieve non-bioreactive conformal coatings onto the same 3D scaffolds, preventing attachment of HDFs yet retaining bulk properties critical to biomedical applications.<sup>40</sup> Again, the thin films conformally coated the morphologically complex materials while retaining desirable bulk properties. The results of these studies imply the tunability of our PECVD techniques could render a range of polymeric constructs non-fouling, allowing for optimization of complex 3D polymeric constructs used in biomaterials.

In addition to tuning surface properties of films deposited by PECVD, we have also used plasma surface modification to controllably impart desirable functionalities. Plasma surface modification describes the interaction of active gas-phase plasma species with a material surface, resulting in functionalization of the material surface. In these processes, energetic species in the plasma break covalent bonds on the surface, forming radicals which react with energetic gas-phase species.<sup>77-78</sup> Functionalization of the surface can be customized, primarily by utilizing

specific plasma systems. Indeed, much of biomaterials research involving plasma surface modification seeks to tune the surface chemistry of materials (i.e., to obtain desirable O/N).<sup>36</sup> For example, a substantial portion of previous Fisher group research demonstrated that low temperature H<sub>2</sub>O<sub>(v)</sub> plasma treatment increases the surface hydrophilicity of polymers, primarily via implantation of oxygen-containing functionalities (e.g., C–OH, O–C=O).<sup>81-84</sup> For modified nitric oxide (NO)-releasing poly(lactic-co-glycolic acid)- based polymers, H<sub>2</sub>O<sub>(v)</sub> plasma surface modification significantly enhanced material wettability and oxygen content in a customizable fashion [verified with water contact angle goniometry (WCA) and X-ray photoelectron spectroscopy (XPS)], further improving properties that are attractive in biomedical applications.<sup>56</sup>

#### **1.4. Plasma processing and characterization of polymeric materials for enhanced antibacterial properties**

As discussed above, applications of plasma include creating antifouling surfaces via manipulation of material hydrophobicity/hydrophilicity or surface charge or via PECVD fabrication of thin films. A large focus of this dissertation, however, lies in the use of antibacterial compounds as PECVD precursors. Specifically, the broad class of compounds of interest are essential oils, many of which have antimicrobial properties supported by extensive clinical trials.<sup>85-93</sup> Indeed, PECVD has successfully fabricated thin films from oils of tea tree, lavender, eucalyptus and lemongrass, as well as some individual constituents;<sup>64, 85-87, 89, 91-105</sup> however, films deposited from these systems have primarily been explored for their optical or electronic properties.<sup>99, 102, 105-108</sup> Few studies have assessed the biological performance of the materials, and even fewer explore essential-oil based thin films deposited on 3D constructs (e.g.,

electrospun fiber mats for wound dressings).<sup>64</sup> The complexity of the film deposition process requires a comprehensive approach to fully elucidate pathways toward optimizing film properties. Generating fundamental knowledge of the film deposition mechanisms and correlating this to film surface and bulk properties and performance could provide an avenue for the development of advanced low-fouling devices for biomaterials applications.

Recent advances in the field of plasma processing also reveal its potential to control the incorporation and release of biocidal agents.<sup>109-114</sup> Plasma processing can accomplish this via several mechanisms, including the deposition of plasma polymerized coating barriers,<sup>111</sup> plasma-assisted grafting of antibiotic small molecules,<sup>12, 16, 73</sup> and tuning surface chemistry and cross linking to control diffusion of biocidal agents from the material or diffusion of biological fluid into the material.<sup>114</sup>

Plasmas are inherently complex systems and become even more so when considering how they alter surfaces during plasma processing. This dissertation utilizes H<sub>2</sub>O<sub>(v)</sub> plasma surface modification for increasing material wettability, oxygen content, and thus, biocompatibility. Because this dissertation focuses on investigating plasma processing as a means to customize antibacterial materials, H<sub>2</sub>O<sub>(v)</sub> plasma treatment is also investigated for tuning the incorporation and release of biocidal agents. Thus, prevalent themes that appear throughout this dissertation include understanding the fundamental processes that occur during plasma surface modification and PECVD, elucidating how plasma parameters can be optimized to customize material properties, and determining how surface properties affect the biological outcomes of the modified biomaterials. Such an approach is critical to this field as further elucidation of the interactions of bacteria, proteins, and other biomacromolecules relies on understanding the fundamental chemistry occurring at the biological-material interface.

Another large area of focus for this work is the quantitative assessment of biological performance, namely fundamental bacteria-surface interactions. There currently exists no clinical tool for the diagnosis for biofilm. In some cases, there may be no symptoms of an infection, yet bacteria with biofilm-forming potential may be present and slow-growing. By the time a biofilm has grown extensively enough to cause visible signs of infection, bacteria are significantly more resistant to treatment. Although development of a “gold standard” biofilm diagnostic tool is a “holy grail” of the biomedical field, materials-focused research should seek to understand the fundamental interactions of bacteria at biomaterial surfaces and the avenues by which biofilm formation can be prevented. Current assays are typically limited to planktonic bacterial cultures and fall short in providing a true measure of biofilm growth *in vivo*, as the material must be removed before the biofilm can be characterized.<sup>11</sup> Planktonic cultures are not representative of clinical settings, wherein bacteria primarily live as biofilms.<sup>1,11</sup> Even fundamental studies often negate the importance of characterizing all life stages of bacteria interacting with a biomaterial surface.

## **1.5. Overview of research**

Despite the widespread use of biomedical devices, surprisingly little is understood about the factors that guide bacterial adhesion and colonization over these materials, as this depends on a variety of surface properties such as wettability, roughness, and surface charge as well as the properties of the bacterial membrane. Accordingly, the works in this dissertation seeks to understand the fundamental interactions of bacteria at surfaces and the avenues by which biofilm formation can be prevented. Chapter 2 contains detailed explanations of experimental methodologies employed for the work described in the forthcoming chapters. Chapter 3

introduces the effect of water (vapor) plasma surface modification, using polymeric ultrafiltration membranes as a first example. Bioanalytical methods used herein range from fundamental flux and fouling studies wherein the performance of an ultrafiltration membrane is tested to determine changes in permeability after fouling by protein or plasma processing. Chapters 4-8 focus on the fabrication and characterization of a range of materials incorporated with biocidal agents or fabricated with antibacterial surfaces. Chapter 4 delves deeper into important aspects of analyzing bactericidal performance, such as considering the clinical relevance of assays employed. Semi-quantitative bacterial assays involve the assessment of bacterial kill rate, revealing the time-resolved decline in bacteria that occurs upon exposure to biocidal agents, as well as bright field, fluorescence, and scanning electron microscopy (SEM) imaging techniques, to understand bacterial attachment and biofilm formation in the days after exposure of the material to bacteria. Chapter 5 contains work completed in collaboration with Prof. Melissa Reynolds' research group detailing the water plasma surface modification of a nitric oxide releasing polymer for control of drug delivery and enhancement of surface wettability. A description of the development and optimization of a PECVD system using essential oil-derived monomers, and the application of these films to complex 3D polymeric materials, are detailed in Chapters 6 and 7, respectively. Chapter 9 contains a summary of the research presented in this dissertation.

## REFERENCES

1. Bryers, J. D., Medical biofilms. *Biotechnol. Bioeng.* **2008**, *100* (1), 1-18.
2. Bryers, J. D.; Ratner, B. D., Bioinspired implant materials befuddle bacteria. *ASM News-American Society for Microbiology* **2004**, *70* (5), 232-232.
3. Stamatialis, D. F.; Papenburg, B. J.; Gironés, M.; Saiful, S.; Bettahalli, S. N.; Schmitmeier, S.; Wessling, M., Medical applications of membranes: drug delivery, artificial organs and tissue engineering. *J. Membr. Sci.* **2008**, *308* (1-2), 1-34.
4. Blass, C.; Jones, C.; Courtney, J., *Biomaterials for blood tubing: the application of plasticised poly (vinyl chloride)*. SAGE Publications Sage UK: London, England: 1992.
5. Woodruff, M. A.; Hutmacher, D. W., The return of a forgotten polymer—Polycaprolactone in the 21st century. *Prog. Polym. Sci.* **2010**, *35* (10), 1217-1256.
6. Donlan, R. M., Biofilms: microbial life on surfaces. *Emerg Infect Dis* **2002**, *8* (9), 881-890.
7. Bryers, J. D., Problems of Biofilms Associated with Medical Devices and Implants. In *Medical Biofilms*, 2008.
8. Scott, R. D., *The Direct Medical Costs of Healthcare-associated Infections in US Hospitals and the Benefits of Prevention*. Centers for Disease Control and Prevention: March 2009.
9. Donlan, R.; Murga, R.; Bell, M.; Toscano, C.; Carr, J.; Novicki, T.; Zuckerman, C.; Corey, L.; Miller, J., Protocol for detection of biofilms on needleless connectors attached to central venous catheters. *J. Clin. Microbiol.* **2001**, *39* (2), 750-753.
10. Stoodley, P.; Sauer, K.; Davies, D. G.; Costerton, J. W., Biofilms as complex differentiated communities. *Annu Rev Microbiol* **2002**, *56*, 187-209.
11. Lindsay, D.; von Holy, A., Bacterial biofilms within the clinical setting: what healthcare professionals should know. *J. Hosp. Infect.* **2006**, *64* (4), 313-325.
12. Salwiczek, M.; Qu, Y.; Gardiner, J.; Strugnell, R. A.; Lithgow, T.; McLean, K. M.; Thissen, H., Emerging rules for effective antimicrobial coatings. *Trends Biotechnol.* **2014**, *32* (2), 82-90.
13. Pringle, J. H.; Fletcher, M., Influence of substratum wettability on attachment of freshwater bacteria to solid surfaces. *Appl. Environ. Microbiol.* **1983**, *45* (3), 811-817.
14. Bendinger, B.; Rijnaarts, H. H.; Altendorf, K.; Zehnder, A. J., Physicochemical cell surface and adhesive properties of coryneform bacteria related to the presence and chain length of mycolic acids. *Appl. Environ. Microbiol.* **1993**, *59* (11), 3973-3977.
15. Fletcher, M.; Loeb, G. I., Influence of substratum characteristics on the attachment of a marine pseudomonad to solid surfaces. *Appl. Environ. Microbiol.* **1979**, *37* (1), 67-72.
16. Bazaka, K.; Jacob, M. V.; Chrzanowski, W.; Ostrikov, K., Anti-bacterial surfaces: natural agents, mechanisms of action, and plasma surface modification. *RSC Adv.* **2015**, *5* (60), 48739-48759.
17. Fletcher, M., *Bacterial adhesion: molecular and ecological diversity*. John Wiley & Sons: 1996; Vol. 19.
18. Linke, D.; Goldman, A., *Bacterial adhesion: chemistry, biology and physics*. Springer Science & Business Media: 2011; Vol. 715.
19. Landry, R. M.; An, D.; Hupp, J. T.; Singh, P. K.; Parsek, M. R., Mucin–*Pseudomonas aeruginosa* interactions promote biofilm formation and antibiotic resistance. *Mol. Microbiol.* **2006**, *59* (1), 142-151.
20. Khoury, A. E.; Lam, K.; Ellis, B.; Costerton, J. W., Prevention and control of bacterial infections associated with medical devices. *ASAIO journal (American Society for Artificial Internal Organs: 1992)* **1992**, *38* (3), M174-178.
21. Souli, M.; Giamarellou, H., Effects of slime produced by clinical isolates of coagulase-negative *Staphylococci* on activities of various antimicrobial agents. *Antimicrob. Agents Chemother.* **1998**, *42* (4), 939-941.

22. Donlan, R. M., Role of biofilms in antimicrobial resistance. *ASAIO journal* **2000**, *46* (6), S47-S52.
23. Percival, S. L.; Suleman, L.; Vuotto, C.; Donelli, G., Healthcare-associated infections, medical devices and biofilms: risk, tolerance and control. *J. Med. Microbiol.* **2015**, *64* (4), 323-334.
24. Hall-Stoodley, L.; Costerton, J. W.; Stoodley, P., Bacterial biofilms: From the natural environment to infectious diseases. *Nat. Rev. Microbiol.* **2004**, *2*, 95.
25. Costerton, J.; Irvin, R.; Cheng, K., The bacterial glycocalyx in nature and disease. *Annu. Rev. Microbiol.* **1981**, *35* (1), 299-324.
26. Nichols, W., Biofilm permeability to antibacterial agents. *Bacterial Biofilms and Their Control in Medicine and Industry. Cardiff, BioLine* **1994**, 141-149.
27. Francolini, I.; Donelli, G., Prevention and control of biofilm-based medical-device-related infections. *FEMS Immunology & Medical Microbiology* **2010**, *59* (3), 227-238.
28. G., D. M.; J., G. K.; S., S. P., Modeling biofilm antimicrobial resistance. *Biotechnol. Bioeng.* **2000**, *68* (4), 456-465.
29. Costerton, J. W.; Lewandowski, Z.; Caldwell, D. E.; Korber, D. R.; Lappin-Scott, H. M., Microbial biofilms. *Annu. Rev. Microbiol.* **1995**, *49* (1), 711-745.
30. Costerton, J. W.; Cheng, K.; Geesey, G. G.; Ladd, T. I.; Nickel, J. C.; Dasgupta, M.; Marrie, T. J., Bacterial biofilms in nature and disease. *Annu. Rev. Microbiol.* **1987**, *41* (1), 435-464.
31. Westgate, S. J.; Percival, S. L.; Knottenbelt, D. C.; Clegg, P. D.; Cochrane, C. A., Chronic equine wounds: What is the role of infection and biofilms? *Wounds: A Compendium of Clinical Research and Practice* **2010**, *22* (6), 138-145.
32. Vasilev, K.; Griesser, S. S.; Griesser, H. J., Antibacterial surfaces and coatings produced by plasma techniques. *Plasma Process. Polym.* **2011**, *8* (11), 1010-1023.
33. Vasilev, K.; Sah, V.; Anselme, K.; Ndi, C.; Mateescu, M.; Dollmann, B.; Martinek, P.; Ys, H.; Ploux, L.; Griesser, H. J., Tunable antibacterial coatings that support mammalian cell growth. *Nano Lett.* **2010**, *10* (1), 202-207.
34. Bryers, J. D.; Giachelli, C. M.; Ratner, B. D., Engineering biomaterials to integrate and heal: the biocompatibility paradigm shifts. *Biotechnol. Bioeng.* **2012**, *109* (8), 1898-1911.
35. Castner, D. G.; Ratner, B. D., Biomedical surface science: Foundations to frontiers. *Surf. Sci.* **2002**, *500* (1-3), 28-60.
36. Jacobs, T. M., R.; Geyter, N.D.; Dubruel, P.; Leys, C., Plasma surface modification of biomedical polymers: Influence on cell-material interaction. *Plasma Chem. Plasma Process* **2012**, *32*, 1039-1073.
37. Khang, G.; Lee, S. J.; Kim, M. S.; Lee, H. B., Biomaterials: Tissue Engineering and Scaffolds. *Encyclopedia of Medical Devices and Instrumentation* **2006**.
38. Yu, Q.; Zhang, Y.; Wang, H.; Brash, J.; Chen, H., Anti-fouling bioactive surfaces. *Acta biomaterialia* **2011**, *7* (4), 1550-1557.
39. Bhattacharya, A.; Misra, B., Grafting: a versatile means to modify polymers: techniques, factors and applications. *Prog. Polym. Sci.* **2004**, *29* (8), 767-814.
40. Hawker, M. J.; Pegalajar-Jurado, A.; Fisher, E. R., Conformal encapsulation of three-dimensional, bioresorbable polymeric scaffolds using plasma-enhanced chemical vapor deposition. *Langmuir* **2014**, *30* (41), 12328-12336.
41. Li, Q.; Bi, Q.-y.; Lin, H.-H.; Bian, L.-X.; Wang, X.-L., A novel ultrafiltration (UF) membrane with controllable selectivity for protein separation. *J. Membr. Sci.* **2013**, *427*, 155-167.
42. Reuben, B. G.; Perl, O.; Morgan, N. L.; Stratford, P.; Dudley, L. Y.; Hawes, C., Phospholipid coatings for the prevention of membrane fouling. *J. Chem. Technol. Biotechnol.* **1995**, *63* (1), 85-91.
43. Jiang, S.; Cao, Z., Ultralow-fouling, functionalizable, and hydrolyzable zwitterionic materials and their derivatives for biological applications. *Adv. Mater.* **2010**, *22* (9), 920-932.
44. Cheng, G.; Li, G.; Xue, H.; Chen, S.; Bryers, J. D.; Jiang, S., Zwitterionic carboxybetaine polymer surfaces and their resistance to long-term biofilm formation. *Biomaterials* **2009**, *30* (28), 5234-5240.

45. Cheng, G.; Zhang, Z.; Chen, S.; Bryers, J. D.; Jiang, S., Inhibition of bacterial adhesion and biofilm formation on zwitterionic surfaces. *Biomaterials* **2007**, *28* (29), 4192-4199.
46. Amirgoulova, E. V.; Groll, J.; Heyes, C. D.; Ameringer, T.; Röcker, C.; Möller, M.; Nienhaus, G. U., Biofunctionalized polymer surfaces exhibiting minimal interaction towards immobilized proteins. *Chem. Phys. Chem* **2004**, *5* (4), 552-555.
47. Ameringer, T.; Fransen, P.; Bean, P.; Johnson, G.; Pereira, S.; Evans, R. A.; Thissen, H.; Meagher, L., Polymer coatings that display specific biological signals while preventing nonspecific interactions. *J. Biomed. Mater. Res. A* **2012**, *100* (2), 370-379.
48. McArthur, S. L.; McLean, K. M.; Kingshott, P.; St John, H. A. W.; Chatelier, R. C.; Griesser, H. J., Effect of polysaccharide structure on protein adsorption. *Colloids Surf., B* **2000**, *17* (1), 37-48.
49. Ista, L. K.; López, G. P., Interfacial tension analysis of oligo (ethylene glycol)-terminated self-assembled monolayers and their resistance to bacterial attachment. *Langmuir* **2012**, *28* (35), 12844-12850.
50. Balamurugan, S.; Ista, L. K.; Yan, J.; López, G. P.; Fick, J.; Himmelhaus, M.; Grunze, M., Reversible protein adsorption and bioadhesion on monolayers terminated with mixtures of oligo (ethylene glycol) and methyl groups. *J. Am. Chem. Soc.* **2005**, *127* (42), 14548-14549.
51. K Ista, L.; Fan, H.; Baca, O.; P López, G., Attachment of bacteria to model solid surfaces: oligo (ethylene glycol) surfaces inhibit bacterial attachment. *FEMS Microbiol. Lett.* **1996**, *142* (1), 59-63.
52. Epstein, A. K.; Wong, T.-S.; Belisle, R. A.; Boggs, E. M.; Aizenberg, J., Liquid-infused structured surfaces with exceptional anti-biofouling performance. *Proc. Natl. Acad. Sci.* **2012**, *109* (33), 13182-13187.
53. Ma, J.; Sun, Y.; Gleichauf, K.; Lou, J.; Li, Q., Nanostructure on taro leaves resists fouling by colloids and bacteria under submerged conditions. *Langmuir* **2011**, *27* (16), 10035-10040.
54. Kull, K. R.; Steen, M. L.; Fisher, E. R., Surface modification with nitrogen-containing plasmas to produce hydrophilic, low-fouling membranes. *J. Membr. Sci.* **2005**, *246* (2), 203-215.
55. Matsuyama, H.; Teramoto, M.; Hirai, K., Effect of plasma treatment on CO<sub>2</sub> permeability and selectivity of poly (dimethylsiloxane) membrane. *J. Membr. Sci.* **1995**, *99* (2), 139-147.
56. Pegalajar-Jurado, A.; Joslin, J. M.; Hawker, M. J.; Reynolds, M. M.; Fisher, E. R., Creation of hydrophilic nitric oxide releasing polymers via plasma surface modification. *ACS Appl. Mater. Interfaces* **2014**, *6* (15), 12307-12320.
57. Hawker, M. J.; Pegalajar-Jurado, A.; Hicks, K. I.; Shearer, J. C.; Fisher, E. R., Allylamine and allyl alcohol plasma copolymerization: Synthesis of customizable biologically-reactive three-dimensional scaffolds. *Plasma Process. Polym.* **2015**, *12* (12), 1435-1450.
58. Chu, P. K. C., J.Y.; Wang, L.P.; Huang, N., Plasma-surface modification of biomaterials. *Mater. Sci. Eng., R* **2002**, *36*, 143-206.
59. Machado, M. C.; Tarquinio, K. M.; Webster, T. J., Decreased Staphylococcus aureus biofilm formation on nanomodified endotracheal tubes: a dynamic airway model. *Int. J. Nanomedicine* **2012**, *7*, 3741.
60. Hochbaum, A. I.; Aizenberg, J., Bacteria pattern spontaneously on periodic nanostructure arrays. *Nano Lett.* **2010**, *10* (9), 3717-3721.
61. Cheng, Y. T.; Rodak, D.; Wong, C.; Hayden, C., Effects of micro- and nano-structures on the self-cleaning behaviour of lotus leaves. *Nanotechnology* **2006**, *17* (5), 1359.
62. Tiller, J. C.; Liao, C.-J.; Lewis, K.; Klivanov, A. M., Designing surfaces that kill bacteria on contact. *Proc. Natl. Acad. Sci.* **2001**, *98* (11), 5981-5985.
63. Murata, H.; Koepsel, R. R.; Matyjaszewski, K.; Russell, A. J., Permanent, non-leaching antibacterial surfaces—2: How high density cationic surfaces kill bacterial cells. *Biomaterials* **2007**, *28* (32), 4870-4879.
64. Abrigo, M.; Kingshott, P.; McArthur, S. L., Bacterial response to different surface chemistries fabricated by plasma polymerization on electrospun nanofibers. *Biointerphases* **2015**, *10* (4), 9.
65. Ciston, S.; Lueptow, R. M.; Gray, K. A., Controlling biofilm growth using reactive ceramic ultrafiltration membranes. *J. Membr. Sci.* **2009**, *342* (1-2), 263-268.



66. Shi, Q.; Meng, J.-Q.; Xu, R.-S.; Du, X.-L.; Zhang, Y.-F., Synthesis of hydrophilic polysulfone membranes having antifouling and boron adsorption properties via blending with an amphiphilic graft glycopolymer. *J. Membr. Sci.* **2013**, *444*, 50-59.
67. Ulbricht, M.; Riedel, M.; Marx, U., Novel photochemical surface functionalization of polysulfone ultrafiltration membranes for covalent immobilization of biomolecules. *J. Membr. Sci.* **1996**, *120* (2), 239-259.
68. Yamagishi, H.; Crivello, J. V.; Belfort, G., Development of a novel photochemical technique for modifying poly (arylsulfone) ultrafiltration membranes. *J. Membr. Sci.* **1995**, *105* (3), 237-247.
69. Yamagishi, H.; Crivello, J. V.; Belfort, G., Evaluation of photochemically modified poly (arylsulfone) ultrafiltration membranes. *J. Membr. Sci.* **1995**, *105* (3), 249-259.
70. Aziz, Z.; Abu, S. F.; Chong, N. J., A systematic review of silver-containing dressings and topical silver agents (used with dressings) for burn wounds. *Burns* **2012**, *38* (3), 307-318.
71. Dallas, P.; Sharma, V. K.; Zboril, R., Silver polymeric nanocomposites as advanced antimicrobial agents: classification, synthetic paths, applications, and perspectives. *Adv. Colloid Interface Sci.* **2011**, *166* (1-2), 119-135.
72. Palza, H.; Quijada, R.; Delgado, K., Antimicrobial polymer composites with copper micro- and nanoparticles: Effect of particle size and polymer matrix. *J. Bioact. Compat. Polym.* **2015**, *30* (4), 366-380.
73. Hasan, J.; Crawford, R. J.; Ivanova, E. P., Antibacterial surfaces: the quest for a new generation of biomaterials. *Trends Biotechnol.* **2013**, *31* (5), 295-304.
74. Glinel, K.; Jonas, A. M.; Jouenne, T.; Leprince, J.; Galas, L.; Huck, W. T., Antibacterial and antifouling polymer brushes incorporating antimicrobial peptide. *Bioconjugate Chem.* **2008**, *20* (1), 71-77.
75. Alves, D.; Olívia Pereira, M., Mini-review: Antimicrobial peptides and enzymes as promising candidates to functionalize biomaterial surfaces. *Biofouling* **2014**, *30* (4), 483-499.
76. Bauer, T.; Torres, A.; Ferrer, R.; Heyer, C.; Schultze-Werninghaus, C.; Rasche, K., Biofilm formation in endotracheal tubes. Association between pneumonia and the persistence of pathogens. *Monaldi archives for chest disease* **2002**, *57* (1), 84-87.
77. Flamm, D. L.; Auciello, O., *Plasma deposition, treatment, and etching of polymers: the treatment and etching of polymers*. Elsevier: 2012.
78. Grill, A., *Cold Plasmas in Materials Fabrications: from fundamentals to applications*. IEEE: New York, 1994.
79. Friedrich, J., Mechanisms of plasma polymerization - Reviewed from a chemical point of view. *Plasma Process. Polym.* **2011**, *8* (9), 783-802.
80. Vasudev, M. C.; Anderson, K. D.; Bunning, T. J.; Tsukruk, V. V.; Naik, R. R., Exploration of plasma-enhanced chemical vapor deposition as a method for thin-film fabrication with biological applications. *ACS Appl Mater Interfaces* **2013**, *5* (10), 3983-3994.
81. Steen, M. L. H., L.; Havey, E. D.; Capps, N. E.; Castner, D. G.; Fisher, E. R., Low temperature plasma treatment of asymmetric polysulfone membranes for permanent hydrophilic surface modification. *J. Membr. Sci.* **2001**, *188*, 97-114.
82. Steen, M. L.; Butoi, C. I.; Fisher, E. R., Identification of gas-phase reactive species and chemical mechanisms occurring at plasma-polymer surface interfaces. *Langmuir* **2001**, *17* (26), 8156-8166.
83. Steen, M. L. J., A. C.; Fisher, E. R., Hydrophilic modification of polymeric membranes by low temperature H<sub>2</sub>O plasma treatment. *J. Membr. Sci.* **2002**, *204*, 341-357.
84. Tompkins, B. D.; Fisher, E. R., Evaluation of polymer hydrophobic recovery behavior following H<sub>2</sub>O plasma processing. *J. Appl. Polym. Sci.* **2015**, *132* (20).
85. Burt, S. A.; Reinders, R. D., Antibacterial activity of selected plant essential oils against *Escherichia coli* O157:H7. *Lett. Appl. Microbiol.* **2003**, *36*.
86. Carson, C. F.; Mee, B. J.; Riley, T. V., Mechanism of action of *Melaleuca alternifolia* (tea tree) oil on *Staphylococcus aureus* determined by time-kill, lysis, leakage, and salt tolerance assays and electron microscopy. *Antimicrob. Agents Chemother.* **2002**, *46* (6), 1914-1920.

87. Edmondson, M.; Newall, N.; Carville, K.; Smith, J.; Riley, T. V.; Carson, C. F., Uncontrolled, open-label, pilot study of tea tree (*Melaleuca alternifolia*) oil solution in the decolonisation of methicillin-resistant *Staphylococcus aureus* positive wounds and its influence on wound healing. *Int. Wound J.* **2011**, *8* (4), 375-384.
88. Li, L.; Li, Z.-W.; Yin, Z.-Q.; Wei, Q.; Jia, R.-Y.; Zhou, L.-J.; Xu, J.; Song, X.; Zhou, Y.; Du, Y.-H.; Peng, L.-C.; Kang, S.; Yu, W., Antibacterial activity of leaf essential oil and its constituents from *Cinnamomum longepaniculatum*. *Int J Clin Exp Med* **2014**, *7* (7), 1721-1727.
89. May, J. C., C.H.; King, A.; Williams, L.; French, G.L., Time-kill studies of tea tree oils on clinical isolates. *J. Antimicrob. Chemother.* **2000**, *45*, 639-643.
90. Hendry, E. R.; Worthington, T.; Conway, B. R.; Lambert, P. A., Antimicrobial efficacy of eucalyptus oil and 1,8-cineole alone and in combination with chlorhexidine digluconate against microorganisms grown in planktonic and biofilm cultures. *J. Antimicrob. Chemother.* **2009**, *64* (6), 1219-1225.
91. Burt, S., Essential oils: their antibacterial properties and potential applications in foods--a review. *Int J Food Microbiol* **2004**, *94* (3), 223-253.
92. Dorman, H. J. D.; Deans, S. G., Antimicrobial agents from plants: antibacterial activity of plant volatile oils. *J Appl Microbiol* **2000**, *88*, 308-316.
93. Dalleau, S.; Cateau, E.; Berges, T.; Berjeaud, J. M.; Imbert, C., *In vitro* activity of terpenes against *Candida* biofilms. *Int J Antimicrob Agents* **2008**, *31* (6), 572-576.
94. Carson, C. F.; Hammer, K. A.; Riley, T. V., *Melaleuca alternifolia* (tea tree) oil: a review of antimicrobial and other medicinal properties. *Clin Microbiol Rev* **2006**, *19* (1), 50-62.
95. Carson, C. F.; Riley, T. V.; Cookson, B. D., Efficacy and safety of tea tree oil as a topical antimicrobial agent. *J. Hosp. Infect.* **1998**, *40*, 175-178.
96. Cox, S. D.; Mann, C. M.; Markham, J. L.; Bell, H. C.; Gustafson, J. E.; Warmington, J. R.; Wyllie, S. G., The mode of antimicrobial action of the essential oil of *Melaleuca alternifolia* (tea tree oil). *J Appl Microbiol* **2000**, *88*, 170-175.
97. Easton, C. D.; Jacob, M. V., Solubility and adhesion characteristics of plasma polymerized thin films derived from *Lavandula angustifolia* essential oil. *J. Appl. Polym. Sci.* **2010**, *115* (1), 404-415.
98. Easton, C. D.; Jacob, M. V.; Shanks, R. A.; Bowden, B. F., Surface and chemical characterization of polyLA thin films fabricated using plasma polymerization. *Chem. Vap. Deposition* **2009**, *15* (7-9), 179-185.
99. Ahmad, J.; Bazaka, K.; Oelgemoller, M.; Jacob, M. V., Wetting, solubility and chemical characteristics of plasma-polymerized 1-isopropyl-4-methyl-1,4-cyclohexadiene thin films. *Coatings* **2014**, *4* (3), 527-552.
100. Ahmad, J.; Bazaka, K.; Whittle, J. D.; Michelmor, A.; Jacob, M. V., Structural characterization of  $\gamma$ -terpinene thin films using mass spectroscopy and X-ray photoelectron spectroscopy. *Plasma Process. Polym.* **2015**, *12* (10), 1085-1094.
101. Bazaka, K.; Jacob, M. V.; Ivanova, E. P., A study of a retention of antimicrobial activity by plasma polymerized terpinen-4-ol thin films. In *Mater. Sci. Forum*, Nie, J. F.; Morton, A., Eds. Trans Tech Publications Ltd: Stafa-Zurich, 2010; Vol. 654, pp 2261-2264.
102. Easton, C. D.; Jacob, M. V., Optical characterisation of radio frequency plasma polymerised *Lavandula angustifolia* essential oil thin films. *Thin Solid Films* **2009**, *517* (15), 4402-4407.
103. Pegalajar-Jurado, A.; Easton, C. D.; Styan, K. E.; McArthur, S. L., Antibacterial activity studies of plasma polymerised cineole films. *J. Mater. Chem. B* **2014**.
104. Jacob, M. V.; Easton, C. D.; Woods, G. S.; Berndt, C. C., Fabrication of a novel organic polymer thin film. *Thin Solid Films* **2008**, *516* (12), 3884-3887.
105. Jacob, M. V.; Olsen, N. S.; Anderson, L. J.; Bazaka, K.; Shanks, R. A., Plasma polymerised thin films for flexible electronic applications. *Thin Solid Films* **2013**, *546*, 167-170.
106. Ahmad, J.; Bazaka, K.; Vasilev, K.; Jacob, M. V., Electrical conduction in plasma polymerized thin films of  $\gamma$ -terpinene. *J. Appl. Polym. Sci.* **2015**, *132* (30).

107. Bazaka, K.; Jacob, M. V.; Ostrikov, K., Sustainable life cycles of natural-precursor-derived nanocarbons. *Chem. Rev.* **2016**, *116* (1), 163-214.
108. Easton, C. D.; Jacob, M. V.; Shanks, R. A., Fabrication and characterisation of polymer thin-films derived from cineole using radio frequency plasma polymerisation. *Polymer* **2009**, *50* (15), 3465-3469.
109. Petlin, D.; Tverdokhlebov, S.; Anissimov, Y., Plasma treatment as an efficient tool for controlled drug release from polymeric materials: A review. *J. Controlled Release* **2017**.
110. Hagiwara, K.; Hasebe, T.; Hotta, A., Effects of plasma treatments on the controlled drug release from poly(ethylene-co-vinyl acetate). *Surf. Coat. Technol.* **2013**, *216*, 318-323.
111. Osaki, S. G.; Chen, M.; Zamora, P. O., Controlled drug release through a plasma polymerized tetramethylcyclo-tetrasiloxane coating barrier. *J. Biomater. Sci., Polym. Ed.* **2012**, *23* (1-4), 483-496.
112. Paradiso, P.; Chu, V.; Santos, L.; Serro, A. P.; Colaco, R.; Saramago, B., Effect of plasma treatment on the performance of two drug-loaded hydrogel formulations for therapeutic contact lenses. *J. Biomed. Mater. Res. B Appl. Biomater.* **2015**, *103* (5), 1059-1068.
113. Simovic, S.; Losic, D.; Vasilev, K., Controlled drug release from porous materials by plasma polymer deposition. *Chem. Commun.* **2010**, *46* (8), 1317-1319.
114. Tajima, S.; Komvopoulos, K., Effect of reactive species on surface crosslinking of plasma-treated polymers investigated by surface force microscopy. *Appl. Phys. Lett.* **2006**, *89* (12), 124102.

## CHAPTER 2

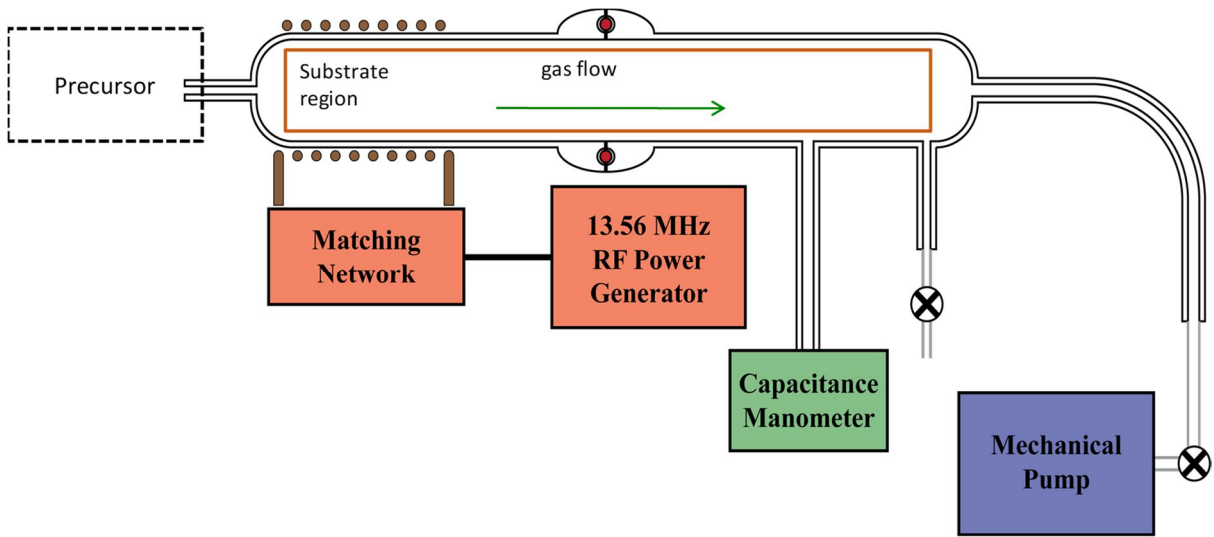
### EXPERIMENTAL METHODS

This chapter provides a detailed description of the materials, methodologies, instruments and techniques used to perform the research presented in this dissertation, including the fabrication, modification, and analysis of biomedically-relevant polymeric constructs. Much of this chapter is adapted from publications that are the basis of Chapters 3 and 5-6; all figures, tables and text have been reproduced here with permission from their respective publishers.<sup>1-3</sup> This chapter comprises six primary sections: plasma reactor set-up and substrate preparation and fabrication (2.1); plasma processing details (2.2), materials and gas-phase characterization (2.3), flux and fouling methodologies (2.4), and biological performance assessment including bacterial assays (2.5) and thromboelastographic measurements (2.6).

#### **2.1 General information**

##### **2.1.1 Plasma reactor set-up**

All plasma surface modifications and PECVD processes described in Chapters 3-8 were performed in a home-built borosilicate glass barrel style plasma reactor (50 mm internal diameter.), illustrated in Fig. 2.1 and previously described.<sup>1,4</sup> Each plasma was ignited by supplying radio frequency (rf) power ( $P$ ) from a 13.56 MHz power supply (RFX 600; Advanced Energy Industries, Inc., Fort Collins, CO) through a matching network to an 8-turn 5 American wire gauge Ni-plated copper induction coil. Vacuum was achieved with a two-stage rotary vane mechanical pump coupled to a liquid-N<sub>2</sub> cold trap, and pressure ( $p$ ) was monitored by a Baratron® capacitance manometer (MKS Instruments Inc., Andover, MA).



**Figure 2.1.** General schematic of the ICP reactor used for the modifications described herein.

### 2.1.2 Precursor and substrate preparation

Depositing essential oil-derived precursors 1,8-cineole, terpinen-4-ol, and  $\alpha$ -terpinene (99%) were purchased from Alfa Aesar (Heysham, England). Other depositing precursors included 1,7-octadiene (98%) and allylamine (allylNH,  $\geq 99\%$ ) and were purchased from Sigma-Aldrich (St. Louis, MO, USA). Deionized (DI) H<sub>2</sub>O (Millipore, 18 m $\Omega$  cm) and all other liquid precursors were each placed in a 50 mL borosilicate sidearm vacuum flask equipped with a Teflon™ stopcock and subjected to three consecutive freeze-pump-thaw cycles to remove dissolved atmospheric gases prior to use. Argon (99.99%, Airgas) was used as received for treatments performed for Chapter 7.

*Two-dimensional (2D) substrate preparation.* Substrates used for film deposition varied depending on experiment; glass slides (VWR micro slides, plain, 1.2 mm thickness), were cut to approximately 12  $\times$  12 mm, *p*-type <100> silicon wafers with 40-60 Å native oxide layer (Wacker-Chemitronic GMBH, Germany) were cut to approximately 6  $\times$  12 mm, and polystyrene (PS) disks (diameter = 13.5 mm) were punched from non-tissue culture (NTC) petri dishes (Fisher Scientific, Fair Lawn, NJ, USA).

*Preparation of commercial ultrafiltration membranes.* A summary of specifications for all commercial filtration membranes employed in this work is provided in Table 2.1. Asymmetric ultrafiltration (UF) polysulfone (UPS) membranes were donated by US Filter, Inc. [molecular weight cut off (MWCO) of 100 kDa]. Ultrafiltration polyethersulfone (PES) membranes (MWCO = 100 kDa) were purchased from Synder Filtration (Vacaville, CA, USA). Circular membrane samples (35 mm diameter) were obtained by punching from the flat sheets (~8.5  $\times$  11") and rinsed with methanol (99.9%; Fisher Scientific), hexanes (98.5%, Mallinkrodt Chemicals), ethanol (absolute anhydrous, ACS grade, PHARMCO-AAPER, Brookfield, CT,

**Table 2.1.** Manufacturer provided details for ultrafiltration and microporous membranes used in this work.

<b>Membrane</b>	<b>Manufacturer</b>	<b>MWCO (kDa)<sup>a</sup></b>	<b>Pore size (μm)</b>	<b>Thickness (μm)</b>	<b>Chapter(s)</b>
PSf	US Filter	100	-----	10	3
PES <sup>b</sup>	Synder Filtration	100	-----	150	8
PVDF <sup>b</sup>	Synder Filtration	100	-----	150	8
PC-TE	Sterlitech Corp.	-----	0.2	10	4, 7

<sup>a</sup> For microporous membranes, pore size is the manufacturer provided measure of pore diameter, whereas the MWCO provides a relative pore size for ultrafiltration membranes.

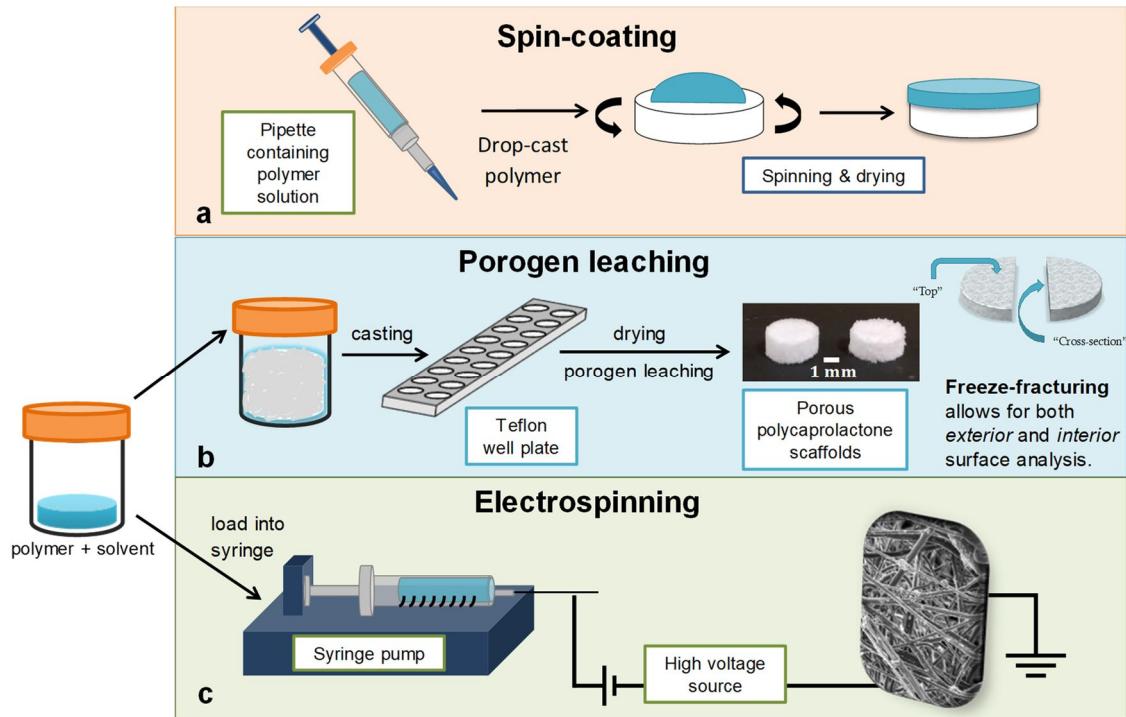
<sup>b</sup> Contains hydrophilic additive.

USA), or a 1% aqueous solution of sodium dodecyl sulfate (SDS; 99%; Fisher Scientific), as specified, prior to use. Soaking times ranged from 5-30 min. Membranes soaked in SDS were rinsed by submerging in DI water for 20 min to remove any residue before drying in a desiccator. For studies specifically investigating the effect of solvent type and soaking time on UF membranes, three membranes were cleaned at once to ensure consistency and gauge reproducibility. Gravimetric studies were completed to assess the effect of cleaning parameters on the membrane by weighing the membrane (Denver Instrument APX-100 analytical balance, precise to 0.1 mg) before and after preparation. As is typical of UF membranes, both a shiny “tight” side (responsible for the filtration capabilities of the membrane) and matte “open” side were visible. Nomenclature regarding asymmetric membranes is described elsewhere.<sup>5</sup>

*Polymer scaffold fabrication and incorporation of silver nanoparticles (AgNPs).*

Polycaprolactone (PCL) scaffolds were fabricated by the porogen leaching method, as depicted in Fig. 2.2.a and described previously.<sup>6-8</sup> Briefly, chloroform ( $\text{CHCl}_3$ ; >99.8%, Fisher Scientific, Fair Lawn, NJ, USA) was added to PCL pellets (average  $M_n = 80,000$ , Sigma-Aldrich, Saint Louis, Missouri, USA) and allowed to dissolve completely (~3 h). Sieved (150-300  $\mu\text{m}$ ) sodium chloride ( $\text{NaCl}$ , Sigma-Aldrich) was added to the dissolved PCL/ $\text{CHCl}_3$  mixture (5/95% w/w PCL/ $\text{NaCl}$ ) to act as a porogen. The polymer slurry was cast into Teflon® PTFE molds (McMaster Carr) machined with 3 mm  $\times$  3 mm wells. Scaffolds were allowed to dry for ~ 3 h to ensure complete evaporation of  $\text{CHCl}_3$ . Scaffolds, still in the molds, were placed in ultrapure water (Millipore, 18  $\text{m}\Omega$  cm) for salt leaching. After 1 d, scaffolds were removed from wells and water was replaced with fresh ultrapure water once per day for 3-5 d, until salt leaching was complete. Scaffolds were dried and stored under ambient laboratory conditions.





**Figure 2.2.** Schematic of select fabrication techniques used to create the polymeric constructs presented in this work.

AgNP-containing scaffolds were prepared by two methods: (1) blending AgNPs with the polymer slurry and (2) drop casting AgNPs onto the polymer surface. To fabricate blended Ag-PCL scaffolds, the desired mass of AgNPs [ $<100$  nm, polyvinylpyrrolidone (PVP) added as dispersant, Sigma-Aldrich] was mixed into the PCL-chloroform mixture along with the NaCl porogen prior to casting in molds. Aliquots of water used for leaching were preserved at several time points for further analysis. For drop casting, a 0.08% w/w solution of AgNPs was prepared in 50 mM aqueous sodium citrate buffer (ACS grade, Fisher Scientific) and sonicated for 30 min. Each scaffold was drop cast with this solution until the top was fully covered ( $\sim 600$   $\mu\text{L}$ ). Scaffolds were dried in air, rinsed with 10 aliquots of 100  $\mu\text{L}$  of ultrapure water to remove salt from the buffer and allowed to dry overnight.

*Electrospun fiber fabrication and incorporation of AgNPs.* Fibers loaded with AgNPs were fabricated by electrospinning, as described elsewhere.<sup>9-11</sup> Two strategies were employed, one with commercial AgNPs blended in as well as *in situ* reduction of  $\text{AgNO}_3$  salt. First, a 7:3 solvent mixture was prepared from dichloromethane (DCM; ACS grade, Macron Fine Chemicals) and methanol (MeOH;  $\geq 99.8\%$  ACS grade, Sigma-Aldrich). 5 mL of 8% w/v PCL was prepared by placing PCL pellets in 7:3 DCM:MeOH and allowing for full dissolution while stirring gently. AgNPs (10% w/v) were then blended with the polymer gel and the Ag-polymer mixture was added to a 5 mL syringe (BD, Luer-Lok™ tip) equipped with a Hamilton 90520 needle. A constant voltage of 25 kV was applied to the end of the needle using a high voltage power supply (Gamma High Voltage Research, model ES30P-20W, Ormond Beach, FL), and a syringe pump (Kent Scientific GenieTouch™, Torrington, CT, USA) was operated such that the Ag-polymer mixture was dispensed at 5 mL  $\text{h}^{-1}$  for 1 h. Electrospun fibers were collected on a clean piece of aluminum foil (approximately 4"  $\times$  4") supported on a large metal sample holder

placed ~15 cm from the end of the needle. The resulting mat (~1-2 mm thick) was peeled from the aluminum foil support and placed in a clean petri dish in a hood for at least 24 h to allow for complete solvent evaporation.

The second strategy employed *in situ* reduction of AgNO<sub>3</sub> salt to form AgNPs within the electrospun mat, as described by Sumitha et al.<sup>11</sup> For this approach, a PCL solution (14% w/v) was prepared in 5:3:2 CHCl<sub>3</sub>: MeOH: N,N-dimethylformamide (DMF; ACS grade, Fisher Scientific). AgNO<sub>3</sub> (99.8%, Fisher Scientific) was added at 10% w/v. The AgNO<sub>3</sub>-polymer slurry was gently stirred for two hours to ensure complete dissolution, then electrospun as described above. Regardless of the strategy employed, at least 3 fiber mats were fabricated per sample type and fiber mats were cut into 2 × 2 cm squares for analysis.

*Fabrication of AgNP-loaded films.* Flat PCL films spin coated onto polystyrene (PS) disks (13.5 mm diameter), punched from NTC Petri dishes (Fisher Scientific), were prepared as substrates for immobilization of AgNPs on surface. A 17% w/v solution of PCL was prepared in CHCl<sub>3</sub> and allowed to dissolve for ~2 h. PCL films were fabricated via spin coater (WS-650-23NPP/LITE, Laurell Technologies). Spin coating was achieved by using a transfer pipette to place a droplet of polymer solution onto PS disks and rotating at 2000 rpm for 2 min followed by 3200 rpm for 1 min. Films were soaked in absolute ethanol for 1 h to remove residual CHCl<sub>3</sub> then dried in a hood overnight.

Spin-coated PCL films were loaded with AgNPs via *in situ* reduction of AgNO<sub>3</sub> salt. Methods for immobilization were chosen based on work published by Cao et al.<sup>12</sup> Briefly, films were placed in the bottom of a 10 mL beaker and covered with enough 0.1 M AgNO<sub>3</sub> solution to completely cover films (~3 mL). The beakers containing films were then placed in a 38 °C water bath for 48 h. A 0.075 M solution of vitamin C was prepared by placing L+ ascorbic acid (99%

purity, Alfa Aesar, Ward Hill, MA, USA) in distilled water, and the pH was adjusted to 6 using NaOH (5.0 M in DI water, Mallinckrodt Baker Inc., Phillipsburg, NJ, USA). Films were placed ~3 mL vitamin C solution to cover films for 15 min to allow for complete reduction. After rinsing, films were allowed to fully dry in a hood. Identical methods were also completed on these flat PCL substrates that were H<sub>2</sub>O<sub>(v)</sub> plasma treated before exposure to AgNO<sub>3</sub> solution.

Films were also fabricated using an alternative method described by Fortunati et al.<sup>13</sup> Here, we followed a slightly modified procedure to fabricate similar films. In our case, polylactic acid (PLA; NatureWorks Ingeo™ Biopolymer grade 6202D) was used in place of polylactic-co-glycolic acid (PLGA). Briefly, PLA was dissolved in CHCl<sub>3</sub> at 10% w/v. AgNPs were added (7% w/v) and the mixture was blended well before spreading on a flat Teflon PTFE surface (McMaster Carr). Films were allowed to fully dry and resulting films (~0.3 mm thick) were stored in a hood protected from light. Films were also made without AgNPs to serve as material controls.

*Fabrication of AgNP-loaded membranes.* Another type of material was fabricated based on a modified method described by Islam et al.<sup>14</sup> Membranes used herein have pores half the size of the membranes reported by Islam et al., thus the ability of bacteria to penetrate the pores should not increase, allowing them to colonize the surface similarly. Polycarbonate track-etched (PC-TE) membranes (13 mm diameter, 200 nm pores, Whatman Nuclepore) were drop cast with AgNP-containing solution (1.1 and 2.2 g L<sup>-1</sup> in distilled water, sonicated 30 min). A 20 µL droplet of solution was added to the surface of the membranes and allowed to dry.

*Synthesis of nitric oxide donor and fabrication of nitric oxide-releasing Tygon® films.* For the studies presented in this dissertation, we used S-nitrosoglutathione (GSNO) as the NO donor, which is prepared by nitrosating the thiol residue of glutathione. All reagents used to prepare

GSNO are described elsewhere; GSNO was synthesized following the protocol published by Hart.<sup>15</sup> Briefly, glutathione (5 mmol) was added to a mixture of 8 mL of ice-cold water and 2.5 mL of 2 M hydrochloric acid. For the nitrosation step, sodium nitrate (5 mmol) was added to the mixture to form nitrous acid as the nitrosating agent. The solution was then stirred on ice for 40 min. The GSNO product was precipitated by adding 10 mL of acetone, and the product was filtered and washed with water to remove any excess of nitrite. The GSNO was subsequently rinsed with acetone, dried under vacuum for 1.5 h protected from direct light, and stored in EPA vials (Fisher Scientific, Fair Lawn, NJ, USA) at  $-20\text{ }^{\circ}\text{C}$  until use to prevent any donor decomposition. Characterization of GSNO was performed by ultraviolet-visible spectroscopy as previously reported.<sup>16</sup>

The model polymer in all studies was Tygon® (Formula R-3603, Saint-Gobain Performance Plastics, Akron, OH, USA). To prepare the Tygon® solution, Tygon® was dissolved in tetrahydrofuran (THF, Fisher Scientific, Fair Lawn, NJ, USA) at a concentration of  $0.075\text{ g mL}^{-1}$ . Tygon® only films were prepared by delivering  $750\text{ }\mu\text{L}$  of the Tygon®/THF solution to the bottom of a 20 mL glass beaker. GSNO-incorporated films were prepared by blending either 5% or 20% w/w GSNO in Tygon® solution (denoted as GSNO5 and GSNO20, respectively) before casting into the beaker. Films were dried overnight at room temperature and protected from light. Resulting Tygon® films were transparent whereas GSNO5 and GSNO20 films are pink in color because of GSNO donor incorporation.<sup>17</sup>

*Clinical consumables as substrates.* Commercial disposable TEG cups and pins were purchased from Haemonetics (Braintree, MA, USA). These commercial consumables were used as received. Customized TEG cups with larger volumes were designed using CAD software

(dimensions published elsewhere)<sup>18</sup> and 3D printed from acrylonitrile butadiene styrene (ABS) using an EnvisionTec 3D printer.

## 2.2 Plasma processing of polymeric materials

A summary of treatment conditions for all precursors and substrates is given in Table 2.2. Treatments described in Chapters 3-5 and Chapter 8 were chosen based on parameters optimized in previous studies.<sup>4, 7, 19-22</sup> The parameters most commonly varied herein include the applied rf  $P$ , precursor  $p$ , treatment time, and substrate location in the reactor.

Except for membranes, materials were placed on clean glass slides (typically 3 at a time in the case of scaffolds or Tygon® films) inside the plasma reactor. Before introducing each plasma precursor, the chamber was evacuated to base pressure (<10 mTorr). Precursors were introduced through a 6 mm internal diameter inlet via either a needle metering valve (in the case of liquid precursors) or a mass flow controller (for gaseous precursors such as Ar). In the case of film deposition, the reactor was pre-conditioned by operating the plasma at the desired conditions without a substrate. The chamber was purged with precursor gas for  $\geq 5$  min, and pressure was allowed to stabilize before igniting the plasma. After plasma processing, the chamber was once again purged with precursor vapor  $\geq 5$  min to quench any remaining active sites on the substrate surface that could react with atmospheric gases. Post processing, all materials were stored under ambient laboratory conditions, protected from light.

Throughout this dissertation, several shorthand notations are used to describe materials after plasma processing. For materials in Chapter 3, the shorthand notation UPS-0 indicates untreated UPS membranes, whereas treated membranes are labeled using the corresponding plasma

**Table 2.2.** List of parameters for each plasma system described in this work.

Precursor	$P$ (W)	$p$ (mTorr)	Treatment time (min)	Substrate placement (cm downstream from coil)	Chapter(s)	Material modified or deposited
H <sub>2</sub> O	30	50	0.5-5	20	3	PSf
		200	10		8	PES
	25	50	2	10		PVDF
	20	200	2	15	4	Ag materials
			5		5	Tygon®
		50	2	10	6-8	ppCin
1,8-cineole	50-150	15-100	5-60 <sup>a</sup>	in coil, 10, 15	6	ppCin on glass
1,7-octadiene	25	100	10	10		ppOct on glass
terpinen-4-ol <sup>b</sup>	50	5	10	10	7	ppT-4-ol on glass, scaffolds, membranes
$\alpha$ -terpinene	25	60	10	10	7	ppTer on glass, scaffolds, membranes

<sup>a</sup> Treatment time was varied for ppCin deposition rate studies. Films for all other analyses in Chapters 6-7 were deposited for 5 min, unless otherwise noted.

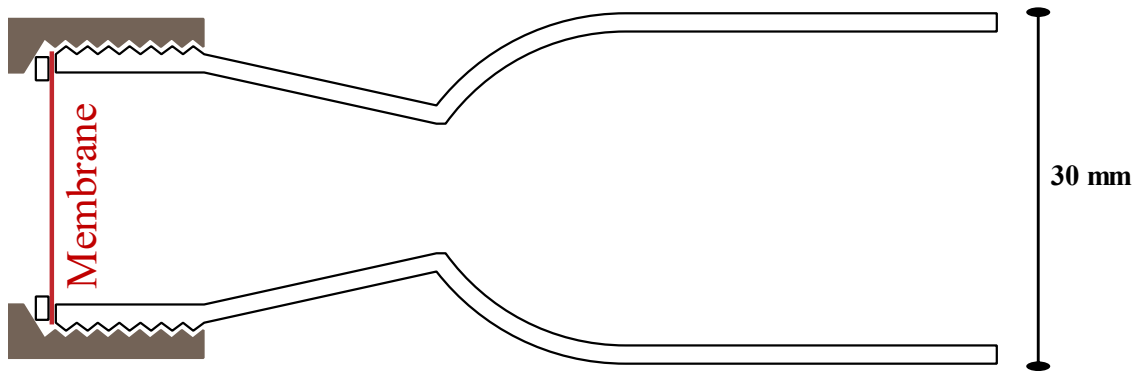
<sup>b</sup> Films from terpinen-4-ol were also deposited via plasma graft polymerization for studies in Chapter 7, as described in Section 2.2.

treatment time: UPS-0.5 for 30 s, UPS-1 for 1 min, UPS-2 for 2 min, UPS-3 for 3 min, and UPS-5 for 5 min treatment. The prefix *pp* is typically given to plasma polymerized thin films in this work. (e.g., ppCin for films resulting from the plasma polymerization of 1,8-cineole; ppOct for films from 1,7-octadiene). A list of abbreviations for all films is provided in Table 2.2.

*Membrane and suture modification.* For all membrane plasma treatments, an additional cylindrical glass membrane holder (30 mm diameter) was used to orient the membrane perpendicular to the gas flow, as previously described (Fig. 2.3).<sup>1, 20</sup> To reduce plasma-induced damage to the membranes, the holder was typically placed ~10-20 cm downstream from the most intense region of the plasma glow, as this is known to reduce etching from high-energy species or temperature-related damage to the polymer.<sup>23</sup> The open side of the membrane is oriented upstream (unless specified otherwise) and facing the plasma glow, while the tight side faced downstream, once again to reduce damage during modification.

*Plasma graft polymerization.* Because the terpinen-4-ol parameter space was limited by the low vapor pressure of the monomer, plasma graft polymerization was another method chosen to deposit ppT-4-ol films. Substrates were placed in the reactor in a similar manner as described above (e.g., membranes were placed in the membrane holder) and subjected to surface activation by Ar for 10 min at  $p = 150$  mTorr and  $P = 40$  W.<sup>22</sup> Ar flow was immediately stopped after plasma was turned off, and terpinen-4-ol was flowed in at the maximum allowable rate for one hour. Neither terpinen-4-ol pressure nor flow rate were quantifiable because the low vapor pressure of the precursor resulted in a total chamber pressure indistinguishable from the base pressure.





**Figure 2.3.** Schematic of holder for modification of commercial membranes.

Precursor flow could, however, be verified, as an initial spike in pressure upon opening the precursor bulb was observed, and a faint residual essential oil odor was apparent after the plasma reactor chamber was opened. After the 1 h flow of terpinen-4-ol, the precursor bulb was closed, the chamber pumped out, and the substrate allowed to remain in the chamber for an extended period of time (>1 h) to ensure no activated sites remained to react with atmosphere.

### **2.3 Gas-phase and material characterization techniques**

*Gas phase analysis.* Optical emission spectroscopy (OES) was used to investigate select plasmas *in situ*, specifically to detect excited state species during plasma deposition. Optical emission spectra were obtained by modifying the reactor depicted in Fig. 2.1 to include a replaceable fused quartz window at the upstream end (~5 cm from the coil). Emitted radiation was gathered coaxially through a cable comprising four fiber optical strands and dispersed onto a 10  $\mu\text{m}$  entrance slit of an Avantes AvaSpec-2048-USB2 multichannel spectrometer equipped with four fiber gratings, 3648 pixel charge-coupled array detectors, detectable wavelength range of 187 – 1016 nm, and a 0.1 nm full width at half maximum (FWHM) resolution. Spectra were collected by averaging 600 scans, each with a 50 ms integration time with background/dark spectra collected during the initial 5 min gas flow while emission spectra were collected for the entire 5 min plasma deposition.

For all surface characterization described herein, materials were analyzed immediately after modification (unless otherwise noted), and measurements were repeated for a minimum of  $n = 3$  to gauge reproducibility of the plasma deposition processes. Prior to analysis of PCL scaffolds, the scaffold interior was exposed by immersion in liquid nitrogen followed by slicing vertically with a scalpel. This allowed for analysis of both the tops and cross sections of the 3D materials.

*Water contact angle (WCA) goniometry.* WCA ( $\theta$ ) was measured using a Krüss DSA30S contact angle goniometer (Matthews, NC, USA). A 2  $\mu\text{L}$  drop of ultrapure water (Millipore, 18 m $\Omega$  cm) was applied to the material surface and the static WCA ( $\theta_{\text{static}}$ ) was measured using high-speed video recording for 10 s at 64 frames per second (fps). Data were analyzed with onboard Krüss software; the circle fitting method was used for low WCA ( $<30^\circ$ ), and the tangent line fitting method was used for WCA values larger than  $30^\circ$ .<sup>24</sup> Probe liquid parameters included density = 0.9970 g/mL, viscosity = 0.0010 cP, and surface tension = 72.16 mN/m.  $\theta_{\text{static}}$  values are reported as mean  $\pm$  standard deviation for  $n \geq 9$  measurements.

Some samples (e.g.,  $\text{H}_2\text{O}_{(\text{v})}$  plasma treated ultrafiltration membranes) did not reach a  $\theta_{\text{static}}$ ,<sup>5</sup> thus WCA ( $\theta$ ) as a function of time or “age of the drop” after the 2  $\mu\text{L}$  water drop contacts the membrane surface, referred to hereafter as dynamic WCA, was measured with a Krüss DSA10 or Krüss DSA30S contact angle goniometer (Matthews, NC, USA). A video was collected at 25-64 fps for  $\geq 10$  s and  $\theta$  was obtained for each frame by fitting the data using the Krüss onboard software (using circle fitting and identical probe liquid parameters). As a criterion for determining if the material is “completely wettable”, we established that the drop must be absorbed ( $\theta \leq 20^\circ$ ) into the membrane in  $\leq 2$  s after the drop contacts the membrane surface. Dynamic WCA values for samples treated in  $\text{H}_2\text{O}_{(\text{v})}$  plasmas were measured within one hour of removing the membrane from the reactor, designated as “freshly-treated” materials.

*WCA assessment of modified material aging.* Select materials in Chapters 3 and 6 were aged in ambient laboratory conditions for various time spans to assess any hydrophobic recovery that may occur in the days or months following plasma processing. Membranes discussed in Chapter 3 were aged for up to 2 months and dynamic WCA measurements were repeated in an identical manner as described above. As-deposited ppCin and ppOct films and  $\text{H}_2\text{O}_{(\text{v})}$  plasma

treated ppCin films discussed in Chapter 6 were aged under ambient laboratory conditions to assess changes in WCA after 24 h, 1 week, 2 weeks, 1 month, and 2 months.

*Fourier-transform infrared (FTIR) spectroscopy.* FTIR analysis was performed using a Thermo Scientific Nicolet 6700 FTIR spectrometer (Madison, WI). Spectra were collected in transmission mode at a resolution of  $4\text{ cm}^{-1}$  and averaged over 120 scans. For analysis of the monomers, freshly cleaned, polished KBr or NaCl windows were covered with a thin layer of liquid, whereas films were deposited on either KBr pellets (pressed from FTIR-grade KBr, Sigma-Aldrich, St. Louis, MO, USA) or Si wafers for FTIR analysis. To minimize atmospheric signal, the instrument was purged with  $\text{N}_2$  gas  $>2$  h before and during analysis. For all spectra, atmospheric signals were suppressed and baseline was corrected using the onboard software (Omic v8.2).

*X-ray photoelectron spectroscopy (XPS).* XPS was performed using a Physical Electronics PE5800 ESCA/AES system (Chanhassen, MN, USA) equipped with an Al  $K_{\alpha}$  monochromatic X-ray source (1486.6 eV), hemispherical electron analyzer, and multichannel detector. Samples were mounted to the sample holder using double sided conductive carbon tape. A  $45^{\circ}$  take off angle and low energy electron flood gun (5 – 15 eV) were employed for collection of spectra with minimal artifacts from surface charging. Survey spectra were collected for 5 min over 50 – 1100 eV to obtain approximate elemental composition, whereas high-resolution spectra were collected for 15 min for all elements present in  $>1\%$  amounts including  $\text{C}_{1s}$ ,  $\text{O}_{1s}$ , and, in some cases,  $\text{N}_{1s}$ ,  $\text{Ag}_{3d}$ , and  $\text{Si}_{2p}$ . Each of at least three samples was analyzed in three distinct spots to determine homogeneity of surface composition. CasaXPS software (Casa Software Ltd., Cheshire, UK) was used for deconvolution of all high-resolution spectra with Gaussian-

Lorentzian (70:30) fits and FWHM constrained to  $\leq 2.0$  eV.<sup>25</sup> High-resolution C<sub>1s</sub> spectra were charge corrected by setting the C–C/C–H component to 285.0 eV for all samples.<sup>20, 25</sup>

*Scanning Electron Microscopy-Energy Dispersive Spectroscopy (SEM-EDS).* Material morphology was assessed by SEM. All polymer samples were secured to an aluminum stub with double sided conductive carbon tape, and sputter coated with Au film (~10 nm) to minimize charging. SEM-EDS data were obtained using a JEOL JSM-6500F microscope operated at a working distance of ~10.0 mm and an accelerating voltage of 2-5 kV (for imaging) and 10 kV (for EDS data collection). The gold coating step was omitted for EDS data collection.

*Optical profilometry.* PECVD allows for relatively fast (on the scale of seconds to minutes) deposition of films with controllable thickness. To concurrently characterize the deposition rate of our systems and roughness of the resulting films, we performed optical profilometry analyses. Glass substrates were masked with either PS or a silicon wafer to obtain a clean edge of the film for measuring step heights; deposition time varied from 2 to 60 min. A Zometrics ZeScope optical profilometer (Middlefield, CT, USA) was used to collect scans over a 250  $\mu\text{m}$   $\times$  350  $\mu\text{m}$  area at 20 $\times$  magnification. The scan length was set to 100  $\mu\text{m}$  in the z-axis and signal threshold to 1.0%. Optical profilometry data were used to determine film roughness parameters, specifically,  $R_a$ , the arithmetic average height of film heights and valleys, and  $R_q$ , the geometric average or root-mean-square roughness. The mean deposition rate was calculated using the individual step heights measured; results for deposition rates and roughness parameters were obtained from a minimum  $n = 3$ ; and error reported is one standard deviation of the mean.

*Analysis of nitric oxide release.* To determine the effect of plasma treatment on NO release, nitric oxide analyzers (NOAs, Sievers 280i, GE Analytical Instruments, Boulder, CO, USA) were used to measure NO release from polymer films before and after plasma treatment. This

technique is highly selective and sensitive for the direct chemiluminescent detection of NO.<sup>26</sup> Prior to data collection, NOAs were calibrated using zero gas (UHP N<sub>2</sub>) and 45 ppm NO/N<sub>2</sub>. Samples were introduced (uncovered) to the NOA cell containing nutrient broth media (NBM) at 37 °C to mimic bacterial culture conditions and the sample intervals were 5 s and 1 min for 24 and 72 h, respectively. NO released from the polymer samples was swept into the reaction cells by N<sub>2</sub> flow gas at 200 mL min<sup>-1</sup>. Average concentration data collected over the sample interval were converted to moles of NO using a previously determined calibration constant. By calculating the theoretical amount of NO in each film (assumed to be unchanged by plasma treatment) the percentage of NO released from each film could be determined. The time to reach maximum NO release was determined for each trial. Surface flux was calculated by dividing the amount of NO released by the film surface area as a function of time. All measurements were performed in triplicate, and statistical analyses were completed using a two-tailed t-test with significance considered at  $p \leq 0.05$ .

*Film stability analysis.* The quality of film adhesion was assessed by testing film stability in biologically-relevant media for both glass and PS substrates. Each film was immersed in sterile physiological saline (10 mL; 0.85% w/v NaCl, certified ACS grade, Fisher Scientific, Fair Lawn, NJ, USA) and incubated at room temperature for 18 h, before carefully rinsing 3 times with copious amounts of Millipore water. After drying, films were then visually inspected to observe film integrity, and, if film presence or quality was not visually clear, WCA analysis was performed to confirm or deny film presence and integrity.

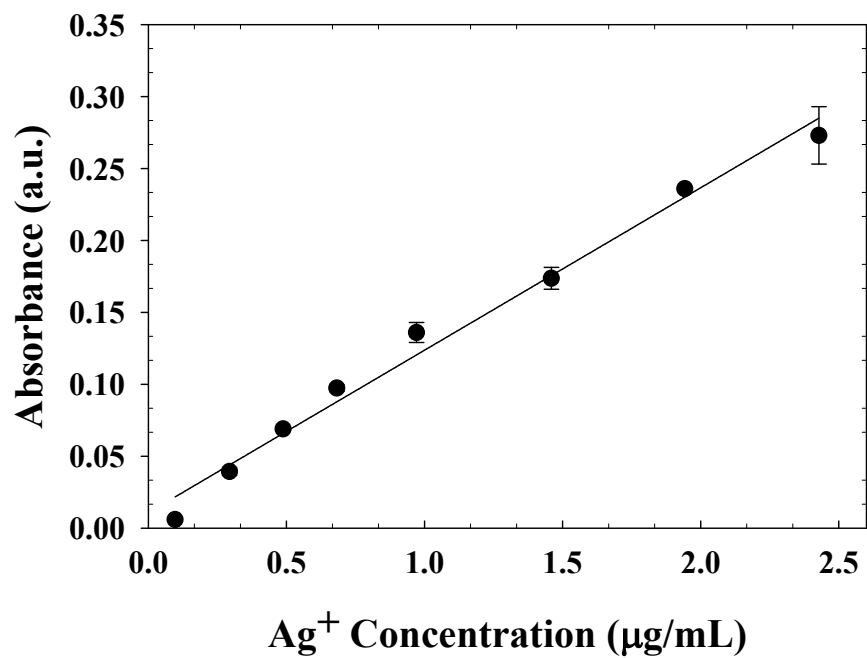
*Ag leaching analysis.* Flame atomic absorption spectroscopy (AAS) was employed for Ag leaching studies on the 0.024% and 2.4% w/w Ag blended scaffolds.<sup>27-29</sup> Measurements were made using a Varian SpectrAA 50 single beam spectrometer equipped with a Varian Ag hollow

cathode lamp, aligned to maximize signal. The lamp was operated at a current of 4 mA and slit width was set to 0.5 nm. The flame was ignited using acetylene fuel with air as support and absorbance at 328.1 nm was monitored to correlate to Ag concentration. Distilled water was used before measurements to zero the instrument as well as between measurements to ensure it gave no measurable absorbance. Silver standards of concentrations 0.1-2.5 ppm were prepared by digestion of AgNPs with nitric acid (ACS grade, Mallinckrodt, St. Louis, Missouri, USA), and absorbance values were collected in triplicate for each standard to create a calibration curve for Ag quantification (Fig. 2.4). Samples of ethanol and water used for the leaching of 0.024% Ag scaffolds were analyzed and each absorbance value was converted to Ag concentration (in ppm) using the standard curve.

## **2.4 Strategies for assessment of membrane performance**

Chapters 3 and 7 detail the performance of filtration membranes modified by several different plasma systems. This section describes how the hydrodynamic performance and fouling resistance of these materials were measured.

*Observation of protein layer by XPS.* Surfaces exposed to biological environments adsorb proteins and other biomolecules that can affect the delivery of a drug from the material.<sup>30</sup> Because many biomolecules contain high levels of nitrogen, XPS can be used to estimate adsorbed protein on a variety of substrates.<sup>30-33</sup> Untreated and treated Tygon® and GSNO20 films were placed in 2 mL of NBM in well plates for 24 h (protected from light). The atomic percentage of nitrogen from XPS survey scans was obtained for 3 distinct spots on each film to estimate the amount of protein adsorbed during the kill rate assays.

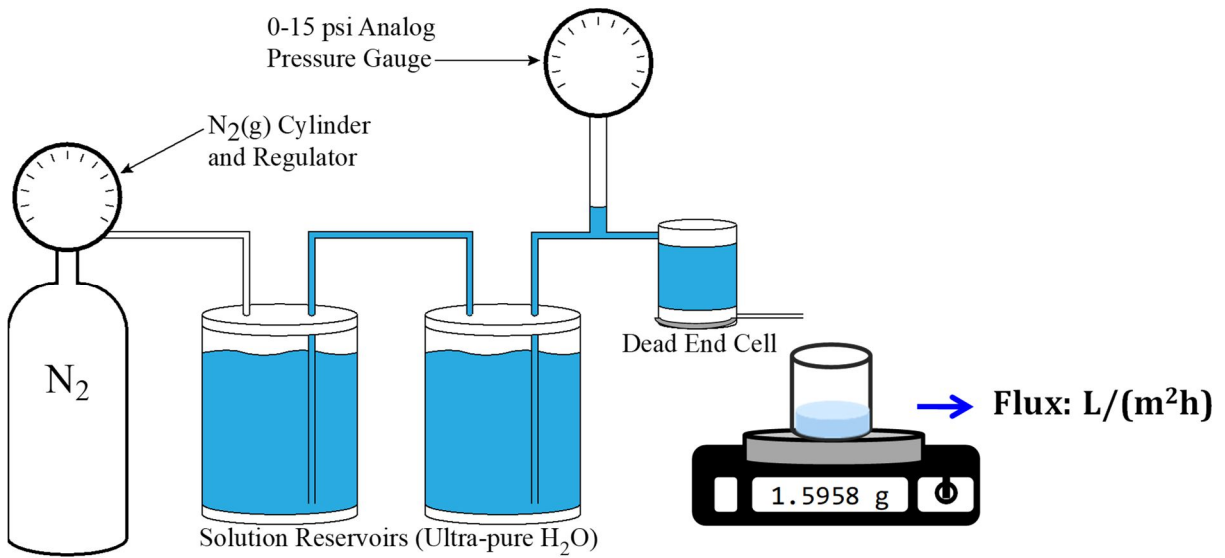


**Figure 2.4.** Calibration curve created for the analysis of Ag<sup>+</sup> content by flame AAS. Data represent the mean  $\pm$  standard deviation of  $n \geq 3$ .



*Gravimetric analysis of protein fouling.* Protein mass gained by membranes was measured under both static and dynamic (i.e., during flux experiments) conditions. For static conditions, 4 mL of a 10% aqueous bovine serum albumin (BSA, initial fractionation by heat shock, >98%, A9430, obtained from Sigma Chemical) solution were added to membranes in 6-well tissue culture (TC, VWR, Arlington Heights, IL, USA) well plates and allowed to sit for the specified time (18-36 h). Membranes were rinsed 3 times with 4 mL aliquots of ultrapure water and allowed to dry in clean well plates. Membranes were weighed before and after exposure to protein and rinsed using a Denver Instrument APX-100 analytical balance, precise to 0.1 mg. The difference in mass was assumed to be the mass of protein adsorbed to the membrane surface. For dynamic fouling studies, the membrane was weighed prior to undergoing a protein flux experiment and after protein filtration and rinsing with ultrapure water.

*Flux studies.* Ultrafiltration experiments were conducted using a 10 mL dead-end stirred UF cell (Model 8010, Amicon Div., Danvers Millipore Corp.) connected to a nitrogen gas cylinder by an acrylic solution reservoir (>2 L of solution) that allows continuous liquid flow. A schematic of this device is shown in Fig. 2.5. The bulk solution in the UF cell was stirred with a magnetic stir bar at 400 rpm. The active membrane area was 3.46 cm<sup>2</sup>. Because the untreated membranes are hydrophobic, UPS-0 was exposed to a preconditioning treatment as described in detail elsewhere.<sup>23</sup> Briefly, UPS-0 was wet in 50% (v/v) isopropyl alcohol in DI water solution prior to filtration. The isopropyl alcohol was gradually replaced with DI water to effectively wet the membrane, where each untreated membrane remained in DI water for 12 h prior to use. All treated membranes were simply wet in water for 5 min prior to filtration as they were already nominally hydrophilic.



**Figure 2.5.** Schematic of dead-end stirred cell setup for flux measurements.

Wet membranes were placed in the stirred cell and secured with the included o-ring. The system was sealed and filled with DI water. The water was then pressurized through the membrane using N<sub>2</sub> (103.4 kPa, 15 psi) for 15 min to compact the membrane. The pressure was then reduced to operating pressure (68.9 kPa, 10 psi) and the water flux was measured every 30 min for 1 h. Initial water flux and water flux after 1 h of filtration are referred to as  $J_0$  and  $J_1$ , respectively. As pressure can affect these measurements, all flux values obtained were normalized using the operating pressure (i.e., flux units of L m<sup>-2</sup> kPa<sup>-1</sup> h<sup>-1</sup>).

A 1% w/v solution of bovine serum albumin (BSA) was prepared by dissolving BSA powder in DI water at room temperature. This protein solution was autoclaved prior to experiments. Without removing the membrane from the test cell, the dead-end stirred UF cell was filled with 1% BSA solution. The membrane was initially exposed to the protein solution for 2 h without stirring and the solution was then stirred for 1 h while protein flux was measured every 30 min ( $J_2$  is the protein flux after 1 h of protein filtration). The tendency of the membrane to foul was assessed by calculating the % RFR exhibited by the membrane when exposed to the BSA solution. The % RFR was estimated using equation 2.1:

$$\text{Relative flux reduction (\% RFR)} = \left(1 - \frac{J_2}{J_1}\right) * 100 \quad (2.1)$$

After UF of the BSA solution, the membrane was cleaned by rinsing twice with DI water. The water flux was once again measured after cleaning ( $J_3$  – water flux after 1 h of water filtration) to calculate the % FRR (equation 2.2). The % FRR provides an indication of the recovery of the membrane after fouling.

$$\text{Flux recovery ratio (\% FRR)} = \left(\frac{J_3}{J_1}\right) * 100 \quad (2.2)$$

The amount of protein adsorbed on the membrane was evaluated by gravimetric analysis. Every membrane was weighed with an accuracy of 0.01 mg before and after performance testing

to estimate the mass of the deposited protein. It was assumed a homogeneous deposition of the protein over the entire membrane and the  $\mu\text{g}$  of protein per  $\text{cm}^2$  of membrane were calculated based on the active membrane area. A paired-samples t-test was conducted to determine any significant impact of the surface modification on the membrane performance.

*Effect of the compaction-pressure release cycles on overall performance.* As control experiments, UPS-0, UPS-2, and UPS-5 membranes were exposed to the filtration set-up described above, in the absence of protein solution. These experiments provided insight into the effect of the compaction-pressure release cycles on membrane performance in the presence of pure water and the absence of foulant. Membranes were placed in the stirred cell, the system was filled with DI water, and the water was pressurized through the membrane with  $\text{N}_2$  for 15 min. The pressure was then reduced to operating pressure (68.9 kPa) and the water flux was measured every 30 min for 1 h ( $J_{0c}$ ). The water flux after 1 h of filtration is labeled as  $J_{1c}$ . The reservoir was emptied and filled with new ultrapure water; the membrane was subsequently exposed to ultrapure water for 2 h without stirring (mimicking the replacement of the water with protein solution for the fouling experiments). The water was stirred and  $J_{2c}$  was calculated after 1 h of filtration. The membrane was cleaned by rinsing twice with DI water and the water flux  $J_{3c}$ —water flux after 1 h of water filtration was obtained. The minimum % RFR and the maximum % FRR were calculated after exposing membranes to aforementioned pressure cycles. A one-way repeated measures ANOVA was conducted to compare the effect of compaction-pressure release cycles on membrane performance after different treatments [Wilks' Lambda = 0.17,  $F(2,7) = 17.19$ ,  $p < 0.05$ , multivariate partial eta squared = 0.83].

*Effect of the length of the fouling period on overall performance.* A second set of control studies was performed to understand the relationship between the length of the fouling cycle and

the overall recovery of performance of the material after fouling. Wet untreated membranes were placed in the stirred cell and the system was filled with DI water. The water was pressurized through the membrane with nitrogen (at 103.4 kPa) for 15 min. The pressure was then reduced to operating pressure (68.9 kPa) and the water flux was measured every 30 min for 1 h. The water flux after 1 h of filtration is labeled as  $J_1$ . Untreated membranes were then exposed to the protein solution for 1 h while protein flux was measured every 30 min ( $J_{2,1}$  is the protein flux after 1 h of protein filtration). After UF of the BSA solution, the membrane was cleaned by rinsing twice with DI water. Water was filtered again at an operating pressure of 68.9 kPa and water flux values were obtained every 30 min for 1 h. The membrane fouling procedure was repeated two more times following the above methodology, the protein flux after the second and third fouling cycle were labeled as  $J_{2,2}$  and  $J_{2,3}$ , respectively. The water flux was once again measured after the third cleaning ( $J_3$  – water flux after 1 h of water filtration). The tendency of the membrane to foul was assessed by calculating the % RFR exhibited by the membrane when exposed to the BSA solution for  $n \geq 3$ . The % FRR was calculated by comparing  $J_1$  and  $J_3$ .

## 2.5 Bacterial assays

*Preparation of bacterial culture.* The bactericidal activity of samples of interest was determined following a modified protocol based on the National Committee for Clinical Laboratory Standards guidelines.<sup>25, 34</sup> *E. coli* (ATCC 25922) and *S. aureus* (ATCC 29213) were obtained from American Type Culture Collection (ATCC, Manassas, VA, USA). Lyophilized bacteria were grown in warm NBM (Oxoid™ OXCM0001B, Fisher Scientific, Fair Lawn, NJ, USA) overnight at 37 °C and 150 rpm. The overnight (OV) culture was diluted 1:1 in 30% v/v

glycerol ( $\geq 99.5\%$ , Sigma-Aldrich, St. Louis, MO, USA) solution and stored at  $-80\text{ }^{\circ}\text{C}$  until use. For each trial, a tube of culture was thawed at room temperature and centrifuged at 4700 rpm for 10 min. The resulting pellet was dispersed in warm NBM and incubated overnight at  $37\text{ }^{\circ}\text{C}$  and 150 rpm. The optical density at 600 nm ( $\text{O.D.}_{600\text{nm}}$ ) of the overnight culture was analyzed via UV-vis spectroscopy (Thermo Scientific, Genesys 20), and the culture was diluted with fresh warm NBM to an  $\text{O.D.}_{600\text{nm}}$  of  $\sim 0.1$  a.u. The culture was incubated at  $37\text{ }^{\circ}\text{C}$  and 100 rpm until it reached the logarithmic growth phase ( $\text{O.D.}_{600\text{nm}} \sim 0.3$  a.u.) prior to exposing the bacterial culture to the sample of interest. All bactericidal activity assays were performed in  $37\text{ }^{\circ}\text{C}$  NBM to closely mimic *in vivo* conditions and to ensure excess nutrients were available to allow for continuous growth of bacterium during the testing period.

*Kill-rate assays.* For biocidal materials and solutions described in Chapters 4-7, bactericidal activity was determined according to a modified protocol by the Clinical and Laboratory Standards Institute (CLSI) protocol.<sup>34</sup> Both liquid (essential oils or aqueous AgNP solutions) and polymeric constructs were assessed via slightly modified kill rate colony counting techniques. For nanoparticles, AgNPs in the desired concentration were added to scintillation vials containing bacterial culture (typically 6 mL of culture per vial, enough for triplicate analyses) and vortexed before placing in 3 separate wells of a TC 12-well plate. For liquid samples (essential oils and octadiene), the monomer was added to vials in the desired concentration containing 6 mL of bacterial solution and vortexed to disperse the monomer. For material testing, polymeric constructs were added to wells in TC 6-well plates and bacterial culture (2 mL) in logarithmic growth phase ( $\text{O.D.}_{600\text{nm}} \sim 0.3$  a.u.) was added to wells containing Ag-loaded polymeric constructs. Identical polymeric constructs without Ag were always tested as controls to rule out any biocidal effect of the polymer itself or its degradation byproducts.

Regardless of whether materials or AgNPs alone were being tested, bacterial culture (2 mL) was placed in empty wells as positive controls.

Well plates containing samples were placed in a static incubator at 37 °C for the duration of the assay. Monitoring of bacterial population, quantified as colony forming units per mL of bacterial culture (CFU mL<sup>-1</sup>), occurred at defined time points (typically 2, 4, and 24 h and, in some cases, 48 h). At each of these times, 100 µL aliquots of culture were removed from each well and placed in 1.5 mL centrifuge tubes (Eppendorf, Hauppauge, NY, USA) each containing 900 µL of sterile 0.85% w/v aqueous NaCl to undergo serial 10-fold dilutions to a factor of 10<sup>6</sup> or 10<sup>7</sup>, as necessary to achieve a countable number of colonies on each plate. A diluted aliquot (50 µL) of each sample was plated twice per well on nutrient agar (NA, Oxoid™ OXCM0003B, Fisher Scientific, Fair Lawn, NJ, USA) TC plates. Plates were incubated overnight in a static incubator at 37 °C, colonies were counted, and CFU mL<sup>-1</sup> values were calculated using equation 2.3.

$$\frac{\text{colony forming units (CFU)}}{\text{volume (mL)}} = \frac{\text{number of colonies}}{\text{dilution factor} \times \text{plated volume (mL)}} \quad (2.3)$$

In cases where no colonies were observed, an undiluted aliquot was plated to confirm no bacteria grew; thereafter, we nominally have 1 CFU mL<sup>-1</sup>, corresponding to the limit of detection (LOD) of the technique, according to the American Society for Testing and Materials (ASTM) and Current Good Manufacturing Practice (CGMP) for the United States Food and Drug Administration (FDA).<sup>35-37</sup> The limit of quantification (LOQ) for this technique is estimated to be 25 CFU mL<sup>-1</sup>.

To determine the log reduction of viable cells in each sample at each time point, the CFU mL<sup>-1</sup> in each well was compared to that of the positive control.<sup>35</sup> The survival fraction (SF) and log reduction in the sample being testing were calculated using equations 2.4 and 2.5.<sup>35</sup>

$$SF = \frac{\frac{\text{CFU after exposure to biocidal agent}}{\text{mL}}}{\frac{\text{CFU control sample}}{\text{mL}}} \quad (2.4)$$

$$\log \text{ reduction} = \log_{10} (SF^{-1}) \quad (2.5)$$

All kill rate assays were completed for  $n \geq 9$  and CFU mL<sup>-1</sup> and log reduction values are expressed as mean  $\pm$  one standard deviation. Statistical analysis was completed using a one-tailed Student's t-test with significance considered at  $p < 0.05$ .

*Zone of inhibition assays.* Zone of inhibition, or Kirby-Bauer, assays were completed for the studies described in Chapter 4 based on established CLSI protocols.<sup>38-40</sup> The *E. coli* OV culture was prepared as described above. The OV culture (O.D.<sub>600 nm</sub>  $\approx$  1 a.u.) was then diluted to O.D.<sub>600 nm</sub> = 0.1 a.u. and grown  $\sim$ 2 h until population reached  $\sim 10^9$  CFUs mL<sup>-1</sup> as seen by O.D.<sub>600 nm</sub> = 0.3 a.u. Autoclaved cotton swabs were used to obtain culture and spread onto Mueller-Hinton (MH) agar plates (Hardy Diagnostics, Santa Maria, CA, USA). Plates were rotated 60° between swabs for a total of three swabs for even coverage. Plates were allowed to dry for 3-5 min before Antibiotic BD BBL™ Sensi-Disc Susceptibility Test Gentamicin Discs (10  $\mu$ g, Fisher Scientific, Fair Lawn, NJ, USA) were placed at the center of each MH agar plate as controls. Test samples were cut approximately to size ( $\sim$ 6 mm diameter) of the control discs and placed on MH agar plates  $\sim$ 20 cm apart. Plates were incubated a full 36 h, with visual assessment made at 18, 24, and 36 h to determine inhibition zone diameters.

*Bacterial attachment and growth assays.* To determine the propensity for *E. coli* and *S. aureus* to attach to each sample surface, bacterial attachment and growth assays were performed. In addition to ppCin and H<sub>2</sub>O<sub>(v)</sub> plasma treated ppCin films, ppOct films were used as a hydrophobic control, and glass slides were used as positive, hydrophilic, controls. Films were placed in 12-well TC plates (VWR, Arlington Heights, IL, USA). and 2 mL of prepared bacterial



culture were added to each well. After 24 h of incubation at 37 °C, NBM was removed and each film was rinsed 3 times with sterile 0.85% w/v NaCl without being allowed to dry out. Propidium iodide (PI, 1.0 mg mL<sup>-1</sup> in water) and SYTO9 (5 mM in DMSO) fluorescence stains were purchased from Life Technologies Corporation (Carlsbad, CA). A working solution of stain was prepared with concentrations of 3 μM PI and 0.5 μM SYTO9; this solution was refrigerated between uses for a maximum of 1 month. Each sample was covered with 500 μL of staining solution containing PI and SYTO9 and allowed to incubate protected from light for 20 min before stain was removed and samples were rinsed 3 times with Millipore water. Films were air dried covered from light. Images were obtained using an Olympus IX73 fluorescence microscope and processed using Olympus CellSens software (v1.14). PI fluoresces red, with excitation and emission wavelengths of 543 nm and 617 nm, respectively, whereas SYTO9 appears green, with excitation and emission wavelengths of 488 nm and 500 nm, respectively. The red-fluorescent PI stain intercalates with DNA and cannot permeate intact cell membranes; thus, PI only stains non-viable bacterial cells. In contrast, green-fluorescent SYTO9 enters both viable and non-viable cells. Images displayed herein depict signals from PI and SYTO9 overlaid to observe both viable and nonviable bacteria. Yellow signal sometimes arises when red and green filters overlap because SYTO9 was not completely displaced from the cell by PI, thus both stains remain in the cell, and we may assume the cells are nonviable.<sup>41</sup> Minimal processing was performed when necessary to eliminate background auto-fluorescence of the film, likely arising from unsaturated carbon bonds within the plasma polymer.<sup>42</sup>

To quantify bacterial attachment on opaque materials (i.e., microporous membranes), *E. coli* culture was placed on the material surface and allowed to incubate in the same manner as described above. After the specified time period, however, the membranes were sonicated

(30 min, VWR® Ultrasonic Cleaner, 117 V, 60 Hz) in fresh NBM. An aliquot of the sonicated liquid then underwent serial dilutions, plating, incubation, and colony counting, as described above.

*Biofilm formation assays.* The use of viability assays in combination with biofilm formation assays allow for a more comprehensive assessment of antibiofouling behavior. Biofilm formation assays commenced in the same manner as the bacterial attachment assays described above, but the incubation period was extended to 5 d to allow for observation of biofilm growth. Warm NBM was replaced each day until the end of the assay, after which NBM was removed from each sample well, and slides were rinsed 3 times with 2 mL of physiological 0.85% w/v saline solution, without being allowed to dry out. Crystal violet stain (750  $\mu$ L, 1% aqueous solution, Sigma-Aldrich, St. Louis, MO, USA, diluted 1:10 in ultrapure water) was added to each well. After well plates were incubated at room temperature for 20 min, the stain was removed from each well, and samples were rinsed 3 times with copious amounts of Millipore water (taking care not to disturb film integrity). Finally, samples were dried at room temperature, and bright field images were obtained using an Olympus IX73 fluorescence microscope and processed using Olympus CellSens software (v1.14).

ImageJ image analysis software (v1.6; National Institutes of Health, USA) was used to assess extent of biofilm surface coverage for control samples and films.<sup>25, 43</sup> Bright field images were converted to 8-bit and binary format. The threshold was adjusted so that each pixel of the converted image accurately represented the original image. A minimum of 9 images were analyzed per sample type and the mean  $\pm$  standard deviation is reported.

## 2.6 Analysis of blood coagulation dynamics

*Thromboelastography (TEG) analyses.* Methodologies described in this section correspond to data presented in Chapter 8. Here, select materials were interfaced with canine blood plasma and a commercial thromboelastography instrument [TEG® 5000 Thromboelastograph® Hemostasis System (Haemonetics Corporation)] was used to measure coagulation dynamics. Both standard consumable cups and cups designed with modified dimensions based on previous work in our group were used.<sup>18</sup> Canine blood plasma was harvested from citrated canine whole blood following centrifugation at  $4500 \times g$  for 10 min. Harvested plasma was distributed into 2 mL cryogenic vials in 700  $\mu\text{L}$  aliquots. Aliquots were stored in a  $-80\text{ }^\circ\text{C}$  freezer until analysis, for no longer than 1 week.

Porogen leached scaffolds were quartered by freeze fracturing (Section 2.3), and placed into 3D-printed acrylonitrile butadiene styrene (ABS) TEG cups. TEG experiments were completed within 24 h of modification. One vial of plasma was prepared for each run by thawing for 1 min in a  $37\text{ }^\circ\text{C}$  water bath with gentle shaking. Each vial was kept on ice until use ( $<10$  min). The standard disposable TEG cap with pin was loaded into the instrument and either the standard or modified cup was loaded into the instrument base. For modified cups, a piece of machined Teflon® was placed under the cup to ensure a flush fit with the instrument. 10  $\mu\text{L}$  of tissue factor solution [TriniCLOT PT Excel Reagent (TCoag) and DI water] were added to the cup, followed by 330  $\mu\text{L}$  of thawed plasma, to give a final 1% w/v TCoag concentration. For experiments involving a polymeric construct (i.e., scaffold, membrane), the material was immediately added to the plasma mixture. The cup contents were allowed to equilibrate to the temperature of the TEG ( $37\text{ }^\circ\text{C}$ ,  $\sim 2$  min), and 20  $\mu\text{L}$  of  $\text{CaCl}_2$  (0.2 M, Haemonetics Corp.) were added and quickly mixed via pipette to initiate coagulation. The TEG run was initiated and

allowed to run until the maximum amplitude (MA) was reached. Data reported are the mean  $\pm$  standard deviation for  $n \geq 3$  replicate samples.

Data that can be obtained from TEG analyses are thoroughly discussed elsewhere.<sup>44-47</sup> In short, data are output as standard TEG traces (amplitude vs time) and velocity curves, corresponding to the first derivative of the TEG trace. From the standard trace, one can obtain reaction time (R), MA, and time to MA (TMA). Velocity curves provide additional clotting information including maximum rate of thrombus generation (MRTG, the maximum velocity of clot growth), the time to MRTG (TMRTG, the time elapsed before maximum clot growth rate is reached), and total thrombus generation (TTG, the total area under the velocity curve, providing a measure of total clot growth).

## REFERENCES

1. Pegalajar-Jurado, A.; Mann, M. N.; Maynard, M. R.; Fisher, E. R., Hydrophilic modification of polysulfone ultrafiltration membranes by low temperature water vapor plasma treatment to enhance performance. *Plasma Process. Polym.* **2016**, (13), 598.
2. Mann, M. N.; Neufeld, B. H.; Hawker, M. J.; Pegalajar-Jurado, A.; Paricio, L. N.; Reynolds, M. M.; Fisher, E. R., Plasma-modified nitric oxide-releasing polymer films exhibit time-delayed 8-log reduction in growth of bacteria. *Biointerphases* **2016**, *11* (3), 11.
3. Mann, M. N.; Fisher, E. R., Investigation of antibacterial 1, 8-cineole-derived thin films formed via plasma-enhanced chemical vapor deposition. *ACS Appl Mater Interfaces* **2017**, *9* (42), 36548-36560.
4. Steen, M. L.; Jordan, A. C.; Fisher, E. R., Hydrophilic modification of polymeric membranes by low temperature H<sub>2</sub>O plasma treatment. *J. Membr. Sci.* **2002**, *204*, 341-357.
5. Hawker, M. J.; Pegalajar-Jurado, A.; Fisher, E. R., Innovative applications of surface wettability measurements for plasma modified three-dimensional porous polymeric materials: A review. *Plasma Proc. Polym.* **2015**, *12*
6. Fisher, E. R., Challenges in the characterization of plasma-processed three-dimensional polymeric scaffolds for biomedical applications. *ACS Appl Mater Interfaces* **2013**, *5* (19), 9312-9321.
7. Hawker, M. J.; Pegalajar-Jurado, A.; Hicks, K. I.; Shearer, J. C.; Fisher, E. R., Allylamine and allyl alcohol plasma copolymerization: synthesis of customizable biologically-reactive three-dimensional scaffolds. *Plasma Process. Polym.* **2015**, *12* (12), 1435-1450.
8. Hawker, M. J.; Pegalajar-Jurado, A.; Fisher, E. R., Conformal encapsulation of three-dimensional, bioresorbable polymeric scaffolds using plasma-enhanced chemical vapor deposition. *Langmuir* **2014**, *30* (41), 12328-12336.
9. Liu, S.; Zhao, J.; Ruan, H.; Wang, W.; Wu, T.; Cui, W.; Fan, C., Antibacterial and anti-adhesion effects of the silver nanoparticles-loaded poly(L-lactide) fibrous membrane. *Mater. Sci. Eng., C* **2013**, *33* (3), 1176-1182.
10. Sheikh, F. A.; Barakat, N. A. M.; Kanjwal, M. A.; Jeon, S.-H.; Kang, H.-S.; Kim, H.-Y., Self synthesize of silver nanoparticles in/on polyurethane nanofibers: Nano-biotechnological approach. *J. Appl. Polym. Sci.* **2010**, *115* (6), 3189-3198.
11. Sumitha, M. S.; Shalumon, K. T.; Sreeja, V. N.; Jayakumar, R.; Nair, S. V.; Menon, D., Biocompatible and antibacterial nanofibrous poly( $\epsilon$ -caprolactone)-nanosilver composite scaffolds for tissue engineering applications. *J. Macromol. Sci., Pure Appl. Chem.* **2012**, *49* (2), 131-138.
12. Cao, X.; Tang, M.; Liu, F.; Nie, Y.; Zhao, C., Immobilization of silver nanoparticles onto sulfonated polyethersulfone membranes as antibacterial materials. *Colloids Surf B Biointerfaces* **2010**, *81* (2), 555-562.
13. Fortunati, E.; Mattioli, S.; Visai, L.; Imbriani, M.; Fierro, J. L. G.; Kenny, J. M.; Armentano, I., Combined effects of Ag nanoparticles and oxygen plasma treatment on PLGA morphological, chemical, and antibacterial properties. *Biomacromolecules* **2013**, *14* (3), 626-636.
14. Islam, M. S.; Larimer, C.; Ojha, A.; Nettleship, I., Antimycobacterial efficacy of silver nanoparticles as deposited on porous membrane filters. *Mater. Sci. Eng., C* **2013**, *33* (8), 4575-4581.
15. Hart, T. W., Some observations concerning the S-nitroso and S-phenylsulphonyl derivatives of L-cysteine and glutathione. *Tetrahedron Letters* **1985**, *26* (16), 2013-2016.
16. Damodaran, V. B.; Joslin, J. M.; Wold, K. A.; Lantvit, S. M.; Reynolds, M. M., S-nitrosated biodegradable polymers for biomedical applications: synthesis, characterization and impact of thiol structure on the physicochemical properties. *J. Mater. Chem.* **2012**, *22* (13), 5990-6001.
17. Kuo, W. N.; Kocis, J. M.; Nibbs, J., Nitrosation of cysteine and reduced glutathione by nitrite at physiological pH. *Frontiers in Bioscience* **2003**, *8*, A62-A69.

18. Hawker, M. J.; Olver, C. S.; Fisher, E. R., Modification of a commercial thromboelastography instrument to measure coagulation dynamics with three-dimensional biomaterials. *Biointerphases* **2016**, *11* (2), 029602.
19. Pegalajar-Jurado, A.; Joslin, J. M.; Hawker, M. J.; Reynolds, M. M.; Fisher, E. R., Creation of hydrophilic nitric oxide releasing polymers via plasma surface modification. *ACS Appl. Mater. Interfaces* **2014**, *6* (15), 12307-12320.
20. Tompkins, B. D.; Dennison, J. M.; Fisher, E. R., H<sub>2</sub>O plasma modification of track-etched polymer membranes for increased wettability and improved performance. *J. Membr. Sci.* **2013**, *428*, 576-588.
21. Wavhal, D. S.; Kull, K. R.; Steen, M. L.; Fisher, E. R., Hydrophilic surface modification of microporous polymer membranes using a variety of low-temperature plasma treatments. *Mat. Res. Soc. Symp. Proc.* **2003**, *752*, 53-58
22. Wavhal, D. S.; Fisher, E. R., Membrane surface modification by plasma-induced polymerization of acrylamide for improved surface properties and reduced protein fouling. *Langmuir* **2003**, *19* (1), 79-85.
23. Wavhal, D. S.; Fisher, E. R., Modification of polysulfone ultrafiltration membrane by CO<sub>2</sub> plasma treatment. *Desalination* **2005**, *172*, 189-205.
24. DSA4 Software for Drop Shape Analysis: User Manual. Krüss GmbH: Hamburg, 2004-2014; p 49.
25. Pegalajar-Jurado, A.; Easton, C. D.; Styan, K. E.; McArthur, S. L., Antibacterial activity studies of plasma polymerised cineole films. *J. Mater. Chem. B* **2014**.
26. Bates, J. N., Nitric oxide measurement by chemiluminescence detection. *Neuroprotocols* **1992**, *1*, 141-149.
27. Zeng, F.; Hou, C.; Wu, S.; Liu, X.; Tong, Z.; Yu, S., Silver nanoparticles directly formed on natural macroporous matrix and their anti-microbial activities. *Nanotechnology* **2007**, *18* (5), 055605.
28. D'Britto, V.; Kapse, H.; Babrekar, H.; Prabhune, A. A.; Bhoraskar, S. V.; Premnath, V.; Prasad, B. L. V., Silver nanoparticle studded porous polyethylene scaffolds: bacteria struggle to grow on them while mammalian cells thrive. *Nanoscale* **2011**, *3* (7), 2957.
29. Cavanagh, M. H.; Burrell, R. E.; Nadworny, P. L., Evaluating antimicrobial efficacy of new commercially available silver dressings. *Int Wound J* **2010**, *7* (5), 394-405.
30. McArthur, S. L., Applications of XPS in bioengineering. *Surf. Interface Anal.* **2006**, *38* (11), 1380-1385.
31. Fitzpatrick, H.; Luckham, P.; Eriksen, S.; Hammond, K., Use of X-ray photoelectron spectroscopy to study protein adsorption to mica surfaces. *J. Colloid Interface Sci.* **1992**, *149* (1), 1-9.
32. McArthur, S. L.; McLean, K. M.; Kingshott, P.; St John, H. A.; Chatelier, R. C.; Griesser, H. J., Effect of polysaccharide structure on protein adsorption. *Colloids Surf., B* **2000**, *17* (1), 37-48.
33. Paynter, R. W., Ratner, B. D., *The Study of Interfacial Proteins and Biomolecules by X-ray Photoelectron Spectroscopy*. Plenum Press: New York, 1985.
34. Barry, A. L.; Craig, W. A.; Nadler, H.; Reller, L. B.; Sanders, C. C.; Swenson, J. M., *Methods for Determining Bactericidal Activity of Antimicrobial Agents; Approved Guideline*. 1999; Vol. 19.
35. Hamilton, M. A., *The Log Reduction (LR) Measure of Disinfectant Efficacy*. MSU Center for Biofilm Engineering: Montana State University, 2010.
36. Sutton, S., Accuracy of plate counts. *Journal of Validation Technology* **2011**, *17*, 42-46.
37. Sutton, S., The limitations of CFU: compliance to CGMP requires good science. *Journal of GXP Compliance* **2012**, *16* (1), 74.
38. Reller, L. B.; Weinstein, M.; Jorgensen, J. H.; Ferraro, M. J., Antimicrobial susceptibility testing: A review of general principles and contemporary practices. *Clin Infect Dis* **2009**, *49* (11), 1749-1755.
39. Bauer, A.; Kirby, W.; Sherris, J. C.; Turck, M., Antibiotic susceptibility testing by a standardized single disk method. *Am J Clin Pathol* **1966**, *45* (4), 493.
40. Institute, C. L. S., Performance standards for antimicrobial disk susceptibility tests. Clinical and Laboratory Standards Institute: Wayne, PA, 2009.

41. Stiefel, P.; Schmidt-Emrich, S.; Maniura-Weber, K.; Ren, Q., Critical aspects of using bacterial cell viability assays with the fluorophores SYTO9 and propidium iodide. *BMC Microbiol.* **2015**, *15*, 9.
42. Sauer, M.; Hofkens, J., *Handbook of Fluorescence Spectroscopy and Imaging: from Ensemble to Single Molecules*. John Wiley & Sons: 2010.
43. Pasmore, M.; Todd, P.; Smith, S.; Baker, D.; Silverstein, J.; Coons, D.; Bowman, C. N., Effects of ultrafiltration membrane surface properties on *Pseudomonas aeruginosa* biofilm initiation for the purpose of reducing biofouling. *J. Membr. Sci.* **2001**, *194* (1), 15-32.
44. Bolliger, D.; Seeberger, M. D.; Tanaka, K. A., Principles and practice of thromboelastography in clinical coagulation management and transfusion practice. *Transfusion medicine reviews* **2012**, *26* (1), 1-13.
45. Luddington, R., Thrombelastography/thromboelastometry. *International Journal of Laboratory Hematology* **2005**, *27* (2), 81-90.
46. Nielsen, V. G., Beyond cell based models of coagulation: Analyses of coagulation with clot “lifespan” resistance–time relationships. *Thrombosis research* **2008**, *122* (2), 145-152.
47. Ellis, T. C.; Nielsen, V. G.; Marques, M. B.; Kirklin, J. K., Thrombelastographic measures of clot propagation: a comparison of alpha with the maximum rate of thrombus generation. *Blood coagulation & fibrinolysis* **2007**, *18* (1), 45-48.

## CHAPTER 3

### HYDROPHILIC MODIFICATION OF ULTRAFILTRATION MEMBRANES BY LOW TEMPERATURE H<sub>2</sub>O<sub>(v)</sub> PLASMA TREATMENT TO ENHANCE PERFORMANCE

This chapter details the water plasma surface modification of commercial ultrafiltration membranes to enhance surface wettability and reduce protein fouling for improved filtration performance. A portion of this chapter is based on work published in *Plasma Processes and Polymers* by Adoracion Pegalajar-Jurado, Michelle N. Mann, Matthew R. Maynard, and Ellen R. Fisher and is reproduced with permission from *Plasma Process. Polym.*, 13: 598-610, Wiley 2016 (license number 4380811204591). This work was supported by the National Science Foundation (CHE-1152963) and the Camille and Henry Dreyfus Foundation. I would like to thank Dr. Adoracion Pegalajar-Jurado for contributions to this work, specifically in mentorship during training and data collection and Mr. Matthew R. Maynard for assistance with data collection. I also want to thank Dr. Patrick McCurdy for assistance with SEM and XPS analyses and Dr. Brendan Tompkins and Dr. Dattatray S. Wavhal for assistance with the experimental design and preliminary work for filtration and fouling experiments.

#### **3.1 Introduction**

Ultrafiltration (UF) technology has expanded significantly since the 1960s, finding widespread use in applications requiring separations including medical, dairy, chemical recovery, and water treatment industries.<sup>1-3</sup> In each of these applications, UF membranes are exposed to different foulants including colloidal particles, biological specimens, and organic compounds, contributing to a reduction in membrane performance.<sup>4</sup> Membrane biofouling



results in part from protein macromolecules present in the liquid streams being filtered, and is enhanced by hydrophobic interactions between the surface and protein molecules,<sup>5-6</sup> ultimately leading to fouling that cannot be reversed by mild cleaning (e.g., rinsing with water). Absorbed protein must typically be removed using caustic agents, a difficult procedure that requires shutdown of the filtration unit for extended periods of time and can cause extensive damage to the membranes. Ideally, the majority of foulants would be removed by a hydraulic backwash procedure, reducing or eliminating the need for cleaning using caustic chemicals. Over longer periods of operation, however, foulants can accumulate, thereby requiring higher transmembrane pressure to achieve effective filtration.<sup>2, 4, 7</sup> Thus, employing hydrophilic polymeric membranes could enhance membrane performance and allow for partial fouling reversibility, ultimately improving the applicability and extending the lifetime of membrane-based devices.

LTPs can be used to modify the surface properties of polymeric membranes via film deposition, functional group implantation, or plasma graft copolymerization.<sup>1, 8-16</sup> Some limitations of plasma-based techniques include possible damage to the membrane by interactions with plasma species, non-uniform plasma treatment across the thickness of the membrane, as well as the potential for short-lived modification depending on the treatment parameters and material properties. Indeed, plasma-induced damage such as mass loss and/or pore size enlargement or reduction has been reported.<sup>8-13</sup> For example, polypropylene microfiltration membranes were modified using NH<sub>3</sub>, air, and CO<sub>2</sub> rf plasmas to enhance surface wettability, yet pore enlargement was observed as a result of plasma-induced damage of the membranes.<sup>8-10</sup> Despite the possible downsides, there are significant advantages in using LTPs to modify polymeric membranes. Indeed, both wettability and antifouling properties of microfiltration and UF membranes have been enhanced by plasma treatment,<sup>1, 15, 17</sup> with the primary key being

appropriate selection of plasma parameters and feed gases so as to minimize damage and maintain membrane structure.

Polysulfone (PSf) is widely used as an UF membrane material as it has good thermal and chemical stabilities.<sup>18</sup> Despite these desirable properties, PSf UF membranes require preconditioning for applications in aqueous-based separations because of their hydrophobic nature,<sup>19</sup> and they also tend to suffer from irreversible fouling.<sup>20</sup> Gancarz and coworkers treated PSf UF membranes in microwave plasmas containing N<sub>2</sub>, NH<sub>3</sub>, and CO<sub>2</sub> and demonstrated an improvement in membrane wettability, but at the expense of pore size enlargement.<sup>11-13</sup> Another study modified PSf UF membranes with an rf O<sub>2</sub> plasma, resulting in WCA ~30° after a 120 s treatment, but membrane morphology after plasma treatment was not assessed.<sup>21</sup> Thus, it is not clear whether the modification was the result of chemical or morphological changes. We previously reported inductively coupled rf water vapor [H<sub>2</sub>O<sub>(v)</sub>] plasma treatment of sub-micron PSf membranes.<sup>1, 15-16</sup> In these studies, the membrane was placed perpendicular to the gas flow, ~9 cm downstream from the most intense region of the plasma glow to achieve gas flow through the membrane and minimize membrane damage. Complete modification of the entire cross-section of the membrane as well as the downstream exterior membrane surface was observed, indicating the plasma penetrates the thickness of the membrane. Although minimal structural damage was observed in this system for short treatment times, evidence of pore enlargement for microporous membranes was reported. Extending this work, Wavhal *et al.* reported the modification of asymmetric UF PSf membranes via rf CO<sub>2</sub> plasma treatment using a similar membrane configuration.<sup>17</sup> In this study, however, the membranes were placed 20 cm downstream from the most intense region of the plasma glow. This extreme downstream placement could further limit damage to the delicate UF PSf materials, but it presents a more

challenging situation as surface modifying plasma species may recombine prior to reaching the membrane, decreasing modification efficiency. Although penetration of the plasma through the UF membrane cross-section is more difficult in this configuration, these studies demonstrated successful modification across the membrane thickness with no membrane damage, indicating plasma treatment is a promising route for modifying UF membranes.

In the present work, we have extended  $\text{H}_2\text{O}_{(v)}$  plasma treatments to asymmetric UF PSf membranes and explored their anti-fouling properties. Building off the work of Wavhal *et al.*, we placed the membranes 20 cm downstream from the plasma glow. Changes in surface chemistry are measured using XPS and FTIR, whereas changes in surface wettability are described by WCA goniometry data. Variations in the physical structure of the membranes after plasma treatment were analyzed by % mass loss and SEM images. The fouling properties of both untreated and treated membranes were studied using BSA as a model protein. The tendency of the membrane to foul (relative flux reduction, RFR), and the ability of the membrane to recover after fouling (flux recovery ratio, FRR) were assessed, taking into consideration the effect of the compaction-pressure release cycles on membrane performance in the absence of foulants. Overall, we illustrate that  $\text{H}_2\text{O}_{(v)}$  plasma treatments can be used to impart lasting (>2 months) functionalization of the UF PSf membrane surfaces with minimal damage, enhancing the global performance of the membranes.

## **3.2 Results**

### **3.2.1. Surface chemistry**

XPS was used to assess changes in the surface chemistry of the PSf membranes after plasma modification. Atomic compositions and binding environments for UPS-0, UPS-2, and UPS-5 are

summarized in Table 3.1. To verify the penetration of the plasma throughout the cross-section of the UF membrane, both sides of the membrane were analyzed. For the open side of the membrane (oriented upstream and facing the plasma glow), the O content increases from ~15% for the untreated membrane (UPS-0) to ~25% and 28% for the 2 min and 5 min treatments, respectively. Focusing on the tight side (oriented downstream), the O concentration increases from ~14% for UPS-0 to ~19% for UPS-2, and reaches ~24% for UPS-5. For both sides, the S content varies only slightly from ~3% for UPS-0 to ~2.5% for UPS-2, and <2.5% for UPS-5. One striking difference in the modification of the open and tight side of the membrane is that N moieties are incorporated on the open side only (<1%).

High-resolution  $C_{1s}$  XPS spectra were collected to evaluate the introduction of functional groups after plasma treatment. Representative high-resolution  $C_{1s}$  spectra of UPS-0 and UPS-2 are shown in Fig. 3.1. The  $C_{1s}$  spectra of UPS-0 could be deconstructed into four peaks (Fig. 3.1a and b) based on the reference measurements of Beamson and Briggs.<sup>22</sup> The primary peaks in the  $C_{1s}$  envelopes are at (i) BE ~284.7 eV, corresponding to carbon atoms involved in C–C/C–H bonds; (ii) at BE ~285.3 eV, corresponding to carbon atoms bonded to sulfur (C–SO<sub>2</sub>); and (iii) at BE ~286.34 eV corresponding to carbon atoms in ether groups (C–O–R).

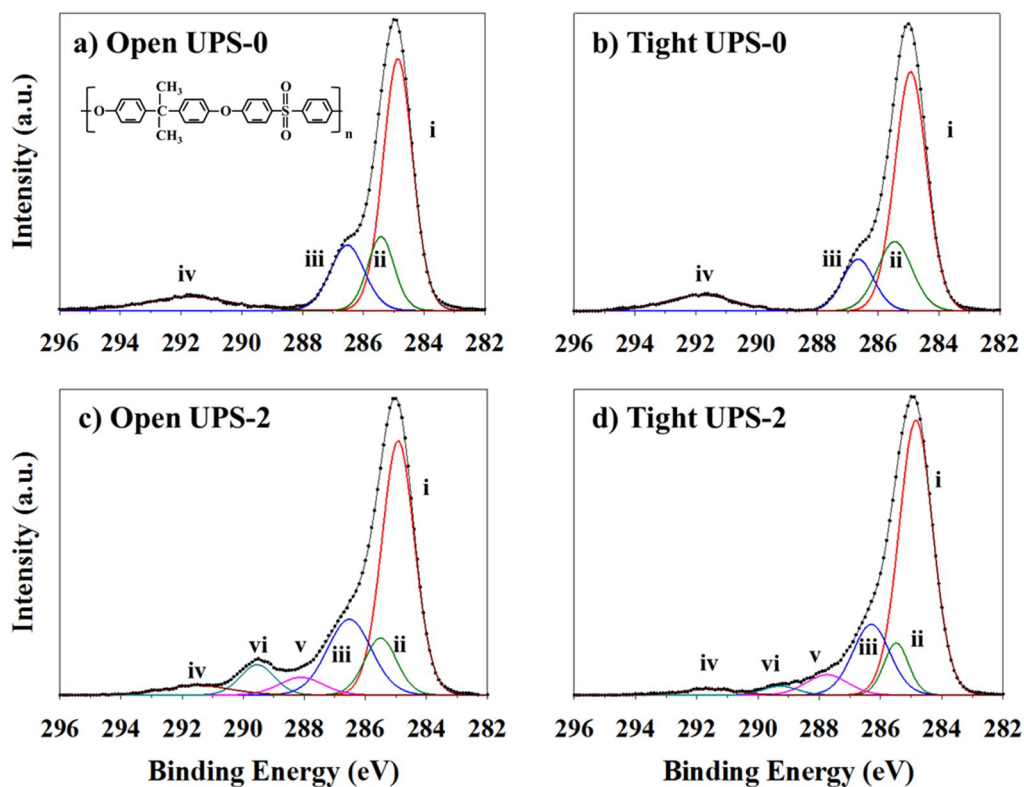
In addition, a peak arising from the  $\pi$ - $\pi^*$  shake-up satellite at ~291.6 eV (iv) establishes the aromaticity of the PSf polymer.<sup>17, 22-23</sup> High-resolution  $C_{1s}$  spectra of both sides of a H<sub>2</sub>O(v) plasma treated membrane (UPS-2) are shown in Fig. 3.1c and d. Deconstructing the spectra of the treated membrane reveals the presence of two new components:  $C_{1s}$  (v) at ~287.5 eV corresponds to carbonyl groups (C=O/O–C–O), and  $C_{1s}$  (vi) at ~289.5 eV is attributed to carboxylic functionality (CCOO). In plasma-modified membranes, the  $C_{1s}$  (ii) peak likely

**Table 3.1.** XPS elemental composition and binding environment percentages for untreated and treated membranes.<sup>a</sup>

Plasma treatment		% C	% O	% S	C-C/ C-H	C-SO <sub>2</sub> / <u>CCOO</u> <sup>b</sup>	C-OR/ C-OH	C=O/ O-C-O	<u>CCOO</u>	$\pi$ - $\pi^*$
Membrane Side										
UPS-0	Tight	83.0 (0.1)	13.7 (0.1)	3.4 (0.1)	60.4 (1.1)	19.4 (0.5)	12.1 (0.6)	-	-	8.2 (0.5)
UPS-0	Open	81.7 (0.1)	15.2 (0.1)	3.1 (0.1)	56.7 (1.6)	17.1 (1.5)	18.0 (1.3)	-	-	8.2 (1.0)
UPS-2	Tight	78.1 (0.2)	19.4 (0.3)	2.5 (0.1)	61.8 (1.3)	8.2 (0.7)	20.5 (1.8)	4.9 (0.6)	2.0 (0.1)	2.5 (0.4)
UPS-2	Open	76.1 (0.4)	25.9 (0.4)	2.5 (0.1)	54.3 (1.6)	11.1 (0.4)	19.1 (1.6)	5.1 (0.2)	6.1 (0.5)	4.4 (0.3)
UPS-5	Tight	74.5 (0.6)	23.9 (0.7)	1.6 (0.1)	-	-	-	-	-	-
UPS-5	Open	69.6 (0.6)	27.9 (0.6)	2.5 (0.1)	-	-	-	-	-	-

<sup>a</sup>As determined from deconstructed C<sub>1s</sub> XPS spectra. All analyses were performed for n = 9; the mean ± standard deviation (in parentheses) is reported.

<sup>b</sup>CCOO only present in H<sub>2</sub>O<sub>(v)</sub> plasma treated polysulfone membranes.

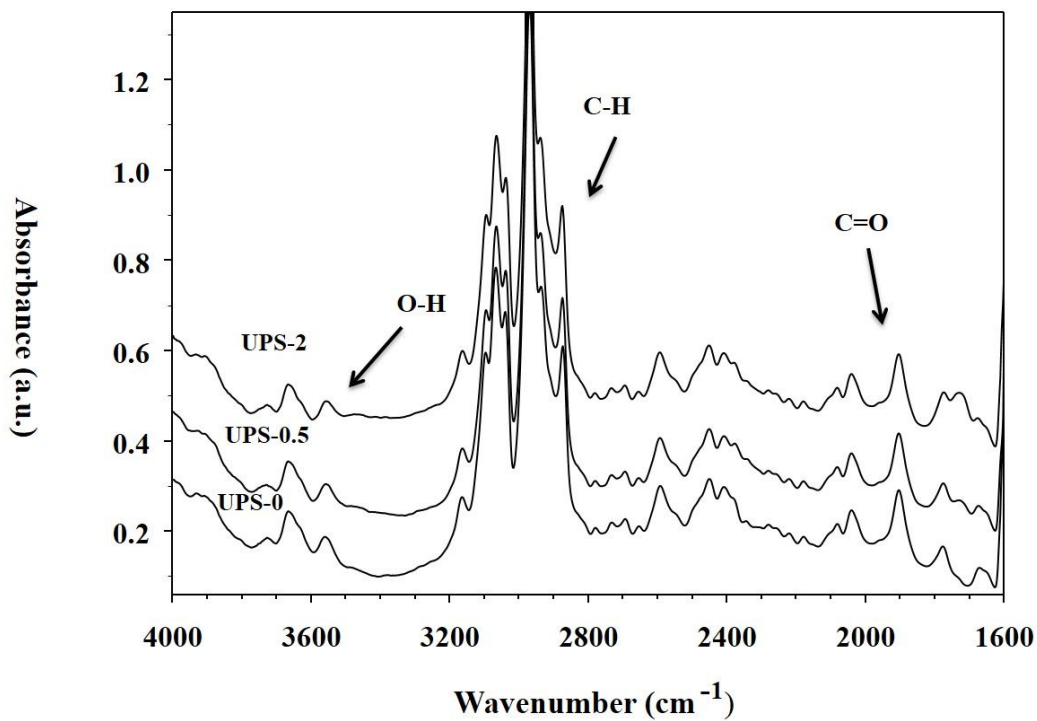


**Figure 3.1.** Representative high-resolution  $C_{1s}$  XPS spectra and fits for (a) UPS-0 open side, (b) UPS-0 tight side, (c) UPS-2 open side and (d) UPS-2 tight side. Deconstructed fits represent (i) C–C/C–H; (ii) C–SO<sub>2</sub> (UPS-0) or C–SO<sub>2</sub>,  $\underline{C}$ –COO (UPS-2); (iii) C–O–R/C–OH; (iv)  $\pi \rightarrow \pi^*$ ; (v) C=O/O–C–O; and (vi)  $\underline{C}\underline{C}\underline{O}\underline{O}$ .

contains contributions from both carbon atoms in C–SO<sub>2</sub> and from carboxyl secondary shift (C–COO). Both sides of the UPS-2 membranes are similarly modified as shown by the relative areas of the different components of the C<sub>1s</sub> envelope (Table 3.1). Comparing UPS-0 with UPS-2, the contribution from C–O–R/C–OH functionality increases after treatment (Fig. 3.1, Table 3.1), indicating the presence of species containing C–O bonds (e.g., alcohol or ether groups) after plasma treatment. The surfaces of plasma-modified membranes also contain additional oxidized carbon species, including C=O/O–C–O and C–COO. Notably, the contribution from the  $\pi$ - $\pi^*$  satellite peak is smaller in the spectra of plasma-treated membranes, likely as a result of graphitization of the polymer surface arising from dehydrogenation of the phenyl ring and disruption in the aromaticity.<sup>24</sup>

In previous work, we reported that the permanency of the surface modification is related to chemical changes in UPS membranes as a result of plasma treatment. These changes could arise from the incorporation of new, more hydrophilic functional groups (C=O, C–O, OH, and O–C=O) that are covalently bound to the polymeric backbone.<sup>1</sup> To corroborate the implantation of these functional groups (such as C=O and OH) after treatment, we performed FTIR analysis on UPS-0, UPS-0.5, and UPS-2 (Fig. 3.2).

A broad absorption band centered at 1733 cm<sup>-1</sup> is apparent in spectra of all plasma-modified membranes and increases in intensity with increasing treatment time (for times  $\geq 3$  min). This relatively broad absorption band indicates the presence of carbon-oxygen double bond-containing species (i.e., aldehyde, ketone, acid, and ester groups), although we cannot distinguish between these functional groups using FTIR alone. Furthermore, the absorption peaks in the 3300 to 3500 cm<sup>-1</sup> region verify the presence of hydroxyl groups.<sup>25</sup> These results, in conjunction with XPS data corroborate the implantation of both C=O and OH functional groups.



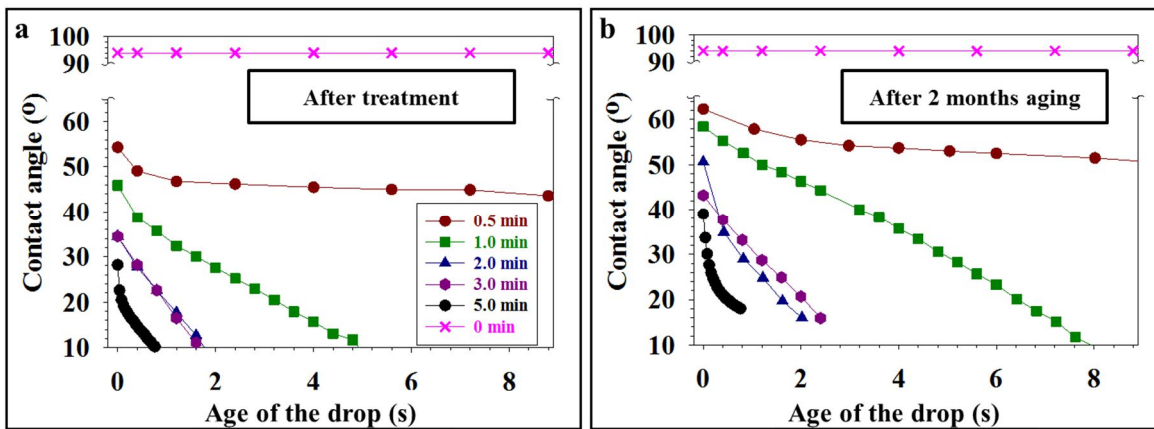
**Figure 3.2.** Representative FTIR spectra for UPS-0, UPS-0.5 and UPS-2 membranes. Functional groups observed include carbonyl (C=O, 1733 cm<sup>-1</sup>), hydrocarbon (C-H, 3100-3000 cm<sup>-1</sup>) and hydroxyl (O-H, 3500-3300 cm<sup>-1</sup>), as labeled.



### 3.2.2. Changes in surface wettability and architecture

The average  $\theta_{\text{static}}$  of the open and tight sides of UPS-0 are  $\sim 85^\circ$  and  $\sim 94^\circ$ , respectively, and the values do not change significantly over the data collection time (10 s). The open sides of all plasma-treated membranes (regardless of treatment time) are hydrophilic, whereby water drops disappeared in significantly less than a second, limiting the ability to perform static or even time-resolved (dynamic) measurements. The tight sides of all treated membranes are also more hydrophilic than UPS-0 but slightly less hydrophilic than the open sides. In these measurements, the drop never reaches a static plateau that would allow measurement of a  $\theta_{\text{static}}$ . Nevertheless, we were able to collect dynamic WCA data (Fig. 3.3a) on these surfaces. The water drop on the tight sides of UPS-2, UPS-3, and UPS-5 membranes disappears (i.e.,  $\theta \leq 20^\circ$ ) in  $\leq 2$  s, demonstrating improved surface wettability in comparison to UPS-0. Based on the established criterion, UPS-2, UPS-3, and UPS-5 are considered “completely wettable” materials in this context. The water drop disappears in  $\leq 6$  s for UPS-1 (Fig. 3.1a) and does not disappear for UPS-0.5, suggesting that, although those membranes do not meet the “completely wettable” criterion established in this chapter, they are significantly more hydrophilic than UPS-0. Note that these measurements were made on the downstream side of the membranes, further evidence that the membrane treatment is penetrating through the thickness of the membrane, even with the more remote (20 cm downstream) placement of the sample.

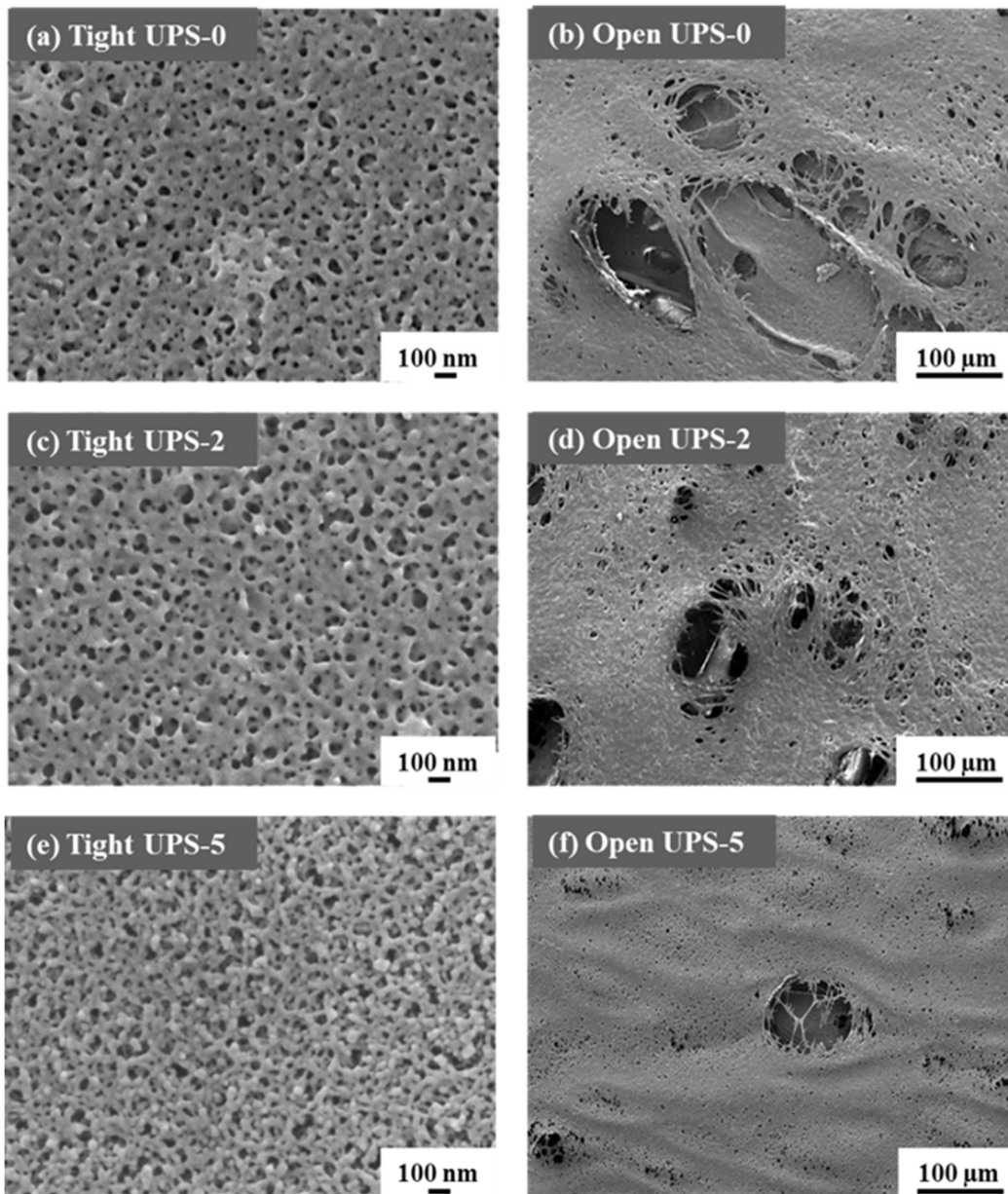
Although enhancing UPS membrane wettability is necessary to improve filtration performance, the stability of the modification over time is critical in terms of product shelf life. To study the effect of membrane aging on wettability, modified membranes were stored, covered, under ambient laboratory conditions for 2 months. No chemical or physical treatment



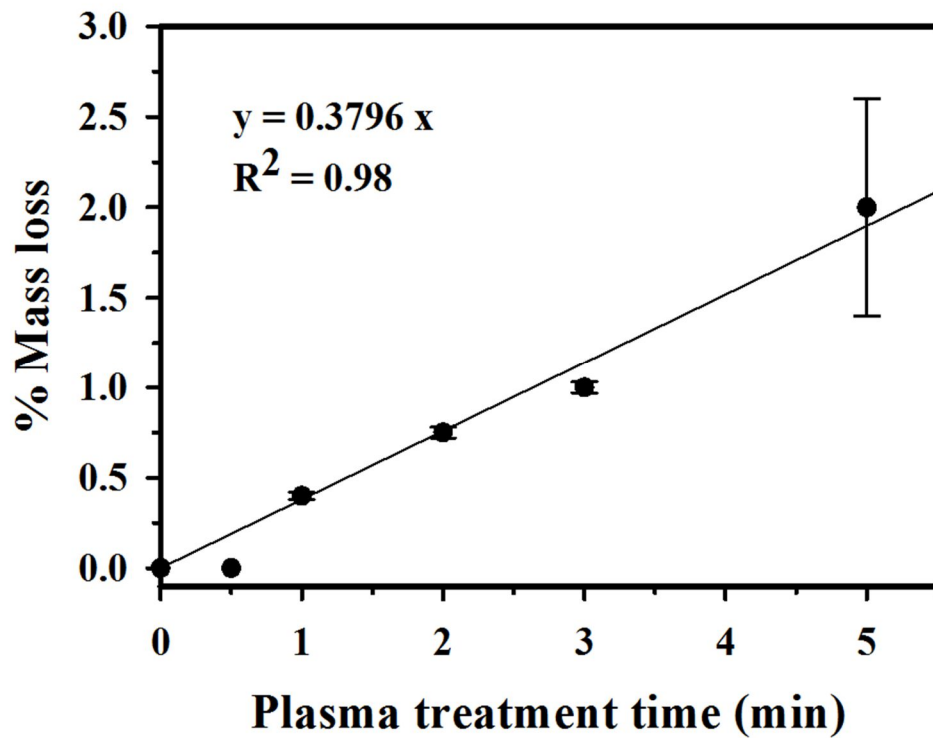
**Figure 3.3.** Representative WCA ( $^{\circ}$ ) as a function of time or water drop age (s) for tight sides of UPS-0, UPS-0.5, UPS-1, UPS-2, UPS-3 and UPS-5 measured a) immediately after treatment and b) after 2 months aging under ambient laboratory conditions (lines added only to guide the eye).

was applied to the samples. WCA measurements on aged samples were collected in the same fashion as on freshly treated materials, revealing that water drops on the tight side of the aged UPS-2, UPS-3, and UPS-5 membranes still disappeared in  $\sim 2$  s (Fig. 3.3b). Thus, aged membranes exhibited similar wetting behavior as that observed on their freshly treated counterparts. In the case of UPS-1, however, the drop vanished in  $\leq 8$  s, somewhat longer than that observed for its freshly treated counterpart. Notably, the WCA on the tight side of UPS-0.5 increases after stabilization from  $\sim 48^\circ$  to  $\sim 58^\circ$  after 2 months of aging. Overall, the data in Fig. 3.3b are very similar to those shown in Fig. 3.3a for freshly treated materials with treatment time  $\geq 2$  min. This illustrates that the tight sides of UPS-1, UPS-2, UPS-3, and UPS-5 membranes remain “completely wettable” after 2 months of aging under ambient laboratory conditions, experiencing minimal hydrophobic recovery.

Although the membrane is placed  $\sim 20$  cm from the glow, significantly minimizing the exposure to ionizing radiation,<sup>26</sup> plasma-induced damage could still occur. SEM micrographs of both sides of untreated and treated membranes are shown in Fig. 3.4. SEM images suggest no changes in the bulk architecture of the open (Fig. 3.4b, d) and tight (Fig. 3.4a, c) sides of the UPS-2 membranes. The tight side of UPS-5 (Fig. 3.4e), however, displays a slight shrinkage of the membrane pores, although it is not possible to quantify the damage visually. Examination of membrane mass loss after plasma treatment (Fig. 3.5), however, reveals a linear correlation ( $R^2 = 0.98$ ) between % mass loss and plasma treatment time, with the greatest mass loss ( $\sim 2\%$ ) occurring after a 5 min treatment. In addition, the UPS-5 membranes exhibit a relatively large standard deviation in % mass loss, indicative of greater variability in the amount of induced damage for this treatment time; this is discussed further below. This linear trend holds for longer



**Figure 3.4.** SEM images of UPS-0 (a) tight side (50,000 $\times$ , scale bar 100 nm) and (b) open side (200 $\times$ , scale bar 100  $\mu$ m); UPS-2 (c) tight side and (d) open side; and UPS-5 (e) tight side and (f) open side.



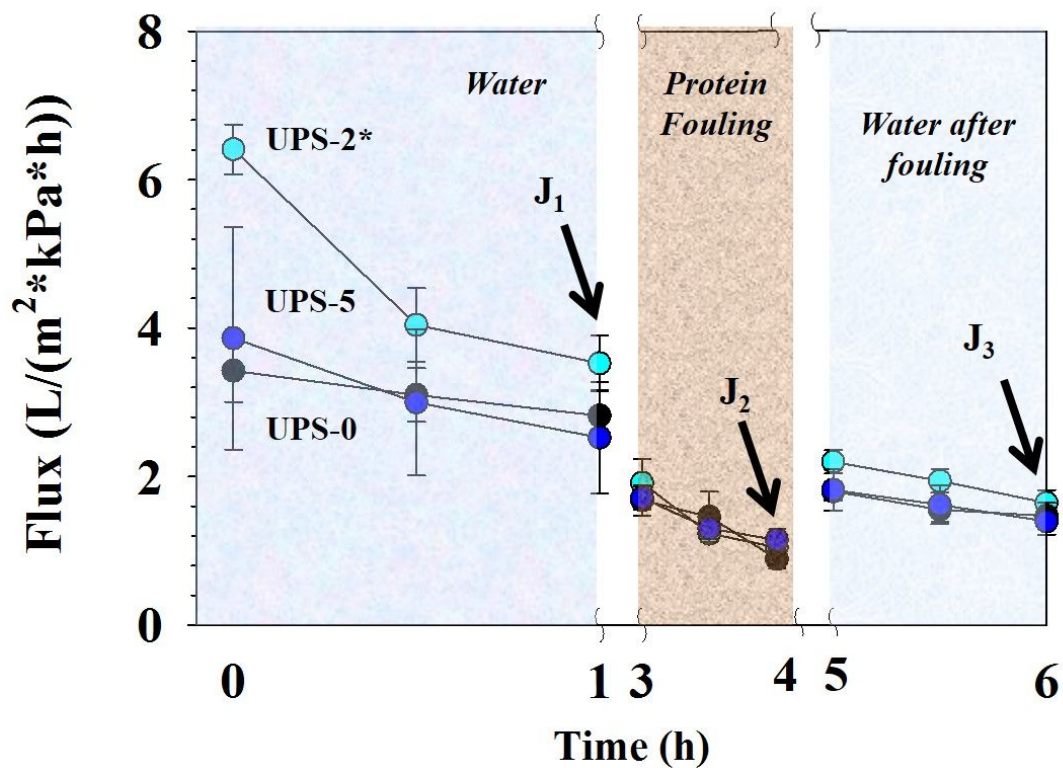
**Figure 3.5.** Percent mass loss as a function of plasma treatment time. All analyses were performed for an  $n \geq 3$ ; error bars represent  $\pm 1$  standard deviation from the mean. Data were fit with a linear least squares analysis;  $R^2$  values  $\geq 0.98$ .

treatments times (8 and 10 min), indicating that treatments times  $\geq 5$  min impart considerable damage to the membrane.

### 3.2.3. Ultrafiltration experiments

XPS and WCA data corroborated that the cross-section of the membranes is modified after  $\text{H}_2\text{O}_{(v)}$  plasma treatment, likely affecting the filtration properties of the membrane.<sup>12, 27-29</sup> To evaluate enhancement of the filtration properties of the membranes after plasma modification, the permeability of water through UPS-0, UPS-2, and UPS-5 membranes was studied via water flux experiments. UPS-2 membranes were selected for water permeability measurements as they remained hydrophilic even 2 months after plasma treatment, and this improvement in wettability occurred with minimal mass loss ( $\leq 1\%$ ). Water flux through UPS-5 membranes was also investigated to further explore the indications of pore damage for these membranes and as an upper bound on effects of the % mass loss, which reached 2%.

Representative experimental data of flux as a function of time is given in Fig. 3.6, and corresponding figures of merit are summarized in Table 3.2. The water flux for all membranes declines at approximately the same rate over the initial water filtration period (1 h) regardless of plasma treatment. Note, however, that the water flux for UPS-2 is significantly higher than for UPS-0 and UPS-5 (Table 3.2). Indeed, the stable water flux (i.e., the average of flux values after 1 h) for UPS-2 has increased by  $\sim 26\%$  when compared to UPS-0 (Table 3.2). This is likely the result of the higher hydrophilicity of the UPS-2 membranes in comparison to UPS-0. The same argument does not, however, apply for UPS-5. The initial water flux for UPS-5 does not differ from UPS-0, even though UPS-5 is significantly more wettable than UPS-0. In addition, the experimental error associated with the flux experiment reaches almost 40%. The lower than



**Figure 3.6.** Water flux ( $J_1$ ), protein flux ( $J_2$ ) and water flux after fouling ( $J_3$ ) in  $L m^{-2} kPa^{-1} h^{-1}$  for UPS-0, UPS-2 and UPS-5 membranes. All analyses were performed for  $n \geq 3$ ; error bars represent  $\pm 1$  standard deviation from the mean ( $p < 0.05$ ).

**Table 3.2.** Water flux, protein flux, and water flux after fouling.<sup>a</sup>

Plasma treatment		Initial water flux ( $J_0$ )	Water flux after 1 h filtration ( $J_1$ )	Protein flux ( $J_2$ )	Water flux after fouling ( $J_3$ )
Membrane	Time (min)	$\text{L m}^{-2} \text{kPa}^{-1} \text{h}^{-1}$	$\text{L m}^{-2} \text{kPa}^{-1} \text{h}^{-1}$	$\text{L m}^{-2} \text{kPa}^{-1} \text{h}^{-1}$	$\text{L m}^{-2} \text{kPa}^{-1} \text{h}^{-1}$
UPS-0	0	$3.4 \pm 0.4$	$2.8 \pm 0.3$	$0.9 \pm 0.1$	$1.5 \pm 0.2$
UPS-2	2	$6.4 \pm 0.3$	$3.5 \pm 0.4$	$1.0 \pm 0.1$	$1.6 \pm 0.2$
UPS-5	5	$3.9 \pm 1.5$	$2.5 \pm 0.8$	$1.1 \pm 0.1$	$1.4 \pm 0.2$

<sup>a</sup>All analyses were performed for  $n \geq 3$ ; the mean  $\pm$  standard deviation is reported.



expected water flux and associated error for UPS-5 are likely attributed to plasma-induced damage suffered by these materials; this is elaborated on below.

#### **3.2.4. Fouling experiments**

Untreated and treated membranes were exposed to 1% BSA solution to determine the tendency of the membranes to foul by protein adsorption. No significant differences are observed in the protein flux values for UPS-0, UPS-2, and UPS-5 after membrane fouling ( $J_2$ , Table 3.2). The % RFR for UPS-5 is somewhat lower than for UPS-0 and UPS-2, indicating a lower reduction in the measured flux after fouling (Table 3.2). The large error associated with these materials and the lack of improvement observed in the initial water flux, however, makes UPS-5 a less reliable filtration membrane than UPS-2.

After fouling, membranes were rinsed with DI water and the post-fouling water flux was measured ( $J_3$ , Table 3.2). Similar water flux after fouling values and % FRR are obtained for the three membranes independent of plasma modification. Although comparable protein adsorption is observed for UPS-0 and UPS-2, UPS-5 exhibits somewhat lower values of BSA adsorption.

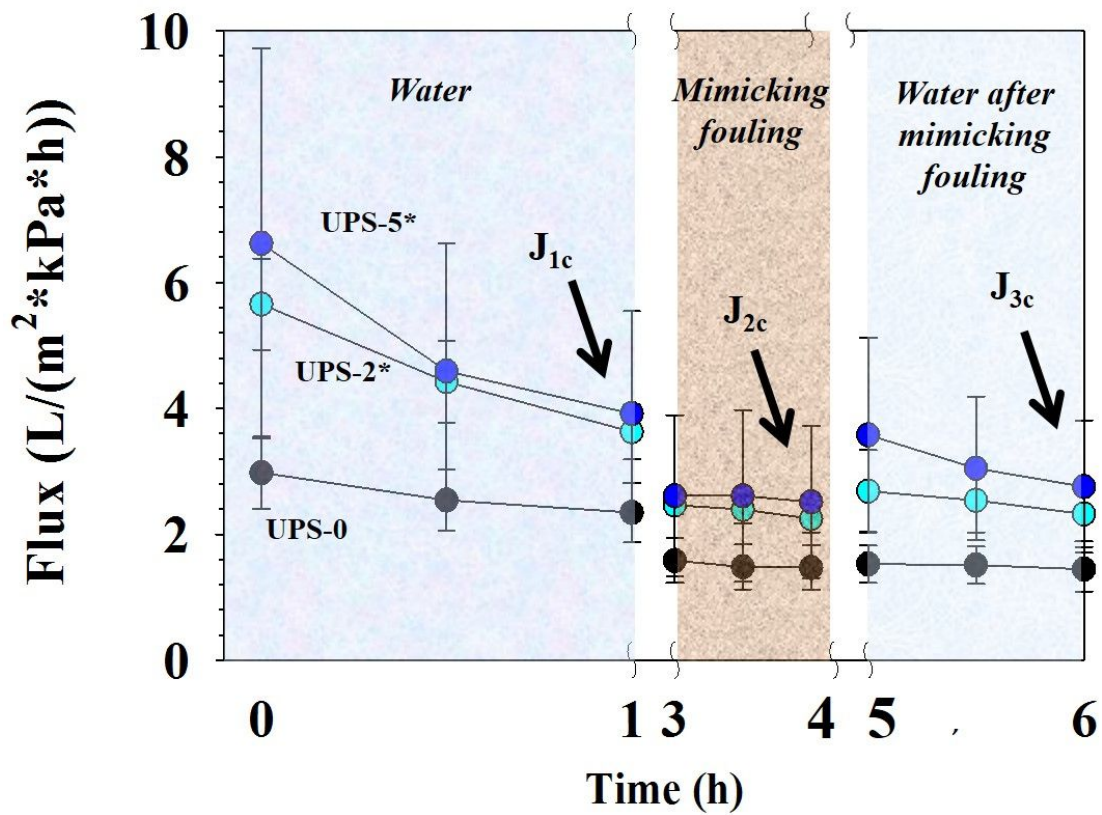
#### **3.2.5. Control ultrafiltration experiments**

*Effect of the compaction-pressure release cycles on overall performance.* Control water flux experiments were performed to understand the effect of the compaction-pressure release cycles used for the fouling experiments on the parent material. The compaction process alone results in an irreversible loss of membrane performance over time.<sup>30</sup> These control water flux experiments therefore allow understanding of the decline in the membrane performance associated with compaction-pressure release cycles during the entire fouling experiment as opposed to the effect

of the protein adsorption on the performance of the material. Fig. 3.7 depicts experimental data of control flux as a function of time, and corresponding figures of merit are summarized in Table 3.3.

The control water flux for all membranes declines at approximately the same rate over the initial water filtration period (1 h) as observed in Fig. 3.7. Here, the variability in the results observed for UPS-5 reaches almost 50%, further evidence that UPS-5 is a less reliable filtration membrane than UPS-2 (Table 3.3). The % RFR for untreated and treated membranes obtained in the control ultrafiltration experiments reached ~40%, and this value represents the minimum relative flux reduction achievable when the material is exposed to the compaction-pressure release cycles (Table 3.4). The % FRR was calculated for the control ultrafiltration experiments, indicating the maximum achievable recovery after exposing the material to the compaction-pressure release cycles. The calculated flux recovery ratio reveals that a maximum of ~60% of the membrane performance can be recovered after the compaction-pressure release cycles, independent of the plasma treatment, indicating the membrane underwent full compaction and did not recover initial flux values. These control results illustrate the importance of understanding how the design of a filtration experiment affects the material before interpreting fouling data. Additionally, the significant difference observed between the effects of compaction-pressure release cycles on the three different materials also highlights the importance of studying the effect for each type of material.

*Effect of the length of the fouling period on overall performance.* Control fouling experiments were performed to understand the effect of the length of the fouling period on the parent material. For the fouling experiments reported above, we explored an experimental set-up designed to provide a realistic approach to a filtration process wherein a UF membrane is



**Figure 3.7.** Water flux ( $J_{1c}$ ), water flux mimicking protein fouling flux ( $J_{2c}$ ) and water flux after mimicking fouling ( $J_{3c}$ ) in  $L m^{-2} kPa^{-1} h^{-1}$  for control ultrafiltration experiments using UPS-0, UPS-2 and UPS-5. All analyses were performed for  $n \geq 3$ ; error bars represent  $\pm 1$  standard deviation from the mean ( $p < 0.05$ ).

**Table 3.3.** Water flux, protein flux, and water flux for control experiments.<sup>a</sup>

Plasma treatment		Initial water flux ( $J_{0c}$ )	Water flux after 1 h filtration ( $J_{1c}$ )	Water flux mimicking protein fouling ( $J_{2c}$ )	Water flux after mimicking fouling ( $J_{3c}$ )
Membrane	Time (min)	$L m^{-2} kPa^{-1} h^{-1}$	$L m^{-2} kPa^{-1} h^{-1}$	$L m^{-2} kPa^{-1} h^{-1}$	$L m^{-2} kPa^{-1} h^{-1}$
UPS-0	0	$3.0 \pm 0.6$	$2.3 \pm 0.5$	$1.5 \pm 0.4$	$1.4 \pm 0.4$
UPS-2	2	$5.7 \pm 0.7$	$3.6 \pm 0.4$	$2.2 \pm 0.2$	$2.3 \pm 0.4$
UPS-5	5	$6.6 \pm 3.1$	$3.9 \pm 1.6$	$2.5 \pm 1.2$	$2.8 \pm 1.1$

<sup>a</sup>All analyses were performed for  $n \geq 3$ ; the mean  $\pm$  standard deviation is reported.

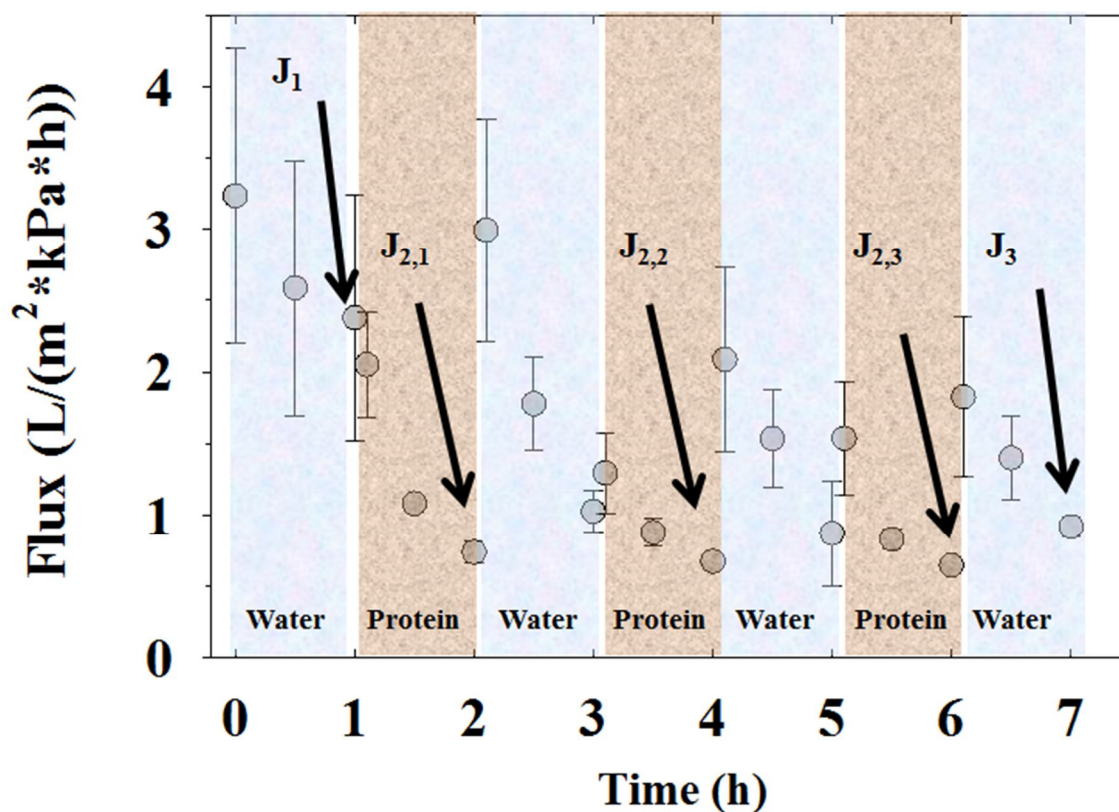
**Table 3.4.** Relative flux reduction, flux recovery ratio, protein adsorption, and control RFR, FRR.<sup>a</sup>

Plasma treatment		Relative flux reduction (% <b>, RFR)</b>	Flux recovery ratio (% <b>, FRR)</b>	Protein adsorption ( $\mu\text{g}/\text{cm}^2$ )	Minimum relative flux reduction achievable (% <b>, RFR)</b>	Maximum flux recovery ratio achievable (% <b>, FRR)</b>
Membrane	Time (min)					
UPS-0	0	69 ± 1	52 ± 2	114 ± 13	38 ± 3	61 ± 3
UPS-2	2	70 ± 2	47 ± 7	126 ± 67	39 ± 2	60 ± 6
UPS-5	5	52 ± 9	58 ± 9	34 ± 5	37 ± 7	71 ± 14

<sup>a</sup>All analyses were performed for  $n \geq 3$ ; the mean ± standard deviation is reported.

exposed to foulants for extended periods of time. It is, however, important to also identify whether any differences arise in the FRR if the parent material is exposed to three shorter (1 h) fouling cycles instead of one longer (3 h) fouling period. These control fouling experiments therefore allow understanding of the decline in the membrane performance associated with each fouling cycles and the foulant accumulation overtime. Fig. 3.8 depicts experimental data of control flux as a function of time, and corresponding figures of merit are summarized in Table 3.5.

The water flux declines at approximately the same rate over the initial water filtration period (1 h) for an untreated membrane as observed in Fig. 3.7 and Fig. 3.8. After the first fouling cycle, the % RFR<sub>1st cycle</sub> reaches ~70%. The water flux after the first membrane cleaning with DI water recovers some of the initial flux and FRR<sub>1st cycle</sub> ≈ 40% is obtained. Similar values of % RFR and FRR are observed for the two subsequent fouling cycles and the overall values for % RFR and % FRR are presented in Table 3.5 with values of ~70% and ~45% respectively. These values are comparable to the values reported in Table 3.4 for UPS-0 indicating that, regardless of whether the fouling cycle is three 1 h cycles or one 3 h cycle, the accumulation of foulants is comparable. The error associated with the % FRR (±15%, Table 3.5) with the multiple cycles experiment, however, suggests that the compaction-pressure release cycles used in these fouling control experiments have an effect on the reproducibility of the experiments.



**Figure 3.8.** Water flux ( $J_1$ ), protein flux after first fouling cycle ( $J_{2,1}$ ), protein flux after second fouling cycle ( $J_{2,2}$ ), protein flux after third fouling cycle ( $J_{2,3}$ ) and water flux after three fouling cycles ( $J_3$ ) for UPS-0 membranes. All analyses were performed for  $n \geq 3$ ; error bars represent  $\pm 1$  standard deviation from the mean.

**Table 3.5.** Water flux, protein flux, and water flux after fouling  $\text{L m}^{-2} \text{kPa}^{-1} \text{h}^{-1}$ .<sup>a</sup>

<b>Plasma treatment</b>	<b>Water flux after 1 h filtration (<math>J_1</math>)</b>	<b>Protein flux (<math>J_{2,1}</math>)</b>	<b>Protein flux (<math>J_{2,2}</math>)</b>	<b>Protein flux (<math>J_{2,3}</math>)</b>	<b>Water flux after fouling (<math>J_3</math>)</b>	<b>Overall % RFR</b>	<b>Overall %FRR achievable</b>
<b>Membrane</b>							
UPS-0	$2.2 \pm 0.9$	$0.7 \pm 0.1$	$0.7 \pm <0.1$	$0.6 \pm <0.1$	$1 \pm 0.1$	$70 \pm 9$	$44 \pm 15$

<sup>a</sup>All analyses were performed for  $n \geq 3$ ; the mean  $\pm$  standard deviation is reported.



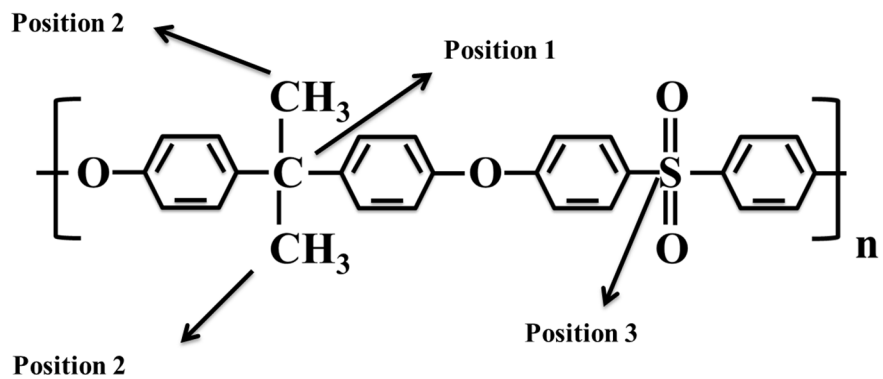
### 3.3 Discussion

This study demonstrates that  $\text{H}_2\text{O}_{(v)}$  plasmas can effectively modify the surface chemistry of PSf UF membranes while retaining the bulk architecture, and that this modification results in improved hydrodynamic characteristics and partial reversibility of protein adsorption. Compositional data obtained via XPS and FTIR experiments indicates that modification of the membrane cross section occurs, confirming previously reported results for complete cross section modification of asymmetric UF membranes using  $\text{CO}_2$  plasma treatments.<sup>17</sup> In both studies, membrane orientation and downstream placement allows the plasma to penetrate through the thickness of the porous membrane, thereby facilitating modification of the entire membrane cross-section.

The XPS and FTIR data clearly demonstrate that plasma treatment results in implantation of a variety of oxygen-containing functional groups regardless of treatment time. Notably, key factors contributing to the chemical modification of the membrane using  $\text{H}_2\text{O}_{(v)}$ -based plasma systems are the treatment parameters used and the active species in the plasma. We have previously performed extensive gas-phase diagnostics on  $\text{H}_2\text{O}_{(v)}$  plasma systems, with and without a polymer substrate.<sup>1, 15</sup> OES of  $\text{H}_2\text{O}_{(v)}$  plasmas revealed the presence of excited-state OH radicals and H atoms.<sup>1</sup> When a PSf membrane was placed horizontally directly in the coil region of the plasma reactor, additional emission lines attributed to CO were observed,<sup>1</sup> indicating the membranes were being oxidized during plasma treatment.<sup>31-32</sup> Based on radical-surface interaction experiments, gas-phase OH radicals are believed responsible for the oxidation of the membrane surface<sup>1</sup>. As shown by Steen, *et al.*,<sup>1</sup> there are three main positions in the backbone of PSf at which oxidation can occur during  $\text{H}_2\text{O}_{(v)}$  plasma exposure (Fig. 3.9), including the quaternary carbon, the methyl group, and the sulfur group. Oxidation at the

quaternary carbon (Position 1) yields ketone functionalities, oxidation at the methyl groups (Position 2) forms aldehydes that can be further oxidized to carboxylic acid groups, and oxidation at the sulfur group (Position 3) yields sulfate-like groups.<sup>1</sup> XPS and FTIR composition data for plasma-modified UF membranes indicate carbonyl groups, such as aldehyde, ketone, and carboxylic functionalities were introduced by plasma treatment. Reactions between OH radicals and the membrane surface must occur through cleavage of C–S, C–C, C–O, or C–H bonds. Cleavage of the C–H bond on the methyl group by OH (Position 2) is the most reasonable path that would result in direct formation of an alcohol group on the membrane surface. Given that an OH stretching peak is observed in FTIR spectra of treated membranes, it appears that despite the relatively high C–H bond energy (4.5 eV), some alcohol groups were incorporated via C–H bond cleavage during treatment. A secondary oxidation pathway at the sulfur (Position 3) results in sulfate-like groups that are observed in the high-resolution S<sub>2p</sub> spectra (data not shown). In addition, our XPS results also indicate the presence of nitrogen on the upstream (open) side of treated samples, possibly occurring via reaction at the methyl group. The incorporation of nitrogen is attributed to higher concentrations of radicals produced on the upstream side of the membrane directly facing the plasma, which upon exposure to air can react with atmospheric nitrogen.<sup>33</sup> Overall, these XPS and FTIR data indicate two possible oxidative reaction pathways between OH and PSf membranes during plasma treatment.

Plasma oxidation of the membranes via introduction of oxygen functionality also dramatically changes the wettability of the membranes. In particular, dynamic WCA data for the tight sides of all treated membranes confirmed that, after plasma treatment, the membranes were significantly more hydrophilic than UPS-0 (Fig. 3.3a). As the UPS-0.5 and UPS-1 membranes did not meet the established wettability criterion, it is clear that treatment time must exceed 60 s



**Figure 3.9.** Schematic of polysulfone structure indicating the three main positions where oxidation can occur during H<sub>2</sub>O<sub>(v)</sub> plasma exposure.<sup>1</sup>

to meet the established criterion. Likewise, previous work has demonstrated plasma exposure times  $\geq 60$  s are required to lastingly (longer than 9 months) and completely modify asymmetric microporous PSf, PES, and PE membranes using both  $\text{CO}_2$  and  $\text{H}_2\text{O}_{(v)}$  plasmas.<sup>1, 15, 17</sup> Notably, here we observe that some membrane damage occurs with a plasma treatment time of 5 min, suggesting treatment times between 1 and 5 min are ideal to obtain long-lasting hydrophilic surfaces with minimal damage to the membrane structure.

Aging studies demonstrated that the tight sides of treated membranes remain hydrophilic after two months of aging in air. Only UPS-2, UPS-3, and UPS-5 are, however, still considered “completely wetting” after this aging period based on our established criterion. The observed aging of membranes treated for  $< 2$  min suggests these samples are losing hydrophilicity over time. Hydrophobic recovery is terminology used to describe the loss of hydrophilic characteristics (acquired by plasma treatment), accompanied by a return to the hydrophobic nature of the parent material, usually shortly after treatment. This phenomenon generally occurs via polymer rearrangement, whereby the hydrophilic functional groups migrate away from the surface and become buried within the bulk of the polymer. Here, hydrophobic recovery manifested differently for our UPS materials. In particular, for aged UPS-1, water drops merely took longer to absorb than they did for freshly treated UPS-1 membranes. In contrast, for UPS-0.5, the WCA increased by  $10^\circ$  on aged materials relative to the freshly treated membranes. Perhaps more notable, no significant hydrophobic recovery was observed for UPS-2, UPS-3 or UPS-5. Such behavior has been widely observed for plasma-treated polymeric materials, including but not limited to UF membranes.<sup>15, 17, 34-39</sup> In a worst-case scenario, recovery can occur for PSf membranes within 24 h of plasma treatment,<sup>36</sup> indicating a poor choice of

treatment conditions. Here, we demonstrate how optimizing plasma parameters (specifically treatment time) allow us to avoid hydrophobic recovery for our treated materials.

The water flux for both untreated and treated membranes decreased at approximately the same rate to reach a stable water flux during the initial water filtration. The flux decline is partially attributed to the compaction of the membrane structure under pressure and formation of microscopic bubbles on the permeate side of the membranes as a result of gas dissolved in the feed water.<sup>40</sup> Our control ultrafiltration experiments confirm that ~40% of the flux decline observed is directly related to the compaction-pressure release cycles regardless of plasma modification. Nevertheless, UPS-2 showed significant improvement in the hydrodynamic characteristics of the membrane in comparison to UPS-0. UPS-5, however, demonstrated no significant improvement in comparison to UPS-0, corroborating that longer treatment times ( $\geq 5$  min) resulted in plasma-induced damage and potentially shrinkage of pore size. Therefore, to ensure bench-top stability with minimal structural damage and enhancement of membrane filtration performance, the optimized treatment time is 2 min.

The propensity of the membrane to foul, or % RFR, reached ~70% for UPS-0 and UPS-2, providing an opportunity to evaluate the effect of  $\text{H}_2\text{O}_{(v)}$  plasma treatments on PSf UF membrane performance. The values obtained for UPS-0 and UPS-2 represent a combination of compaction-pressure release cycles as shown by control ultrafiltration experiments (~40%) and protein fouling (~30%). The main mechanisms involved in the fouling of the membrane include (1) adsorption of matter within the membrane pores, (2) pore clogging and (3) adsorption of matter on top of the membrane surface or “cake formation”.<sup>41</sup> The first two mechanisms often result in irreversible fouling, whereas the third mechanism may be partially reversed. Membrane fouling caused by the accumulation of protein aggregates at the membrane surface occurs regardless of

the membrane used.<sup>40, 42</sup> Nevertheless, sometimes the fouling associated with the third mechanism has been partially reversed on plasma treated membranes.<sup>8-10, 17, 21, 42-48</sup> Several studies have shown that membranes with enhanced hydrophilicity in comparison to the parent material demonstrate higher flux recoveries and better antifouling properties.<sup>12, 27, 29</sup> It has been hypothesized that when water comes in contact with a hydrophilic membrane, it will form a hydration layer, reducing subsequent interactions with potential foulants.<sup>41</sup> This may result in looser binding of protein to the membrane and therefore increasing the reversibility of the fouling. Several studies report the use of harsh chemicals such as sodium hydroxide and ethylenediaminetetraacetic acid<sup>8-10, 43-44</sup> to clean fouled membranes, as well as more mild approaches such as PBS,<sup>45-46</sup> DI water,<sup>17, 21, 42</sup> or a backwash approach<sup>47-48</sup> to reverse membrane fouling. Herein, the membranes were simply rinsed with ultrapure water after fouling to assess the level of reversibility of membrane fouling we could achieve. The amount of protein adsorbed on the material and the % FRR were used to compare the ability to recover after fouling for UPS-0 and UPS-2. In addition, the control experiments performed to assess the effect of the length of the fouling period on overall performance of untreated membranes indicated that the amount of foulant accumulated in the parent material over 3 h is equivalent regardless if the fouling occurs over a single 3 h period of time or occurs over three consecutive 1 h fouling cycle.

Based on previously reported static protein adsorption studies on hydrophilic and hydrophobic surfaces,<sup>49-51</sup> we anticipated a significantly larger amount of BSA would adsorb to the hydrophilic UPS-2 surface compared to the hydrophobic UPS-0. The potential formation of a hydration layer on the hydrophilic membrane prior to exposure to the foulants (i.e., BSA), however, mitigated the ability of the proteins to adsorb to the membrane.<sup>41</sup> This is supported by

the observation that a similar amount of protein adsorption was measured for UPS-0 and UPS-2 membranes, which can be attributed to 1) the partial reversibility of the protein layer on UPS-2 as a result of rinsing the membranes with ultrapure water because of weaker protein binding to the hydrophilic membrane; and 2) less protein interacting with the hydrated membrane surface.<sup>41</sup> As a final note, the ability of the membranes to recover filtration capabilities after reversing fouling was assessed based on % FRR. For both UPS-0 and UPS-2, the calculated % FRR reached ~50%. Control ultrafiltration experiments, however, indicated that the maximum FRR achievable after the compaction-pressure release cycles in the absence of foulants is ~60%. Hence, comparing control ultrafiltration experiments with fouling experiments for UPS-2 demonstrated a 70-90% recovery based on the maximum FRR achievable ( $60 \pm 6$ ) shown by control ultrafiltration experiments (Table 3.4).

This indicates that these plasma treatment conditions enhance hydrodynamic characteristics of the membranes, eliminate preconditioning requirements, and allow significant recovery after fouling by rinsing the membrane with ultrapure water alone.

### **3.4 Summary and conclusions**

Overall, the results highlighted here are in concordance with our past studies of plasma modification of UF membranes. Surface analyses confirmed the penetration of the plasma through the porous membrane thickness and the modification of the membrane cross section. The surface wettability of the PSf UF membranes was significantly enhanced without imparting substantial damage to the membrane structure. Limited hydrophobic recovery was observed for membranes treated for <2 min. Control ultrafiltration experiments highlighted the importance of understanding the compaction-pressure release cycles and the effect of the length of the fouling

period on membrane performance. The hydrodynamic characteristics of the plasma modified membranes were improved and the protein adsorption on modified membranes was partially reversed by simply rinsing with ultrapure water. These findings support the hypothesis that  $\text{H}_2\text{O}_{(v)}$  plasma treatments show real promise for lastingly modifying polymeric membranes while retaining their structure and pore network.



## REFERENCES

1. Steen, M. L.; Hymas, L.; Havey, E. D.; Capps, N. E.; Fisher, E. R., Low temperature plasma treatment of asymmetric polysulfone membranes for permanent hydrophilic surface modification. *J. Membr. Sci.* **2001**, *188*, 97.
2. Shi, X.; Tal, G.; Hankins, N. P.; Gitis, V., Fouling and cleaning of ultrafiltration membranes: a review. *Journal of Water Process Engineering* **2014**, *1*, 121-138.
3. Cheryan, M., *Ultrafiltration handbook*. Technomic Publishing Co. Inc.: 1986.
4. Li, N. N.; Fane, A. G.; Ho, W. W.; Matsuura, T., *Advanced membrane technology and applications*. John Wiley & Sons: 2011.
5. Israelachvili, J. N., *Intermolecular and Surface Forces*. 2 ed.; Academic Press: London, 1985.
6. Feast, W. J., *Polymer Surfaces and Interfaces*. H.S. Munro (Ed.) ed.; Wiley: Chichester, 1987.
7. Nguyen, T.; Roddick, F. A.; Fan, L., Biofouling of water treatment membranes: a review of the underlying causes, monitoring techniques and control measures. *Membranes* **2012**, *2* (4), 804-840.
8. Yu, H.-Y.; Liu, L.-Q.; Tang, Z.-Q.; Yan, M.-G.; Gu, J.-S.; Wei, X.-W., Surface modification of polypropylene microporous membrane to improve its antifouling characteristics in an SMBR: Air plasma treatment. *J. Membr. Sci.* **2008**, *311* (1–2), 216-224.
9. Yu, H.-Y.; Xie, Y.-J.; Hu, M.-X.; Wang, J.-L.; Wang, S.-Y.; Xu, Z.-K., Surface modification of polypropylene microporous membrane to improve its antifouling property in MBR: CO<sub>2</sub> plasma treatment. *J. Membr. Sci.* **2005**, *254* (1), 219-227.
10. Yu, H.-Y.; Hu, M.-X.; Xu, Z.-K.; Wang, J.-L.; Wang, S.-Y., Surface modification of polypropylene microporous membranes to improve their antifouling property in MBR: NH<sub>3</sub> plasma treatment. *Sep. Purif. Technol.* **2005**, *45* (1), 8-15.
11. Gancarz, I.; Poźniak, G.; Bryjak, M., Modification of polysulfone membranes 1. CO<sub>2</sub> plasma treatment. *Eur. Polym. J.* **1999**, *35* (8), 1419-1428.
12. Gancarz, I.; Pozniak, G.; Bryjak, M., Modification of polysulfone membranes 3. Effect of nitrogen plasma. *Eur. Polym. J.* **2000**, *36*, 1563.
13. Bryjak, M.; Gancarz, I.; Poźniak, G.; Tylus, W., Modification of polysulfone membranes 4. Ammonia plasma treatment. *Eur. Polym. J.* **2002**, *38* (4), 717-726.
14. Wavhal, D. S.; Fisher, E. R., Hydrophilic modification of polyethersulfone membranes by low temperature plasma-induced graft polymerization. *J. Membr. Sci.* **2002**, *209*, 255.
15. Steen, M. L.; Jordan, A. C.; Fisher, E. R., Hydrophilic modification of polymeric membranes by low temperature H<sub>2</sub>O plasma treatment. *J. Membr. Sci.* **2002**, *204*, 341.
16. Wavhal, D. S.; Kull, K. R.; Steen, M. L.; Fisher, E. R., Hydrophilic surface modification of microporous polymer membranes using a variety of low-temperature plasma treatments. *Mat. Res. Soc. Symp. Proc.* **2003**, *752*, 53-58
17. Wavhal, D. S.; Fisher, E. R., Modification of polysulfone ultrafiltration membrane by CO<sub>2</sub> plasma treatment. *Desalination* **2005**, *172*, 189-205.
18. van Reis, R.; Zydney, A., Membrane separations in biotechnology. *Current Opinion in Biotechnology* **2001**, *12* (2), 208-211.
19. Wu, S., *Polymer Interface and Adhesion*. 2nd ed.; Chapman and Hall: London, 1987.
20. Mok, S.; Worsfold, D. J.; Fouda, A.; Matsuura, T., Surface modification of polyethersulfone hollow fiber membranes by  $\gamma$ -ray irradiation. *J. Appl. Polym. Sci.* **1994**, *51*, 193.
21. Kim, K. S.; Lee, K. H.; Cho, K.; Park, C. E., Surface modification of polysulfone ultrafiltration membrane by oxygen plasma treatment. *J. Membr. Sci.* **2002**, *199*, 135.
22. Beamson, G.; Briggs, D., *High Resolution of XPS of Organic Polymers*. New York, 1992.
23. Kull, K. R.; Steen, M. L.; Fisher, E. R., Surface modification with nitrogen-containing plasmas to produce hydrophilic, low-fouling membranes. *J. Membr. Sci.* **2005**, *246* (2), 203-215.

24. Collaud-Coen, M.; Gröning, P.; Dietler, G.; Schlapbach, L., Creation of a conductive surface-layer on polypropylene samples by low-pressure plasma treatments. *J. Appl. Phys* **1995**, *77*, 5695.
25. Belfer, S.; Fainchtain, R.; Purinson, Y.; Kedem, O., Surface characterization by FTIR-ATR spectroscopy of polyethersulfone membranes-unmodified, modified and protein fouled. *J. Membr. Sci.* **2000**, *172*, 113.
26. Steen, M. L.; Butoi, C. I.; Fisher, E. R., Identification of gas-phase reactive species and chemical mechanisms occurring at plasma-polymer surface interfaces. *Langmuir* **2001**, *17*, 8156.
27. Capannelli, G.; Bottino, A.; Gekas, V.; Tragardh, G., Protein fouling behavior of ultrafiltration membranes prepared with varying degrees of hydrophilicity. *Process Biochemistry Internat.* **1990**, *25* (6), 221-224.
28. Kang, M. S.; Chun, B.; Kim, S. S., Surface modification of polypropylene membrane by low-temperature plasma treatment. *J. Appl. Polym. Sci.* **2001**, *81*, 1555.
29. Fujimoto, K.; Tadokoro, H.; Ueda, Y.; Ikada, Y., Polyurethane surface modification by graft polymerization of acrylamide for reduced protein adsorption and platelet adhesion. *Biomaterials* **1993**, *14*, 442.
30. Stade, S.; Kallioinen, M.; Mikkola, A.; Tuuva, T.; Mänttari, M., Reversible and irreversible compaction of ultrafiltration membranes. *Sep. Purif. Technol.* **2013**, *118* (0), 127-134.
31. Harshbarger, W. R.; Porter, R. A.; Miller, T. A.; Norton, P., *Appl. Spectrosc.* **1977**, *31*, 201.
32. Degenkolb, E. O.; Mogab, C. J.; Goldrich, M. R.; Griffiths, J. E., *Appl. Spectrosc.* **1976**, *30*, 520.
33. Morosoff, N., An introduction to plasma polymerization In *Plasma deposition, treatment, and etching of polymers: the treatment and etching of polymers*, Flamm, D. L.; Auciello, O.; d'Agostino, R., Eds. Academic Press, Inc.: London, 1990.
34. Bodas, D.; Khan-Malek, C., Hydrophilization and hydrophobic recovery of PDMS by oxygen plasma and chemical treatment—An SEM investigation. *Sensor. Actuat. B-Chem.* **2007**, *123* (1), 368-373.
35. Tompkins, B. D.; Dennison, J. M.; Fisher, E. R., H<sub>2</sub>O plasma modification of track-etched polymer membranes for increased wettability and improved performance. *J. Membr. Sci.* **2013**, *428*, 576-588.
36. J. Ditter, Personal Communication. US Filter, Inc.
37. Gengenbach, T. R.; Chatelier, R. C.; Griesser, H. J., Characterization of the ageing of plasma-deposited polymer films: Global analysis of X-ray photoelectron spectroscopy data. *Surf. Interface Anal.* **1996**, *24* (4), 271-281.
38. Tarasova, A.; Hamilton-Brown, P.; Gengenbach, T.; Griesser, H. J.; Meagher, L., Colloid probe AFM and XPS study of time-dependent aging of amine plasma polymer coatings in aqueous media. *Plasma Proc. Polym.* **2008**, *5* (2), 175-185.
39. Griesser, H. J.; Da, Y.; Hughes, A. E.; Gengenbach, T. R.; Mau, A. W., Shallow reorientation in the surface dynamics of plasma-treated fluorinated ethylene-propylene polymer. *Langmuir* **1991**, *7* (11), 2484-2491.
40. Mueller, J.; Davis, R. H., Protein fouling of surface-modified polymeric microfiltration membranes. *J. Membr. Sci.* **1996**, *116*, 47.
41. Kumar, R.; Ismail, A. F., Fouling control on microfiltration/ultrafiltration membranes: Effects of morphology, hydrophilicity, and charge. *J. Appl. Polym. Sci.* **2015**, *132* (21), DOI: 10.1002/app.42042.
42. McVerry, B. T.; Temple, J. A.; Huang, X.; Marsh, K. L.; Hoek, E. M.; Kaner, R. B., Fabrication of low-fouling ultrafiltration membranes using a hydrophilic, self-doping polyaniline additive. *Chem. Mater.* **2013**, *25* (18), 3597-3602.
43. Hong, S.; Elimelech, M., Chemical and physical aspects of natural organic matter (NOM) fouling of nanofiltration membranes. *J. Membr. Sci.* **1997**, *132* (2), 159-181.
44. Lim, A.; Bai, R., Membrane fouling and cleaning in microfiltration of activated sludge wastewater. *J. Membr. Sci.* **2003**, *216* (1), 279-290.
45. Park, J. Y.; Acar, M. H.; Akthakul, A.; Kuhlman, W.; Mayes, A. M., Polysulfone-graft-poly(ethylene glycol) graft copolymers for surface modification of polysulfone membranes. *Biomaterials* **2006**, *27* (6), 856-865.

46. Wavhal, D. S.; Fisher, E. R., Membrane surface modification by plasma-induced polymerization of acrylamide for improved surface properties and reduced protein fouling. *Langmuir* **2003**, *19*, 79.
47. Qu, F.; Liang, H.; Zhou, J.; Nan, J.; Shao, S.; Zhang, J.; Li, G., Ultrafiltration membrane fouling caused by extracellular organic matter (EOM) from *Microcystis aeruginosa*: Effects of membrane pore size and surface hydrophobicity. *J. Membr. Sci.* **2014**, *449*, 58-66.
48. Nabe, A.; Staude, E.; Belfort, G., Surface modification of polysulfone ultrafiltration membranes and fouling by BSA solutions. *J. Membr. Sci.* **1997**, *133* (1), 57-72.
49. Wagner, M. S.; McArthur, S. L.; Shen, M.; Horbett, T. A.; Castner, D. G., Limits of detection for time of flight secondary ion mass spectrometry (ToF-SIMS) and X-ray photoelectron spectroscopy (XPS): detection of low amounts of adsorbed protein. *J. Biomater. Sci. Polym. Ed.* **2002**, *13* (4), 407-428.
50. Rubio, C. C., D.; Bellon-Fontaine, M.N.; Relkin, P.; Pradier, C.M.; Marcus, P., Characterization of bovine serum albumin adsorption on chromium and AISI 304 stainless steel, consequences for the *Pseudomonas fragi* K1 adhesion. *Colloids Surf., B* **2002**, *24*, 193-205.
51. Jeyachandran, Y.; Mielczarski, E.; Rai, B.; Mielczarski, J., Quantitative and qualitative evaluation of adsorption/desorption of bovine serum albumin on hydrophilic and hydrophobic surfaces. *Langmuir* **2009**, *25* (19), 11614-11620.

## CHAPTER 4

### FABRICATION AND CHARACTERIZATION OF POLYMERIC CONSTRUCTS LOADED WITH ANTIBACTERIAL AG NANOPARTICLES

This chapter details the incorporation of biocidal silver nanoparticles into several polymeric constructs with different morphologies. Select materials are H<sub>2</sub>O<sub>(v)</sub> plasma surface modified to enhance material wettability and aid nanoparticle incorporation. The antibacterial performance of the resulting Ag-loaded constructs is investigated and the results are discussed in a clinical context. This chapter is largely based on an invited article submitted to *Biointerphases* by Michelle N. Mann and Ellen R. Fisher. Financial support for this work was provided by the National Science Foundation (CHE-1152963), the Camille and Henry Dreyfus Foundation, and the Colorado State University's Office of the Vice President for Research Catalyst for Innovative Partnerships Program. I would like to thank Dr. Adoracion Pegalajar-Jurado for mentorship during training and data collection, and Dr. Morgan J. Hawker, Mr. Matthew R. Maynard, and Mr. Cyrus Salvani for assistance with a review of the literature, as well as SEM and biological data collection. I also want to thank Dr. Patrick McCurdy for assistance with SEM-EDS and XPS analyses, Dr. Christine Olver for assistance with TEG analyses, and Dr. Joseph DiVerdi for assistance with flame atomic absorption spectroscopic analyses.

#### 4.1 Introduction

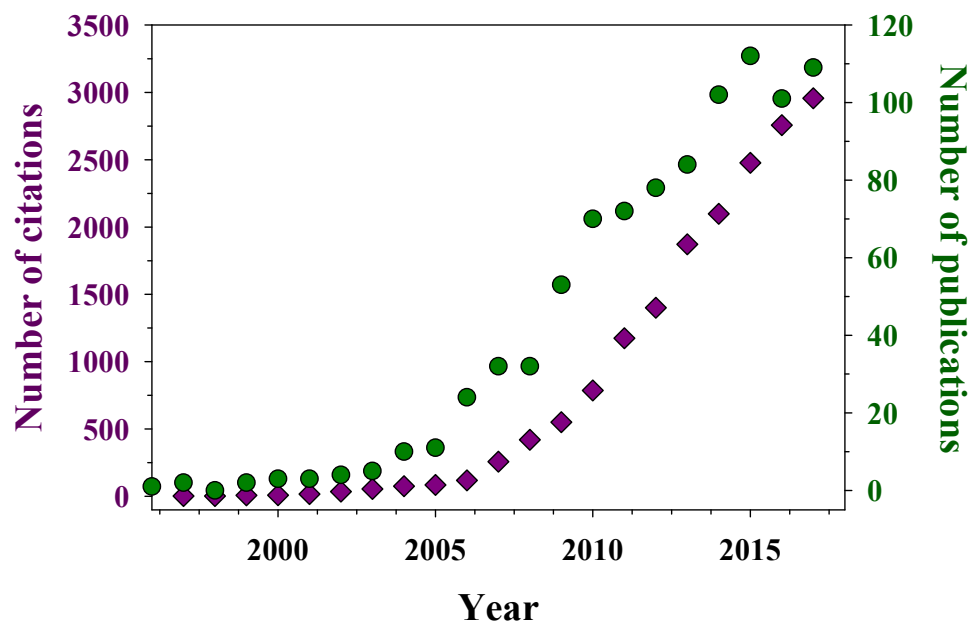
Surgical site infections (SSIs) are the most prevalent form of hospital-acquired infections (HAIs), with ~300,000 per year in the United States.<sup>1-2</sup> Each SSI can add an additional 7-11 days to a given hospital stay and up to \$45,000 in healthcare costs, culminating in an estimated

\$3.5-10 billion annual healthcare costs.<sup>1-2</sup> The monetary impact, combined with the 2-11 times higher risk of patient death, requires that prevention and management of wound infection remain a major priority in post-operative care.<sup>1</sup> As such, research contributing to the emergence of antimicrobial wound dressings has exploded in recent decades.<sup>3-7</sup> Ag is a common biocidal agent investigated for use in medical settings as it has fast-acting, broad-spectrum biocidal activity.<sup>5, 8-12</sup> The toxicity of Ag arises from release of Ag<sup>+</sup> that causes multiple phenomena (e.g., binding of Ag<sup>+</sup> to bacterial cell membranes and interfering with DNA replication) that lead to cell death in most bacterial strains.<sup>13</sup> Now, wound dressings and ointments containing Ag [e.g., Acticoat®, silver sulfadiazine (SSD) creams] are prevalent in the treatment of burn wounds.<sup>14-17</sup> Discrepancies surrounding the delivery of Ag at the wound site exist within the literature, however, with some studies finding significant absorption of Ag occurs at burn sites treated with SSD,<sup>18-19</sup> whereas others find little Ag is absorbed.<sup>20-21</sup> This confusion arises, in part, from the nature of silver delivery from silver nitrate-containing dressings or SSD creams.<sup>16-17, 22</sup> As Ag is often rapidly inactivated through the formation of chloride complexes, frequent dressing changes are required.<sup>17</sup> The overuse of dressings, however, can deliver a large excess of Ag to the wound. Indeed, excess amounts of Ag (up to 3200 ppm) are often observed after treatment.<sup>17</sup>

To circumvent the rapid Ag depletion that can occur after application of AgNO<sub>3</sub> and SSD, Ag nanoparticles (AgNPs) have been employed to serve as a reservoir for active Ag species. AgNPs can provide a greater total amount of Ag, yet Ag<sup>0</sup> is much more slowly depleted than its oxidized form. Much of the progress in the past 20 years has thus focused on efforts to incorporate AgNPs throughout porous three-dimensional (3D) biomaterials (e.g., fibrous mats for wound healing and scaffolds for tissue engineering) to controllably deliver Ag at the wound

or implant site. Controlled and prolonged delivery of Ag may mean longer lifetime and efficacy of the biomaterial and a speedier healing time. The ideal Ag-containing material would also exhibit fast-acting, broad spectrum antimicrobial activity, and be otherwise nontoxic and nonirritating. The body of literature on such materials has increased exponentially in past decades, as evidenced by the growing number of publications and citations (Fig. 4.1). Indeed, in the first five months of 2018, no fewer than 45 publications have appeared. Table 4.1 summarizes select methodologies commonly used for the fabrication of Ag-loaded polymeric materials. Various approaches used for incorporating AgNPs into polymeric devices include polymerization of the polymer matrix around AgNPs; blending of AgNPs into polymer mixtures; or introduction of AgNPs onto polymeric construct surfaces by spreading of a slurry or in situ reduction from Ag-containing salts (e.g., AgNO<sub>3</sub>).

The performance of Ag-polymer composite biomaterials has been impeded by several factors surrounding the nature of AgNP incorporation into polymers. One downside to blending AgNPs into polymers includes the difficulty in homogeneously distributing the AgNPs, as they tend to agglomerate in the highly viscous polymer solutions.<sup>23</sup> Furthermore, Ag leachability from AgNPs can be difficult to predict as it depends on particle size, morphology, and the surrounding matrix.<sup>24</sup> Other major limitations include the tendency to encapsulate the AgNP, preventing the release of Ag<sup>+</sup> from the bulk nanoparticle.<sup>25-26</sup> Placing AgNPs on polymer surfaces, however, often results in instantaneous release and thus short-term effects, or otherwise difficult-to-tune release of Ag from the construct. Some studies suggest that increasing material hydrophilicity can improve silver release.<sup>27-28</sup> Plasma surface modification is one strategy often employed to improve overall material wettability and biocompatibility; this approach has also been used to



**Figure 4.1.** Number of publications (left axis) and citations (right axis) as a function of year for the Web of Science search term “Ag nanoparticle polymers” as of December 2017.

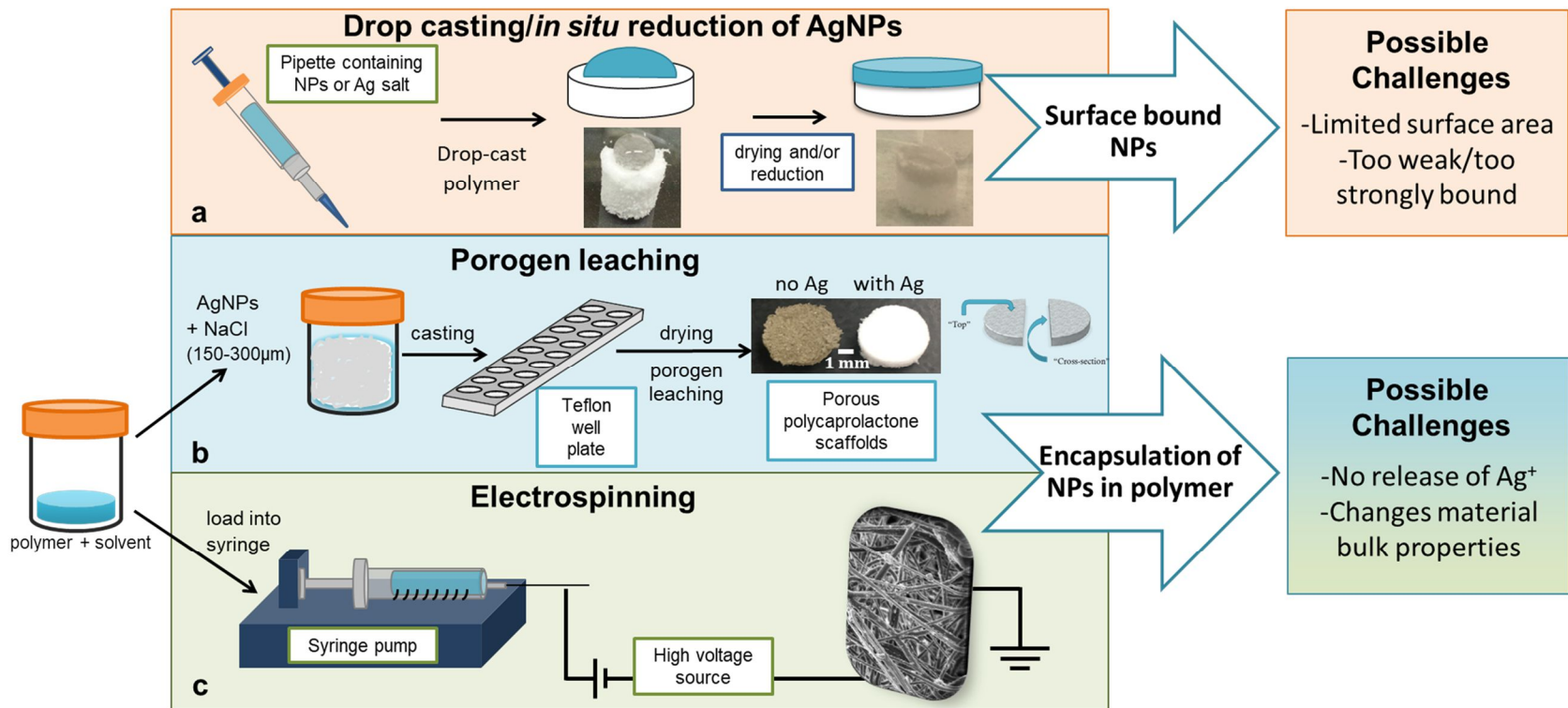
**Table 4.1.** Summary of fabrication and analytical methods for selected AgNP-incorporated porous materials.

Method of Ag incorporation	Material	Bacterial strain(s)	Antibacterial assays	Bactericidal results	Ref
Surface immobilization/ <i>in situ</i> reduction from Ag-containing salts	PE scaffolds	<i>B. subtilis</i> , <i>S. aureus</i> , <i>P. aeruginosa</i>	Kill rate by colony counting method	1-2-log reduction after 12 h	29
	PES membranes	<i>S. aureus</i> , <i>S. albus</i> , <i>E. coli</i>	Zone of inhibition; kill rate by colony counting method	~1-log reduction	30
	PET mesh	<i>E. coli</i> , <i>S. aureus</i>	Zone of inhibition; kill rate by UV-vis spectroscopy	~3-log reduction (>99.7% killed)	31
Drop casting/slurry with commercial AgNPs	Ceramic membranes	<i>E. coli</i>	Adhesion measured with atomic force microscopy (AFM)	Ag increases <i>E. coli</i> adhesion to surface	32
	PC-TE membranes	<i>M. avium</i> , <i>M. smegmatis</i> , <i>M. marinum</i>	Attachment via SEM imaging; kill rate by colony counting method	<1-log reduction after 48 h	33
Blending commercial AgNPs into polymer during fabrication	PLGA films	<i>E. coli</i> , <i>S. aureus</i>	Attachment via imaging; kill rate by colony counting method	<1-log reduction after 24 h; ~20% reduction in adhesion	34
	Electrospun PLA fibers	<i>S. epidermidis</i> , <i>S. aureus</i> , <i>P. aeruginosa</i>	Attachment and live-dead imaging assays	~1-log reduction in attachment after 24 h	35
	PSf UF membranes	<i>E. coli</i> , <i>P. mendocina</i>	Biofilm formation; kill rate by colony counting method	1-2-log reduction	36



control the delivery of biocidal agents from polymeric constructs, whether by enhancing wettability through surface activation/functionalization<sup>37-38</sup> or via thin film deposition or cross-linked layer formation.<sup>28, 39-42</sup>

Perhaps the most critical factor inhibiting the progress is the lack of quantitative analysis surrounding the antibacterial efficacy of Ag-releasing constructs. Equally as important is the development of standards by which to determine and discuss the effectiveness of such devices. Here, we fabricate a variety of Ag-loaded polymeric constructs, Fig. 4.2, such as those commonly fabricated for use as wound dressings, ultrafiltration membranes and tissue engineering scaffolds, to examine their efficacy against *E. coli*, a common strain isolated from hospital acquired infections. Using materials fabricated previously in our lab as well as materials reproduced from other relevant studies, we seek to explore the efficacy of AgNP-loaded materials as antibacterial devices, but also to provide a critical examination of the current literature and evaluation techniques employed for these materials. As such, this work attempts to understand how Ag can be incorporated, how Ag is retained, and characterize the nature of leaching, ultimately helping to assess whether these devices could be feasible to combat rising incidences of SSIs. In addition, we provide suggestions for best practices that could address some of the short comings in the literature and allow for a more rigorous approach to evaluating antibacterial biomaterials. Finally, we present select proof-of-concept blood TEG data that can be used in clinical settings to determine the practicality of interfacing a biomaterial with blood.



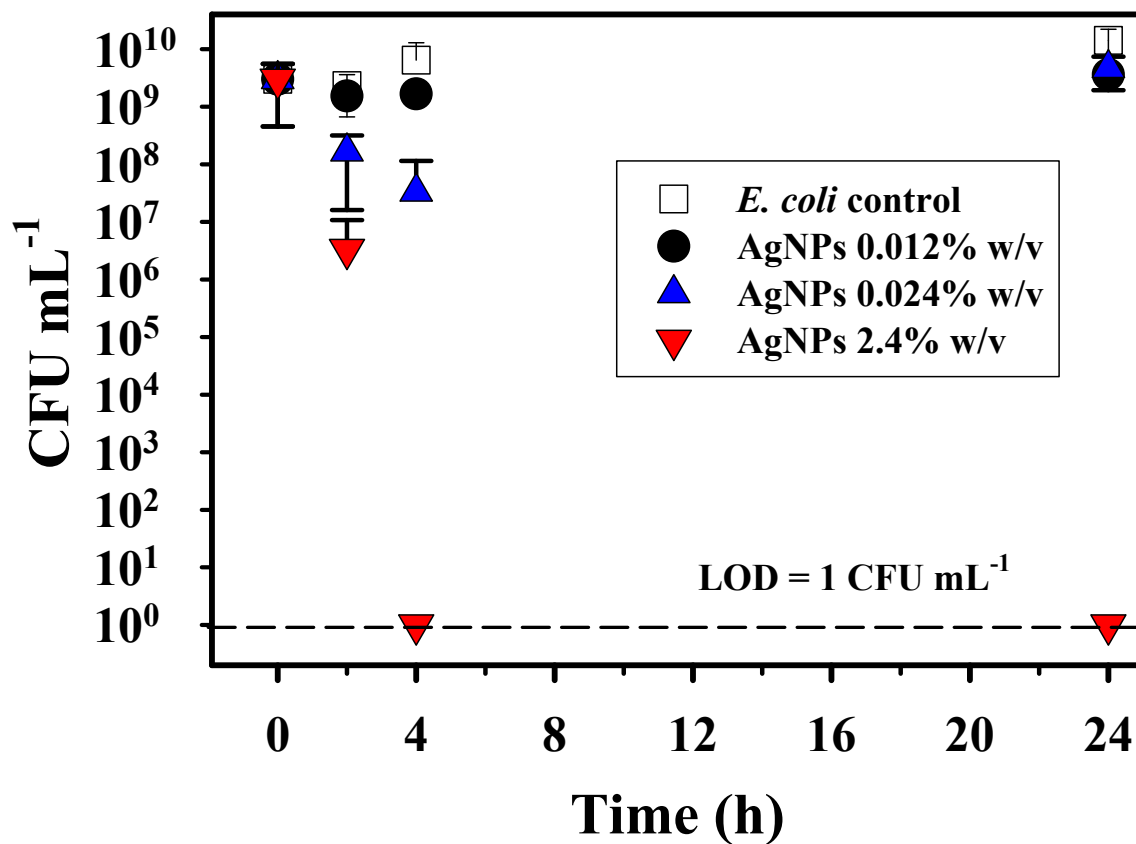
**Figure 4.2.** Schematic of the three fabrication techniques used to create the Ag-loaded polymeric constructs presented in this work.

## 4.2 Results

A range of fabrication and modification methodologies was explored to determine the efficacy of each technique to successfully incorporate AgNPs into polymeric constructs. A combination of surface and bulk compositional analysis as well as evaluation of Ag leaching from materials allows us to determine the ability of our Ag-loaded materials to release the biocidal agent into solution where it can act on bacteria.

As proof-of-concept, the biocidal activity of our commercial AgNPs was investigated via a colony-counting kill rate assay. Three concentrations of AgNPs in *E. coli* culture were examined and the number of CFUs per mL of culture is presented as a function of time in Figure 4.3. From these data, we observe the reduction in bacterial population depends on AgNP concentration. At the lowest concentration (0.012% w/v) of AgNPs, no noticeable reduction is observed after 2 h, and a <1-log decrease is observed after 4 h. After 24 h, there is no measurable population decline. When the concentration of AgNPs was doubled (0.024% w/v), a more substantial reduction was observed at both 2 and 4 h, ~1- and 2-log, respectively. After 24 h, however, the population of bacteria fully recovered to that of the *E. coli* control. This indicates that, at relatively low levels of AgNPs, bacteria could fully recover after 24 h, despite an initial observed reduction. When the concentration was significantly increased 100-fold to 2.4% w/v AgNPs, a 1-log reduction was observed after 2 h, and no colonies were observed after only 4 h, corresponding to a >7-log decrease. When the assay is extended to 24 h, we no longer observe bacterial recovery and the population remains such that no bacterial colonies are observed on plates, suggesting a much longer-lasting antibacterial effect.

*Incorporation of AgNPs.* As bacterial assays with AgNPs alone revealed the importance of concentration, a variety of concentrations were used for our constructs. The first metric to

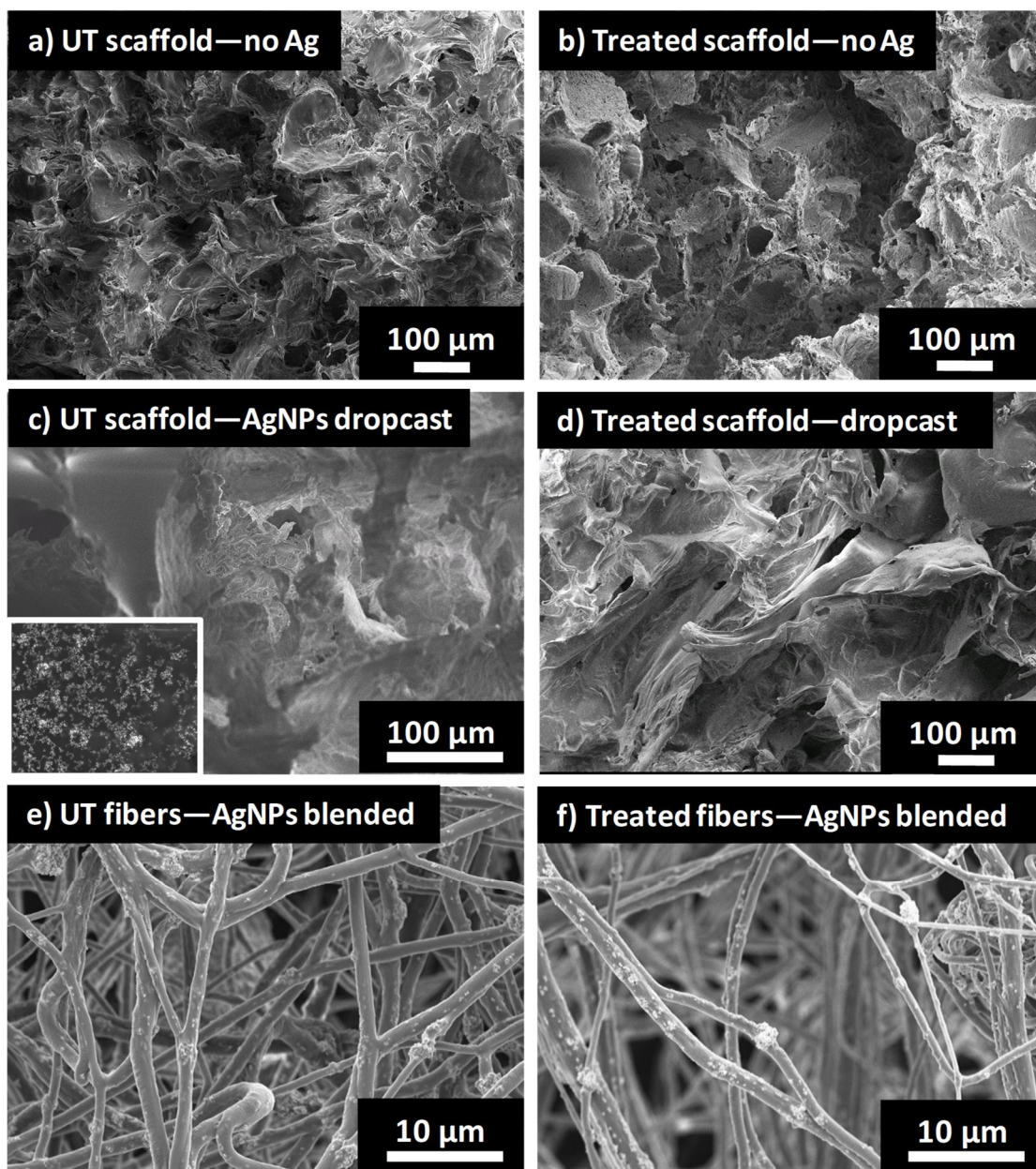


**Figure 4.3.** Number of CFUs mL<sup>-1</sup> versus time for various concentrations of AgNPs in *E. coli* culture.

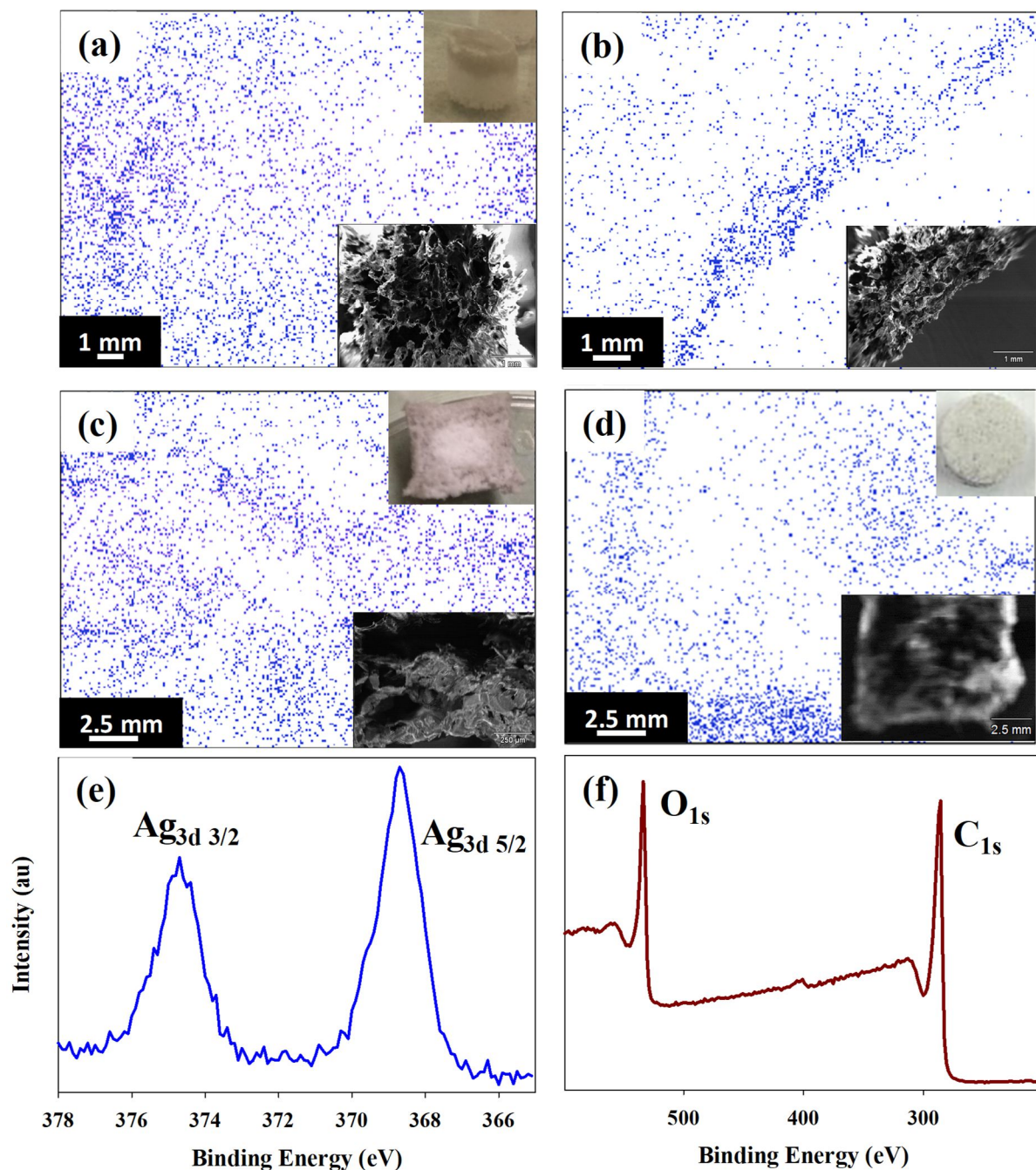
determine success of AgNP incorporation was visual inspection and identification of Ag in the bulk material. AgNPs were incorporated into 3D PCL scaffolds by drop-casting and blending into the polymer-solvent slurry, Fig. 4.2. Figure 4.2b shows a photograph of a AgNP-incorporated PCL scaffold alongside a PCL scaffold with no additives, with the color change showing that the Ag is indeed incorporated.

Although inspection of all materials revealed visible incorporation of AgNPs, SEM-EDS was used to map Ag in both the tops and cross sections of select Ag-loaded constructs. SEM images of PCL scaffolds before and after plasma surface modification (Fig. 4.4a-b) clearly show the porous interconnected morphology is maintained. Figures 4.4c-d show both untreated and plasma-treated scaffolds after dropcasting with AgNPs. These images demonstrate the bulk morphology undergoes no apparent change after AgNPs dropcasting. The inset provided in Figure 4.4c allows examination of AgNPs on the scaffold surface at higher magnification ( $\times 1500$ ). Similarly, SEM micrographs of the electrospun PCL fiber mats, wherein the AgNPs were blended during the fabrication process, indicate no apparent change in morphology or damage to the fibrous network result from AgNP incorporation or  $\text{H}_2\text{O}_{(v)}$  plasma surface modification (Fig. 4.4e-f).

Figure 4.5 shows SEM-EDS data for both the top and cross sections of PCL scaffolds loaded with AgNPs via drop casting and blending. EDS maps for untreated PCL scaffolds after drop casting are shown in Figure 4.5a-b. Viewing the scaffold from the top, Figure 4.5a, AgNPs appear relatively uniformly dispersed throughout the scaffold bulk. When viewing the cross-section, however, AgNPs primarily remain near the external surface of the material, as revealed by the band of Ag present in the map of the scaffold cross section, Figure 4.5b. In contrast, both the blending method and the method of drop casting AgNPs onto plasma-treated scaffolds



**Figure 4.4.** Representative SEM images showing (a) PCL scaffold as fabricated before Ag loading ( $\times 100$ ); (b)  $\text{H}_2\text{O}_{(\text{v})}$  plasma modified PCL scaffold before Ag loading ( $\times 100$ ); (c) top of PCL scaffold after dropcasting ( $\times 100$ ) with inset showing the cross section at  $\times 1500$  magnification; (d) cross section of  $\text{H}_2\text{O}_{(\text{v})}$  plasma treated scaffold after dropcasting ( $\times 100$ ); (e) 10% w/v AgNP-loaded PCL fibers ( $\times 2000$ ); and (f) AgNP-loaded  $\text{H}_2\text{O}_{(\text{v})}$  plasma modified PCL fibers ( $\times 2000$ ).



**Figure 4.5.** Representative EDS maps showing (a) untreated AgNP drop cast scaffold top and (b) cross section; (c) H<sub>2</sub>O(v) plasma treated AgNP drop cast scaffold cross section; and (d) cross section of scaffolds with 2.4% w/v AgNPs incorporated via blending. Insets in (a)-(d) show corresponding SEM image for each EDS map. A representative Ag<sub>3d</sub> XPS spectrum is shown in (e) for drop cast scaffolds and a survey scan is shown in (f) for scaffolds with blended AgNPs.

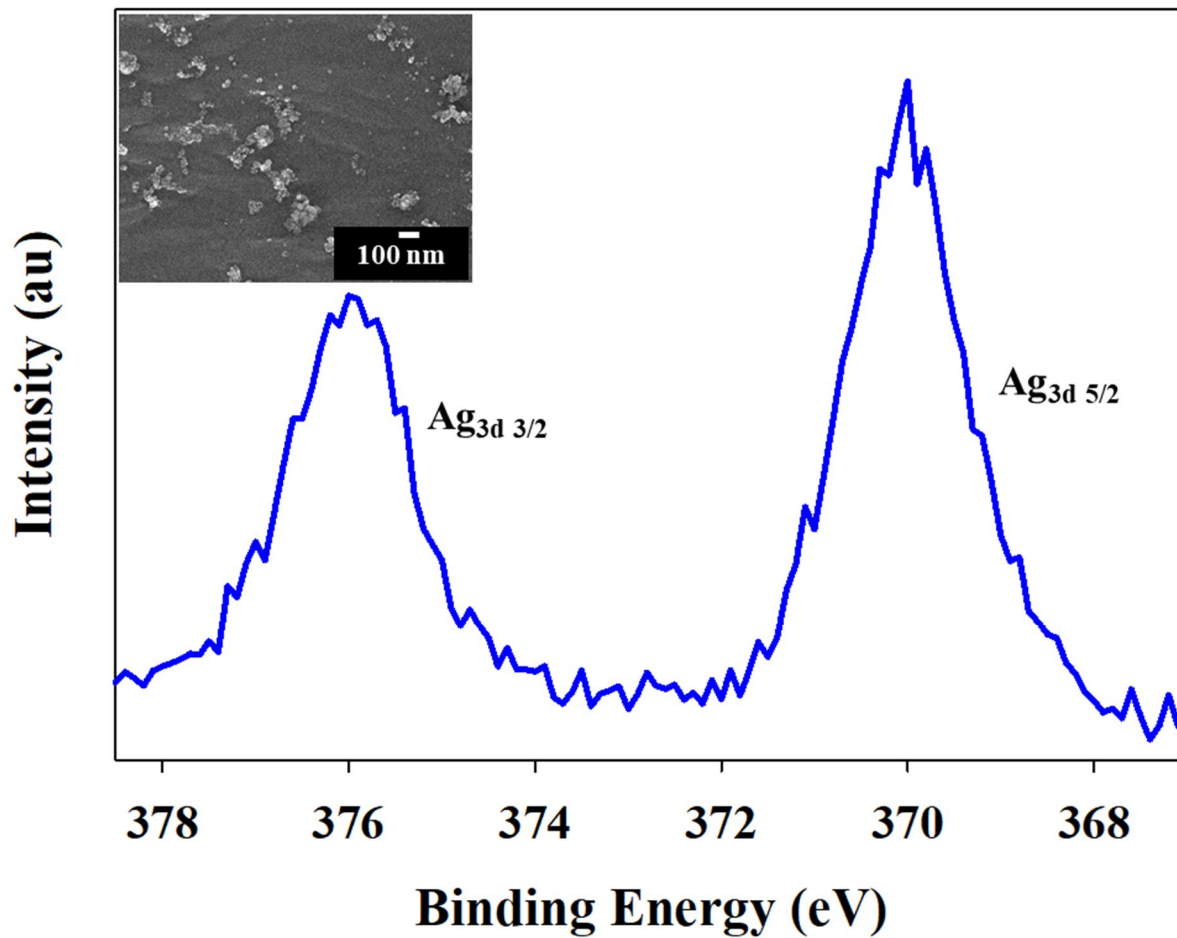
provide superior results with respect to dispersed incorporation of commercial AgNPs, Fig. 4.5c-d.

*Surface analysis (XPS and WCA goniometry).* As plasma surface modification was performed to increase AgNP incorporation by enhancing material wettability, WCA goniometry was completed on materials as fabricated, after Ag incorporation, and after plasma treatment. Untreated PCL scaffolds with no AgNPs have a static water contact angle of  $\sim 120^\circ$ . Upon AgNP incorporation, the water contact angle is unchanged. After water plasma surface modification, however, dynamic WCA measurements on treated PCL scaffolds show drop absorption occurs in  $< 1.5$  s, thus our scaffolds are nominally hydrophilic.

As surface-available Ag is critical to the success of Ag-loaded constructs for drug delivery systems, XPS was used to determine surface Ag composition of drop cast scaffolds, blended scaffolds and PCL films with surface immobilized AgNPs. A representative Ag<sub>3d</sub> high-resolution XPS spectrum for drop cast AgNP-loaded scaffolds is shown in Fig. 4.5e, revealing significant Ag on the surface ( $\sim 20\%$ ). Scaffolds loaded with AgNPs via blending, however, exhibited no detectable Ag presence on the surface, Fig. 4.5f, despite having a significantly higher concentration of AgNPs. Spin coated PCL films with AgNPs reduced *in situ* contained a significant amount of Ag ( $54.2 \pm 0.4\%$ ) on the surface (spectra with SEM image shown in Figure 4.6).

*Biocidal Evaluation of Ag-loaded constructs.* Having determined how bacteria are sensitive to  $[\text{Ag}^+]$  in solution, it is critical to determine how to incorporate AgNPs into polymeric constructs such that  $[\text{Ag}^+]$  released is sufficient and controllable. Table 4.2 summarizes results from kill rate assays using commercial AgNPs and Ag-loaded constructs fabricated in our lab, as well as other biocidal materials we have previously fabricated, to serve as a comparison. As





**Figure 4.6.** Representative  $Ag_{3d}$  XPS spectrum for Ag-loaded spin-coated PCL films with SEM image inset (30,000  $\times$ ).

**Table 4.2.** Summary of results from kill rate assays for Ag-loaded polymeric materials.<sup>a, b</sup>

Antimicrobial agent	Material	% reduction			Strain(s)	Ref
		2 h	24 h	48 h		
AgNPs	AgNP solution (2.4%)	99 ± 3	99.999999 <sup>c</sup>	99.999999 <sup>c</sup>	<i>E. coli</i>	this work
	Ag scaffolds (2.4% blended)	10 ± 45	~0	53 ± 2	<i>E. coli</i>	this work
	Ag fibers (10% blended)	71 ± 23	31 ± 42	7 ± 20	<i>E. coli</i>	this work; 12
	Ag-PCL film ( <i>in situ</i> reduction)	67 ± 54	~0	~0	<i>E. coli</i>	30
	AgNP drop cast UF membranes	—	—	36 ± 27	<i>E. coli</i>	33
NO	NO-releasing Tygon® films	~0	99.999999 <sup>c</sup>	99.999999 <sup>c</sup>	<i>E. coli</i> and <i>S. aureus</i>	37
	<i>S</i> -nitrosated dextran-cysteamine	99.99-99.9999 <sup>d</sup>	99.999999 <sup>c</sup>	99.999999 <sup>c,e</sup>	<i>E. coli</i> , <i>A. baumannii</i> , and <i>S. aureus</i>	43

<sup>a</sup> Values reported as mean ± standard deviation for n ≥ 9

<sup>b</sup> ~0% indicates no measurable reduction was achieved whereas “—” indicates measurement was not made

<sup>c</sup> 8-log reduction; assumes assay LOD = 1 CFU mL<sup>-1</sup> and starting CFU mL<sup>-1</sup> on the order of 10<sup>9</sup>

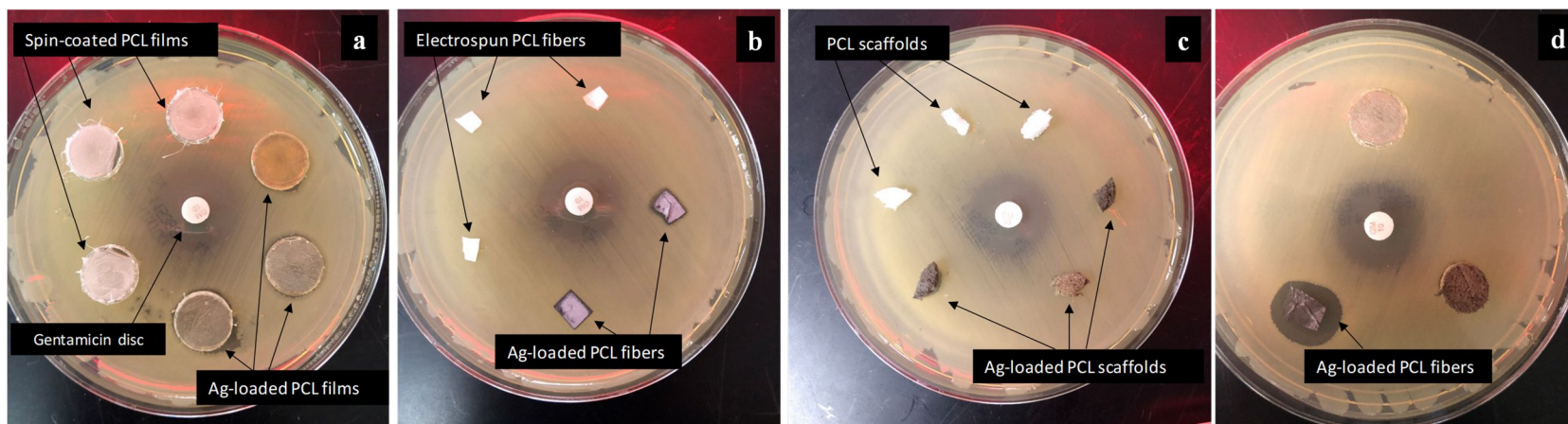
<sup>d</sup> ~2-4-log reduction was observed, depending on bacterial strain

<sup>e</sup> 8-log reduction was observed up to 72 h

discussed above, AgNPs (2.4% w/v) in solution exhibit a 2-log reduction after 2 h and an 8-log reduction after 24 h. This antibacterial activity was maintained up to 48 h. For polymeric materials loaded with AgNPs as a biocidal agent, however, we observe no substantial reduction (i.e., <1-log) in bacterial population, even after 48 h. This lack of biocidal activity resulting from Ag-loaded constructs appears independent of the method of Ag loading or material fabrication.

*Zone of inhibition method.* Zone of inhibition assays were employed as a potential alternative method to assess biocidal activity of the Ag-loaded constructs. Representative photographs showing zone of inhibition results are presented in Figure 4.7 for AgNP-loaded PCL films (Fig. 4.7a), fibers, (Fig. 4.7b), and scaffolds (Fig. 4.7c). Identical materials without AgNPs were also analyzed to serve as material controls. No zones of inhibition were observed for any materials not containing AgNPs. For control Gentamicin antibiotic disks, inhibition zones measured  $6 \pm 1$  mm. In general, no zones of inhibition were observed for any of our Ag-loaded materials. We observed one notable exception to this, evident when comparing the Ag-loaded fibers in Fig. 4.7b ( $\sim 6 \times 4$  mm) to those in Fig. 4.7d ( $\sim 8 \times 6$  mm). A zone of inhibition of  $5 \pm 2$  mm was observed for the larger fiber mats, yet none was observed for the fiber mats of smaller dimensions, despite being cut from the same fiber mat.

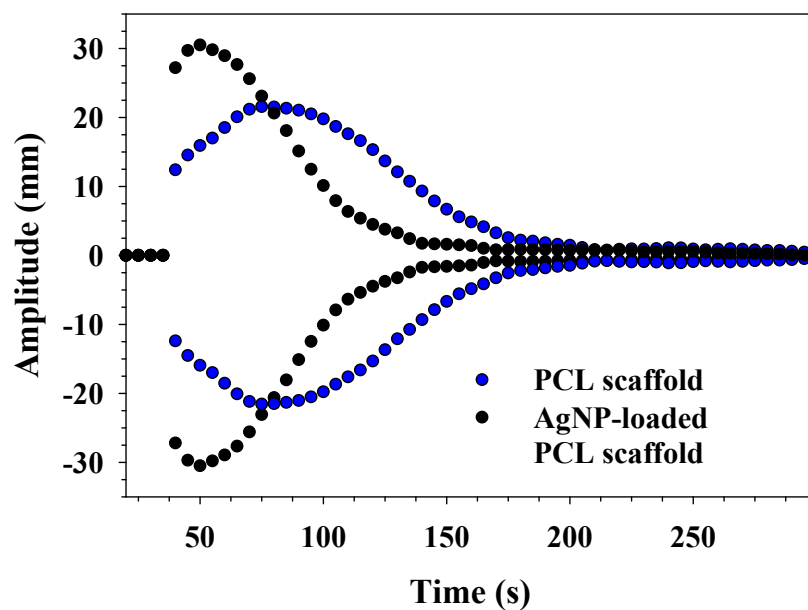
*Leaching analysis.* Leaching studies were also completed for PCL scaffolds loaded with 0.024% and 2.4% w/v AgNPs. As the nature of the scaffold fabrication process inherently exposes Ag-loaded scaffolds to water, the water used for the salt leaching steps was subjected to analysis of Ag content via AAS to determine if any loss of Ag occurred for the blended constructs. Testing aliquots shortly after immersion of AgNP-loaded scaffolds in water for porogen leaching accounts for any unblended Ag lost from the surface to be measured. In contrast, analyzing water used for porogen leaching in the days after the initial immersion allows



**Figure 4.7.** Representative photographs of zone of inhibition assay for (a) spin-coated PCL films; (b) small ( $\sim 6 \times 4$  mm) electrospun PCL fibers mats; (c) PCL scaffolds; (d) large Ag-loaded PCL fiber mats ( $\sim 8 \times 6$  mm).

us to determine if Ag is continually released after any surface Ag is lost. In summary, for AgNP-loaded scaffolds at both 0.024% and 2.4%, very low (~ppb) concentrations of  $\text{Ag}^+$  were detected in water after ~4 h of leaching. No Ag was detected beyond 24 h of leaching. Results from testing water used for leaching 0.024% Ag scaffolds revealed a maximum of <0.1 ppm Ag was reached during the entire leaching process. Leaching of 2.4% Ag scaffolds revealed  $[\text{Ag}] < 0.5$  ppm. For fabricated films with Ag immobilized on the surface,  $[\text{Ag}^+] < 0.1$  ppm was reached after 1 h, reaching a maximum of 0.13 ppm after 24 h. Overall, we found minimal amounts of  $\text{Ag}^+$  were released from the scaffolds (<0.5 ppm) and films (~0.1 ppm) upon immersion in aqueous solutions.

Finally, as proof-of-concept, we completed an initial assessment of the blood coagulation dynamics of our AgNP-loaded scaffolds and electrospun fibers. Fig. 4.8. displays traces from TEG measurements for unmodified and AgNP-loaded PCL scaffolds. In short, the black trace corresponding to AgNP-loaded PCL scaffolds has both a larger maximum amplitude and a faster time to maximum amplitude, revealing PCL scaffolds become somewhat thrombogenic upon loading with AgNPs. Values derived from these traces emphasize this result (Table 4.3). The average maximum amplitude for PCL scaffolds is equal to  $35.1 \pm 0.6$  mm whereas the average amplitude increases to  $65.5 \pm 15.5$  mm upon AgNP incorporation. Note the time to maximum amplitude also increases from  $6.3 \pm 2.4$  mm to  $12.4 \pm 5.6$  mm upon nanoparticle addition, yet this increase is not statistically significant within combined experimental error. The maximum rate of thrombin generation appears to increase dramatically from  $12.3 \pm 1.1$   $\text{dyn cm}^{-2} \text{ s}^{-1}$  to  $57.4 \pm 35.0$   $\text{dyn cm}^{-2} \text{ s}^{-1}$ , yet we note the large error on this value for AgNP-scaffolds. For AgNP-loaded electrospun fibers, we see no notable change in blood coagulation dynamics compared to control PCL fibers.



**Figure 4.8.** Thromboelastographic traces demonstrating the clotting formation dynamics for canine blood plasma interfaced with both as-fabricated (blue) and biocide-loaded (black) porous polycaprolactone (PCL) scaffolds. Traces are representative of  $n = 3$  samples examined.

**Table 4.3.** Thromboelastographic data for blank cups, control scaffolds and fibers, and AgNP-loaded scaffolds and fibers.<sup>a</sup>

<b>Material [tested with canine blood plasma]</b>	<b>Reaction time (min)</b>	<b>MA (mm)</b>	<b>TA (min)</b>	<b>MRTG [(dyn/cm<sup>2</sup>)/s]</b>	<b>TMRTG (min)</b>
Blank cup (no substrate)	1.3 ± 0.7	19.4 ± 3.7	4.9 ± 3.7	5.5 ± 1.3	1.8 ± 0.2
PCL scaffold	1.2 ± 0.6	35.1 ± 0.6	6.3 ± 2.4	12.3 ± 1.1	1.7 ± 0.5
10% Ag PCL scaffold	0.8 ± <0.1	65.5 ± 15.5	12.4 ± 5.6	57.4 ± 35.0	0.7 ± 0.5
Electrospun PCL fibers	0.5 ± 0.3	25.5 ± 2.2	8.2 ± 0.2	7.7 ± 0.8	1.1 ± 0.3
10% Ag PCL fibers	0.6 ± 0.3	21.6 ± 3.1	6.9 ± 1.5	5.5 ± 2.6	1.4 ± 0.5

<sup>a</sup> Values reported as mean ± standard deviation for n ≥ 3

### 4.3 Discussion

The development of biomedical devices that deliver AgNPs and similar biocidal agents requires comprehensive assessment of the agent-bacterial interactions as the drug is released from the polymer. Here, we discuss the antibacterial efficacy of several AgNP-loaded polymeric materials as well as how this relates to the method of incorporation (e.g., covalently bound vs. “resting” (i.e., physisorbed) on surface vs. physically encapsulated).

*Evaluating bactericidal efficacy.* For AgNPs alone, kill rate assays revealed antibacterial activity over time clearly depends on Ag concentration. Because the colony counting method allows us to distinguish between both small (<1-log) and large (>8-log) reductions, we can observe small declines in bacterial populations after 2 and 4 h with lower concentrations of Ag, indicating that there may be an initial biocidal action, but recovery occurs before 24 h of exposure has passed. For larger concentrations, however, this population decline remains over time, indicating bacteria are likely fully eradicated. Because 99% of bacteria can be killed and the remaining 1% is sufficient to lead to a substantial and rapid recovery in population, it was critical that we analyze bacterial population over both longer and shorter time scales, as recovery phenomena can and do occur. Moreover, achieving sufficient AgNP incorporation and tunable Ag<sup>+</sup> release is imperative in the development of our polymeric constructs loaded with AgNPs.

Kill rate data for drug-incorporated polymeric constructs fabricated in our laboratory are displayed in Table 4.2. Also listed in Table 4.2 for comparison are selected previously published data for nitric oxide (NO)-releasing polymeric materials, highlighting our ability to fabricate and analyze drug-loaded polymeric materials that result in very large (>8-log) bacterial population reductions.<sup>37, 44</sup> Compared to other drug-releasing polymers and AgNPs in solution, however, our AgNP-loaded constructs are largely ineffective at killing bacteria in bulk solution.



Moreover, our zone of inhibition results appear consistent with the kill rate studies, with both assays revealing no biocidal activity (likely signifying no Ag release) after up to 36 h. One notable exception manifested in two outcomes for AgNP-loaded electrospun fibers, reinforcing the strong dependence of the zone of inhibition method on sample size, and reiterating the importance of controlling Ag delivery from these materials. In comparing our biological performance outcomes to those in the associated literature (Tables 4.1 and 4.2), we see that our results are largely in agreement, namely having only small, insignificant reductions in population and no reproducible zone of inhibition results observed. Overall, neither the short nor long term effects of these materials live up to what we observe with commercial antibiotics. It is notable that the literature is rife with studies claiming strong antibacterial activity using the zone of inhibition method as the sole method of evaluating this claim. Given that there is often little or no information regarding the impact of sample size on the stated results, this represents an opportunity for the community to enhance the rigor of the evaluation methods used for antimicrobial biomaterials. This is discussed further below.

*Evaluating success of Ag incorporation.* If we define “incorporation of AgNPs” as AgNPs existing either on the material surface or in the bulk construct, here we have demonstrated AgNPs are successfully incorporated in polymeric constructs using various fabrication methodologies. For AgNP drop casting onto PCL scaffolds, we found plasma treatment significantly improves the uniformity of incorporation, likely because of improved hydrophilicity induced by the surface modification that allows for deeper penetration of the AgNP-containing solution. Importantly, the porous morphologies of our scaffolds and fibers are maintained after H<sub>2</sub>O<sub>(v)</sub> plasma surface modification as well as after AgNP incorporation. As wettability depends on both surface chemical composition and surface roughness, and SEM micrographs of untreated

and treated PCL scaffolds indicate no apparent change in morphology or damage to the interconnected porous network (Fig. 4.4), we can attribute the observed increase in wettability primarily to the chemical modification of the polymer. Previously reported XPS spectra for H<sub>2</sub>O<sub>(v)</sub> plasma modified PCL scaffolds and similar polymeric materials indicates surface oxygen content is significantly enhanced by plasma treatment, rendering polymeric materials more wettable.<sup>37, 44-45</sup>

A key objective of this work is to determine via compositional analysis techniques if AgNPs are on the surface and thus capable of being oxidized to Ag<sup>+</sup> upon exposure to biological environments. XPS and EDS aided in determination of both surface and bulk composition, respectively. Some challenges arose when assessing the composition of materials loaded with AgNPs, specifically difficulty in measuring elemental Ag on the surface of the constructs using XPS. For example, XPS detected no Ag on the blended scaffold top or cross section surface. EDS, however, revealed the presence of AgNPs throughout the bulk of the construct, signifying, along with photographs and leaching data, the incorporated Ag remained in the polymeric constructs, even after the soaking process. For both materials loaded with AgNPs via *in situ* reduction, Ag was detected on the surface via XPS. Compared to films ( $54.2 \pm 0.4\%$  Ag), porous scaffolds exhibited slightly less Ag (~20%) on the surface, despite their larger surface area. Note, however, that because the materials have drastically different morphologies (flat versus porous and rough), direct comparisons of the surface Ag content are difficult to make.

These results from compositional analyses suggest much of the Ag present may be encapsulated in the polymer matrix in the case of Ag-loaded scaffolds and fibers, as Ag was introduced when the polymer-solvent solution was gel-like and not dried. Upon solvent evaporation and subsequent drying, it is likely that most of the AgNPs are fully surrounded by

polymer, and what remains on the surface is lost during porogen leaching, rinsing steps, or during initial exposure to biological solution (i.e., an initial burst of drug release upon immersion in bacterial culture). Especially for our electrospun fibers, we see biocidal activity may decrease slightly from 2 h ( $71 \pm 23\%$  reduction) to 48 h ( $7 \pm 20\%$  reduction), possibly indicating an initial burst of Ag release. Here, however, we show evidence that leaching of surface available Ag from scaffolds likely occurs on time scales shorter than is necessary to leach the porogen. Similarly, several others hypothesize encapsulation by polymeric matrix prevents release of Ag<sup>+</sup> into biological solution.<sup>46-47</sup> Zodrow and coauthors found that 90% of Ag remains in their polymeric membranes, even after filtration of 4 L of DI water, with Ag lost only from the surface. This depletion of surface Ag was accompanied by a reduction in material antimicrobial performance (for *E. coli* and *Pseudomonas mendocina*), though the percent reduction is unspecified.<sup>36</sup> Martinez Abad et al. found their AgNP-loaded electrospun fibers (fabricated by thermal reduction of Ag-containing salt blended with the solvent mixture prior to electrospinning) were homogeneously incorporated with AgNPs.<sup>46</sup> The nanoparticles, however, were retained in the fibers, substantially decreasing their ability to release (i.e., almost all Ag remained after 24 h soaking time).<sup>46</sup> Moreover, the authors found a correlation between thermal annealing time and decreased antibacterial performance (for *Listeria monocytogenes* and *Salmonella enteric*). For similar electrospun Ag-polyurethane composite nanofibers, Sheikh et al. found the number of nanoparticles in the fiber bulk is high (as seen in TEM images) compared to relatively few on the surface (as assessed via SEM).<sup>48</sup> The authors attribute this not only to encapsulation of the AgNP by the polymer, but also to the branched nature of polyurethane, which provides a matrix that imprisons the AgNPs after fabrication. No Ag is lost from the fibers during a 25 h agitated washing period.<sup>48</sup> In some cases, AgNP encapsulation can

occur even without their incorporation into polymeric materials. In work by El-Kheshen and coworkers, the effect of reducing and protecting agents on AgNP antibacterial activity was investigated.<sup>47</sup> The authors found Ag was encapsulated in the case where glucose was used as a reducing agent; thus, no Ag released and no inhibition zone was observed. This once again illustrates the importance of ensuring AgNPs alone are effective biocidal agents before incorporation into the nanocomposite.

Strategies employed to mitigate poor antibacterial performance. Several studies have extended the fabrication methodologies outlined in Table 1 to further modify materials in an attempt to improve antibacterial performance of AgNP-loaded materials. In particular, some researchers have attempted to circumvent AgNP encapsulation via plasma treatment, as certain plasmas can etch or ablate polymers.<sup>25, 34, 49</sup> In one example, España-Sanchez and coworkers fabricated Ag nanopowder-polypropylene nanocomposites films via melt casting.<sup>25</sup> The as-fabricated materials exhibited no antibacterial behavior; however, when these materials were Ar plasma treated to enhance surface nanoparticle exposure, a small (85-99%) reduction in *S. aureus* and *Pseudomonas aeruginosa* after 3-6 h was observed. During melt mixing, the authors believe nanoparticles become embedded in the polymer. They hypothesize that even the near-surface NPs remain tightly embedded and if ion diffusion occurs, it is slow.<sup>25</sup> As a result of exposure to air after surface activation by the Ar plasma, surface oxygen and nitrogen content increased and the material wettability was enhanced, which the authors posit likely enhanced the interaction of aqueous bacterial cultures with the composite material. In a related study, Fortunati et al. found oxygen plasma treatment of AgNP-loaded PLGA films, similar to those fabricated herein, results in an increase in bacteria killed from ~30% to ~90%. The increases in antibacterial activity of these AgNP-loaded constructs post plasma etching, albeit arguably small,

suggests encapsulation of the nanoparticle may indeed be preventing Ag release. Nevertheless, etching the surrounding polymer from the embedded AgNP may not be a productive route to achieve improved AgNP-loaded materials, as control of AgNP release kinetics and mitigation of possible damage to the polymer matrix is imperative.

In cases where AgNPs are incorporated by *in situ* reduction and/or surface immobilization, there are two possible factors that may compromise construct efficacy. First, AgNPs could be bound too strongly to the surface. Indeed, Monteiro et al. discuss how AgNPs are strongly fixed to the native poly(methyl methacrylate) polymer of their Ag-loaded denture resin such that no release of Ag<sup>+</sup> occurs even after 120 days of leaching.<sup>26</sup> Alternatively, if AgNPs are not bound too strongly and do indeed release, there may be few surface available AgNPs because of limited surface area afforded by the construct architecture. For example, spin-coated polyurethane-Ag nanocomposite films fabricated by Hsu and coauthors released insufficient Ag<sup>+</sup> to reach an effective antibacterial concentration, with all materials exhibiting <2 log reduction in growth for *E. coli* and Ag<sup>+</sup>-resistant *E. coli*.<sup>23</sup> Similar to our leaching results presented herein, the authors of this study also found maximum concentrations of leached Ag<sup>+</sup> of ~0.5 ppb.<sup>23</sup> These polyurethane-Ag composite films are limited in surface area by their relatively flat morphology; without sufficient AgNP interacting with aqueous media, no release of the biocidal Ag<sup>+</sup> will occur.

In an attempt to mitigate limited surface-immobilized Ag, Kumar et al. fabricated Ag-loaded polyethylene terephthalate (PET) mesh materials via *in situ* reduction of AgNO<sub>3</sub>.<sup>31</sup> The authors provide evidence of Ag on the surface, yet, despite the relatively large surface area-to-volume ratio of the mesh material, the authors failed to achieve sufficient Ag release in a controllable manner and described observing a “discontinuous release of inadequate concentration of active

silver ion from metal form.”<sup>31</sup> In these cases, because performance drops sharply over time, these materials are likely unsuitable for long-term use because of the limited amount of surface available Ag, and more importantly, the challenge in controlling Ag<sup>+</sup> delivery. Furthermore, control of Ag delivery is also required to avoid delivering cytotoxic levels of Ag to the patient. Unfortunately, a majority of studies span relatively short time spans ( $\leq 24$  h), thus limiting the ability to discern both the short and long-term efficacy of the material. From this emerges a lack of discussion of how the fabrication methodology may ultimately affect the kinetics of Ag<sup>+</sup> release, potentially limiting our development of longer lasting materials that may shorten healing time.

*Recommendations for Best Practices.* As the efficacy of AgNP-loaded polymeric constructs is disparate throughout the large body of literature focused on fabrication of materials for wound dressings and tissue engineering, our work encourages better evaluation and reporting of such materials towards ultimately reaching a standard of research for these materials. Here, we presented results from biocidal assays for a variety of AgNP-loaded polymeric constructs. In light of the results from our studies and comparison to the literature, we present a few recommendations for the collection and analysis of biological data in the context of determining if AgNP-loaded polymers provide antibacterial effects.

Overall, it is imperative to utilize appropriate techniques that consider the needs of the application in their design. First, full details on fabrication and biological assessment methods must be provided to accurately convey biological results. This includes adhering to appropriate established standardized testing protocols. For example, a common discrepancy in this literature is the use of inoculating cultures of populations that vary by several orders of magnitude (5-6). Starting cultures should have populations of  $>10^6$  CFUs per mL for the assays employed

herein.<sup>50</sup> When smaller starting populations are used, the log reduction that can be measured is inherently limited. For example, when cultures of  $10^5$  are used, at best only 5-log reductions can be measured.<sup>29, 51</sup> Thus, the efficacy and accuracy of the measurement is significantly reduced.

Another glaring gap in the design of biological experiments is the lack of sufficient time points. As surfaces are susceptible to significant bacterial colonization in as few as 6 h after contact, short-term, fast-acting antimicrobial activity is essential. Zone of inhibition and similar semi-quantitative assays can provide rapid, valuable information about the minimum inhibitory concentration of a drug as well as information about resistance; however, these assays are fundamentally incapable of revealing large reductions in bacterial populations.<sup>11, 52</sup> Moreover, there is no quantitative way to measure recovery, thus this technique alone cannot reveal the ability of a wound dressing to resist bacterial proliferation for hours or days after placement. Long-term antibacterial activity (i.e., 2-4 days), however, is also needed to mitigate frequent changing of dressings and prevent disturbance to the wound site. To reveal the immediate effects of a drug-releasing material, the bacterial population should be quantified in the minutes and hours after implementation, using the time kill colony counting or similar method. By combining an array of techniques, studies can achieve the temporal resolution critical to verify biological outcomes of drug-releasing materials.

Next, when analyzing data and considering whether a material falls in the class of antibacterial materials, it is crucial to complete comprehensive characterization to capture both qualitative and quantitative aspects of antibacterial behavior. Cavanagh et al. completed a study comparing the activity of numerous newer commercially available silver dressings.<sup>11</sup> The goal of the study was to confirm assertions of several commercially available Ag-releasing wound dressing products claiming to have antibacterial activity lasting days. Only two of the products

produced a log reduction in CFUs mL<sup>-1</sup>; the largest log reduction was ~3 and most were <1. One sample that produced a measurable zone of inhibition did not result in a log reduction in CFUs mL<sup>-1</sup>. Clearly, these results demonstrate single assays simply do not provide sufficient information to deem a material “antibacterial”. Combinations of complementary tests should be utilized in analysis of drug-loaded wound dressings and similar materials.

As important as utilizing numerous techniques is considering important limitations of each technique, such as the LOD, limit of quantification (LOQ), and the sensitivity, among others. Compared to zone of inhibition and spectroscopic techniques, the colony counting method is advantageous as it has a lower LOD and greater sensitivity.<sup>50, 53</sup> These qualities are critical as relatively small (2-3-log) reductions provide an opportunity for surviving bacteria to easily recover on time scales relevant to the applications discussed herein (<24 h). Too often results are not placed within the context of the biological technique used to gather the data or the needs of the clinical settings where the devices are intended to be deployed. This ultimately leads to a misrepresentation of the biological results and overrepresentation of the clinical relevance of the material.

Lack of language specificity and the reporting of non-quantitative results further complicates the interpretation of the literature. For example, statements claiming materials “caused a reduction in survival from 81% to 10% within 12 h” leading the authors to conclude that “the scaffolds clearly display a broad-spectrum activity” fails to acknowledge that this is <1-log reduction.<sup>29</sup> In another example, Kumar et al. state “high percentage reduction values of >99.7% obtained for both types of bacteria” for their PET mesh materials.<sup>31</sup> Notably, statistical error is not considered in either of these examples, and given the nature of typical bacterial assays and the impact of stochastic behavior, the error associated with the technique alone is often on the



order of 1-2-log. Likewise, vague descriptions of biological observations are unhelpful and do not accurately convey results. Phrases such as “almost no bacterial colony is seen after 12 h of treatment.”<sup>29</sup> and “almost the whole silver content is retained in the fibers”<sup>46</sup> contain vague and contradictory language. When log reductions of 2-3 are deemed adequate, there emerges a failure to consider why larger log reductions (e.g., equivalent to AgNPs alone) are not achieved and how drug release kinetics can be effectively tuned to bring clinically relevant antibacterial results. In short, data should be reported as quantitatively as possible and statistical error must always be considered.

Improving antibacterial materials for advanced medical devices requires appropriate interpretation of bacterial assays to avoid the misinformation often perpetuated by over interpretation of assay results. As important as considering bacterial interactions is the necessary evaluation of blood interactions with biocide-loaded materials. Though not the focus of this chapter, we have also presented selected proof-of-concept data demonstrating how changes in blood coagulation dynamics arising from blood plasma-AgNP interactions are measured. In short, no notable change in thrombogenic behavior is observed after addition of AgNPs into the materials, indicating the potential for *in vivo* implementation. An undeniable amount of progress has been made in the field to enhance the biocompatibility of AgNP-polymer composites, yet many such devices are not approved for medical use. To further advance antibacterial biomaterial development, it is imperative to consider that zone of inhibition assays and time-kill assays are not a sufficient measure of antibacterial efficacy when used alone. The clinical relevance of a material largely depends on the magnitude of antibacterial activity as well as the time frame of killing. Thus, studies on these materials and continued characterization of their leaching and biological behavior upon interfacing with biological systems must be obtained.

#### 4.4 Summary and conclusions

Achieving controllable incorporation and release of Ag and similar biocidal agents, combined with hydrophilic surface modification, is a substantial advancement towards reducing SSI occurrence in hospitals. Overall, the data presented herein suggest challenges arise when AgNPs are incorporated into polymeric constructs like those typically used in biomedical applications. Our results suggest the efficacy of AgNPs as biocidal agents substantially diminishes when encapsulated by the polymer matrix, making it difficult for Ag<sup>+</sup> to reach biological solution to interact with bacterial cells. Plasma surface modification alleviates some of this, but also introduces the potential for polymer degradation. A review of the literature suggests disparate, vague and non-specific language and context are used when discussing results from bacterial assays. In particular only a single antibacterial assay is employed in most studies, where multiple assays would provide better insight into the antimicrobial activity. Furthermore, a discussion of results in the context of biomedical settings is glaringly absent. We argue the importance of critically evaluating the Ag<sup>+</sup> release from these materials and its effect on bacterial populations. Quantitative analysis of these effects using techniques that allow for maximum temporal and spatial resolution is essential to guide further development of materials for drug delivery, wound healing, and tissue engineering.

## REFERENCES

1. Anderson, D. J.; Podgorny, K.; Berrios-Torres, S. I.; Bratzler, D. W.; Dellinger, E. P.; Greene, L.; Nyquist, A. C.; Saiman, L.; Yokoe, D. S.; Maragakis, L. L.; Kaye, K. S., Strategies to prevent surgical site infections in acute care hospitals: 2014 update. *Infect Control Hosp Epidemiol* **2014**, *35* (6), 605-627.
2. Magill, S. S.; Edwards, J. R.; Bamberg, W., Multistate point-prevalence survey of health care-associated infections. *N Engl J Med* **2014**, *370*, 1198-1208.
3. Vasudev, M. C.; Anderson, K. D.; Bunning, T. J.; Tsukruk, V. V.; Naik, R. R., Exploration of plasma-enhanced chemical vapor deposition as a method for thin-film fabrication with biological applications. *ACS Appl Mater Interfaces* **2013**, *5* (10), 3983-3994.
4. Bazaka, K.; Jacob, M. V.; Chrzanowski, W.; Ostrikov, K., Anti-bacterial surfaces: natural agents, mechanisms of action, and plasma surface modification. *RSC Adv* **2015**, *5* (60), 48739-48759.
5. Marambio Jones, C.; Marambio-Jones, C., A review of the antibacterial effects of silver nanomaterials and potential implications for human health and the environment. *J Nanopart Res* **2010**, *12* (5), 1531-1551.
6. Hasan, J.; Crawford, R. J.; Ivanova, E. P., Antibacterial surfaces: the quest for a new generation of biomaterials. *Trends Biotechnol* **2013**, *31* (5), 295-304.
7. Moura, L. I.; Dias, A. M.; Carvalho, E.; de Sousa, H. C., Recent advances on the development of wound dressings for diabetic foot ulcer treatment--a review. *Acta Biomater* **2013**, *9* (7), 7093-7114.
8. Russell, A. D.; Hugo, W. B., Antimicrobial activity and action of silver. *Prog. Med. Chem.* **1994**, *31*, 351-371.
9. Kumar, R.; Munstedt, H., Silver ion release from antimicrobial polyamide/silver composites. *Biomaterials* **2005**, *26* (14), 2081-2088.
10. Taylor, P. L.; Ussher, A. L.; Burrell, R. E., Impact of heat on nanocrystalline silver dressings. Part I: Chemical and biological properties. *Biomaterials* **2005**, *26* (35), 7221-7229.
11. Cavanagh, M. H.; Burrell, R. E.; Nadworny, P. L., Evaluating antimicrobial efficacy of new commercially available silver dressings. *Int Wound J* **2010**, *7* (5), 394-405.
12. Sumitha, M. S.; Shalumon, K. T.; Sreeja, V. N.; Jayakumar, R.; Nair, S. V.; Menon, D., Biocompatible and antibacterial nanofibrous poly( $\epsilon$ -caprolactone)-nanosilver composite scaffolds for tissue engineering applications. *J Macrom Sci* **2012**, *49* (2), 131-138.
13. McDonnell, G.; Russell, A. D., Antiseptics and disinfectants: activity, action, and resistance. *Clin Microbiol Rev* **1999**, *12* (1), 147-179.
14. Klasen, H. J., A historical review of the use of silver in the treatment of burns. II. Renewed interest for silver. *Burns* **2000**, *26* (2), 131-138.
15. Cho Lee, A. R.; Leem, H.; Lee, J.; Park, K. C., Reversal of silver sulfadiazine-impaired wound healing by epidermal growth factor. *Biomaterials* **2005**, *26* (22), 4670-4676.
16. Aziz, Z.; Abu, S. F.; Chong, N. J., A systematic review of silver-containing dressings and topical silver agents (used with dressings) for burn wounds. *Burns* **2012**, *38* (3), 307-318.
17. Atiyeh, B. S.; Costagliola, M.; Hayek, S. N.; Dibo, S. A., Effect of silver on burn wound infection control and healing: review of the literature. *Burns* **2007**, *33* (2), 139-148.
18. Wang, X. W.; Wang, N. Z.; Zhang, O. Z., Tissue deposition of silver following topical use of silver sulfadiazine in extensive burns. *Burns* **1985**, *11*, 197-201.
19. Sano, S.; Fujimori, R.; Takashima, M.; Itokawa, Y., Absorption, excretion and tissue distribution of silver sulfadiazine. *Burns* **1981**, *8*, 278-285.
20. Harrison, H. N., Pharmacology of sulfadiazine silver—its attachment to burned human and rat skin and studies of gastrointestinal absorption and extension. *Arch. Surg.* **1979**, *114*, 281-285.

21. Tsipouras, N.; Colin, R.; Brady, P., Passage of silver ions through membrane-mimetic materials, and its relevance to treatment of burn wounds with silver sulfadiazine cream. *Clinical Chem* **1997**, *43*, 290-301.
22. Carter, M. J.; Tingley-Kelley, K.; Warriner, R. A., 3rd, Silver treatments and silver-impregnated dressings for the healing of leg wounds and ulcers: a systematic review and meta-analysis. *J Am Acad Dermatol* **2010**, *63* (4), 668-679.
23. Hsu, S.-h.; Tseng, H.-J.; Lin, Y.-C., The biocompatibility and antibacterial properties of waterborne polyurethane-silver nanocomposites. *Biomaterials* **2010**, *31* (26), 6796-6808.
24. Madhavan, P.; Hong, P. Y.; Sougrat, R.; Nunes, S. P., Silver-enhanced block copolymer membranes with biocidal activity. *ACS Appl Mater Interfaces* **2014**, *6* (21), 18497-18501.
25. Espana-Sanchez, B. L.; Avila-Orta, C. A.; Padilla-Vaca, F.; Neira-Velazquez, M. G.; Gonzalez-Morones, P.; Rodriguez-Gonzalez, J. A.; Hernandez-Hernandez, E.; Rangel-Serrano, A.; Barriga, E. D.; Yate, L.; Ziolo, R. F., Enhanced antibacterial activity of melt processed poly(propylene) Ag and Cu nanocomposites by argon plasma treatment. *Plasma Proc Polym* **2014**, *11* (4), 353-365.
26. Monteiro, D. R.; Gorup, L. F.; Takamiya, A. S.; de Camargo, E. R.; Barbosa, D. B., Silver distribution and release from an antimicrobial denture base resin containing silver colloidal nanoparticles. *J Prosthodont* **2012**, *21* (1), 7-15.
27. Petlin, D.; Tverdokhlebov, S.; Anissimov, Y., Plasma treatment as an efficient tool for controlled drug release from polymeric materials: A review. *J. Controlled Release* **2017**.
28. Deng, X.; Nikiforov, A. Y.; Coenye, T.; Cools, P.; Aziz, G.; Morent, R.; De Geyter, N.; Leys, C., Antimicrobial nano-silver non-woven polyethylene terephthalate fabric via an atmospheric pressure plasma deposition process. *Scientific reports* **2015**, *5*, 10138.
29. D'Britto, V.; Kapse, H.; Babrekar, H.; Prabhune, A. A.; Bhoraskar, S. V.; Premnath, V.; Prasad, B. L. V., Silver nanoparticle studded porous polyethylene scaffolds: bacteria struggle to grow on them while mammalian cells thrive. *Nanoscale* **2011**, *3* (7), 2957.
30. Cao, X.; Tang, M.; Liu, F.; Nie, Y.; Zhao, C., Immobilization of silver nanoparticles onto sulfonated polyethersulfone membranes as antibacterial materials. *Colloids Surf., B* **2010**, *81* (2), 555-562.
31. Kumar, V.; Jolival, C.; Pulpytel, J.; Jafari, R.; Arefi-Khonsari, F., Development of silver nanoparticle loaded antibacterial polymer mesh using plasma polymerization process. *J Biomed Mater Res A* **2013**, *101* (4), 1121-1132.
32. Yakub, I.; Soboyejo, W. O., Adhesion of *E. coli* to silver- or copper-coated porous clay ceramic surfaces. *Journal of Applied Physics* **2012**, *111* (12), 124324.
33. Islam, M. S.; Larimer, C.; Ojha, A.; Nettleship, I., Antimycobacterial efficacy of silver nanoparticles as deposited on porous membrane filters. *Mater. Sci. Eng., C* **2013**, *33* (8), 4575-4581.
34. Fortunati, E.; Mattioli, S.; Visai, L.; Imbriani, M.; Fierro, J. L. G.; Kenny, J. M.; Armentano, I., Combined effects of Ag nanoparticles and oxygen plasma treatment on PLGA morphological, chemical, and antibacterial properties. *Biomacromolecules* **2013**, *14* (3), 626-636.
35. Liu, S.; Zhao, J.; Ruan, H.; Wang, W.; Wu, T.; Cui, W.; Fan, C., Antibacterial and anti-adhesion effects of the silver nanoparticles-loaded poly(L-lactide) fibrous membrane. *Mater Sci Eng C Mater Biol Appl* **2013**, *33* (3), 1176-1182.
36. Zodrow, K.; Brunet, L.; Mahendra, S.; Li, D.; Zhang, A.; Li, Q.; Alvarez, P. J., Polysulfone ultrafiltration membranes impregnated with silver nanoparticles show improved biofouling resistance and virus removal. *Water Res.* **2009**, *43* (3), 715-723.
37. Mann, M. N.; Neufeld, B. H.; Hawker, M. J.; Pegalajar-Jurado, A.; Paricio, L. N.; Reynolds, M. M.; Fisher, E. R., Plasma-modified nitric oxide-releasing polymer films exhibit time-delayed 8-log reduction in growth of bacteria. *Biointerphases* **2016**, *11* (3), 031005.
38. Zhang, W.; Chu, P. K.; Ji, J.; Zhang, Y.; Liu, X.; Fu, R. K. Y.; Ha, P. C. T.; Yan, Q., Plasma surface modification of poly vinyl chloride for improvement of antibacterial properties. *Biomaterials* **2006**, *27* (1), 44-51.

39. Osaki, S. G.; Chen, M.; Zamora, P. O., Controlled Drug Release through a Plasma Polymerized Tetramethylcyclo-tetrasiloxane Coating Barrier. *J. Biomater. Sci., Polym. Ed.* **2012**, *23* (1-4), 483-496.
40. Susut, C.; Timmons, R. B., Plasma enhanced chemical vapor depositions to encapsulate crystals in thin polymeric films: a new approach to controlling drug release rates. *International Journal of Pharmaceutics* **2005**, *288* (2), 253-261.
41. Simovic, S.; Losic, D.; Vasilev, K., Controlled drug release from porous materials by plasma polymer deposition. *Chemical Communications* **2010**, *46* (8), 1317-1319.
42. Asadinezhad, A.; Novák, I.; Lehocký, M.; Sedlařík, V.; Vesel, A.; Junkar, I.; Sába, P.; Chodák, I., A physicochemical approach to render antibacterial surfaces on plasma-treated medical-grade PVC: Irgasan coating. *Plasma Proc Polym* **2010**, *7* (6), 504-514.
43. Pegalajar-Jurado, A.; Wold, K. A.; Joslin, J. M.; Neufeld, B. H.; Arabea, K. A.; Suazo, L. A.; McDaniel, S. L.; Bowen, R. A.; Reynolds, M. M., Nitric oxide-releasing polysaccharide derivative exhibits 8-log reduction against *Escherichia coli*, *Acinetobacter baumannii* and *Staphylococcus aureus*. *J Control Release* **2015**, *217*, 228-234.
44. Pegalajar-Jurado, A.; Joslin, J. M.; Hawker, M. J.; Reynolds, M. M.; Fisher, E. R., Creation of hydrophilic nitric oxide releasing polymers via plasma surface modification. *ACS Appl Mater Interfaces* **2014**, *6* (15), 12307-12320.
45. Steen, M. L.; Jordan, A. C.; Fisher, E. R., Hydrophilic modification of polymeric membranes by low temperature H<sub>2</sub>O plasma treatment. *J Membr Sci* **2002**, *204*, 341-357.
46. Martínez-Abad, A.; Sanchez, G.; Lagaron, J.; Ocio, M., Influence of speciation in the release profiles and antimicrobial performance of electrospun ethylene vinyl alcohol copolymer (EVOH) fibers containing ionic silver ions and silver nanoparticles. *Colloid Polym Sci* **2013**, *291* (6), 1381-1392.
47. Amany, A.; El-Rab, S. F. G.; Gad, F., Effect of reducing and protecting agents on size of silver nanoparticles and their anti-bacterial activity. *Der Pharma Chemica* **2012**, *4* (1), 53-65.
48. Sheikh, F. A.; Barakat, N. A. M.; Kanjwal, M. A.; Jeon, S.-H.; Kang, H.-S.; Kim, H.-Y., Self synthesise of silver nanoparticles in/on polyurethane nanofibers: Nano-biotechnological approach. *J Appl Polym Sci* **2010**, *115* (6), 3189-3198.
49. Grill, A., *Cold Plasmas in Materials Fabrications: from Fundamentals to applications*. IEEE: New York, 1994.
50. Sutton, S., Accuracy of plate counts. *JVT* **2011**, *17*, 42-46.
51. Duan, Y.-y.; Jia, J.; Wang, S.-h.; Yan, W.; Jin, L.; Wang, Z.-y., Preparation of antimicrobial poly( $\epsilon$ -caprolactone) electrospun nanofibers containing silver-loaded zirconium phosphate nanoparticles. *J Appl Polym Sci* **2007**, *106* (2), 1208-1214.
52. Bauer, A.; Kirby, W.; Sherris, J. C.; Turck, M., Antibiotic susceptibility testing by a standardized single disk method. *Am J Clin Pathol* **1966**, *45* (4), 493.
53. Sutton, S., The limitations of CFU: Compliance to CGMP requires good science. *Journal of GXP Compliance* **2012**, *16* (1), 74.

## CHAPTER 5

### H<sub>2</sub>O<sub>(v)</sub> PLASMA SURFACE MODIFICATION OF NO-RELEASING TYGON FILMS FOR CONTROL OF DRUG RELEASE KINETICS

This chapter details the plasma surface modification of hydrophobic nitric oxide (NO)-releasing poly(vinyl chloride) (PVC)-based polymer films to create hydrophilic materials with controllable drug release. This effort was part of a large collaboration with numerous contributors and demonstrates the utility of plasma processing, not only for modifying surface properties as presented in Chapters 3-8, but also for control of drug release kinetics resulting in tunability of antibacterial behavior. This chapter is based on work published in *Biointerphases* by Michelle N. Mann, Bella H. Neufeld, Morgan J. Hawker, Adoracion Pegalajar-Jurado, Lindsay N. Paricio, Melissa M. Reynolds, and Ellen R. Fisher, and is reproduced with permission, American Institute of Physics, 2016 (license number 4380820668632).<sup>1</sup> This work was supported by the National Science Foundation (CHE-1152963), the Vice President for Research at Colorado State University (Catalyst for Innovative Partnerships), the Camille and Henry Dreyfus Foundation Postdoctoral Program in Environmental Chemistry, the Department of Defense Congressionally Directed Medical Research Program (DOD-CDMRP), and the Boettcher Foundation's Webb-Waring Biomedical Research Program. In decreasing order of contribution, biological analyses were completed by me, Bella Neufeld and Lindsay Paricio, all surface analyses were completed by Dr. Morgan J. Hawker and are published elsewhere.<sup>2</sup> NOA data were collected by Bella Neufeld and analyzed by me.

## 5.1 Introduction

Polymeric tubing derived from medical-grade PVC is prevalent in extracorporeal circuit (ECC) applications, including blood transfusions, hemodialysis, and cardiopulmonary bypasses.<sup>3-</sup>

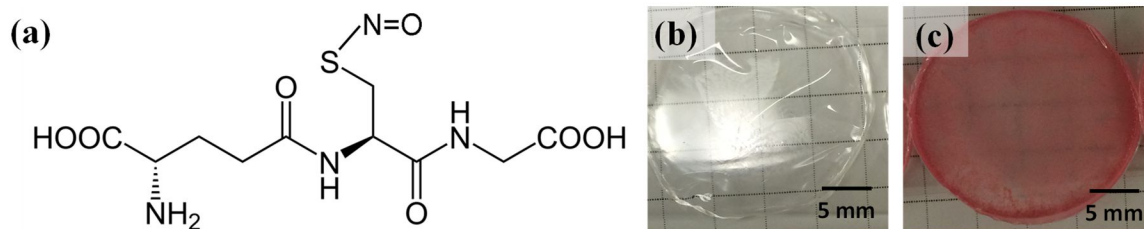
<sup>5</sup> One of the most widely used ECC materials is Tygon®, a proprietary blend of plasticized PVC, because of its inherent strength, flexibility, and transparency.<sup>6-7</sup> Tygon® and other PVC-derived polymers, however, can suffer from bacterial attachment and proliferation that may lead to infection of the bloodstream or at the site of device implantation.<sup>8-10</sup> The mortality rate attributed to these infections has grown in recent years, reaching as high as 50% among elderly patients according to some reports,<sup>9, 10</sup> with the highest risk associated with *S. aureus* infections.<sup>11-12</sup> Recent estimates place the direct costs of *S. aureus* and other HAIs in the United States between \$28 billion and \$45 billion annually with ~60% related to medical devices.<sup>13</sup> Notably, treating HAIs with antibiotics is often ineffective given the emergence of common multidrug resistant bacterial strains; thus, it is critical to shift focus toward development of materials with properties that inherently discourage bacterial attachment or eliminate bacteria before they can attach. Ideal materials for ECC procedures prevent the initial attachment of bacteria while retaining bulk properties (e.g., flexibility, strength), and maintaining biocidal action over clinically-relevant, application-dependent timescales. For example, tubing used during relatively short dialysis procedures requires shorter-term antibacterial properties (hours) than implanted catheter devices (days).

Recent materials-centered approaches to impart antibacterial properties into medical-grade PVC polymers include incorporation of synthetic antibiotics,<sup>14</sup> metal nanoparticles (e.g., Ag, Cu),<sup>15-16</sup> and antimicrobial peptides.<sup>17-19</sup> These methodologies have inherent issues, including cytotoxic complications exhibited by metal nanoparticles<sup>20-21</sup> and the relatively costly (\$50-400

per gram), small-scale commercial synthesis of antimicrobial peptides.<sup>22</sup> Fabrication of materials containing NO has been proposed as a methodology to mitigate these challenges associated with other bactericidal materials. NO, a therapeutic agent produced by endothelial cells that line blood vessels to control coagulation and platelet adhesion, plays an important role in the immune response to inflammation.<sup>23</sup> NO also exhibits multi-targeted bactericidal capabilities: it can directly modify DNA strands via radical induced scission, nitrosate DNA and its repair proteins, and combine with reactive oxygen species to oxidize lipids in bacterial membranes.<sup>24-25</sup> Because NO is endogenous and has multiple mechanisms of antibacterial action, bacteria do not easily develop resistance to NO.<sup>26-28</sup> An inherent challenge of working with NO, however, is that the molecule cannot be retained in polymers because it is highly reactive and short-lived.<sup>29</sup> Thus, to integrate NO into materials, such as tubing used for ECC applications, a variety of NO donors [molecules that release NO upon stimulation (e.g., by light, heat, Cu<sup>2+</sup>)] such as metal nitrosyls, *N*-diazoniumdiolates, and *S*-nitrosothiols (RSNO) can be employed.<sup>25</sup>

Here, Tygon® is used as a model medical-grade PVC polymer, and NO-releasing Tygon® films are fabricated by incorporating 5% and 20% *S*-nitrosoglutathione (GSNO, Fig. 5.1a) donor (denoted GSNO5 and GSNO20, respectively) into a Tygon® solution, as with previous work in our laboratories.<sup>5</sup> Photographs of fabricated films are provided in Fig. 5.1b-c. GSNO as a donor poses minimal risk to the patient as it and its parent glutathione are naturally present in the body.<sup>30</sup> The incorporation of GSNO (or any NO donor) into the Tygon® material, however, will not mitigate bacterial attachment if NO release kinetics cannot be tuned for a specific application. Methods to control NO release from polymer-based platforms include synthetic





**Figure 5.1.** (a) *S*-nitrosoglutathione (GSNO) structure; (b) Tygon® and (c) GSNO20 films immediately after fabrication.

strategies such as the addition of protecting groups to the donor to slow release kinetics,<sup>31</sup> incorporating the NO donor into a nanoparticle,<sup>24,32</sup> and surface modification strategies.<sup>33-34</sup>

Surface modification is perhaps the most facile route to control NO release from polymer constructs as it can be translated to a wide range of material systems. Plasma processing, a specific type of surface modification, is a versatile biomedical polymer material modification as it can alter surface composition while simultaneously sterilizing the surface.<sup>35</sup> Compared to alternative modification strategies, plasma treatment minimizes changes in bulk drug composition because plasmas only modify the outermost surface of the material.<sup>36</sup> We and others have previously demonstrated that H<sub>2</sub>O<sub>(v)</sub> plasma treatment of polymers can dramatically alter surface composition and increase wettability, but less work has been performed towards understanding how plasma processing affects therapeutic, drug-releasing polymers. Thus far, plasma-based methods to control drug delivery have focused on activating the substrate surface prior to drug incorporation or depositing coatings to delay drug release.<sup>14, 23, 36-39</sup> There are fewer reports of plasma surface modification of drug-loaded polymeric devices, such as electrospun fibers loaded with caffeine.<sup>40-42</sup> In addition, our previous work with NO-releasing poly(lactic-co-glycolic acid) (PLGH) films demonstrated that plasma treatment can affect NO release kinetics, as plasma-modified *S*-nitrosated PLGH films had dramatically altered surface properties and lower NO flux when compared to unmodified films.<sup>33</sup>

Although plasma treatment can impact bacterial attachment and cell proliferation by changing surface composition and wettability,<sup>43-44</sup> a more effective method to discourage bacterial proliferation is likely through combining modification with biocidal agent (e.g., NO) addition. This work evaluates the antibacterial activity of plasma treated NO-releasing films against gram-negative *E. coli* and gram-positive *S. aureus*, two planktonic bacteria responsible

for HAIs and known to develop resistance to antibiotics. The overall goals of this work are to determine the effect of H<sub>2</sub>O<sub>(v)</sub> plasma treatment on the properties of NO-releasing Tygon® films and the relationships between material properties (i.e., wettability, roughness, surface chemistry), drug release rate, and the resulting antibacterial efficacy of the films.

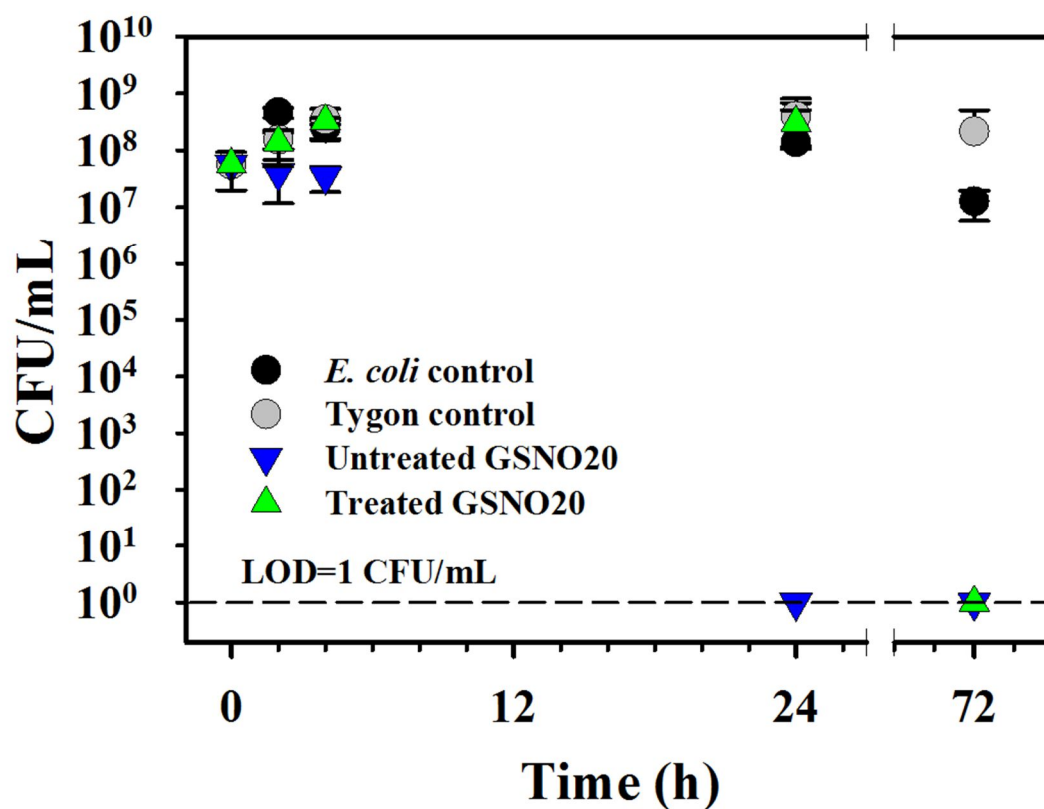
## 5.2 Results

Previous studies have shown H<sub>2</sub>O<sub>(v)</sub> plasma treatments increase the hydrophilicity of polymer surfaces via functional group (e.g., OH) implantation and/or polymer reorganization,<sup>45-48</sup> and that these treatments enhance surface wettability of NO-releasing materials without modifying release capabilities.<sup>33</sup> Indeed, results from surface analysis of GSNO5 and GSNO20, described elsewhere,<sup>2</sup> reveal a substantial increase in film wettability and oxygen content whereas surface roughness is maintained. Results presented herein summarize the antibacterial efficacy of the GSNO20 film and the effect of well-established H<sub>2</sub>O<sub>(v)</sub> plasma treatments on release of NO.<sup>33</sup>

### 5.2.1. Effect of plasma treatment on bactericidal activity of GSNO20 films

The bactericidal activity of our materials was tested against both gram-negative *E. coli* and gram-positive *S. aureus*. For each kill rate assay, a bacterial culture was grown in nutrient-rich media without a film, for use as a positive control. Notably, initial experiments showed that GSNO5 films were ineffective at killing either bacterial strain. Therefore, only untreated and plasma treated GSNO20 films were used for kill rate experiments.

The population of *E. coli* in all wells at time zero was approximately  $\sim 10^8$  CFU mL<sup>-1</sup> (Fig. 5.2 and Table 5.1). After 2 h of exposure to the films, the *E. coli* population had not changed significantly regardless of sample type, with sample wells containing between  $10^8$ - $10^9$



**Figure 5.2.** *E. coli* kill rate represented as concentration of bacteria in CFU mL<sup>-1</sup> as a function of time (h) over 72 h for *E. coli* with blank and Tygon® controls, as well as untreated and plasma-treated GSNO20 films.

**Table 5.1.** CFUs per mL of *E. coli* culture during kill rate assays<sup>a</sup>

<b>Sample</b>	<b>0 h</b>	<b>2 h</b>	<b>4 h</b>	<b>24 h</b>	<b>72 h</b>
<i>E. coli</i>	5.7 (3.7) x 10 <sup>7</sup>	4.7 (0.9) x 10 <sup>8</sup>	2.5 (1.0) x 10 <sup>8</sup>	1.4 (6.7) x 10 <sup>8</sup>	1.3 (0.1) x 10 <sup>7</sup>
Tygon®	5.7 (3.7) x 10 <sup>7</sup>	1.6 (0.5) x 10 <sup>8</sup>	3.5 (1.9) x 10 <sup>8</sup>	4.0 (2.8) x 10 <sup>8</sup>	2.2 (2.9) x 10 <sup>8</sup>
Untreated GSNO20	5.7 (3.7) x 10 <sup>7</sup>	4.0 (2.8) x 10 <sup>7</sup>	3.5 (1.7) x 10 <sup>7</sup>	1 <sup>b</sup>	1 <sup>b</sup>
Treated GSNO20	5.7 (3.7) x 10 <sup>7</sup>	1.4 (0.9) x 10 <sup>8</sup>	3.3 (0.4) x 10 <sup>8</sup>	3.1 (2.0) x 10 <sup>8</sup>	1 <sup>b</sup>

<sup>a</sup> All values reported as the mean ± one standard deviation (n ≥ 9).

<sup>b</sup> The LOD (1 CFU mL<sup>-1</sup>) is reported where no colonies were observed on plates from undiluted aliquots.

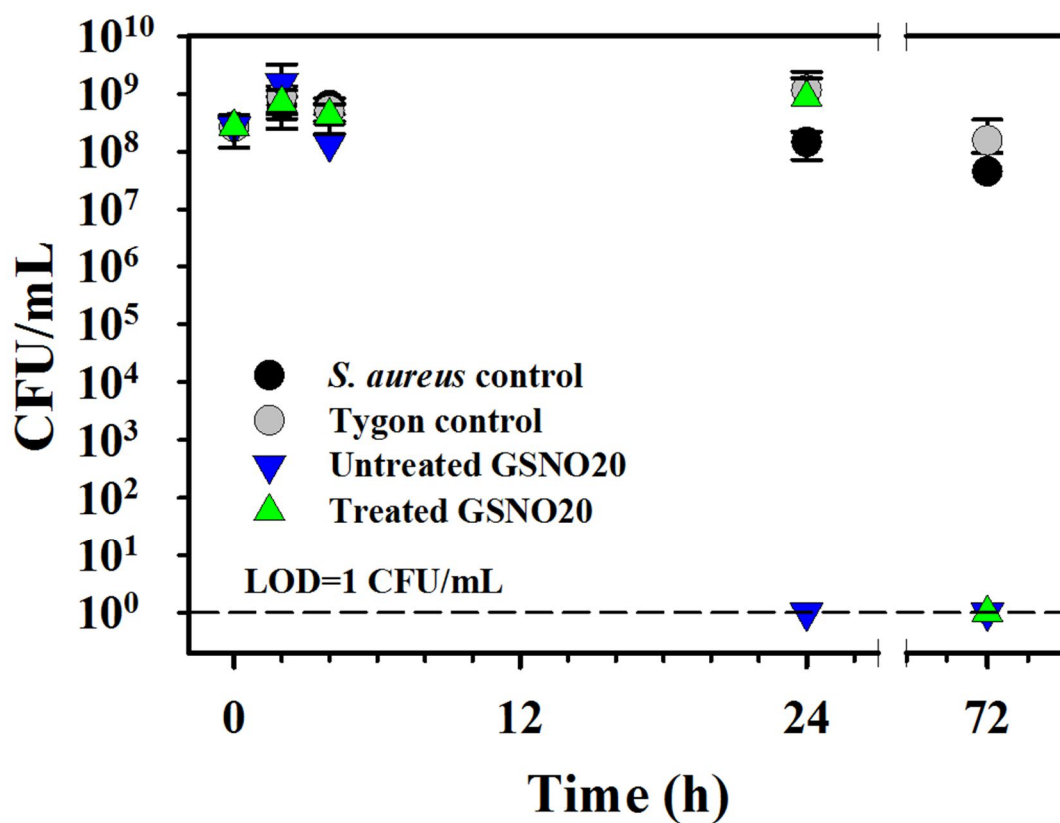
CFU mL<sup>-1</sup>. Four hours after exposure to the NO-releasing films, *E. coli* in the wells with untreated films exhibited a small but not statistically significant decrease in bacterial population.

The treated films maintained a bacterial population similar to the controls. After 24 h of exposure, the *E. coli* population was unchanged in wells containing controls and treated GSNO20 films. In contrast, bacteria in wells containing untreated GSNO20 films were significantly reduced in number (no colonies were present on plates from these wells). To confirm the absence of bacteria, undiluted aliquots were then plated separately and no colonies were observed. Plates were therefore assigned a value of 1 CFU mL<sup>-1</sup> corresponding to the limit of detection of the technique (Chapter 2). Compared to controls, this effect by untreated films represents an 8-log reduction in viable *E. coli*.

To ensure bacteria did not recover from NO exposure, plating at 72 h was also performed. Once again, no colonies were observed on plates from undiluted aliquots from wells containing untreated films. Interestingly, a dramatic decline in bacterial population was also observed for treated films, although on a different timescale. After 72 h of exposure to treated GSNO20 films, no colonies were observed on the plates, even when undiluted aliquots were plated. Thus, *E. coli* exhibited an 8-log reduction in growth after exposure to treated GSNO20 films for 72 h.

Figure 5.3 and Table 5.2 depict the results of the *S. aureus* kill rate assays. Similar kill rate behavior to *E. coli* was observed with *S. aureus*. As with the *E. coli*, untreated GSNO20 films also result in an 8-log reduction in *S. aureus* growth after 24 h. After 72 h, no colonies were present on plates containing aliquots from wells of untreated and treated GSNO20 films, indicating an 8-log reduction in *S. aureus* growth caused by GSNO20 films.

During kill rate assays with both bacterial strains, a color change was observed for both untreated and treated GSNO20 films (Fig. 5.4a-c). After fabrication, films are pink in color,



**Figure 5.3.** *S. aureus* kill rate represented as concentration of bacteria in CFU mL<sup>-1</sup> as a function of time (h) over 72 h for *S. aureus* with blank and Tygon® controls, as well as untreated and plasma-treated GSNO20 films.

**Table 5.2.** CFUs per mL of *S. aureus* culture during kill rate assays<sup>a</sup>

<b>Sample</b>	<b>0 h</b>	<b>2 h</b>	<b>4 h</b>	<b>24 h</b>	<b>72 h</b>
<i>S. aureus</i>	2.7 (1.5) x 10 <sup>8</sup>	6.3 (2.7) x 10 <sup>8</sup>	6.4 (2.0) x 10 <sup>8</sup>	1.5 (0.8) x 10 <sup>8</sup>	4.6 (0.5) x 10 <sup>7</sup>
Tygon®	2.7 (1.5) x 10 <sup>8</sup>	9.0 (4.5) x 10 <sup>8</sup>	5.1 (1.8) x 10 <sup>8</sup>	1.2 (1.3) x 10 <sup>9</sup>	1.6 (2.0) x 10 <sup>8</sup>
Untreated GSNO20	2.7 (1.5) x 10 <sup>8</sup>	1.5 (1.7) x 10 <sup>9</sup>	1.4 (1.6) x 10 <sup>8</sup>	1 <sup>b</sup>	1 <sup>b</sup>
Treated GSNO20	2.7 (1.5) x 10 <sup>8</sup>	7.0 (4.5) x 10 <sup>8</sup>	4.3 (2.3) x 10 <sup>8</sup>	8.7 (9.9) x 10 <sup>8</sup>	1 <sup>b</sup>

<sup>a</sup> All values reported as the mean ± one standard deviation (n ≥ 9).

<sup>b</sup> The LOD (1 CFU mL<sup>-1</sup>) is reported where no colonies were observed on plates from undiluted aliquots.



indicating the presence of the GSNO donor. After 24 h, however, the untreated film lost much of the pink color, whereas the treated GSNO film remained primarily pink in color. After 72 h, both untreated and treated GSNO20 were pale yellow in color.

### 5.2.2. Effect of plasma treatment on NO release

To determine if materials resulted in the sustained release of NO, release profiles were obtained over 24 h for untreated and treated GSNO5 and GSNO20 films. Untreated GSNO5 and GSNO20 films release similar percentages of NO (~40%) within combined experimental error (Table 5.3). No significant difference is observed in the flux or total moles of NO released between untreated and treated GSNO5 (Table 5.3). Untreated GSNO20 films release  $1.30 \pm 0.13 \times 10^{-5}$  moles of NO ( $39 \pm 4\%$ ).  $\text{H}_2\text{O}_{(v)}$  plasma treated GSNO20 films release only  $1.02 \pm 0.11 \times 10^{-5}$  moles of NO ( $31 \pm 3\%$ ) after 24 h; however, these values are not statistically significantly different. Additionally, NO release was measured over 72 h for untreated and treated GSNO20 films (Table 5.3) to correlate NO release kinetics with kill rate experiments (Section 5.2.1). Figure 5.4d shows the moles of NO released (each data point represents an average value over the 1 min sampling interval) from untreated and treated GSNO20 films over 72 h. Untreated films release  $2.61 \pm 0.55 \times 10^{-5}$  moles of NO ( $78 \pm 16\%$ ) whereas treated GSNO20 films deliver  $2.17 \pm 0.31 \times 10^{-5}$  moles of NO ( $65 \pm 9\%$ ) after 72 h, similar within combined experimental error. Interestingly, the time to maximum NO release is clearly earlier for untreated films ( $3.50 \pm 0.13$  h) than treated films ( $6.93 \pm 1.18$  h). This difference was statistically significant (two-tailed t-test,  $p < 0.01$ ).

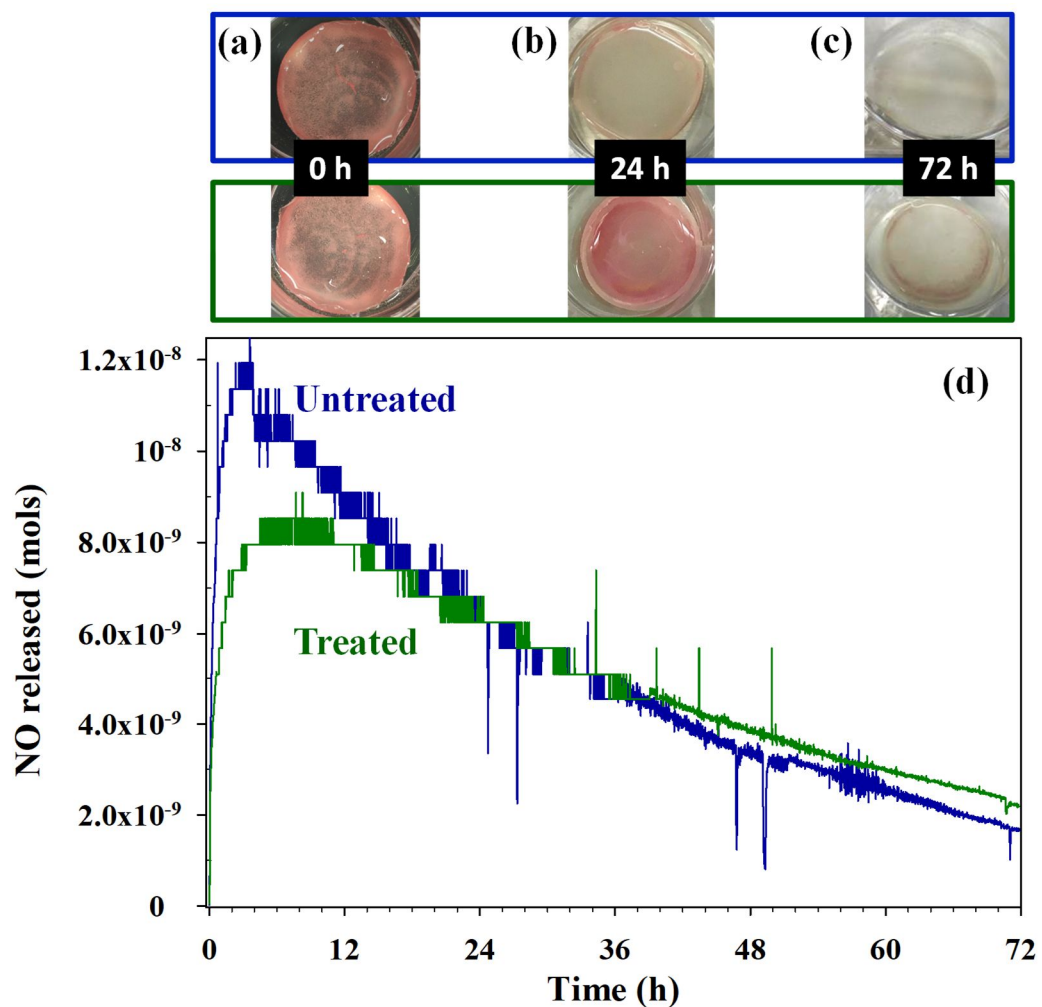
**Table 5.3.** Figures of Merit for NO-release Kinetics for NO-releasing Films

<b>Film</b>	<b>Analysis time (h)</b>	<b>NO flux (nmol cm<sup>-2</sup> min<sup>-1</sup>)<sup>a</sup></b>	<b>Theoretical NO reservoir (×10<sup>-5</sup> mol)<sup>b</sup></b>	<b>Total NO released (×10<sup>-5</sup> mol)</b>	<b>% NO released<sup>c</sup></b>
Untreated GSNO5	24	0.52 ± 0.07	0.84	0.37 ± 0.04	44 ± 5
Treated GSNO5	21	0.52 ± 0.04	0.84	0.30 ± 0.04	36 ± 4
Untreated GSNO20	24	1.73 ± 0.38	3.35	1.30 ± 0.13	39 ± 4
Treated GSNO20	24	1.55 ± 0.27	3.35	1.02 ± 0.11	31 ± 3
Untreated GSNO20	72	1.08 ± 0.58	3.35	2.61 ± 0.55	78 ± 16
Treated GSNO20	72	1.16 ± 0.48	3.35	2.17 ± 0.31	65 ± 9

<sup>a</sup> Average of representative trace over time.

<sup>b</sup> Assumes no loss of NO during plasma treatment.

<sup>c</sup> Error represents standard deviation propagated from total NO released.



**Figure 5.4.** Photographs of untreated (top) and treated (bottom) GSNO20 films during kill rate assays (a) at 0 h, (b) 24 h (c) 72 h. Representative traces of moles of NO released are shown in (d) for untreated and treated GSNO20 films in NBM over 72 h.

### 5.2.3. Evaluation of film nitrogen content by XPS

XPS was used to assess any increase in nitrogen content upon exposure to NBM, presumed to result from the adsorption of protein, on untreated and treated Tygon® and GSNO20 films. For untreated Tygon® films, no nitrogen was observed on the surface, whereas if plasma treated, exposure to NBM results in an increase to  $3.4 \pm 0.2\%$  nitrogen on the film surface. With 20% GSNO incorporation, exposure to NBM results in  $1.5 \pm 0.2\%$  nitrogen on the surface. Plasma treated GSNO20 films have  $3.6 \pm 0.4\%$  nitrogen on the surface after NBM exposure. It is well documented that plasma surface modification can be used to alter protein adsorption on polymer surfaces,<sup>49-50</sup> and that the extent of protein adsorption tends to correlate with surface hydrophilicity.<sup>51-52</sup> If protein adsorption were severe enough to significantly impact NO release, we would expect to see a measurable change in NO release upon plasma treatment and a subsequent lower log reduction for treated materials. Because no attempt was made to reverse protein adsorption on the NO-releasing films, and bactericidal efficacy is retained after treatment, it is likely not the primary reason for the observed differences in bactericidal kill rate.

### 5.3 Effect of plasma treatment on bactericidal activity and NO release kinetics

Data presented herein demonstrate that 20% GSNO loading results in an 8-log reduction, indicating these films are bactericidal against both *E. coli* and *S. aureus*. The concentration of bacteria in control wells was effectively constant throughout the experiment. The slight decline in the population of control wells to  $\sim 10^7$ - $10^8$  CFU mL<sup>-1</sup> after 72 h is not surprising because media was not replaced over the course of the experiment. Notably, no bacterial reduction was observed in wells containing Tygon® films without GSNO, indicating the Tygon® polymer is not responsible for the observed bactericidal activity. Plasma treatment clearly affects NO

release from GSNO-loaded films, manifested primarily in delay of biocidal activity. This is not surprising given that unmodified and plasma-modified NO-releasing Tygon® films had disparate surface properties.<sup>2</sup> Photographs of the films at intervals during kill rate assays (Fig. 5.4a-c) provide additional evidence of delayed NO release as untreated GSNO20 films clearly experience a loss of pink color (indicating cleavage of the S-NO bond) earlier than treated films.

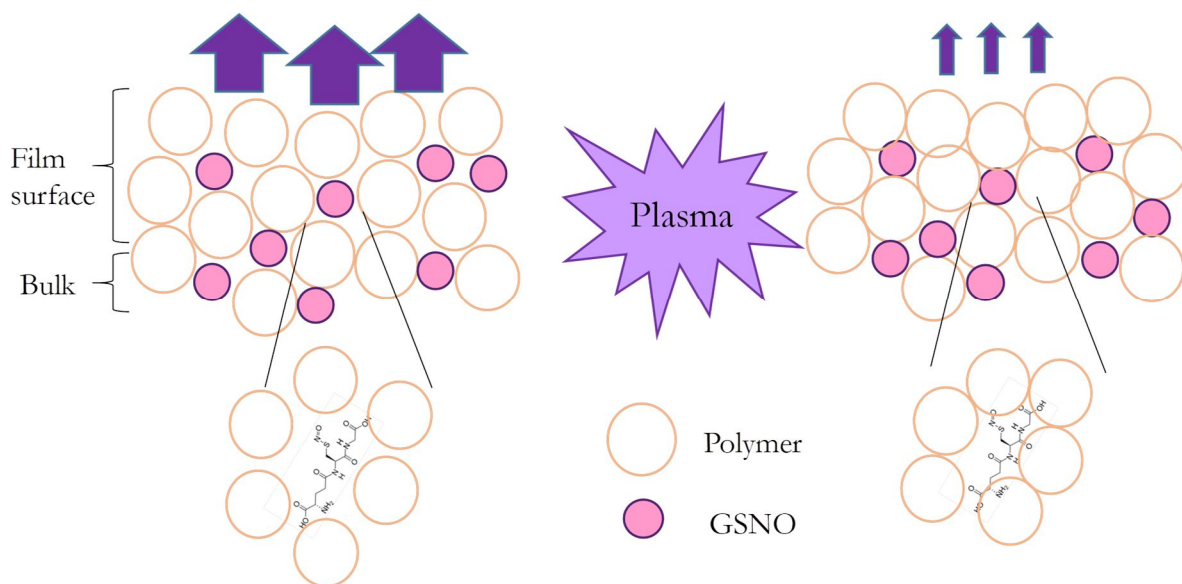
The altered surface properties of the modified GSNO20 films likely cause differences in NO release from the polymer, which directly impact the timescale of bactericidal activity. The NO release profiles for GSNO20 films over 24 h show no noticeable difference in flux of NO for treated versus untreated films; however, the total moles of NO released over the time frame and percentage of NO released is decreased for the former. Although we experimentally show that treated films release a smaller number of moles of NO than untreated films, this difference is not statistically significant. There is, however, a clear difference in the time to reach maximum NO release for treated versus untreated GSNO20, indicating that plasma treatment slows the initial release from GSNO20 films. The shift in time of maximum NO release is on the scale of hours, not days, indicating that plasma treatment has potential for tuning drug release from polymeric materials over clinically-relevant timescales.

The delayed kill rate for plasma treated GSNO20 most likely results from changes in surface properties and chemical composition induced by plasma treatment, specifically the increase of cross-linking, known to occur in plasma treatment of polymers through recombination of radicals produced in the plasma.<sup>36, 41-42, 53</sup> Although the wettability of treated GSNO20 films is increased by plasma treatment, it may also cause cross-linking at the polymer surface which may decrease water penetration into the bulk of the film and limit donor degradation.<sup>36</sup> A conceptual rendering

of this hypothesis is depicted in Figure 5.5. This phenomenon has been observed with drug-incorporated plasma polymerized coatings on stainless steel<sup>36</sup> and with plasma treatment of polymeric devices.<sup>41-42</sup> For example, the drug release rate from stents treated with argon, oxygen, and nitrogen plasmas was found to depend on the degree of cross-linking in the modified polymers.<sup>42</sup> The highest release rate occurred after oxygen plasma treatment where the degree of crosslinking (caused by oxygen cross-linking between molecular chains) was much lower than that by argon or nitrogen plasmas, where cross-linking is induced by free radicals.<sup>42</sup>

It is important to note, however, that NO is not directly responsible for the biocidal activity observed here because of its high reactivity and short lifetime. This seems reasonable, given data demonstrating that NO is released relatively quickly (within the first 5 min of exposure to NBM, Fig. 5.4), but no biocidal activity is observed within the first 4 h of exposure. The observed antibacterial activity of NO is typically attributed to secondary species, such as peroxyxynitrite ( $\text{OONO}^\cdot$ ) that may form from the reaction of NO with  $\text{O}_2^-$  and is more stable than NO itself,<sup>54</sup> or dinitrogen trioxide ( $\text{N}_2\text{O}_3$ ) which can form from the autoxidation of NO or from the reaction of NO with iron and thiols.<sup>55</sup> As donor stability and NO release kinetics can be influenced by the surrounding chemistry,<sup>56</sup> plasma treatment likely delays the formation of these secondary species, resulting in the delayed kill rate by treated GSNO20 films.

Initial experiments demonstrated that both unmodified and modified GSNO5 films failed to reduce *E. coli* and *S. aureus* growth over 24 h. GSNO20 films may be more effective antibacterial materials because the increased donor loading allows the release of more than double the number of moles of NO than GSNO5 films. Previous work wherein we evaluated bactericidal activity of a different NO releasing material (*S*-nitrosated dextran-cysteamine)



**Figure 5.5.** Conceptual cartoon depiction of cross-linking phenomena and the resulting delayed NO release that may occur via  $H_2O_{(v)}$  plasma surface modification.

against *E. coli* and *S. aureus* suggests less than half the concentration of NO released by GSNO5 films (Table 5.3) was needed to achieve an 8-log reduction.<sup>57</sup> Thus, it is somewhat surprising that GSNO5 films failed to reduce bacterial growth given the amount of NO released (Table 5.3). It is important to note, however, that the medium for NO delivery differs substantially between the previous work and the current study (a water-soluble polymer solution compared to a water-insoluble polymeric film, respectively). Herein, the films provide a surface to which bacteria attach, and it is well documented that bacteria present in a biofilm have superior defenses against biocidal agents than planktonic bacteria.<sup>9, 58</sup> Overall, our results suggest plasma treatment delays donor degradation and the initial release of NO from treated GSNO20 films, which may delay the formation of secondary species that are likely more bactericidal than NO itself. The resulting postponement of biocidal activity demonstrates the promising ability to tune the biological response of an NO-releasing material for applications requiring prevention of bacterial infection.

#### **5.4 Summary and conclusions**

Through H<sub>2</sub>O<sub>(v)</sub> plasma treatment, desirable surface properties of NO-releasing polymer films were achieved while NO release capabilities and biocidal activity were maintained. The resulting plasma treated films displayed an NO release profile with a clear difference in time of maximum NO release, likely explaining the delayed but equivalent 8-log reduction in growth of *E. coli* and *S. aureus* over 72 h. We hypothesize that cross-linking, known to occur during plasma treatment of polymers, slows diffusion of NO from the polymer surface, delaying the formation of biocidal byproducts. This suggests plasma treatment may be a valuable avenue for tuning the release of NO from therapeutic materials used as biomedical devices, as the large parameter space available during plasma modification processes likely affords some tunability



over the degree of crosslinking. Future studies should aim to elucidate the role of plasma processing parameters on the capability to control drug release by tuning surface crosslinking in polymeric devices. The incorporation of biocidal agents coupled with the controlled release of the agent represents a holy grail in biomedical device research. Thus, the results presented herein greatly advance fundamental materials research aimed at reducing the morbidity and mortality rate associated with HAIs.

## REFERENCES

1. Mann, M. N.; Neufeld, B. H.; Hawker, M. J.; Pegalajar-Jurado, A.; Paricio, L. N.; Reynolds, M. M.; Fisher, E. R., Plasma-modified nitric oxide-releasing polymer films exhibit time-delayed 8-log reduction in growth of bacteria. *Biointerphases* **2016**, *11* (3), 11.
2. Hawker, M. J. Part I. Development of Plasma Surface Modification and Characterization Strategies for Three-Dimensional Polymer Constructs used in Biological Applications and Part II. Exploring General Chemistry Students' Metacognitive Monitoring on Examinations. Doctoral Dissertation, Colorado State University, Colorado State University Libraries, 2016.
3. Peek, G. J.; Scott, R.; Killer, H. M.; Firmin, R. K., An *in vitro* method for comparing biocompatibility of materials for extracorporeal circulation. *Perfusion-UK* **2002**, *17* (2), 125-132.
4. Hong, J.; Larsson, A.; Ekdahl, K. N.; Elgue, G.; Larsson, R.; Nilsson, B., Contact between a polymer and whole blood: Sequence of events leading to thrombin generation. *J. Lab. Clin. Med.* **2001**, *138* (2), 139-145.
5. Joslin, J. M.; Lantvit, S. M.; Reynolds, M. M., Nitric oxide releasing Tygon materials: Studies in donor leaching and localized nitric oxide release at a polymer-buffer interface. *ACS Appl. Mater. Interfaces* **2013**, *5* (19), 9285-9294.
6. Shi, W.; Zhang, J.; Shi, X.-M.; Jiang, G.-D., Different photodegradation processes of PVC with different average degrees of polymerization. *J. Appl. Polym. Sci.* **2008**, *107* (1), 528-540.
7. Silapasorn, K.; Sombatsompop, K.; Kositchaiyong, A.; Wimolmala, E.; Markpin, T.; Sombatsompop, N., Effect of chemical structure of thermoplastics on antibacterial activity and physical diffusion of triclosan doped in vinyl thermoplastics and their composites with CaCO<sub>3</sub>. *J. Appl. Polym. Sci.* **2011**, *121* (1), 253-261.
8. Lambert, M.-L.; Suetens, C.; Savey, A.; Palomar, M.; Hiesmayr, M.; Morales, I.; Agodi, A.; Frank, U.; Mertens, K.; Schumacher, M.; Wolkewitz, M., Clinical outcomes of health-care-associated infections and antimicrobial resistance in patients admitted to European intensive-care units: a cohort study. *Lancet Infect. Dis.* **2011**, *11* (1), 30-38.
9. Costerton, J. W.; Stewart, P. S.; Greenberg, E. P., Bacterial biofilms: A common cause of persistent infections. *Science* **1999**, *284*, 1318-1322.
10. Speranza, G.; Gottardi, G.; Pederzoli, C.; Lunelli, L.; Canteri, R.; Pasquardini, L.; Carli, E.; Lui, A.; Maniglio, D.; Brugnara, M.; Anderle, M., Role of chemical interactions in bacterial adhesion to polymer surfaces. *Biomaterials* **2004**, *25* (11), 2029-2037.
11. Malani, P. N.; Rana, M. M.; Banerjee, M.; Bradley, S. F., *Staphylococcus aureus* bloodstream infections: the association between age and mortality and functional status. *J. Am. Geriatr. Soc.* **2008**, *56* (8), 1485-1489.
12. Yasmin, M.; El Hage, H.; Obeid, R.; El Haddad, H.; Zaarour, M.; Khalil, A., Epidemiology of bloodstream infections caused by methicillin-resistant *Staphylococcus aureus* at a tertiary care hospital in New York. *Am. J. Infect. Control* **2016**, *44* (1), 41-46.
13. Scott, R. D., *The Direct Medical Costs of Healthcare-associated Infections in US Hospitals and the Benefits of Prevention*. Centers for Disease Control and Prevention: March 2009.
14. Zhang, W.; Chu, P. K.; Ji, J.; Zhang, Y.; Liu, X.; Fu, R. K. Y.; Ha, P. C. T.; Yan, Q., Plasma surface modification of poly vinyl chloride for improvement of antibacterial properties. *Biomaterials* **2006**, *27* (1), 44-51.
15. Chinkamonthong, R.; Kositchaiyong, A.; Sombatsompop, N., Effects of thermal and UV aging on antibacterial properties of linear low-density polyethylene and poly(vinyl chloride) films containing nano-silver colloid. *J. Plast. Film Sheeting* **2012**, *29* (2), 144-162.

16. Balazs, D. J.; Triandafillu, K.; Wood, P.; Chevolut, Y.; van Delden, C.; Harms, H.; Hollenstein, C.; Mathieu, H. J., Inhibition of bacterial adhesion on PVC endotracheal tubes by RF-oxygen glow discharge, sodium hydroxide and silver nitrate treatments. *Biomaterials* **2004**, *25* (11), 2139-2151.
17. Vreuls, C.; Zocchi, G.; Thierry, B.; Garitte, G.; Griesser, S. S.; Archambeau, C.; Van de Weerd, C. V.; Martial, J.; Griesser, H., Prevention of bacterial biofilms by covalent immobilization of peptides onto plasma polymer functionalized substrates. *J. Mater. Chem.* **2010**, *20* (37), 8092-8098.
18. Santoro, D.; Maddox, C. W., Canine antimicrobial peptides are effective against resistant bacteria and yeasts. *Veterinary Dermatology* **2014**, *25* (1), 35-e12.
19. Hancock, R. E. W., Peptide antibiotics. *Lancet* **1997**, *349* (9049), 418-422.
20. Poon, V. K.; Burd, A., *In vitro* cytotoxicity of silver: implication for clinical wound care. *Burns* **2004**, *30* (2), 140-147.
21. Cho Lee, A. R.; Leem, H.; Lee, J.; Park, K. C., Reversal of silver sulfadiazine-impaired wound healing by epidermal growth factor. *Biomaterials* **2005**, *26* (22), 4670-4676.
22. Marr, A. K.; Gooderham, W. J.; Hancock, R. E., Antibacterial peptides for therapeutic use: obstacles and realistic outlook. *Curr. Opin. Pharmacol.* **2006**, *6* (5), 468-472.
23. Feng, Y.; Zhao, H.; Lu, J.; Guo, J., Nitric oxide release from polycarbonate-urethane films containing copper(II) complexes. *J. Controlled Release* **2011**, *152*, Supplement 1 (0), e202-e204.
24. Quinn, J. F.; Whittaker, M. R.; Davis, T. P., Delivering nitric oxide with nanoparticles. *J. Controlled Release* **2015**, *205* (0), 190-205.
25. Heilman, B. J.; St John, J.; Oliver, S. R.; Mascharak, P. K., Light-triggered eradication of *Acinetobacter baumannii* by means of NO delivery from a porous material with an entrapped metal nitrosyl. *J. Am. Chem. Soc.* **2012**, *134* (28), 11573-11582.
26. Gardner, P. R.; Gardner, A. M.; Martin, L. A.; Salzman, A. L., Nitric oxide dioxygenase: An enzymic function for flavohemoglobin. *Proc. Natl. Acad. Sci.* **1998**, *95* (18), 10378-10383.
27. Privett, B. J.; Broadnax, A. D.; Bauman, S. J.; Riccio, D. A.; Schoenfisch, M. H., Examination of bacterial resistance to exogenous nitric oxide. *Nitric Oxide-Biol. Chem.* **2012**, *26* (3), 169-173.
28. Slomberg, D.; Lu, Y.; Broadnax, A.; Hunter, R.; Carpenter, A.; Schoenfisch, M., Role of size and shape on biofilm eradication for nitric oxide-releasing silica nanoparticles. *ACS Appl. Mater. Interfaces* **2013**, *5* (19), 9322-9329.
29. Thomas, D. D.; Liu, Z. P.; Kantrow, S. P.; Lancaster, J. R., The biological lifetime of nitric oxide: Implications for the perivascular dynamics of NO and O<sub>2</sub>. *Proc. Natl. Acad. Sci. U.S.A.* **2001**, *98* (1), 355-360.
30. Wang, W.; Ballatori, N., Endogenous glutathione conjugates: Occurrence and biological functions. *Pharmacol. Rev.* **1998**, *50* (3), 335-355.
31. Xu, H.; Reynolds, M. M.; Cook, K. E.; Evans, A. S.; Toscano, J. P., 2-Hydroxy-5-nitrobenzyl as a diazeniumdiolate protecting group: Application in NO-releasing polymers with enhanced biocompatibility. *Organic Letters* **2008**, *10* (20), 4593-4596.
32. Hetrick, E. M.; Shin, J. H.; Stasko, N. A.; Johnson, C. B.; Wespe, D. A.; Holmuhamedov, E.; Schoenfisch, M. H., Bactericidal efficacy of nitric oxide-releasing silica nanoparticles. *ACS Nano* **2008**, *2* (2), 235-246.
33. Pegalajar-Jurado, A.; Joslin, J. M.; Hawker, M. J.; Reynolds, M. M.; Fisher, E. R., Creation of hydrophilic nitric oxide releasing polymers via plasma surface modification. *ACS Appl. Mater. Interfaces* **2014**, *6* (15), 12307-12320.
34. Carpenter, A. W.; Johnson, J. A.; Schoenfisch, M. H., Nitric oxide-releasing silica nanoparticles with varied surface hydrophobicity. *Colloids Surf., A* **2014**, *454*, 144-151.
35. Sohbatzadeh, F.; Hosseinzadeh Colagar, A.; Mirzanejad, S.; Mahmodi, S., *E. coli*, *P. aeruginosa*, and *B. cereus* bacteria sterilization using afterglow of non-thermal plasma at atmospheric pressure. *Appl. Biochem. Biotechnol.* **2010**, *160* (7), 1978-1984.
36. Osaki, S. G.; Chen, M.; Zamora, P. O., Controlled drug release through a plasma polymerized tetramethylcyclo-tetrasiloxane coating barrier. *Journal of Biomaterials Science Polymer Edition* **2012**, *23* (1-4), 483-496.

37. Asadinezhad, A.; Novak, I.; Lehocky, M.; Sedlarik, V.; Vesel, A.; Junkar, I.; Saha, P.; Chodak, I., A physicochemical approach to render antibacterial surfaces on plasma-treated medical-grade PVC: Irganox coating. *Plasma Process. Polym.* **2010**, *7* (6), 504-514.
38. Susut, C.; Timmons, R. B., Plasma enhanced chemical vapor depositions to encapsulate crystals in thin polymeric films: a new approach to controlling drug release rates. *Int. J. Pharm.* **2005**, *288* (2), 253-261.
39. Simovic, S.; Losic, D.; Vasilev, K., Controlled drug release from porous materials by plasma polymer deposition. *Chemical Communications* **2010**, *46* (8), 1317-1319.
40. Labay, C.; Canal, J. M.; Canal, C., Relevance of surface modification of polyamide 6.6 Fibers by air plasma treatment on the release of caffeine. *Plasma Process. Polym.* **2012**, *9* (2), 165-173.
41. Paradiso, P.; Chu, V.; Santos, L.; Serro, A. P.; Colaco, R.; Saramago, B., Effect of plasma treatment on the performance of two drug-loaded hydrogel formulations for therapeutic contact lenses. *J. Biomed. Mater. Res. B Appl. Biomater.* **2015**, *103* (5), 1059-1068.
42. Hagiwara, K.; Hasebe, T.; Hotta, A., Effects of plasma treatments on the controlled drug release from poly(ethylene-co-vinyl acetate). *Surf. Coat. Technol.* **2013**, *216*, 318-323.
43. Abrigo, M.; Kingshott, P.; McArthur, S. L., Bacterial response to different surface chemistries fabricated by plasma polymerization on electrospun nanofibers. *Biointerphases* **2015**, *10* (4), 9.
44. Bazaka, K.; Jacob, M. V.; Chrzanowski, W.; Ostrikov, K., Anti-bacterial surfaces: natural agents, mechanisms of action, and plasma surface modification. *RSC Adv.* **2015**, *5* (60), 48739-48759.
45. Asfardjani, K.; Segui, Y.; Aurelle, Y.; Abidine, N., Effect of Plasma Treatments on Wettability of Polysulfone and Polyetherimide. *J. Appl. Polym. Sci.* **1991**, *43*, 271-281.
46. Steen, M. L.; Hymas, L.; Havey, E. D.; Capps, N. E.; Castner, D. G.; Fisher, E. R., Low Temperature Plasma Treatment of Asymmetric Polysulfone Membranes for Permanent Hydrophilic Surface Modification. *J. Membr. Sci.* **2001**, *188* (1), 97-114.
47. Steen, M. L.; Jordan, A. C.; Fisher, E. R., Hydrophilic Modification of Polymeric Membranes by Low Temperature H<sub>2</sub>O Plasma Treatment. *J. Membr. Sci.* **2002**, *204* (1), 341-357.
48. Tompkins, B. D.; Dennison, J. M.; Fisher, E. R., H<sub>2</sub>O plasma modification of track-etched polymer membranes for increased wettability and improved performance. *J Membr Sci* **2013**, *428*, 576-588.
49. Pegalajar-Jurado, A.; Mann, M. N.; Maynard, M. R.; Fisher, E. R., Hydrophilic modification of polysulfone ultrafiltration membranes by low temperature water vapor plasma treatment to enhance performance. *Plasma Process. Polym.* **2016**, *13* (6), 598-610.
50. Kull, K. R.; Steen, M. L.; Fisher, E. R., Surface modification with nitrogen-containing plasmas to produce hydrophilic, low-fouling membranes. *J. Membr. Sci.* **2005**, *246* (2), 203-215.
51. Stallard, C. P.; McDonnell, K. A.; Onayemi, O. D.; O'Gara, J. P.; Dowling, D. P., Evaluation of protein adsorption on atmospheric plasma deposited coatings exhibiting superhydrophilic to superhydrophobic properties. *Biointerphases* **2012**, *7* (1-4), 12.
52. Xu, L. C.; Siedlecki, C. A., Effects of surface wettability and contact time on protein adhesion to biomaterial surfaces. *Biomaterials* **2007**, *28* (22), 3273-3283.
53. Tajima, S.; Komvopoulos, K., Effect of reactive species on surface crosslinking of plasma-treated polymers investigated by surface force microscopy. *Appl. Phys. Lett.* **2006**, *89* (12), 124102.
54. Pryor, W. A.; Squadrito, G. L., The chemistry of peroxynitrite: a product from the reaction of nitric oxide with superoxide. *Am. J. Physiol. Lung Cell. Mol. Physiol.* **1995**, *268* (5), L699-L722.
55. Fang, F. C., Mechanisms of nitric oxide-related antimicrobial activity. *J. Clin. Invest.* **1997**, *99*, 2818-2825.
56. Damodaran, V. B.; Joslin, J. M.; Wold, K. A.; Lantvit, S. M.; Reynolds, M. M., S-nitrosated biodegradable polymers for biomedical applications: Synthesis, characterization and impact of thiol structure on the physicochemical properties. *J. Mater. Chem.* **2012**, *22* (13), 5990-6001.
57. Pegalajar-Jurado, A.; Wold, K. A.; Joslin, J. M.; Neufeld, B. H.; Arabea, K. A.; Suazo, L. A.; McDaniel, S. L.; Bowen, R. A.; Reynolds, M. M., Nitric oxide-releasing polysaccharide derivative

exhibits 8-log reduction against *Escherichia coli*, *Acinetobacter baumannii* and *Staphylococcus aureus*. *J. Controlled Release* **2015**, *217*, 228-234.

58. Linke, D.; Goldman, A., *Bacterial Adhesion: Chemistry, Biology and Physics*. Springer Science & Business Media: 2011; Vol. 715.

## CHAPTER 6

### INVESTIGATION OF ANTIBACTERIAL ESSENTIAL OIL-DERIVED THIN FILMS FORMED VIA PLASMA ENHANCED CHEMICAL VAPOR DEPOSITION

This chapter details the optimization of a plasma enhanced chemical vapor deposition to create thin films from eucalyptol (1,8-cineole) for low-fouling, antibacterial surfaces. This chapter is based on work published in *ACS Applied Materials and Interfaces* by Michelle N. Mann and Ellen R. Fisher and reprinted with permission from *ACS Appl. Mater. Interfaces*, **2017**, 9 (42), pp 36548–36560, copyright 2017, American Chemical Society. All data collection, analysis and the writing of the manuscript were performed by me, with significant writing and editorial contributions from Ellen Fisher. I would like to thank Mr. Matthew R. Maynard for assistance with depositions, contact angle goniometry and stability studies; Dr. Adoracion Pegalajar-Jurado for helpful discussion and guidance in project development; and Prof. C.S. Henry's research group for profilometry assistance. Funding for this project was provided by the National Science Foundation (CHE-1152963).

#### **6.1 Introduction**

Many polymers used in biomedical devices have limited biocompatibility because they promote bacterial adhesion and subsequent biofilm formation, ultimately leading to infection and device failure. Indeed, HAIs are a primary cause of increased morbidity and mortality in patients worldwide. In the United States alone, an estimated 1 out of 25 hospitalized patients are affected by an HAI at any given time, amounting to ~650,000 patients annually.<sup>1</sup> Although difficult to accurately calculate the cost of infection-related hospitalization, low estimates place the cost of

preventable HAIs at \$5.7 – 6.8 billion.<sup>2</sup> Approximately 80% of chronic infections are biofilm-related, with *E. coli* and *S. aureus* the most frequently isolated strains from these infections.<sup>3-4</sup> Broadly, bacterial infection presents a major challenge to developing advanced biomedical devices, and by extension, treating chronic infections while simultaneously controlling antibiotic resistance and reducing risk to patient health. This, in part, arises from the resilience of bacteria in a biofilm, as they are typically 10 – 1,000 times more resistant to antibiotics than planktonic bacteria.<sup>4</sup> Thus, it is critical to develop tailored surfaces to control bacterial adhesion and growth on polymeric biomaterials before biofilms can form, without promoting antibiotic resistance. Ideally, an antibacterial coating could be deposited on the surface of a biomedical device, allowing for the bulk material to remain unmodified, yet discouraging bacterial growth. Alternatively, a biocidal agent could be incorporated in the polymer to actively kill bacteria. A holy grail in antibacterial coatings for biomedical devices is the creation of a surface modification platform to achieve mechanically and chemically robust films with highly tailorable surface properties for the desired application.

One broad class of compounds being investigated for their medicinal properties are essential oils, many of which have antimicrobial properties supported by extensive clinical trials,<sup>5-13</sup> but are difficult to immobilize by conventional coating methods. Researchers have employed a few techniques to fabricate solid materials with essential oils, including incorporating polysaccharide films with essential oils,<sup>14-18</sup> microencapsulation,<sup>19-21</sup> and PECVD. In PECVD, a nonthermal rf plasma induces radicalization in a monomeric feed gas, creating reactive chemical species that polymerize to form a smooth, conformal coating on a substrate.<sup>22</sup> This technique allows for the fabrication of soft matter thin films from solid, liquid, or gaseous precursors where conventional methods may fail (e.g., monomers with only C–C functionality or ring structures). Plasma

polymerized films from essential oils are often optically transparent and smooth, making them suitable for a range of applications, including medical coatings and dielectric layers for electronics.<sup>23-29</sup> PECVD is ideal for depositing thin coatings on biomedical devices, as it provides a universal dry, single-step and sterile platform for device fabrication at low temperatures (<300 K), where the bulk mechanical properties and architecture of the underlying substrate are retained.<sup>30</sup> Indeed, plasmas have an extensive history of use in cleaning biomedical implant surfaces prior to implantation,<sup>31</sup> improving biocompatibility of medical implants and scaffolds,<sup>32-37</sup> and improving adhesion in complex composite biomaterials.<sup>38</sup> Moreover, changing PECVD parameters alters the degree of monomer fragmentation and crosslinking in the film, thus allowing for tailoring of film properties such as thickness, wettability, and surface chemistry for a desired application.

To date, PECVD has successfully fabricated thin films from oils of tea tree, lavender, eucalyptus and lemongrass, as well as some of their individual constituents.<sup>5-7, 9, 11-13, 23, 26, 28-29, 39-47</sup> 1,8-cineole (also known as eucalyptol) is a major component of tea tree oil that has promising antibacterial, antifungal, and anti-inflammatory capabilities.<sup>10, 39, 48-50</sup> Although it contains no conventionally polymerizable functionalities, 1,8-cineole has nevertheless shown recent success as an antibacterial plasma-polymerized coating on non-polymer (glass) and polymer (i.e., electrospun fiber mesh) substrates.<sup>23, 27, 46</sup> These studies demonstrated the feasibility of depositing 1,8-cineole-based coatings under a single set of plasma conditions; however, little is known about the effect of plasma parameters on film properties. Here, we describe the fabrication and comprehensive characterization of thin films from 1,8-cineole via PECVD (denoted ppCin), including their antibacterial properties. In addition, we utilize optical emission spectroscopy (OES) to determine the role of gas phase excited-state species in the PECVD

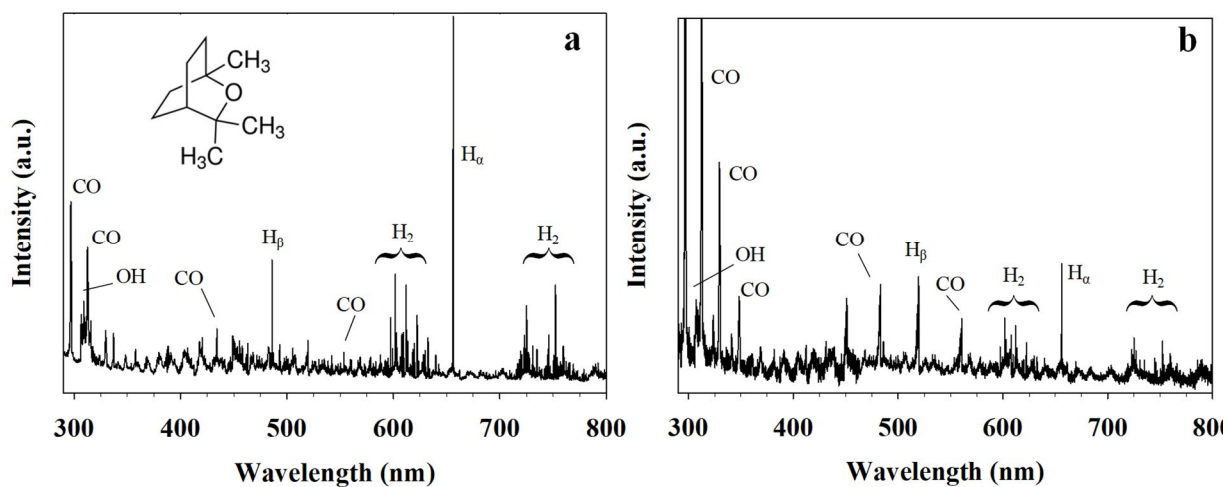


process as a function of plasma parameters. Notably, films deposited in the aforementioned previous studies were hydrophobic, limiting their use in biological environments. To tailor these films for use in biomedical devices, it is therefore advantageous to understand how plasma parameters can be tuned to increase film wettability. To further elucidate the role of wettability in ppCin antibacterial behavior, we employed H<sub>2</sub>O<sub>(v)</sub> plasmas to enhance hydrophilicity, as such an approach has been successful with a range of polymeric materials.<sup>37, 51-53</sup> Biological response is investigated for films of disparate chemistry and wettability [including H<sub>2</sub>O<sub>(v)</sub> plasma treated ppCin films and films fabricated from a hydrocarbon precursor (1,7-octadiene) to serve as a hydrophobic control] by assessing the attachment behavior and biofilm formation of gram-negative *E. coli* and gram-positive *S. aureus*. Specifically, we wish to elucidate to what degree the chemistry and antibacterial properties of the monomer are retained in the plasma polymer. We further seek to understand biofilm formation as a function of both the native antibacterial properties of the polymer and films' physical properties (i.e., roughness, wettability). Film robustness via stability and aging studies is used to demonstrate film practicality for biomedical device applications.

## **6.2 Results**

### **6.2.1. Gas-phase spectroscopy**

Raw OES spectra for 100% cineole plasmas ignited under two different conditions are shown in Figure 6.1. In general, the plasmas contained similar emission signals regardless of the plasma parameters used. The most intense peaks in the plasmas appear at 282.4, 309.1, 485.9, and 656.1 nm, corresponding to emission from CO, OH, H<sub>β</sub> and H<sub>α</sub>, respectively.<sup>54-57</sup> Other



**Figure 6.1.** Representative raw OES spectra for 100% 1,8-cineole plasmas at (a) 15 mTorr 50 W and (b) 100 mTorr 100 W. Panel (a) inset shows the structure of 1,8-cineole. Spectra were acquired with 50 ms integration time and 600 averages.

spectral features include H<sub>2</sub> molecular bands centered at ~610 and ~750 nm.<sup>58</sup> We have previously established that steady state conditions in our systems are reached in <10 s,<sup>59-60</sup> thus neither the presence nor intensity of peaks varied significantly during the 5 min treatment.

Although emitting species did not change with power or pressure, the relative peak intensities did vary. For example, in 100% cineole plasmas operating at 15 mTorr and 50 W, hydrogen species clearly dominate the emission spectrum (Fig. 6.1a), whereas for a plasma operating at higher power and pressure, CO emission intensities approach or exceed those of atomic and molecular hydrogen species (Fig. 6.1b). Because signal intensities can vary, we compared the ratios of emission intensities across all plasma parameters and, thereby, elucidated the effect of  $P$  and  $p$  on relative species' density.<sup>61</sup> The ratios of CO and H<sub>α</sub> species to OH (309.1 nm) are shown in Table 6.1. Notably, both H<sub>α</sub>/OH and CO/OH ratios were ~1 or greater, as CO and H species consistently dominated over OH species. In general, H<sub>α</sub>/OH decreased with increasing pressure (from ~4 – 6 to ~1 – 3) for all powers investigated (50, 100, and 150 W), whereas CO/OH ratios remained lower (ranging from ~2 – 4) at lower pressures and more than doubled at 100 mTorr (ranging from ~6 – 9), for all powers. Some  $P$  dependence may exist, as slightly more H<sub>α</sub> appears as  $P$  increases. Nevertheless, plasma pressure has greater influence than  $P$  in determining which species dominate OH in the plasma.

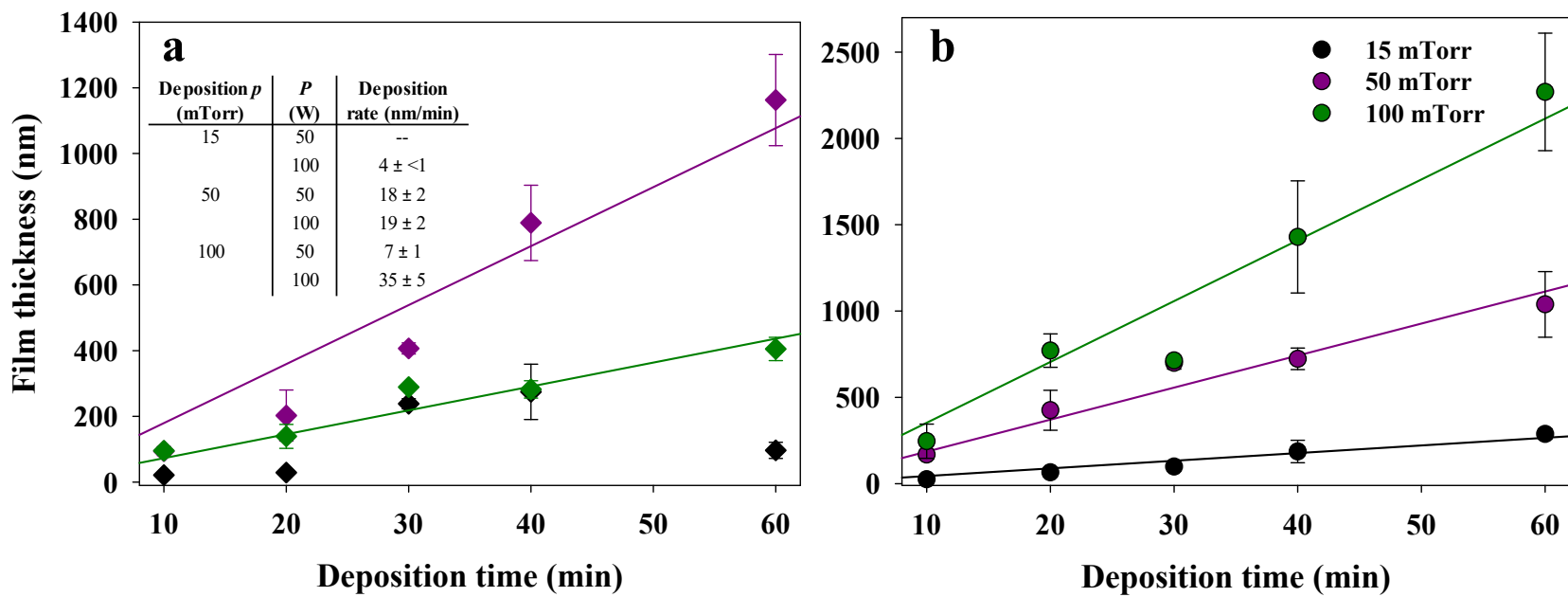
### 6.2.2. Film morphology, roughness, and deposition rate

Film thickness as a function of  $P$  and  $p$  is depicted in Figure 6.2. Deposition of ppCin is linear ( $R^2 > 0.9$ ) for all treatments except ppCin (low  $p, P$ ). Deposition rates vary from  $5 \pm <1 \text{ nm min}^{-1}$  to  $40 \pm 5 \text{ nm min}^{-1}$ . Overall, although increasing  $p$  appears to increase

**Table 6.1.** Ratios of H $\alpha$ /OH and CO/OH as a function of plasma parameters.<sup>a</sup>

Power (W)	Pressure (mTorr)	H $\alpha$ /OH	CO/OH
50	15	4.2 $\pm$ 0.2	2.2 $\pm$ <0.1
	50	2.0 $\pm$ <0.1	2.3 $\pm$ 0.1
	100	0.7 $\pm$ 0.2	7.2 $\pm$ 0.8
100	15	6.0 $\pm$ 1.7	2.5 $\pm$ 0.6
	50	2.8 $\pm$ 0.3	2.6 $\pm$ 0.1
	100	1.5 $\pm$ 0.2	9.4 $\pm$ 1.5
150	15	6.1 $\pm$ 0.4	1.1 $\pm$ 0.1
	50	5.1 $\pm$ 1.6	2.1 $\pm$ 0.4
	100	3.2 $\pm$ 0.5	6.3 $\pm$ 0.4

<sup>a</sup> Peaks at 282.4, 309.1 and 656.1 nm were used to determine intensities of CO, OH, and H $\alpha$ , respectively. Data points represent the mean and standard deviation of  $n \geq 3$ .



**Figure 6.2.** Film thickness as a function of deposition time for 15, 50 and 100 mTorr plasmas at (a) 50 W and (b) 100 W. Inset shows deposition rate provided by a linear fit of each set of plasma parameters ( $R^2 \geq 0.92$ ). Error bars represent standard deviation of the mean ( $n = 3$ ).

deposition rate, no clear relationship between  $P$  and deposition rate can be elucidated from data herein. Deposition rate and roughness data obtained for ppOct deposited in our systems has been previously characterized using optical profilometry. At  $\sim 44 \text{ nm min}^{-1}$ , ppOct is deposited at a comparable rate to that for ppCin (high  $p, P$ ).<sup>62</sup>

Optical profilometry data revealed all films had similar roughness parameters of  $R_a$  and  $R_q \leq 0.05 \text{ }\mu\text{m}$ , similar to those deposited previously.<sup>63</sup> Select  $R_q$  values are shown in Table 6.2. There were few exceptions where films reached  $R_a$  and  $R_q \sim 0.1 \text{ }\mu\text{m}$ ; however, roughness parameters never exceeded  $0.15 \text{ }\mu\text{m}$ , in agreement with SEM data that revealed films with smooth and conformal morphology (Fig. 6.3a-b). In contrast,  $\text{H}_2\text{O}_{(v)}$  plasma treated films display clearly rougher morphology, with raised and pitted regions (Fig. 6.3c). Interestingly, despite appearing to have a rougher morphology in SEM images, no significant changes in  $R_a$  or  $R_q$  were observed after  $\text{H}_2\text{O}_{(v)}$  plasma treatment of films ( $R_a = <0.02$  and  $R_q < 0.04 \text{ }\mu\text{m}$ ). Previously characterized ppOct films were found to have  $R_q = 0.06 \pm 0.04 \text{ }\mu\text{m}$ .<sup>62</sup>

### 6.2.3. Film composition

*Fourier Transform Infrared Spectroscopy.* Monomer FTIR spectra (Fig. 6.4a) showed absorbance peaks for methyl ( $2980, 2969, 2945, 2880 \text{ cm}^{-1}$ ) and methylene stretching ( $2924$  and  $2880 \text{ cm}^{-1}$ ).<sup>64-65</sup> Notable peaks in the spectra for 1,8-cineole include C–H bending at  $1375$  and  $1081 \text{ cm}^{-1}$ , C–C stretching at  $1215 \text{ cm}^{-1}$ , and C–O stretching at  $1168 \text{ cm}^{-1}$ . Spectra for 1,7-octadiene also contained peaks for C=C stretching ( $3062$  and  $1640 \text{ cm}^{-1}$ ) and monosubstituted C–H bending ( $910$  and  $990 \text{ cm}^{-1}$ ). Methyl and methylene stretching are also evidenced in spectra for the plasma polymers as well as an additional band at  $\sim 1706 \text{ cm}^{-1}$ , indicating C=O stretching

**Table 6.2.** Wettability, surface O/C ratio, and binding environment composition of plasma polymerized films.

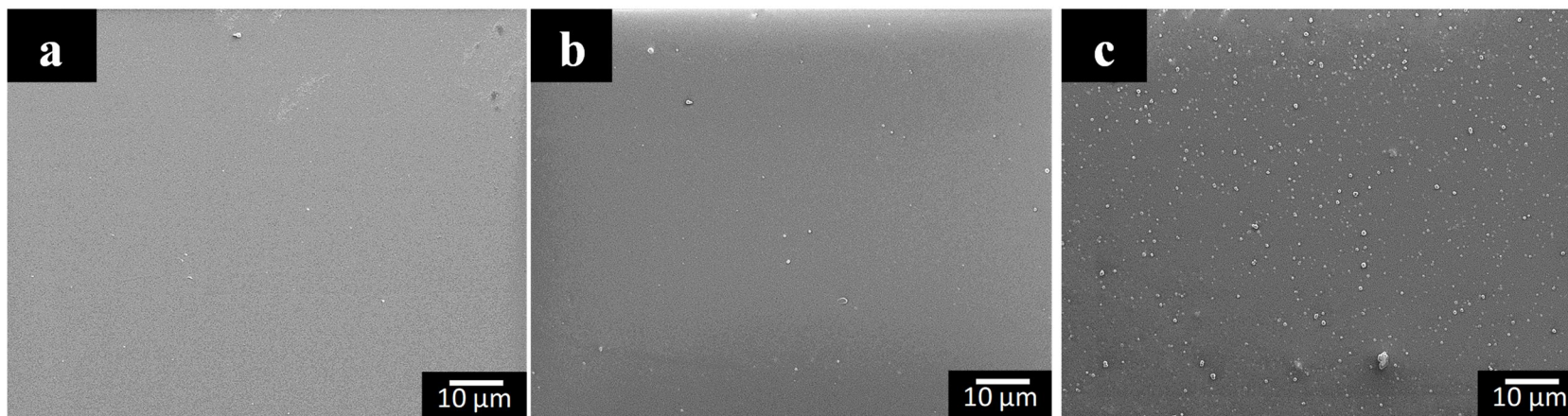
Film <sup>a</sup>	$R_q$ ( $\mu\text{m}$ ) <sup>b</sup>	WCA ( $^\circ$ )	O/C	%C-C/C-H	%C-OH/C-OR	%C=O	%O-C=O
ppOct	$0.06 \pm 0.04^c$	$93.7 \pm 1.4$	$0.14 \pm 0.01$	$85.8 \pm 0.8$	$12.8 \pm 0.9$	$1.5 \pm 0.2$	---
ppCin 15 mTorr 50 W	$<0.01$	$54.3 \pm 4.1$	$0.38 \pm <0.01$	$73.2 \pm 1.7$	$19.9 \pm 1.5$	$7.0 \pm 0.2$	---
ppCin 15 mTorr 100 W	$0.01 \pm <0.01$	$57.7 \pm 2.7$	$0.37 \pm <0.01$	$61.4 \pm 4.3$	$31.8 \pm 4.0$	$6.8 \pm 0.3$	---
ppCin 100 mTorr 100 W	$0.04 \pm 0.01$	$85.6 \pm 1.1$	$0.23 \pm 0.03$	$73.0 \pm 3.5$	$22.7 \pm 2.4$	$4.3 \pm 1.2$	---
Treated <sup>d</sup> ppCin 15 mTorr 50 W	$<0.01$	$20.4 \pm 1.2$	$0.55 \pm 0.02$	$54.7 \pm 1.3$	$29.2 \pm 1.2$	$12.5 \pm 1.0$	$3.6 \pm 1.1$
Treated <sup>d</sup> ppCin 100 mTorr 100 W	$0.04 \pm 0.01$	$34.4 \pm 0.9$	$0.57 \pm 0.01$	$51.3 \pm 2.4$	$30.2 \pm 2.8$	$11.6 \pm 0.6$	$6.8 \pm 0.9$

<sup>a</sup>5 min, 10 cm downstream; on Si

<sup>b</sup> $R_a$  values were similar to  $R_q$  values

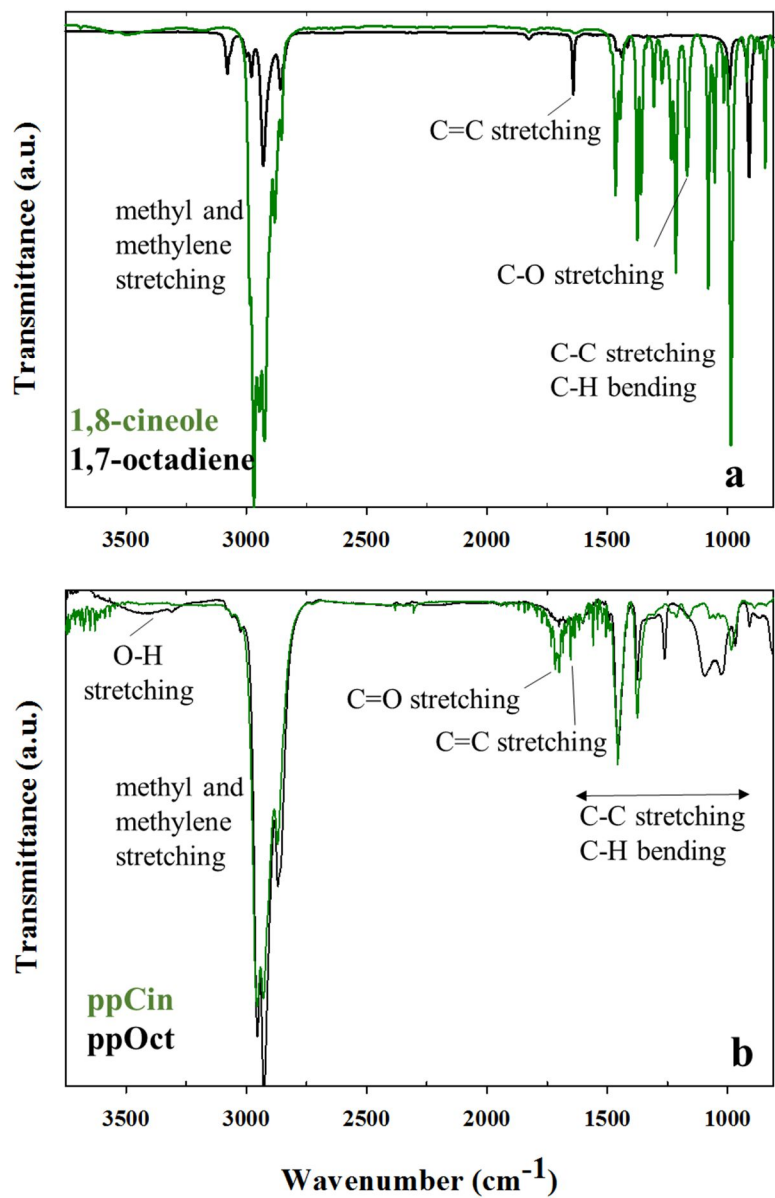
<sup>c</sup>Ref 72

<sup>d</sup>H<sub>2</sub>O<sub>(v)</sub> plasma 50 mTorr, 20 W, 2 min, 10 cm downstream



**Figure 6.3.** Representative SEM images (1000 $\times$ ) of ppCin films deposited at (a) ppCin (low  $p,P$ ) [15 mTorr 50 W] (b) ppCin (high  $p,P$ ) [100 mTorr 100 W] and (c)  $H_2O_{(v)}$  plasma treated ppCin (high  $p,P$ ).



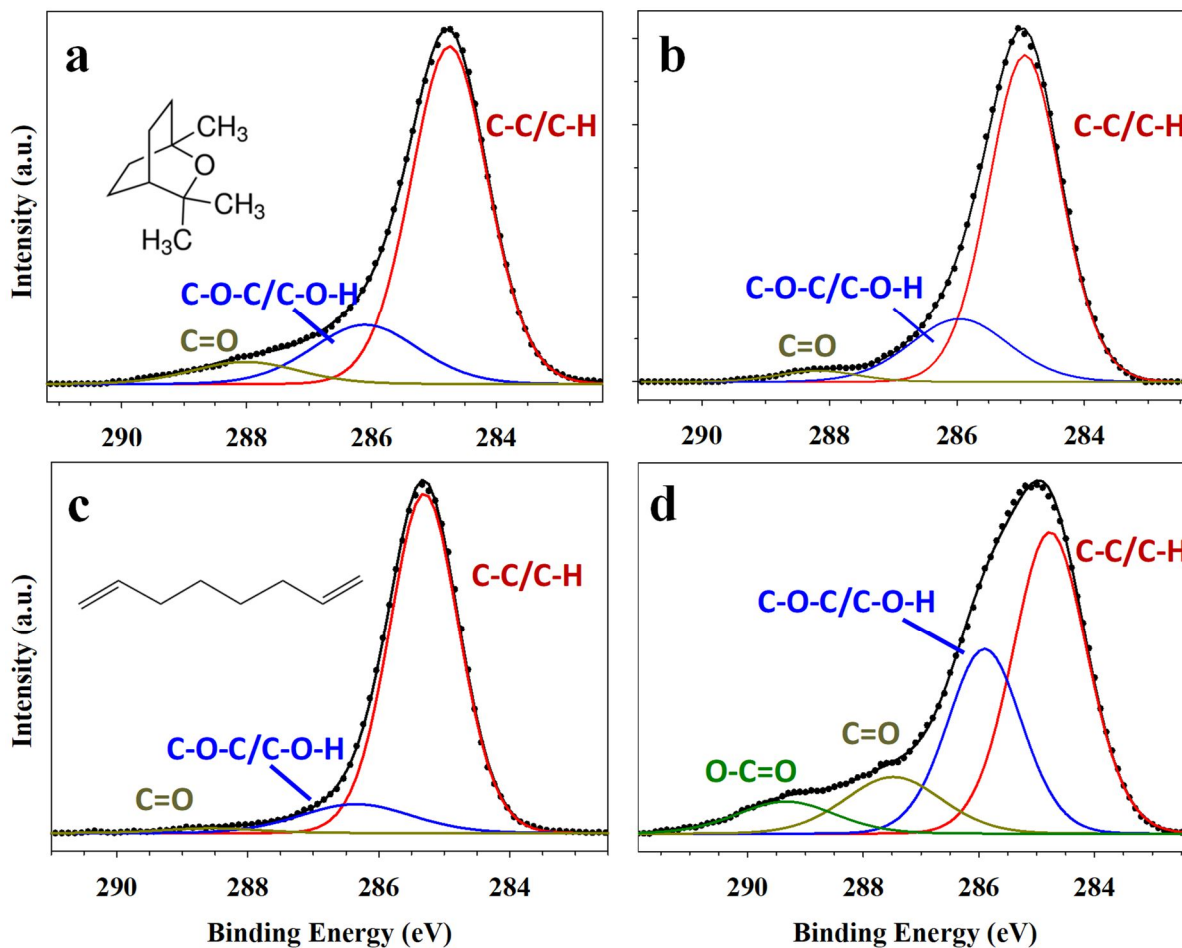


**Figure 6.4.** Representative FTIR spectra for (a) cineole and octadiene monomers (b) ppCin and ppOct films. Note peak intensities should not be compared between samples as neither monomer nor film thickness was controlled.

(Fig. 6.4b). ppOct spectra present additional peaks for C–H bending (1456, 1099 and 1031  $\text{cm}^{-1}$ ) and C–C stretching (1264  $\text{cm}^{-1}$ ) in addition to a very weak and broad O–H stretch centered at  $\sim 3420 \text{ cm}^{-1}$ .  $\text{H}_2\text{O}_{(\text{v})}$  plasma surface modification of ppCin films does not result in FTIR spectral changes (data not shown), which is relatively unsurprising given that FTIR measures the bulk composition of a material.

*X-ray photoelectron spectroscopy.* XPS spectra, Figure 6.5, display the surface composition of ppOct, ppCin and  $\text{H}_2\text{O}_{(\text{v})}$  treated ppCin films. Signal from the underlying Si substrate was not observed, confirming our optical profilometry results that all films were  $>10 \text{ nm}$  thick. ppCin films deposited under all conditions explored herein contain 3 peaks in the  $\text{C}_{1\text{s}}$  spectra: (1) C–C/C–H at 285.0 eV (2) C–OR/C–OH at 286.3 eV, and (3) C=O at 288.1 eV. Quantitative results showing contributions from each functionality are listed in Table 6.2. Compared to films deposited at 15 mTorr and 50 W (Fig. 6.5a), ppCin films fabricated at the same pressure but at  $P = 100 \text{ W}$  contain clearly enhanced alcohol/ether functionality (Table 6.2). Interestingly, O/C ratios are the same within error for films deposited from these two systems and surface carbonyl content is similar (Table 6.2). When  $p$  is increased to 100 mTorr, deposition at  $P = 100 \text{ W}$  (Fig. 6.5b) results in a considerably lower O/C ratio of  $0.23 \pm 0.03$  compared to  $0.37 \pm <0.01$  for ppCin deposited at 15 mTorr and 100 W and less alcohol/ether functionality (reduced to  $22.7 \pm 2.4\%$  from  $31.8 \pm 4.0\%$ ). ppOct films contained the same binding environments as ppCin, although with significantly less C=O functionality than ppCin films (Fig. 6.5c).

$\text{C}_{1\text{s}}$  high resolution XPS spectra for  $\text{H}_2\text{O}_{(\text{v})}$  plasma treated ppCin films are shown in Figure 6.5d. Compared to ppCin films prior to treatment (O/C =  $0.18 \pm 0.01$ ), the corresponding  $\text{H}_2\text{O}_{(\text{v})}$  plasma treated films have an additional  $\text{C}_{1\text{s}}$  peak at 289.1 eV, representing COOR/COOH



**Figure 6.5.** Representative high resolution  $C_{1s}$  XPS spectra for deposited (a) ppCin (low  $p,P$ ) [15 mTorr 50 W], (b) ppCin (high  $p,P$ ) [100 mTorr 100 W], (c) ppOct, and (d)  $H_2O_{(v)}$  treated [50 mTorr 20 W 2 min] ppCin (high  $p,P$ ). Insets in (a) and (b) show the structures of 1,8-cineole and 1,7-octadiene monomers, respectively.

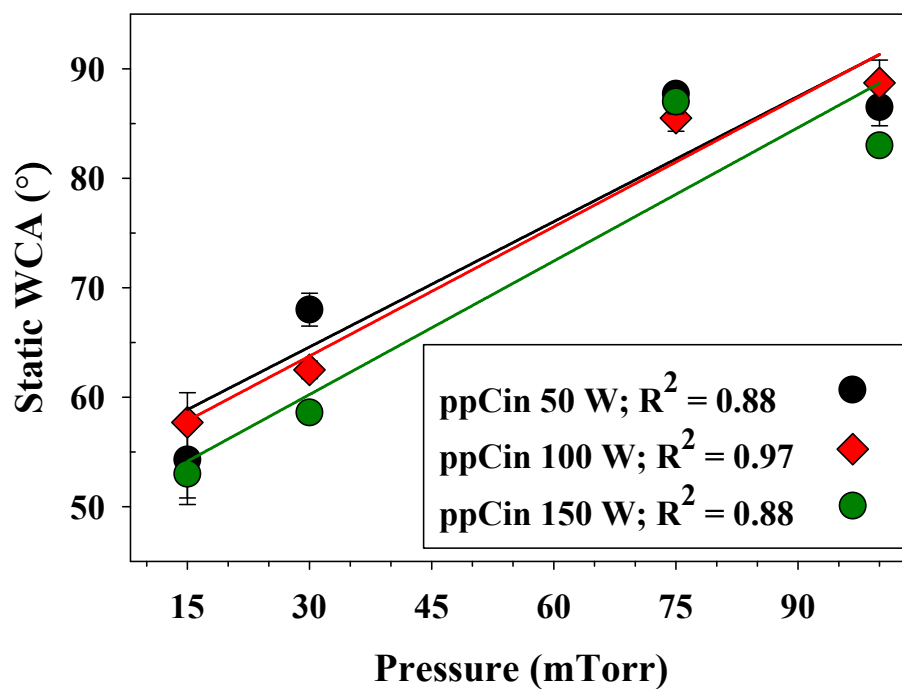
binding environment and a significantly enhanced O/C ratio ( $0.57 \pm <0.01$ , Table 6.2). This O/C ratio enhancement is corroborated by a substantial increase in peak area assigned to alcohol/ether and acid/ester functionality and a concomitant decrease in C–C/C–H binding environment peak area.

#### 6.2.4. Film wettability and aging

*WCA analysis.* Select WCA values for ppCin films are listed in Table 6.2. Also shown are WCAs as a function of monomer gas pressure for  $P = 50 - 150$  W (Fig. 6.6). For reference, clean, unmodified glass slides have a WCA of  $\sim 10^\circ$  and ppOct films have a  $WCA = 93.7 \pm 1.4^\circ$ . In general, at low  $p$  (15 mTorr), a more hydrophilic film results ( $WCA \sim 50 - 60$ ), whereas WCA approaches  $90^\circ$  for all films deposited at  $p = 100$  mTorr. For example, ppCin films with the lowest WCA are deposited in a 50 W, 15 mTorr plasma ( $WCA = 54.3 \pm 4.1^\circ$ ), and when  $p$  is doubled to 30 mTorr, WCA increases to  $68.0 \pm 1.5^\circ$ . At  $p = 100$  mTorr, WCA reaches  $86.5 \pm 1.7^\circ$ , approaching that of ppOct. For all  $P$ , WCA increases linearly with  $p$  ( $R^2 \geq 0.88$ ), Figure 6.6.

All ppCin films became significantly more hydrophilic after  $H_2O_{(v)}$  plasma treatment, Table 6.2. For example, ppCin films deposited at 15 mTorr and 50 W ( $WCA = 54.3 \pm 4.1^\circ$ ) experienced a dramatic increase in wettability after treatment ( $WCA = 20.4 \pm 1.2^\circ$ ). Likewise, ppCin deposited at 100 mTorr and 100 W ( $WCA = 85.6 \pm 1.1^\circ$ ) were rendered significantly more wettable post treatment ( $WCA = 34.4 \pm 0.9^\circ$ ).

*WCA after aging.* Overall, ppCin films exhibited only minor changes in wettability upon aging (Table 6.3). Interestingly, films deposited at  $p < 100$  mTorr experienced a slight WCA



**Figure 6.6.** Static water contact angle as a function of deposition pressure for films deposited in 50, 100, and 150 W plasmas. Error bars represent the standard deviation of the mean (n = 9).

**Table 6.3.** WCA of plasma polymerized films over 2 month aging period.<sup>a</sup>

	<b>Pressure (mTorr)</b>	<b>Power (W)</b>	<i>fresh</i>	<i>1 day</i>	<i>1 week</i>	<i>2 weeks</i>	<i>1 month</i>	<i>2 months</i>
ppCin	15	50	54.3 ± 4.1°	58.6 ± 1.2°	59.7 ± 2.0°	61.0 ± 3.3	62.1 ± 2.2	63.9 ± 1.5°
	30	30	74.4 ± 1.5°	73.8 ± 0.6°	73.0 ± 1.3°	71.9 ± 1.6°	78.2 ± 1.6°	75.7 ± 1.9°
	30	50	68.0 ± 1.5°	72.9 ± 1.0°	75.1 ± 0.6°	71.8 ± 2.6°	78.1 ± 1.5°	76.1 ± 0.6°
	100	25	86.3 ± 1.4°	84.0 ± 1.4°	82.3 ± 1.7°	82.4 ± 1.0°	82.4 ± 1.1°	80.6 ± 0.6°
	100	50	86.5 ± 1.7°	86.5 ± 0.9°	82.4 ± 1.1°	80.7 ± 1.2°	80.9 ± 0.2°	83.0 ± 1.0°
	100	100	85.6 ± 1.1°	85.1 ± 1.2°	81.3 ± 0.5°	79.8 ± 1.0°	81.3 ± 0.8°	81.7 ± 1.7°
Treated <sup>b</sup> ppCin	15	50	20.4 ± 1.2°	34.5 ± 0.9°	42.1 ± 0.6°	43.1 ± 0.6°	44.5 ± 0.7°	44.1 ± 1.0°
ppOct	100	25	93.7 ± 1.4°	90.3 ± 0.8°	85.2 ± 0.6°	85.0 ± 1.0°	83.1 ± 1.4°	82.1 ± 1.5°

<sup>a</sup> All depositions completed on glass placed 10 cm downstream from coil region for 5 min except for ppOct (10 min). Values represent the mean and standard deviation of  $n \geq 9$  measurements.

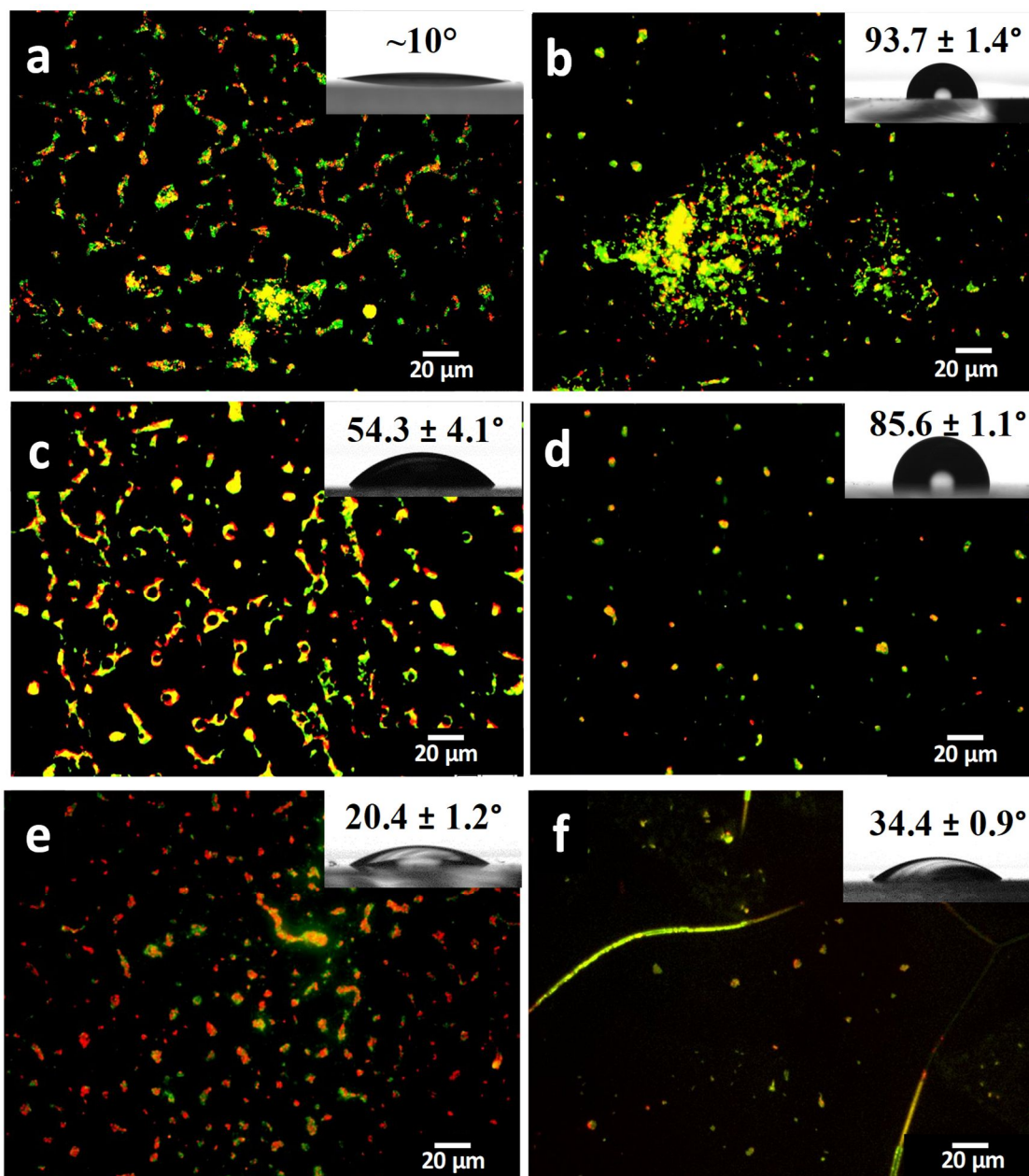
<sup>b</sup> H<sub>2</sub>O<sub>(v)</sub> plasma operating at 50 mTorr and 20 W for 2 min.

increase whereas those deposited at  $p = 100$  mTorr show a small WCA decrease upon aging. For example, WCA for ppCin films deposited at 15 mTorr and 50 W increased  $\sim 10^\circ$  and WCA for ppCin films deposited at 100 mTorr and 100 W decreased  $\sim 4^\circ$ . Importantly, treated ppCin films remained more wettable even after aging than could be achieved in ppCin films as deposited.

### 6.2.5. Bacterial interactions

*Bacterial attachment and growth.* Representative fluorescence microscopy images of attached *E. coli* on controls and ppCin films are shown in Fig. 6.7. *E. coli* attach to both hydrophilic glass slides (Fig. 6.7a) and hydrophobic ppOct film (Fig. 6.7b) controls, forming cluster and chain-like morphologies indicative of colony growth. Both viable (fluoresce green) and nonviable (fluoresce red) bacteria are present on both controls. ppCin (low  $p,P$ ) films (Fig. 6.7c) also exhibit a significant amount of attached *E. coli* in early-stage biofilm growth. ppCin (high  $p,P$ ) films, however, appear to have fewer attached bacteria, and although some appear viable, no initial stages of colony formation are observed (Fig. 6.7d).  $\text{H}_2\text{O}_{(v)}$  plasma treated ppCin films (Fig. 6.7e,f) exhibited similar *E. coli* attachment and growth behavior as their untreated counterparts. A notable difference with bacterial attachment on  $\text{H}_2\text{O}_{(v)}$  plasma treated ppCin films can be observed in Fig. 6.7f, where film instability results in the formation of wrinkles in the film that can be penetrated by bacteria. In these instances, bacteria can attach to the underlying glass slide and grow in channels formed by the wrinkling. Glass slides and ppCin films displayed homogenous attachment behavior across the sample surface, whereas attachment behavior on ppOct films was more heterogeneous.

Identical assays were completed with gram-positive *S. aureus* and similar results to those for *E. coli* were obtained (Fig. 6.8), with some notable differences. In total, bacteria are attached



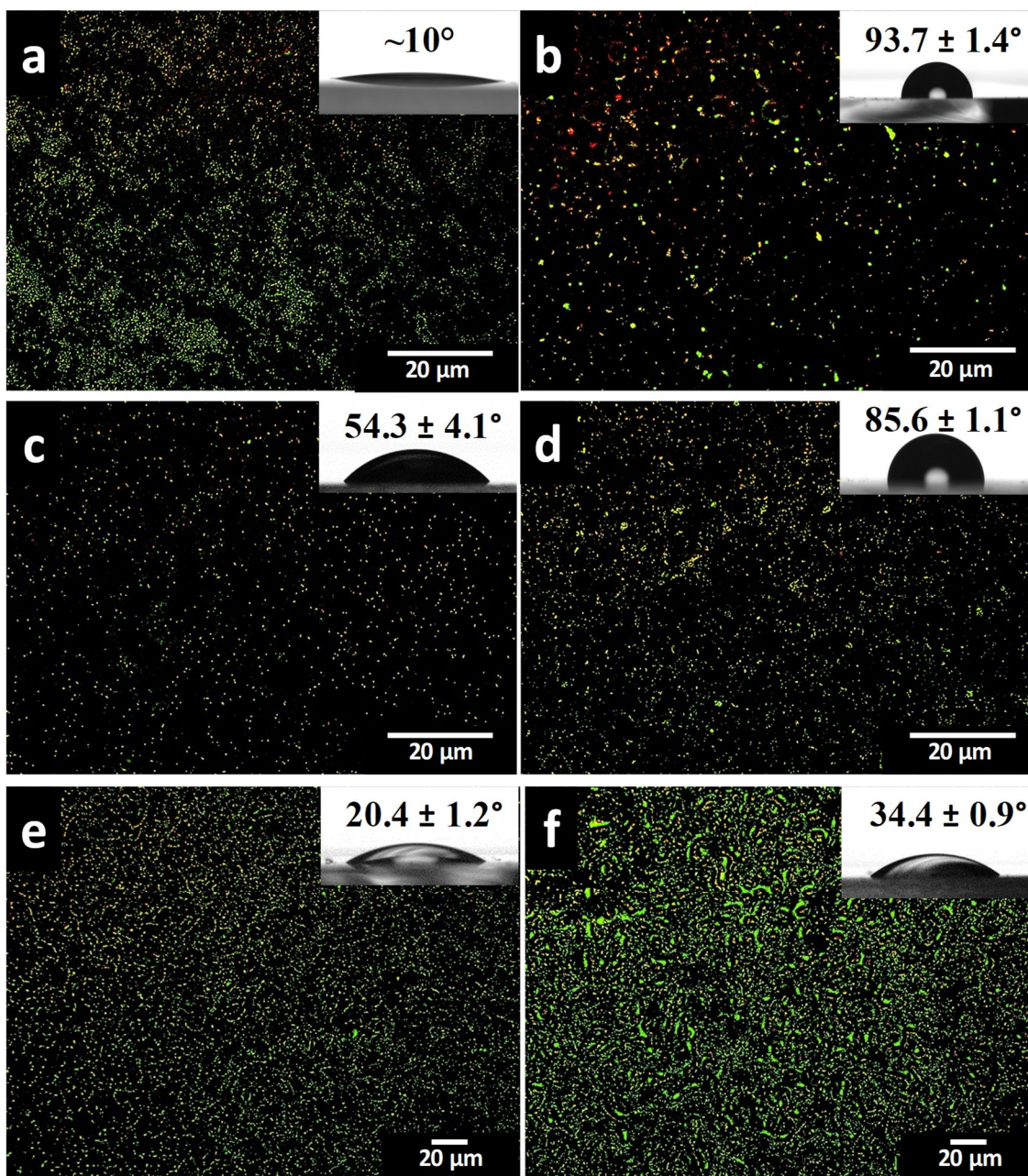
**Figure 6.7.** Fluorescence microscopy images of *E. coli* attached after 24 h incubation to (a) control glass slides and glass slides with films of (b) ppOct; (c) ppCin (low  $p,P$ ) [15 mTorr 50 W]; (d) ppCin (high  $p,P$ ) [100 mTorr 100 W]; (e)  $H_2O_{(v)}$  treated ppCin (low  $p,P$ ); and (f)  $H_2O_{(v)}$  treated ppCin (high  $p,P$ ). Green indicates viable attached bacteria whereas red indicates dead bacteria. Images are representative of  $n \geq 9$  samples examined.



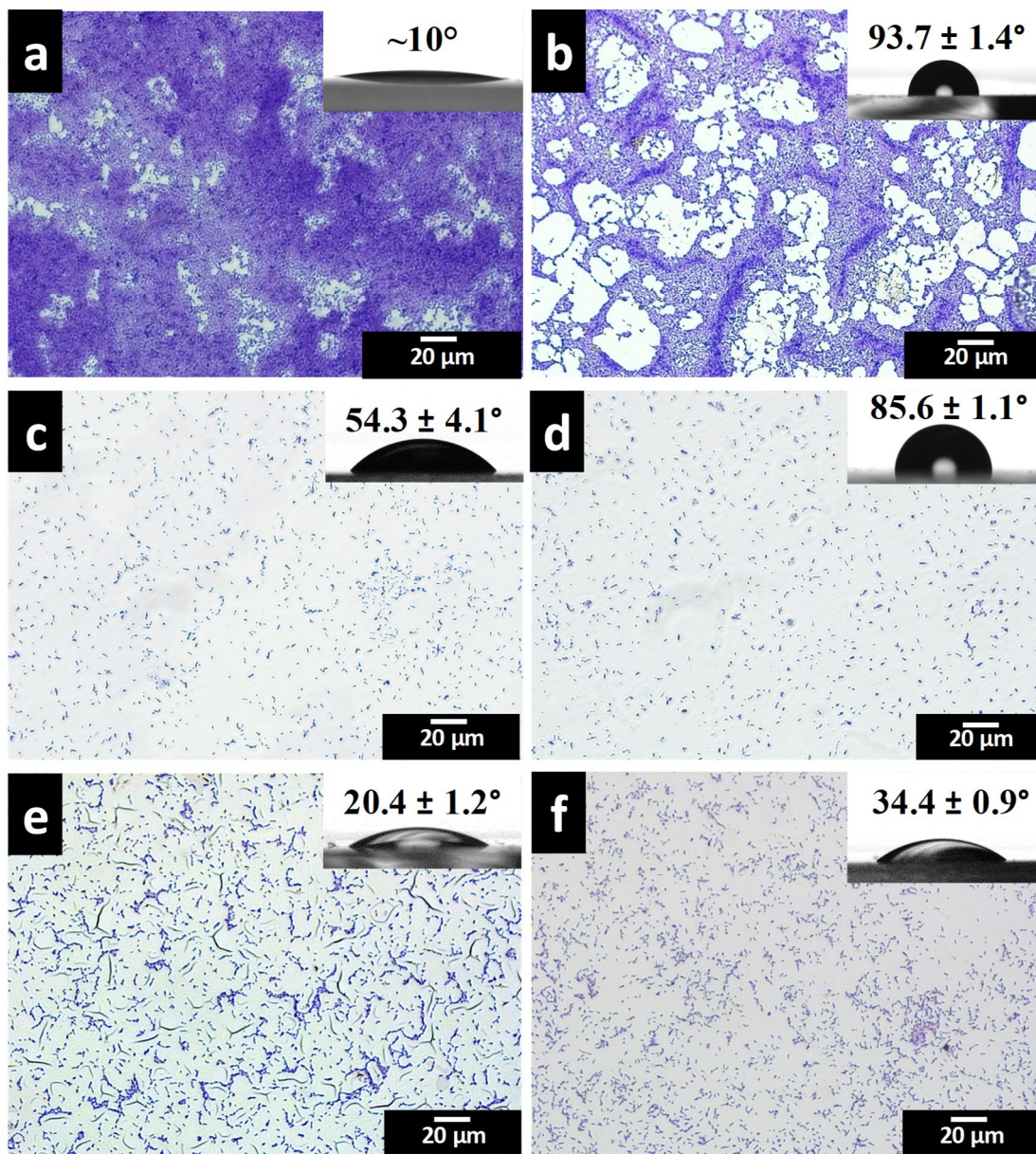
homogenously on all control and films, however, no cluster-like morphologies are present to indicate significant bacterial growth past the initial attachment phase. For glass slides, the presence of green fluorescence indicates a significantly larger number of viable bacteria (Fig. 6.8a) compared to *E. coli* attachment results, but this is not the case with all deposited ppCin films, as there are fewer attached bacteria and most appear nonviable (yellow fluorescence). H<sub>2</sub>O<sub>(v)</sub> plasma treated ppCin films (Fig. 6.8e,f) have slightly more attached *S. aureus* bacteria, with some cluster-like growth (Fig. 6.8f), when compared to results from *E. coli* assays.

*Biofilm formation.* Bright field microscopy images (Fig. 6.9) depict early-stage *E. coli* biofilm growth on samples. Both hydrophilic glass slides (Fig. 6.9a) and hydrophobic ppOct films (Fig. 6.9b) showed significant early-stage biofilm formation, as seen by the cluster-like growth indicative of colonization. We noted ppOct films tended to swell during the 5 d incubation period, resulting in bubble-like features around which bacteria tended to colonize preferentially (Fig. 6.9b). Despite these bubbles, no holes nor delamination were observed. In contrast, ppCin films had little growth of *E. coli* past the initial attachment stage, as indicated by the presence of distinguishable individual bacterial cells (Fig. 6.9c,d). Compared to untreated ppCin, *E. coli* cells further colonized H<sub>2</sub>O<sub>(v)</sub> plasma treated ppCin surfaces, evidenced by the formation of small bacterial clusters on the film surface (Fig. 6.9e,f). Overall, comparable results were obtained from *S. aureus* biofilm formation assays (Fig. 6.10) as those for *E. coli*, with the most notable difference being the overall increased proliferation of *S. aureus* across the ppCin film surface (Fig. 6.10c-f).

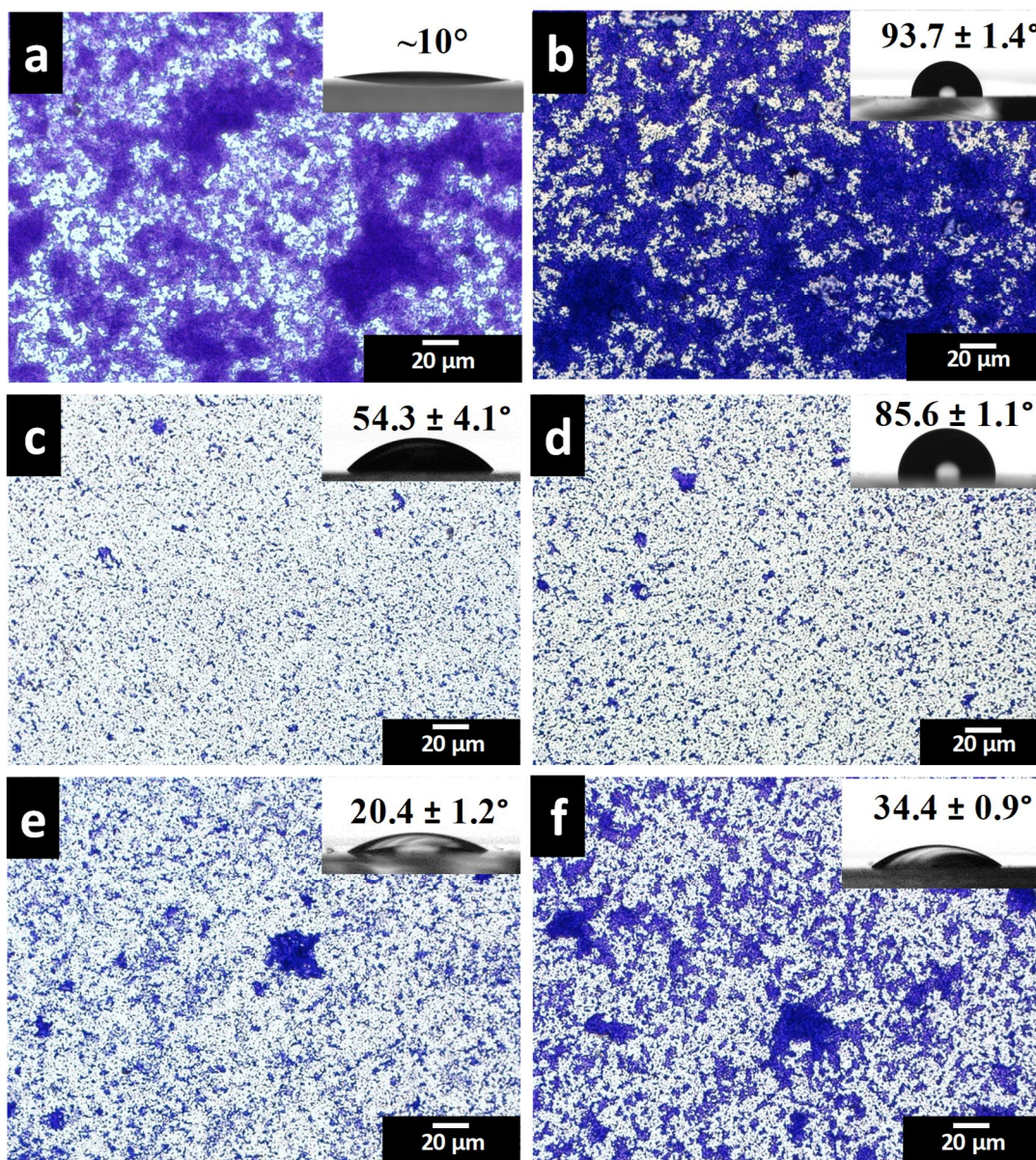
The percentage of each sample covered with biofilm is shown in Fig. 6.11. *E. coli* biofilm covered glass slides and ppOct films to a similar extent ( $37.1 \pm 6.0\%$  and  $39.9 \pm 8.9\%$ , respectively), with more variability observed in ppOct, depending on the extent of film bubbling,



**Figure 6.8.** Fluorescence microscopy images of *S. aureus* attached after 24 h incubation to (a) control glass slides and glass slides with films of (b) ppOct; (c) ppCin (low  $p,P$ ) [15 mTorr 50 W]; (d) ppCin (high  $p,P$ ) [100 mTorr 100 W]; (e)  $H_2O_{(v)}$  treated ppCin (low  $p,P$ ); and (f)  $H_2O_{(v)}$  treated ppCin (high  $p,P$ ). Green indicates viable attached bacteria whereas red indicates dead bacteria. Images are representative of  $n \geq 9$  samples examined.



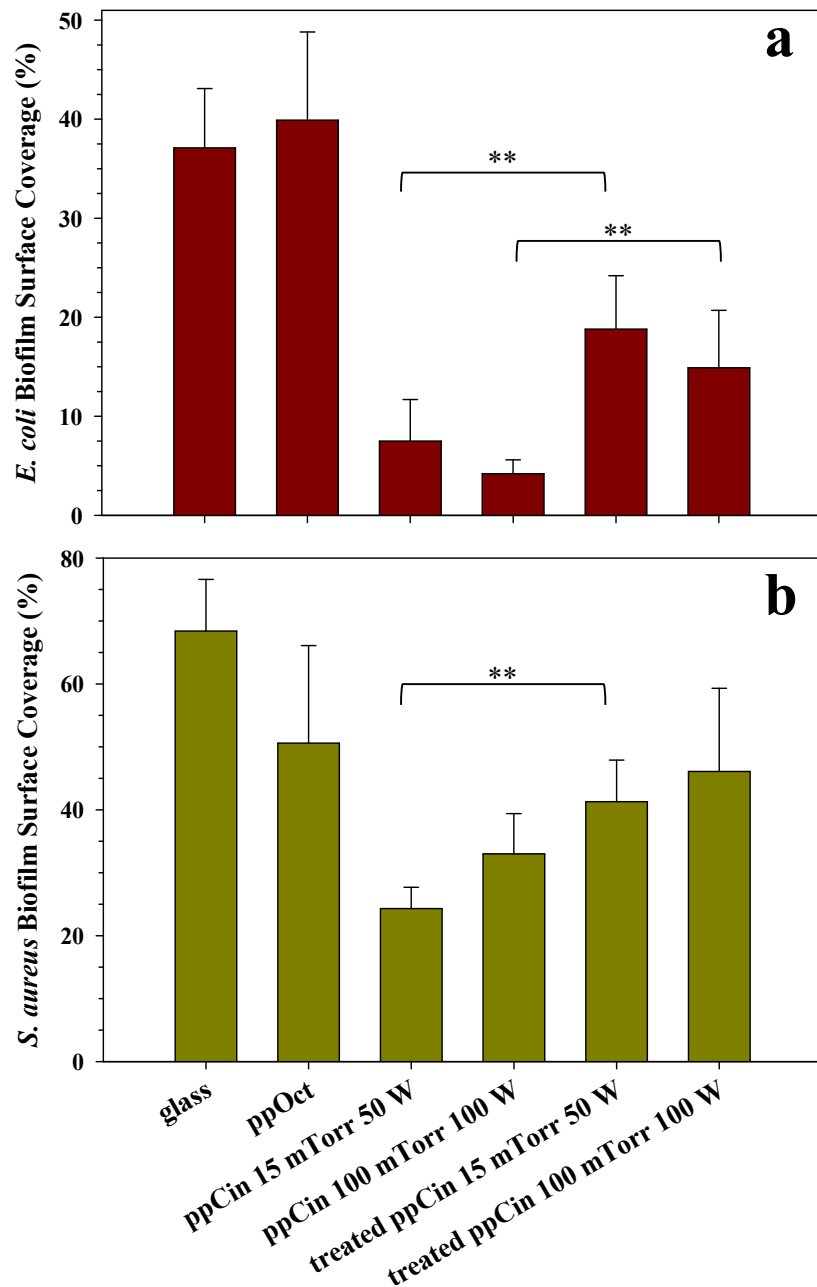
**Figure 6.9.** Bright field microscopy images of *E. coli* biofilm growth after 5 day incubation on (a) control glass slides and glass slides with films of (b) ppOct; (c) ppCin (low  $p,P$ ) [15 mTorr 50 W]; (d) ppCin (high  $p,P$ ) [100 mTorr 100 W]; (e) H<sub>2</sub>O<sub>(v)</sub> treated ppCin (low  $p,P$ ); and (f) H<sub>2</sub>O<sub>(v)</sub> treated ppCin (high  $p,P$ ). Bacteria were stained with crystal violet. Images are representative of  $n \geq 9$  samples examined.



**Figure 6.10.** Bright field microscopy images of *S. aureus* biofilm growth after 5 d incubation on (a) control glass slides and glass slides with films of (b) ppOct; (c) ppCin (low  $p,P$ ) [15 mTorr 50 W]; (d) ppCin (high  $p,P$ ) [100 mTorr 100 W]; (e)  $H_2O_{(v)}$  treated ppCin (low  $p,P$ ); and (f)  $H_2O_{(v)}$  treated ppCin (high  $p,P$ ). Bacteria were stained with crystal violet. Images are representative of  $n \geq 9$  samples examined.

as seen in Fig. 6.9a. Surface biofilm coverage on ppCin (low  $p,P$ ) and ppCin (high  $p,P$ ) was significantly lower ( $<10\%$ ;  $p < 0.01$ ) than on glass or ppOct films (Fig. 6.11a). This confirms that *E. coli* observed during attachment assays (Fig. 6.7c,d) were largely nonviable, and thus, unable to colonize the ppCin surface over the 5 day biofilm formation assay period. In contrast, *S. aureus* surface coverage on glass ( $68.4 \pm 8.2\%$ ) almost doubled that of *E. coli* (Fig. 6.11b). ppOct controls exhibited less *S. aureus* biofilm growth ( $50.6 \pm 15.5\%$ ) than glass ( $p < 0.01$ ), but were the most inconsistent between samples, likely because of film swelling, as discussed above. ppCin films had reduced *S. aureus* biofilm surface coverage compared to either control ( $p < 0.01$ ). ppCin (low  $p,P$ ) had the least surface coverage ( $24.3 \pm 3.4\%$ ) compared to ppCin (high  $p,P$ ) ( $33.0 \pm 6.4\%$ ), reversed from the trend observed during *E. coli* biofilm formation assays.

Surface coverage (Fig. 6.11a) increased to  $18.8 \pm 5.4\%$  for treated ppCin compared to untreated films ( $7.5 \pm 4.2\%$ ;  $p < 0.01$ ), and we also noted the formation of wrinkles in the films' surface after the 5 d assay. Despite increased *E. coli* biofilm coverage on the  $H_2O_{(v)}$  plasma treated ppCin (low  $p,P$ ), coverage remained significantly lower than that on glass or ppOct controls ( $p < 0.01$ ). Treated ppCin (high  $p,P$ ), displayed a significant increase in bacterial cluster formation (Fig. 6.9f) over the untreated film. Surface coverage increases to  $14.9 \pm 5.8\%$  after  $H_2O_{(v)}$  plasma treatment compared to  $4.2 \pm 1.4\%$  for the untreated film ( $p < 0.01$ ), though the *E. coli* biofilm coverage on treated films remains significantly smaller than controls ( $p < 0.01$ ). For treated ppCin (low  $p,P$ ), *S. aureus* biofilm growth significantly increased to  $41.3 \pm 6.6\%$  ( $p < 0.01$ ; Fig. 6.8b).  $H_2O_{(v)}$  plasma treated ppCin (high  $p,P$ ) exhibited  $46.1 \pm 13.2\%$  surface coverage, but this increase was not significant compared to films as deposited. *S. aureus* biofilm growth for  $H_2O_{(v)}$  treated ppCin (high  $p,P$ ) and  $H_2O_{(v)}$  treated ppCin (low  $p,P$ ) remained lower



**Figure 6.11.** Percent surface coverage of (a) *E. coli* and (b) *S. aureus* on control glass slides and deposited films. Statistical significance is marked by \*\* ( $p < 0.01$ ), except for control films. For *E. coli*,  $p < 0.01$  for both controls compared to untreated and treated ppCin films. For *S. aureus*,  $p < 0.01$  for glass compared to all films, and  $p < 0.01$  for ppOct compared to both untreated ppCin films. Values represent mean  $\pm$  standard deviation for  $n \geq 9$  samples.

than that on glass slides ( $p < 0.01$ ), but was not different than that observed on ppOct. Moreover, treated ppCin (high  $p,P$ ) films were stable, exhibiting no bubble or wrinkle formation, after 5 d in bacterial media.

### 6.3 Discussion

Despite numerous clinical trials<sup>10, 39, 48-50</sup> demonstrating the efficacy of tea tree oil as an antibiotic, little is known about how each individual constituent contributes to its antibacterial activity, and even less is understood about how antibacterial components can be retained in the plasma polymerized film. Herein, we discuss the role of plasma parameters in influencing the subsequent interactions of bacteria with our films, ultimately leading to low-fouling coatings that can be applied to biomedical devices with the aim of reducing the high rate of HAIs.

#### 6.3.1 Understanding how plasma chemistry influences film deposition and functionality

*Film and monomer bulk composition.* Our FTIR spectra of cineole monomer and films generally confirm results by Easton *et al.*,<sup>27</sup> indicating a primarily hydrocarbon film comprising methyl and methylene functionalities. Differences in the spectra between the monomer and film likely arise from rearrangement of the monomer C–C/C–H structure upon film deposition; the large number of strong methyl peaks suggests highly cross-linked films comprising short polymer chains, as is common with plasma polymers upon hydrogenation of broken chains.<sup>66</sup> Additionally, our data suggest formation of C=O functionality upon polymerization of 1,8-cineole, supported by the presence of C=O and COOH species in XPS spectra. Others have observed similar bulk composition for films deposited from essential oil-based precursors, such

as *Lavandula angustifolia* (LA), an essential oil with 1,8-cineole as a major component (0.1 – 20%). Easton *et al.* found that polyLA films contained less alcohol/ether functionality as  $P$  increases,<sup>43</sup> similar to what is revealed in our ppCin XPS spectra. Notably, we observe FTIR absorption peaks from C=O and OH species also arise from polymerization of 1,7-octadiene, but XPS spectra suggest these species are incorporated to a lesser degree, likely arising from post deposition oxidation.

Collectively, XPS and OES data reveal that gas-phase species are connected to the resulting film composition. As the density of plasma species has a greater dependence on  $p$  than  $P$ , collisional effects and recombination may play a greater role in determining species formation than monomer fragmentation. Indeed, XPS results reveal that  $p$  plays a significant role in determining oxygen functionality, with ~50% increase in O/C as  $p$  is decreased from 100 mTorr to 15 mTorr (Table 6.2). The incorporation of C–OH and C=O species increases, likely because of the greater OH gas-phase density at  $p < 100$  mTorr. Likewise, our data show clearly enhanced alcohol/ether, carbonyl, and acid/ester functionality at higher  $P$ , a trend that has been observed during the fabrication of films from similar precursors. For example, Ahmad *et al.* related  $P$  to degree of oxygen incorporation for fabrication of films from  $\gamma$ -terpinene.<sup>44</sup> They observed monomer structure is retained to a greater degree at lower  $P$ , attributed to ion-surface interactions that promote grafting of neutral monomer [i.e., ion energy increases linearly with  $P$  over a relatively narrow range (10 – 50 W)] as well as a decrease in the density of intact monomer as  $P$  increases.

XPS analysis of H<sub>2</sub>O<sub>(v)</sub> plasma treated ppCin reveals surface oxygen content is dramatically increased, in the form of carboxylic acid and alcohol/ether functionality (Fig. 6.5d), as observed reproducibly from H<sub>2</sub>O<sub>(v)</sub> plasma treatment of numerous polymeric materials.<sup>51-53, 67</sup> Our



previously published data established this functionalization occurs from reaction of excited-state OH radicals and H atoms at the material interface.<sup>53, 68</sup> Specifically, results from our radical-surface interaction studies indicate that OH radicals oxidize the film surface to result in ketone, aldehyde functionalities, as well as carboxylic functionalities.<sup>56, 68</sup> Additionally, increased surface oxygen may occur from polymer rearrangement during H<sub>2</sub>O<sub>(v)</sub> plasma treatment, as hydrophilic domains in the polymer preferentially orient towards the plasma.

*Deposition rate and morphology.* PECVD deposition rates are strongly dependent on reactor setup, substrate, and plasma parameters. Deposition rate increasing with  $p$ , Fig. 6.2, is to be expected given the mean free path of plasma species decreases at higher  $p$ , limiting interaction of both intact and fragmented monomer species with high energy plasma species.<sup>22</sup> Specifically, we hypothesize film growth at higher  $p$  may be driven by an increased rate at which ions in the plasma initiate the incorporation of whole monomer adsorbed on the surface of the growing film. Indeed, for PECVD of 2-hydroxyethyl methacrylate (HEMA)-based films, Lopez and Ratner find an increase in intact monomer incorporation with decreasing power to pressure ratios, and attribute this to an increased rate of charged particle bombardment at increased  $p$ , facilitating incorporation of intact monomer.<sup>69</sup> Although the degree of ionization in cold plasmas is typically low ( $10^{-7} - 10^{-5}$ ), ion driven reactions at the growing film surface can play a large role in determining the deposition rate of the film.<sup>22</sup> As electron energy decreases with increasing  $p$ , it is likely that the monomer is less fragmented and arrives at the film surface intact to undergo this ion-initiated incorporation.

Under most conditions, deposition of ppCin films in our system follows a linear trend, ranging from  $\sim 4$  to  $35 \text{ nm min}^{-1}$ . Under similar ppCin deposition conditions to those presented here, Easton and coworkers obtained a constant deposition rate of  $\sim 55 \text{ nm min}^{-1}$ .<sup>27</sup> Furthermore,

polyLA films deposited by Jacob *et al.* showed similar deposition rate of  $\sim 40 \text{ nm min}^{-1}$ , although it is not described in detail.<sup>47</sup> These studies imply films can be fabricated in fairly short time frames, and the linearity of ppCin deposition can be maintained between distinct reactor setups. Notably, there are some exceptions to this relationship in our study; our data indicate concomitant etching may occur during film deposition. Indeed, we observe thinner films with longer deposition times for ppCin (low  $p,P$ ), implying etching occurs at a faster rate than film deposition under these conditions, making it difficult to determine an accurate deposition rate. Moreover, SEM reveals a rougher morphology for  $\text{H}_2\text{O}_{(v)}$  plasma treated ppCin films, potentially resulting from etching and subsequent re-deposition of polymer fragments. Nevertheless, our system allows for relatively efficient deposition under a wide range of plasma conditions.

### 6.3.2 Understanding how plasma chemistry influences film wettability and aging

Although the XPS spectra presented in Fig. 6.3 do not appear disparate overall, the subtle differences in oxygen content have a direct impact on film wettability. Overall, our OES data suggest that despite higher  $\text{OH}_{(g)}$  densities as  $p$  increases, the density of CO species dominates over OH radicals in 1,8-cineole plasmas, manifesting in lower alcohol/ether functionality and possibly explaining why more hydrophobic films are deposited at higher  $p$  (Fig. 6.6). Moreover, ppCin (high  $p,P$ ) and ppOct films (Fig. 6.5b and 6.5c, respectively) have very similar surface composition and thus have similar WCA values. Interestingly, the plasma polymerized ppOct surface likely undergoes oxidation upon exposure to the atmosphere because of long-lived radical sites on the film surface, giving rise to a partially oxygenated film.<sup>70-71</sup>

There is no clear dependence of WCA on  $P$  for our data. In contrast, work by Easton and coworkers on similar essential oil-based plasma polymers, shows a small  $P$  dependence for

polyLA films deposited at 250 mTorr, with WCA decreasing  $\sim 10^\circ$  as  $P$  decreases from 75 W to 10 W.<sup>43</sup> Easton *et al.* obtained WCA values of  $\sim 90^\circ$  for cineole-based plasma polymers (higher than ours here) but do not report an O/C ratio.<sup>27</sup> Interestingly, O/C values obtained here are 2 to 4-fold those obtained by others for cineole films,<sup>63</sup> yet WCA values are similar ( $77 \pm 2^\circ$ ). The slight disparities in surface properties may arise from surface roughness differences, as films deposited at 250 mTorr and 25 W by Easton *et al.* had average roughness an order of magnitude greater than those here. Overall, the dependence of film surface properties, such as roughness and wettability, on plasma deposition parameters indicates there is potential to tailor film surfaces for biological applications based on the selected plasma parameters.

Interestingly, upon aging, some ppCin films display an increase in WCA and some a decrease in WCA. Alexander and Duc suggest that a loss of oxygen, manifesting as an increase in WCA, may occur because physisorbed low molecular weight polymer chains evaporate from the film surface.<sup>72</sup> Alternatively, a decrease in WCA may arise from a rapid uptake of atmospheric oxygen by trapped, highly reactive radicals remaining in the film surface (as described by Gengenbach and Griesser<sup>73</sup>). Indeed, films that increase in wettability seem to do so much faster ( $<1$  week) than films with decreasing wettability, which occurs more steadily over the 2 month aging period. Upon aging, WCA data for  $\text{H}_2\text{O}_{(v)}$  plasma treated ppCin films indicate some hydrophobic recovery occurs. This post-modification phenomenon where the polymer chains reorient to bury hydrophilic functionalities in the polymer bulk, regaining some hydrophobicity, has been observed previously for some polymers.<sup>51-53</sup>

In addition to exploring film aging, film stability in biological media was investigated to demonstrate the feasibility of the films as functionalized coatings on biomaterials. Film instability was exhibited in various ways, including the appearance of wrinkles or bubbles and

partial or complete delamination. In general, no clear trends emerged between adhesion and plasma parameters ( $P$  and  $p$ ); however, film stability was dependent on substrate position in the reactor, with adhesion generally improving on substrates placed further downstream from the plasma glow. Our ppOct films behaved similarly to previous results as they displayed features indicative of film swelling when placed in biological media.<sup>74</sup> All films (ppCin and ppOct) were also stable on PS substrates and exhibited similar WCAs to those on glass substrates, indicating their potential for use as functionalized coatings for biomaterials.

### 6.3.3 Understanding how biological performance varies with film properties

Using a kill rate technique similar to that here, Pegalajar-Jurado *et al.* characterized the biocidal behavior of cineole in solution (0.5% v/v), finding it killed *E. coli* more effectively than *S. aureus*, which recovered from any population decline, whereas *E. coli* did not recover.<sup>63</sup> Results from our studies corroborate this observation to some extent; however, we found 1,8-cineole resulted in substantial killing of both bacterial strains. The log reduction arising from exposure to the 1,8-cineole monomer here is significantly greater (8 – 9-log) than that of the previous study (2 – 3-log),<sup>63</sup> a discrepancy that may partially arise from the method of evaluation of bacterial population. The previous study used UV-vis spectroscopy, assuming absorbance of bacterial culture is directly proportional to bacterial population, whereas our analysis utilizes the more quantitative plating method.<sup>11</sup>

Notably, we also performed kill rate analysis on ppCin films to determine if they were biocidal against planktonic bacteria in bulk solution, perhaps caused by retained monomer or other agents leaching from the ppCin films. None of the plasma polymerized films caused a detectable reduction in population of *E. coli* in bulk solution; thus, we could rule out killing of

planktonic bacteria by leachables from the film as the cause of the observed reduction in biofilm formation.

Although leaching of essential oil monomer or small molecular weight compounds is not sufficient to kill *E. coli* in bulk solution, these compounds may play a role in the antifouling behavior of ppCin films. One possible reason for the antibacterial properties of ppCin films is ion-initiated incorporation of intact monomer into the film (discussed above). This has been previously hypothesized by Bazaka and coworkers who found relatively low *P* conditions (10 W) resulted in PECVD films from terpinen-4-ol (structurally similar to 1,8-cineole and a primary component of tea tree oil) that retained the monomer chemistry as well as its biological activity. At higher *P* (25 W), antibacterial activity was completely lost, attributed to lack of intact monomer incorporation.

Here, we focus on wettability to gain insight into factors that control bacterial attachment and growth. As roughness does not change appreciably with plasma parameters, it likely has no significant role in altering film wettability or bacterial interactions in these systems. The presence of viable attached bacteria on hydrophilic glass and hydrophobic ppOct films, however, establishes that altering wettability alone is not sufficient to create a low-fouling surface. Surface chemistry also plays a large role in bacterial-surface interactions, although specific functionalities that drive the attachment and growth processes are not fully elucidated.<sup>75-76</sup> Moreover, Pegalajar-Jurado *et al.* concluded that CH<sub>3</sub> groups likely limit *E. coli* attachment, whereas COOH functionality promoted attachment.<sup>74</sup> Thus, the increased biofilm formation observed for H<sub>2</sub>O<sub>(v)</sub> treated ppCin films likely arises from the increase in COOH functionality and accompanying decrease in WCA.

Interestingly, we observed the overall number of attached *E. coli*, Fig. 6.7, consistently appeared significantly fewer than the number of attached *S. aureus* cells, Fig. 6.8. Essential oils appear to act on the bacterial membrane, causing an increase in membrane permeability, and alteration of membrane fatty acid and proteins.<sup>77</sup> Moreover, hydrocarbons are thought to have a permeabilizing effect on the cytoplasmic membrane.<sup>78</sup> As such, others have used this reasoning to explain the observation that *E. coli* can be more resistant than *S. aureus*, which do not have an outer cell membrane.<sup>12</sup> Others argue that the outer membrane of gram-negative *E. coli* leaves it more susceptible than *S. aureus*.<sup>11,79</sup> Our results here seem to indicate the latter is true for our plasma polymerized antimicrobial films.

As a final note, it is critical to maintain mammalian cell viability while controlling bacterial growth. Although little work has been done, preliminary studies by Pegalajar-Jurado *et al.* suggest murine fibroblast cells do not attach to ppCin films but do attach to the surrounding TC plate, indicating no toxicity to cells in bulk media. Some essential oils and their components in liquid form demonstrate cytotoxicity (although this is strongly dependent on concentration); however, limited studies indicate polymers fabricated from tea tree oil and its components 1,8-cineole and terpinen-4-ol have been shown to be cytocompatible.<sup>80-82</sup> Additional work in this area must be completed before it will be feasible to interface such coatings with mammalian cells for use in biomedical devices. Nevertheless, PECVD of essential oil films represents a promising low-temperature route to obtain antifouling, biofilm-retarding surfaces for temperature-sensitive, morphologically complex biomaterials. Future studies should further elucidate mechanisms of resistance to bacterial attachment as well as film formation mechanisms by probing fragmented species with techniques such as *in situ* mass spectrometry. Ultimately, obtaining such insight will advance deposition of ppCin and other antifouling films on

biomedical devices to create stable, highly adherent surfaces that prevent bacterial attachment without contributing to antimicrobial resistance.

#### **6.4 Summary and conclusions**

The ability to create robust antimicrobial materials with tailorable surface properties remains an overarching goal for many biomedical applications such as wound dressings, tissue engineering and implanted devices. Results presented here demonstrate the use of plasma processing methods to fabricate and modify essential oil-derived plasma polymerized thin films, including characterization of their biological interactions with two strains of bacteria. Our findings suggest ppCin films retain some structure and antimicrobial behavior characteristic of the monomer, even after H<sub>2</sub>O<sub>(v)</sub> plasma treatments, which serve to increase their wettability, a property critical for success in biological environments. Over a wide range of plasma parameters, we produced highly adherent, conformal, and smooth films all of which displayed strong antimicrobial behavior. Furthermore, our comprehensive approach allowed us to correlate excited state plasma gas-phase species densities with resulting ppCin film properties. Film analyses via XPS and WCA studies, as well as the use of hydrophilic and hydrophobic controls, help elucidate the impact of ppCin film properties on attachment and growth of *E. coli* and *S. aureus* on the film surface. Overall, the low-fouling behavior combined with improved wettability of our ppCin films suggest these tunable films have substantial promise for reducing HAIs when used as coatings for biomedical devices.

## REFERENCES

1. Magill, S. S.; Edwards, J. R.; Bamberg, W., Multistate point-prevalence survey of health care-associated infections. *N Engl J Med* **2014**, *370*, 1198-1208.
2. Scott, R. D., *The Direct Medical Costs of Healthcare-associated Infections in US Hospitals and the Benefits of Prevention*. Centers for Disease Control and Prevention: 2009.
3. Harro, J. M.; Peters, B. M.; O'May, G. A.; Archer, N.; Kerns, P.; Prabhakara, R.; Shirliff, M. E., Vaccine development in *Staphylococcus aureus*: Taking the biofilm phenotype into consideration. *FEMS Immunol. Med. Microbiol.* **2010**, *59* (3), 306-323.
4. Monroe, D., Looking for chinks in the armor of bacterial biofilms. *PLoS Biology* **2007**, *5* (11), 2458-2461.
5. Burt, S. A.; Reinders, R. D., Antibacterial activity of selected plant essential oils against *Escherichia coli* O157:H7. *Lett. Appl. Microbiol.* **2003**, *36*, 162-167.
6. Carson, C. F.; Mee, B. J.; Riley, T. V., Mechanism of action of *Melaleuca alternifolia* (tea tree) oil on *Staphylococcus aureus* determined by time-kill, lysis, leakage, and salt tolerance assays and electron microscopy. *Antimicrob. Agents Chemother.* **2002**, *46* (6), 1914-1920.
7. Edmondson, M.; Newall, N.; Carville, K.; Smith, J.; Riley, T. V.; Carson, C. F., Uncontrolled, open-label, pilot study of tea tree (*Melaleuca alternifolia*) oil solution in the decolonisation of methicillin-resistant *Staphylococcus aureus* positive wounds and its influence on wound healing. *Int Wound J* **2011**, *8* (4), 375-384.
8. Li, L.; Li, Z.-W.; Yin, Z.-Q.; Wei, Q.; Jia, R.-Y.; Zhou, L.-J.; Xu, J.; Song, X.; Zhou, Y.; Du, Y.-H.; Peng, L.-C.; Kang, S.; Yu, W., Antibacterial activity of leaf essential oil and its constituents from *Cinnamomum longepaniculatum*. *Int J Clin Exp Med* **2014**, *7* (7), 1721-1727.
9. May, J.; Chan, C. H.; King, A.; Williams, L.; French, G. L., Time-kill studies of tea tree oils on clinical isolates. *J. Antimicrob. Chemother.* **2000**, *45*, 639-643.
10. Hendry, E. R.; Worthington, T.; Conway, B. R.; Lambert, P. A., Antimicrobial efficacy of eucalyptus oil and 1,8-cineole alone and in combination with chlorhexidine digluconate against microorganisms grown in planktonic and biofilm cultures. *J. Antimicrob. Chemother.* **2009**, *64* (6), 1219-1225.
11. Burt, S., Essential oils: their antibacterial properties and potential applications in foods—a review. *Int J Food Microbiol* **2004**, *94* (3), 223-253.
12. Dorman, H. J. D.; Deans, S. G., Antimicrobial agents from plants: antibacterial activity of plant volatile oils. *J Appl Microbiol* **2000**, *88*, 308-316.
13. Dalleau, S.; Cateau, E.; Berges, T.; Berjeaud, J. M.; Imbert, C., *In vitro* activity of terpenes against *Candida* biofilms. *Int J Antimicrob Agents* **2008**, *31* (6), 572-576.
14. Sánchez-González, L.; Cháfer, M.; Hernández, M.; Chiralt, A.; González-Martínez, C., Antimicrobial activity of polysaccharide films containing essential oils. *Food Control* **2011**, *22* (8), 1302-1310.
15. Rieger, K. A.; Eagan, N. M.; Schiffman, J. D., Encapsulation of cinnamaldehyde into nanostructured chitosan films. *J. Appl. Polym. Sci.* **2015**, *132* (13).
16. Sánchez-González, L.; González-Martínez, C.; Chiralt, A.; Cháfer, M., Physical and antimicrobial properties of chitosan–tea tree essential oil composite films. *J. Food Eng.* **2010**, *98* (4), 443-452.
17. Zivanovic, S.; Chi, S.; Draughon, A. F., Antimicrobial activity of chitosan films enriched with essential oils. *J. Food Sci.* **2005**, *70* (1), M45-M51.
18. Salmieri, S.; Lacroix, M., Physicochemical properties of alginate/polycaprolactone-based films containing essential oils. *J. Agric. Food Chem.* **2006**, *54* (26), 10205-10214.



19. Bakry, A. M.; Abbas, S.; Ali, B.; Majeed, H.; Abouelwafa, M. Y.; Mousa, A.; Liang, L., Microencapsulation of oils: A comprehensive review of benefits, techniques, and applications. *Compr. Rev. Food. Sci. Food Saf.* **2016**, *15* (1), 143-182.
20. Wu, J. L.; Liu, H.; Ge, S. Y.; Wang, S.; Qin, Z. Q.; Chen, L.; Zheng, Q. H.; Liu, Q. Y.; Zhang, Q. Q., The preparation, characterization, antimicrobial stability and *in vitro* release evaluation of fish gelatin films incorporated with cinnamon essential oil nanoliposomes. *Food Hydrocoll.* **2015**, *43*, 427-435.
21. Ge, Y.; Ge, M. Q., Development of tea tree oil-loaded liposomal formulation using response surface methodology. *J. Liposome Res.* **2015**, *25* (3), 222-231.
22. d'Agostino, R., *Plasma Deposition, Treatment, and Etching of Polymers*. Academic Press, Inc.: London, 1990.
23. Abrigo, M.; Kingshott, P.; McArthur, S. L., Bacterial response to different surface chemistries fabricated by plasma polymerization on electrospun nanofibers. *Biointerphases* **2015**, *10* (4), 04A301.
24. Ahmad, J.; Bazaka, K.; Vasilev, K.; Jacob, M. V., Electrical conduction in plasma polymerized thin films of  $\gamma$ -terpinene. *J. Appl. Polym. Sci.* **2015**, *132* (30).
25. Bazaka, K.; Jacob, M. V.; Ostrikov, K., Sustainable life cycles of natural-precursor-derived nanocarbons. *Chem. Rev.* **2016**, *116* (1), 163-214.
26. Easton, C. D.; Jacob, M. V., Optical characterisation of radio frequency plasma polymerised *Lavandula angustifolia* essential oil thin films. *Thin Solid Films* **2009**, *517* (15), 4402-4407.
27. Easton, C. D.; Jacob, M. V.; Shanks, R. A., Fabrication and characterisation of polymer thin-films derived from cineole using radio frequency plasma polymerisation. *Polymer* **2009**, *50* (15), 3465-3469.
28. Jacob, M. V.; Olsen, N. S.; Anderson, L. J.; Bazaka, K.; Shanks, R. A., Plasma polymerised thin films for flexible electronic applications. *Thin Solid Films* **2013**, *546*, 167-170.
29. Ahmad, J.; Bazaka, K.; Oelgemoller, M.; Jacob, M. V., Wetting, solubility and chemical characteristics of plasma-polymerized 1-isopropyl-4-methyl-1,4-cyclohexadiene thin films. *Coatings* **2014**, *4* (3), 527-552.
30. Grill, A., *Cold Plasmas in Materials Fabrications: from Fundamentals to Applications*. IEEE: New York, 1994.
31. Baier, R. E.; Meyer, A. E.; Natiella, J. R.; Natiella, R. R.; Carter, J. M., Surface properties determine bioadhesive outcomes—methods and results. *J. Biomed. Mater. Res.* **1984**, *18* (4), 337-355.
32. Vasudev, M. C.; Anderson, K. D.; Bunning, T. J.; Tsukruk, V. V.; Naik, R. R., Exploration of plasma-enhanced chemical vapor deposition as a method for thin-film fabrication with biological applications. *ACS Appl. Mater. Interfaces* **2013**, *5* (10), 3983-3994.
33. Jacobs, T.; Morent, R.; Geyter, N. D.; Dubruel, P.; Leys, C., Plasma surface modification of biomedical polymers: Influence on cell-material interaction. *Plasma Chem. Plasma Process* **2012**, *32*, 1039-1073.
34. Vasilev, K.; Griesser, S. S.; Griesser, H. J., Antibacterial surfaces and coatings produced by plasma techniques. *Plasma Process. Polym.* **2011**, *8* (11), 1010-1023.
35. Pashkuleva, I.; Marques, A. P.; Vaz, F.; Reis, R. L., Surface modification of starch based biomaterials by oxygen plasma or UV-irradiation. *J. Mater. Sci.: Mater. Med.* **2010**, *21* (1), 21-32.
36. Yasuda, H.; Gazicki, M., Biomedical applications of plasma polymerization and plasma treatment of polymer surfaces. *Biomaterials* **1982**, *3*, 68-77.
37. Mann, M. N.; Neufeld, B. H.; Hawker, M. J.; Pegalajar-Jurado, A.; Paricio, L. N.; Reynolds, M. M.; Fisher, E. R., Plasma-modified nitric oxide-releasing polymer films exhibit time-delayed 8-log reduction in growth of bacteria. *Biointerphases* **2016**, *11* (3), 031005.
38. Winkler, S.; Wongthai, P., Increasing the bond strength of metal-ceramic restorations. *J. Prosthet. Dent.* **1986**, *56* (4), 396-401.
39. Carson, C. F.; Hammer, K. A.; Riley, T. V., *Melaleuca alternifolia* (tea tree) oil: a review of antimicrobial and other medicinal properties. *Clinical Microbiology Reviews* **2006**, *19* (1), 50-62.
40. Carson, C. F.; Riley, T. V.; Cookson, B. D., Efficacy and safety of tea tree oil as a topical antimicrobial agent. *J. Hosp. Infect.* **1998**, *40*, 175-178.

41. Cox, S. D.; Mann, C. M.; Markham, J. L.; Bell, H. C.; Gustafson, J. E.; Warmington, J. R.; Wyllie, S. G., The mode of antimicrobial action of the essential oil of *Melaleuca alternifolia* (tea tree oil). *J Appl Microbiol* **2000**, *88*, 170-175.
42. Easton, C. D.; Jacob, M. V., Solubility and adhesion characteristics of plasma polymerized thin films derived from *Lavandula angustifolia* essential oil. *J. Appl. Polym. Sci.* **2010**, *115* (1), 404-415.
43. Easton, C. D.; Jacob, M. V.; Shanks, R. A.; Bowden, B. F., Surface and chemical characterization of polyLA thin films fabricated using plasma polymerization. *Chem. Vap. Deposition* **2009**, *15* (7-9), 179-185.
44. Ahmad, J.; Bazaka, K.; Whittle, J. D.; Michelmore, A.; Jacob, M. V., Structural Characterization of  $\gamma$ -Terpinene Thin Films Using Mass Spectroscopy and X-Ray Photoelectron Spectroscopy. *Plasma Process. Polym.* **2015**, *12* (10), 1085-1094.
45. Bazaka, K.; Jacob, M. V.; Ivanova, E. P., A study of a retention of antimicrobial activity by plasma polymerized terpinen-4-ol thin films. In *Mater. Sci. Forum*, Nie, J. F.; Morton, A., Eds. Trans Tech Publications Ltd: Stafa-Zurich, 2010; Vol. 654-656, pp 2261-2264.
46. Pegalajar-Jurado, A.; Easton, C. D.; Styan, K. E.; McArthur, S. L., Antibacterial activity studies of plasma polymerised cineole films. *J. Mater. Chem. B.* **2014**, *2* (31), 4993-5002.
47. Jacob, M. V.; Easton, C. D.; Woods, G. S.; Berndt, C. C., Fabrication of a novel organic polymer thin film. *Thin Solid Films* **2008**, *516* (12), 3884-3887.
48. De Vincenzi, M.; Silano, M.; De Vincenzi, A.; Maialetti, F.; Scazzocchio, B., Constituents of aromatic plants: Eucalyptol. *Fitoterapia* **2002**, *73*, 269-275.
49. Juergens, U. R.; Dethlefsen, U.; Steinkamp, G.; Gillissen, A.; Repges, R.; Vetter, H., Anti-inflammatory activity of 1,8-cineole (eucalyptol) in bronchial asthma: a double-blind placebo-controlled trial. *Respiratory Medicine* **2003**, *97*, 250-256.
50. Halcon, L.; Milkus, K., *Staphylococcus aureus* and wounds: a review of tea tree oil as a promising antimicrobial. *Am. J. Infect. Control* **2004**, *32* (7), 402-408.
51. Pegalajar-Jurado, A.; Mann, M. N.; Maynard, M. R.; Fisher, E. R., Hydrophilic modification of polysulfone ultrafiltration membranes by low temperature water vapor plasma treatment to enhance performance. *Plasma Process. Polym.* **2016**, (13), 598.
52. Steen, M. L.; Jordan, A. C.; Fisher, E. R., Hydrophilic modification of polymeric membranes by low temperature H<sub>2</sub>O plasma treatment. *J Membr Sci* **2002**, *204*, 341-357.
53. Tompkins, B. D.; Dennison, J. M.; Fisher, E. R., H<sub>2</sub>O plasma modification of track-etched polymer membranes for increased wettability and improved performance. *J Membr Sci* **2013**, *428*, 576-588.
54. Cho, B.-O.; Lao, S.; Sha, L.; Chang, J. P., Spectroscopic study of plasma using zirconium tetra-tert-butoxide for the plasma enhanced chemical vapor deposition of zirconium oxide. *J. Vac. Sci. Technol. A* **2001**, *19* (6), 2751-2761.
55. Harshbarger, W.; Porter, R.; Miller, T. A.; Norton, P., A study of the optical emission from an rf plasma during semiconductor etching. *Appl. Spectrosc.* **1977**, *31* (3), 201-207.
56. Steen, M. L.; Hymas, L.; Havey, E. D.; Capps, N. E.; Castner, D. G.; Fisher, E. R., Low temperature plasma treatment of asymmetric polysulfone membranes for permanent hydrophilic surface modification. *J Membr Sci* **2001**, *188*, 97-114.
57. Pearse, R. W. B.; Gaydon, A. G., *Identification of Molecular Spectra*. Chapman and Hall: 1976.
58. Liu, D.; Zhou, J.; Fisher, E. R., Correlation of gas-phase composition with film properties in the plasma-enhanced chemical vapor deposition of hydrogenated amorphous carbon nitride films. *J. Appl. Phys.* **2007**, *101* (2), 023304.
59. Parker, J., Rotational and vibrational relaxation in diatomic gases. *The Physics of Fluids* **1959**, *2* (4), 449-462.
60. Cuddy, M. F.; Fisher, E. R., Contributions of CF and CF<sub>2</sub> Species to Fluorocarbon Film Composition and Properties for C<sub>x</sub>F<sub>y</sub> Plasma-Enhanced Chemical Vapor Deposition. *ACS Appl. Mater. Interfaces* **2012**, *4* (3), 1733-1741.

61. Lou, Q. W.; Kaler, S.; Donnelly, V. M.; Economou, D. J., Optical emission spectroscopic studies and comparisons of CH<sub>3</sub>F/CO<sub>2</sub> and CH<sub>3</sub>F/O<sub>2</sub> inductively coupled plasmas. *J. Vac. Sci. Technol. A* **2015**, *33* (2), 10.
62. Hawker, M. J. Part I. Development of Plasma Surface Modification and Characterization Strategies for Three-Dimensional Polymer Constructs used in Biological Applications and Part II. Exploring General Chemistry Students' Metacognitive Monitoring on Examinations. Doctoral Dissertation, Colorado State University, Colorado State University Libraries, 2016.
63. Pegalajar-Jurado, A.; Easton, C. D.; Styan, K. E.; McArthur, S. L., Antibacterial activity studies of plasma polymerised cineole films. *J. Mater. Chem. B* **2014**.
64. Coates, J., Interpretation of infrared spectra, a practical approach. *Encyclopedia of Analytical Chemistry* **2000**.
65. Silverstein, M. S.; Visoly-Fisher, I., Plasma polymerized thiophene: Molecular structure and electrical properties. *Polymer* **2002**, *43* (1), 11-20.
66. Retzko, I.; Friedrich, J. F.; Lippitz, A.; Unger, W. E. S., Chemical analysis of plasma-polymerized films: the application of x-ray photoelectron spectroscopy (XPS), x-ray absorption spectroscopy (NEXAFS) and fourier transform infrared spectroscopy (FTIR). *J. Electron. Spectrosc. Relat. Phenom.* **2001**, *121* (1-3), 111-129.
67. Mann, M. N.; Neufeld, B. H.; Hawker, M. J.; Pegalajar-Jurado, A.; Paricio, L. N.; Reynolds, M. M.; Fisher, E. R., Plasma-modified nitric oxide-releasing polymer films exhibit time-delayed 8-log reduction in growth of bacteria. *Biointerphases* **2016**, *11* (3), 11.
68. Steen, M. L.; Butoi, C. I.; Fisher, E. R., Identification of gas-phase reactive species and chemical mechanisms occurring at plasma-polymer surface interfaces. *Langmuir* **2001**, *17* (26), 8156-8166.
69. López, G. P.; Ratner, B. D., Substrate temperature effects on film chemistry in plasma depositions of organics. II. Polymerizable precursors. *J. Polym. Sci., Part A: Polym. Chem.* **1992**, *30* (11), 2415-2425.
70. Salim, M.; Wright, P. C.; McArthur, S. L., Studies of electroosmotic flow and the effects of protein adsorption in plasma-polymerized microchannel surfaces. *Electrophoresis* **2009**, *30* (11), 1877-1887.
71. Whittle, J. D.; Short, R.; Douglas, C.; Davies, J., Differences in the aging of allyl alcohol, acrylic acid, allylamine, and octa-1, 7-diene plasma polymers as studied by x-ray photoelectron spectroscopy. *Chem. Mater.* **2000**, *12* (9), 2664-2671.
72. Alexander, M. R.; Duc, T. M., The chemistry of deposits formed from acrylic acid plasmas. *J. Mater. Chem.* **1998**, *8* (4), 937-943.
73. Gengenbach, T.; Griesser, H., Deposition conditions influence the postdeposition oxidation of methyl methacrylate plasma polymer films. *J Polym Sci A: Polym Chem* **1998**, *36*, 985-1000.
74. Pegalajar-Jurado, A.; Easton, C. D.; Crawford, R. J.; McArthur, S. L., Fabrication of a platform to isolate the influences of surface nanotopography from chemistry on bacterial attachment and growth. *Biointerphases* **2015**, *10* (1), 10.
75. Abrigo, M.; Kingshott, P.; McArthur, S. L., Bacterial response to different surface chemistries fabricated by plasma polymerization on electrospun nanofibers. *Biointerphases* **2015**, *10* (4), 9.
76. Linke, D.; Goldman, A., *Bacterial Adhesion: Chemistry, Biology and Physics*. Springer Science & Business Media: 2011; Vol. 715.
77. Knobloch, K.; Weigand, H.; Weis, N.; Schwarm, H.; Vogenschow, H., *Action of Terpenoids on Energy Metabolism*. Walter de Gruyter: Berlin, Germany: 1986.
78. Bazaka, K.; Jacob, M. V.; Crawford, R. J.; Ivanova, E. P., Plasma-assisted surface modification of organic biopolymers to prevent bacterial attachment. *Acta Biomater.* **2011**, *7* (5), 2015-2028.
79. Deans, S.; Ritchie, G., Antibacterial properties of plant essential oils. *Int. J. Food. Microbiol.* **1987**, *5* (2), 165-180.
80. Bagchi, B.; Banerjee, S.; Kool, A.; Thakur, P.; Bhandary, S.; Hoque, N. A.; Das, S., Synthesis of eucalyptus/tea tree oil absorbed biphasic calcium phosphate-PVDF polymer nanocomposite films: a

surface active antimicrobial system for biomedical applications. *Phys. Chem. Chem. Phys.* **2016**, *18* (25), 16775-16785.

81. Ozkan, A.; Erdogan, A., Membrane and DNA damaging/protective effects of eugenol, eucalyptol, terpinen-4-ol, and camphor at various concentrations on parental and drug-resistant H1299 cells. *Turk. J. Biol.* **2013**, *37* (4), 405-413.

82. Pereira, T. S.; de Sant'Anna, J. R.; Silva, E. L.; Pinheiro, A. L.; de Castro-Prado, M. A. A., *In vitro* genotoxicity of *Melaleuca alternifolia* essential oil in human lymphocytes. *J. Ethnopharmacol.* **2014**, *151* (2), 852-857.

## CHAPTER 7

### FABRICATION OF ESSENTIAL OIL-DERIVED THIN FILMS FOR COMPLEX 3D BIOMEDICAL CONSTRUCTS

This chapter describes the further optimization of essential oil-based PECVD systems, including the continued development of ppCin films and the addition of films from terpinen-4-ol and  $\alpha$ -terpinene. The focus of this chapter is to extend these additional systems and the 1,8-cineole PECVD system optimized in Chapter 6 to deposition onto 3D polymeric constructs. Much of the work contained herein represent preliminary, proof-of-concept results. A substantial portion of this work was assisted by three undergraduate researchers, in decreasing order of contribution. Ms. Brianna Fox completed a large portion of the terpinen-4-ol and  $\alpha$ -terpinene system parameter space optimization, as well as preliminary surface analyses. Mr. Cyrus Salvani performed preliminary biological imaging and kill rate assays for monomers and films. Ms. M. Cristina Lara assisted with substrate preparation and film deposition for all studies described in this chapter. Brianna acknowledges funding from the Research Experiences for Undergraduates (REU) site in the Department of Chemistry at Colorado State University (NSF CHE-1461040). This research was supported by Colorado State University's Office of the Provost and the Office of the Vice President for Research Catalyst for Innovative Partnerships Program. The content is solely the responsibility of the authors and does not necessarily represent the official views of the funding sources.

## 7.1. Introduction

Plant-derived essential oils are a renewable, inexpensive, and abundant resource, and many display antibacterial properties without cytotoxicity.<sup>1-12</sup> For example, tea tree oil has been shown to be a highly effective antibiotic, acting against a broad-spectrum of strains including methicillin-resistant *S. aureus* (MRSA), yet it exhibits low toxicity to human fibroblasts.<sup>3-5, 15</sup> It is generally agreed that the antibacterial activity of the oils likely results from a synergistic effect of their various components.<sup>2, 6, 16</sup> Essential oils are complex mixtures of phenols, aldehydes, ketones, alcohols, esters, ethers, and hydrocarbons.<sup>1-2, 12, 16-17</sup> Some attribute the biocidal behavior of essential oils to the presence of phenolic functionalities,<sup>18-19</sup> which are present in several major tea tree oil components (e.g., carvacrol, thymol, terpinen-4-ol), yet some speculate it is the components present in much smaller amounts that exhibit the most broad-spectrum biocidal activity.<sup>3, 6, 16, 20</sup> Because of their complex chemistry and the multiple mechanisms by which each component likely functions, especially when compared to synthetic antibiotics, these oils carry a far smaller tendency to contribute to antibacterial resistance.<sup>1, 4</sup> As such, there is vast potential for the use of essential oils as a non-petrochemical hydrocarbon resource for the fabrication of “green” antifouling biomedical device surfaces.<sup>8, 11-12, 21</sup>

Immobilizing essential oil-based coatings on biomedical polymeric constructs is challenging via wet chemical methods, as these can be destructive to the polymer. Moreover, the physical and chemical properties of the essential oil components differ greatly, making some difficult to polymerize via conventional methods and introducing challenges with controlling coating chemistry and conformality.<sup>22</sup> Unlike many conventional surface coating methods, PECVD is a solvent-free, one-step method to fabricate conformal thin films, even for complex 3D morphologies, as demonstrated in work by our group<sup>23-24</sup> and others.<sup>25</sup>

For thin film fabrication from tea tree oil or its constituents, it is useful to understand the properties of a film deposited from a single component. In Chapter 6, ppCin films were optimized on 2D substrates, allowing us to better study the properties of the film itself. We investigated the effect of film wettability on bacterial attachment, and determined it is both driven by hydrophilicity as well as discouraged by some intrinsic properties of the 1,8-cineole monomer. We found some biocidal properties of the monomer molecule were retained, with <10% of the coated material surface covered in biofilm after 5 days of incubation. Elucidating the bactericidal properties of each individual component upon plasma polymerization allows for an understanding of any synergistic or antagonistic effects of the oils in thin film form. Thus, our approach involves studying each system independently, ultimately advancing the development of platforms (e.g., copolymerization systems) for biomaterials coatings.

Results from numerous studies (including that in Chapter 6) show biocidal activity depends on film chemistry.<sup>25-27</sup> In one study, *E. coli* attachment was limited by CH<sub>3</sub> functionality, yet promoted by COOH groups.<sup>28</sup> In another example, Bazaka and coworkers found terpinen-4-ol plasma polymers retained much of the monomer structure,<sup>26</sup> but only at low rf power. We observed the same trend for ppCin films. As such, we hypothesize retaining the monomer functionalities of these oils may help create antibacterial, biocompatible films. Plasma polymerization, however, does not inherently retain the monomer structures.<sup>29-30</sup> In fact, extensive fragmentation commonly occurs during PECVD, especially under certain conditions (e.g., higher powers).<sup>29-30</sup> We wish to ascertain, however, the dependence of the plasma polymer properties on the functionalities present in the monomer molecule.

Terpinen-4-ol is a major component of tea tree oil known to be responsible in part for its therapeutic properties, making up anywhere from 35-50%, depending on extraction methods and

cultivation conditions. It is structurally similar to 1,8-cineole, but differs in that it has alcohol functionality instead of epoxide.<sup>3</sup> Terpinen-4-ol exhibits non-specific biocidal activity towards several known biofilm forming ( e.g., *E. coli*, *P. aeruginosa*, *A. baumannii*) as well as MRSA.<sup>12, 17, 31</sup> Specifically, plasma polymers from terpinen-4-ol have demonstrated versatile biological activity that can be tailored to control protein adsorption and cell attachment.<sup>32-33</sup> We also investigate another component of tea tree oil,  $\alpha$ -terpinene, a cyclic hydrocarbon also known to have biocidal properties, although higher concentrations are required (Table 7.1).<sup>13-14</sup>


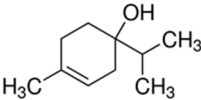
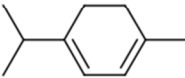
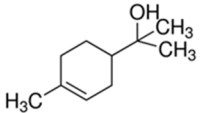
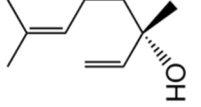
A holy grail in antibacterial coatings for biomedical devices is a surface modification platform to achieve mechanically and chemically robust films with highly tailorable surface properties depending on the desired application. Here, we seek to determine whether these structurally-different essential oil derivatives can result in stable, adherent, low-fouling films on glass as well as 3D, porous biomedically-relevant substrates, including PCL scaffolds and PC-TE membranes. We present data from initial investigations of the parameter spaces and exploratory biological studies, allowing us to begin to explore the role of monomer chemistry and plasma parameters in film properties and biological outcome. By comprehensively investigating the gas phase, the surface and the surface-biological interactions, we can optimize our fabrication platform to create biocompatible, antibacterial coatings.

## 7.2. Results

The first exploration into other potential biocidal monomers involved assessing antibacterial activity of terpinen-4-ol and  $\alpha$ -terpinene using kill rate assays. For comparison, the minimum inhibitory concentration (MIC) values for these oils are listed in Table 7.1.



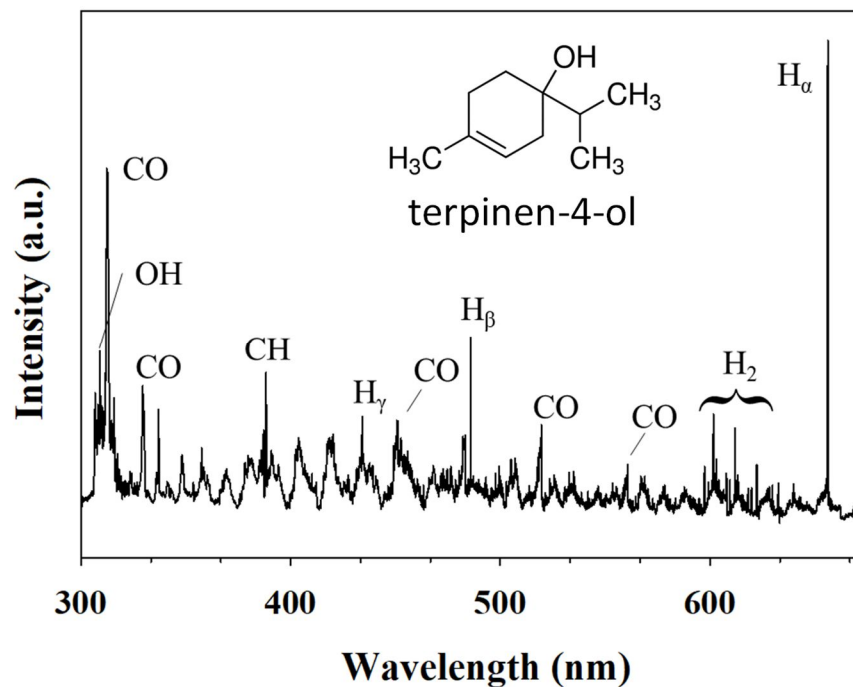
**Table 7.1.** Antibacterial essential oil-derived precursors and their minimum inhibitory concentrations (MICs) for *S. aureus* bacteria.<sup>13-14</sup>

Oil	Structure	MIC values for <i>S. aureus</i> (%)
1,8-cineole		0.5
terpinen-4-ol		0.25
$\alpha$ -terpinene		2
$\alpha$ -terpineol		0.45 – >0.9
linalool		1

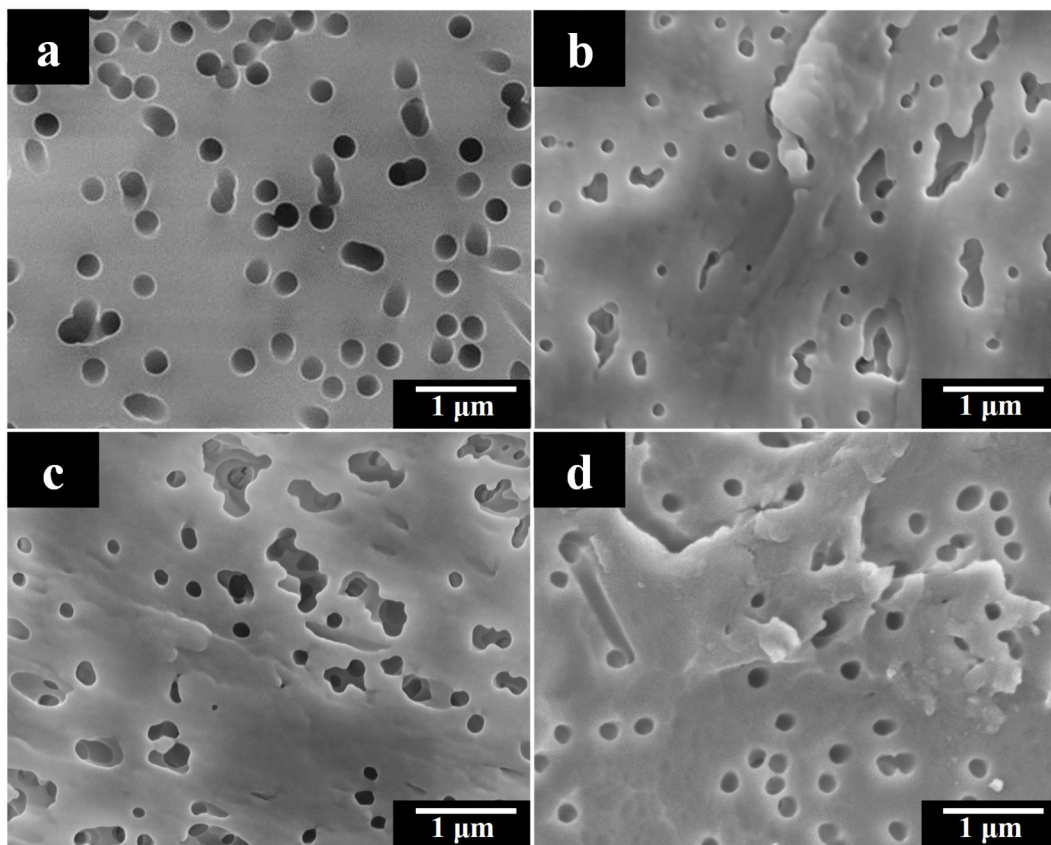
After 2 h of exposure, terpinen-4-ol (0.1% w/v) resulted in a >9-log reduction for *E. coli*, with no colonies observed on the plates, even for undiluted aliquots of culture. This biocidal activity is equal to that of 1,8-cineole (0.5% w/v) described in Chapter 6. No recovery of bacterial population was observed up to 24 h later. No significant reduction was observed for  $\alpha$ -terpinene, even up to concentrations of 2% w/v.

Terpinen-4-ol plasmas were probed using OES, and the species observed were compared to spectra for 1,8-cineole presented in Chapter 6. A representative OES spectrum for a 100% terpinen-4-ol plasma operating at  $P = 50$  W and  $p = 5$  mTorr is displayed in Figure 7.1. The most intense spectral features include peaks corresponding to OH at 309.1 nm, CO at 313.4, 330.1, 450.6, and 520.3 nm, CH at 388.8 nm,  $H_{\beta}$  at 485.9 nm, and  $H_{\alpha}$  at 656.2 nm. Of these, all are also observed in 1,8-cineole plasmas except for CH at 388.8 nm. We also wish to note here that the relative intensities of CO to OH species do appear to vary from what we observed with cineole. Specifically, for a terpinen-4-ol plasma operating at relatively low power and pressure, we see more CO than was observed for 1,8-cineole plasmas operating under similar conditions. There appears to be a smaller relative density of CO to OH than plasmas producing ppCin (high  $p,P$ ) films.

For reference, an uncoated 0.2  $\mu\text{m}$  PC-TE membrane is shown in Fig. 7.2a, where the track-etched porous morphology can be observed. For ppCin deposited on a 0.2  $\mu\text{m}$  PC-TE membrane, Fig. 7.2b, the coating conforms to the morphology of the PC-TE membrane in that the pores remain visible and few appear covered by the coating. It is apparent, however, that the overall morphology of the material is changed by the introduction of a rougher surface and a change in the morphology of the pores. Specifically, the edges of the pores appear smoother and somewhat raised. After  $\text{H}_2\text{O}_{(v)}$  plasma treatment, the morphology of the ppCin (high  $p,P$ ) film is



**Figure 7.1.** Representative raw optical emission spectra for a 100% terpinen-4-ol plasma operating at  $P = 50$  W and  $p = 5$  mTorr. Inset shows the monomer structure. Spectra were acquired with 50 ms integration time and 600 averages.



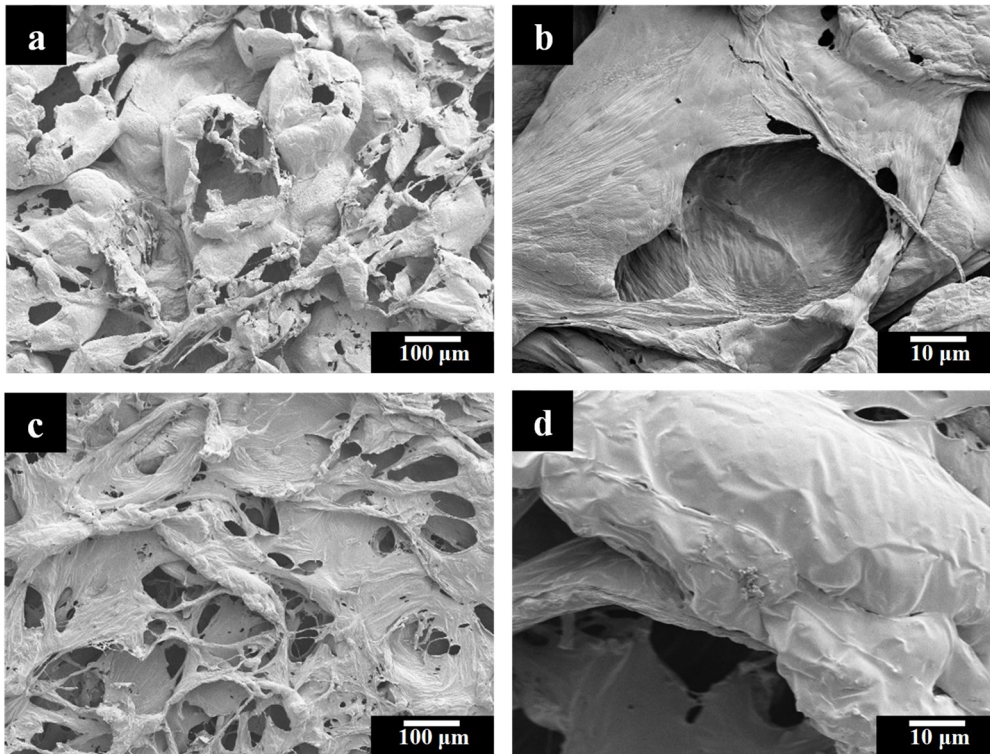
**Figure 7.2.** Representative SEM images of (a) as-received 0.2  $\mu\text{m}$  PC-TE membranes (22,000 $\times$ ); (b) ppCin films [100 mTorr 100 W 5 min] deposited on 0.2  $\mu\text{m}$  PC-TE membranes (22,000 $\times$ ); (c) ppCin films [100 mTorr 100 W 5 min] deposited on 0.2  $\mu\text{m}$  PC-TE membranes and  $\text{H}_2\text{O}_{(\text{v})}$  plasma treated [50 mTorr 20 W 2 min] (22,000 $\times$ ); and (d) ppT-4-ol on PC-TE membranes (22,000 $\times$ ).

retained and no evidence of damage is observed (Fig. 7.2c). ppT-4-ol deposition on PC-TE manifests as a slightly rougher coating than ppCin, but nevertheless appears conformal.

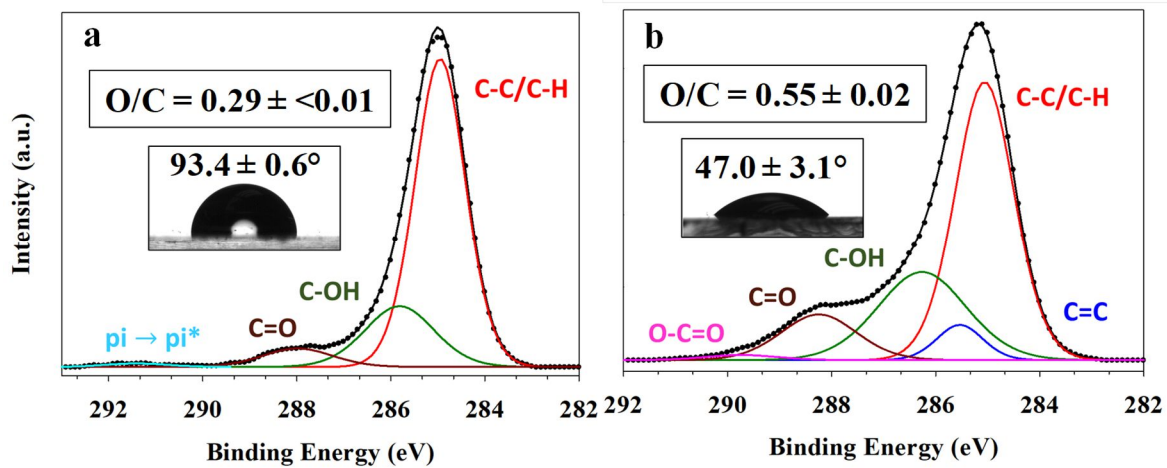
SEM images in Figure 7.3 correspond to PCL scaffolds coated with ppCin and ppT-4-ol. An SEM image of as-fabricated PCL scaffold is provided in Chapter 4, Fig. 4.4a. In Fig. 7.3a and b, we see ppCin (high  $p,P$ ) deposited onto PCL scaffold at low and high magnification, respectively. The ppCin coating appears conformal and does not change the interconnected porous morphology of the material. Fig. 7.3c-d show PCL scaffolds coated with ppT-4-ol films. ppT-4-ol films also appear to affect scaffold morphology. Interestingly, we see features introduced into the scaffold that may be indicative of a coating, specifically the folded, ripple-like appearance of the scaffold surface in Fig. 7.4d. We have previously observed these features in scaffolds that have been plasma polymerized with FC coatings (unpublished data).

Figure 7.4 shows representative XPS spectra for ppTer (Fig. 7.4a) and ppT-4-ol (Fig. 7.4b) films. O/C and WCA values with accompanying photographs are depicted as insets. Four binding environments are present in ppTer films: (1) C–C/C–H at 285.0 eV; (2) C–OH at 285.8 eV; (3); C=O at 288.0 eV; and (4)  $\pi \rightarrow \pi^*$  at 291.4 eV. ppT-4-ol films also contain peaks 1, 2, and 3, as well as two additional peaks corresponding to C=C at 286.0 eV and O–C=O at 289.7 eV. An overall O/C ratio equal to  $0.29 \pm <0.01$  corresponds to ppTer films whereas  $O/C = 0.55 \pm 0.02$  for ppT-4-ol films. Accordingly, the  $\theta_{\text{static}}$  for ppT-4-ol films is significantly lower at  $47.0 \pm 3.1^\circ$  than that for ppTer films ( $\theta_{\text{static}} = 93.4 \pm 0.6^\circ$ ).

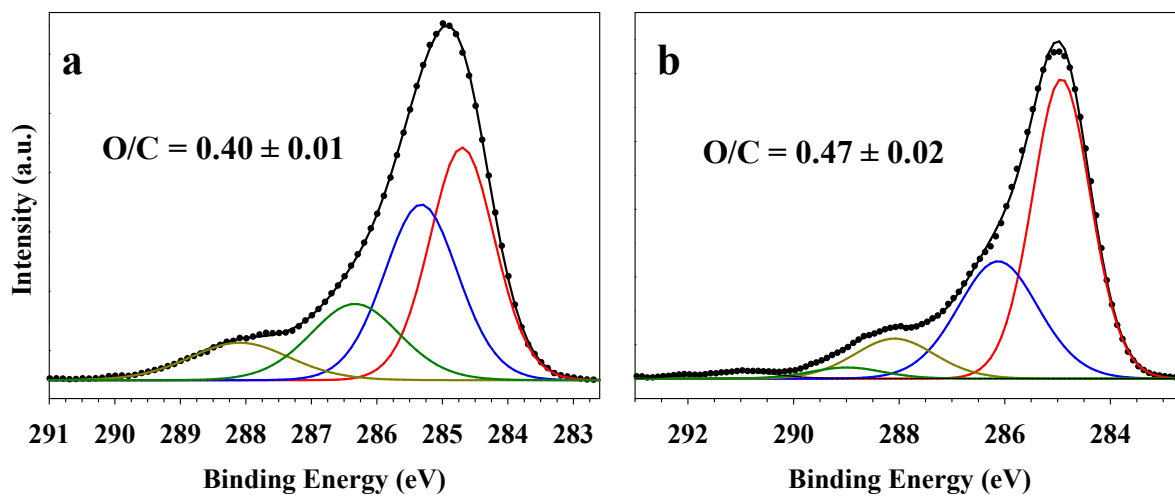
ppT-4-ol films were fabricated via plasma graft polymerization through Ar surface activation followed by 1 h of terpinen-4-ol exposure. Figure 7.5 depicts  $C_{1s}$  XPS spectra for PC-TE membranes treated with Argon only (Fig. 7.5a) and treated with Argon followed by terpinen-4-ol flow (Fig. 7.5b). For spectra corresponding to Argon treated PC-TE, we observe binding



**Figure 7.3.** Representative SEM images of (a-b) ppCin (high  $p,P$ ) on PCL and (c-d) ppT-4-ol on PCL. Images in (a) and (c) are at 100 $\times$  magnification. Images in (b) and (d) are 400 $\times$  and 1000 $\times$ , respectively.



**Figure 7.4.** XPS spectra with inset WCA data for plasma polymerized (a)  $\alpha$ -terpinene ( $P = 25$  W,  $p = 60$  mTorr, 5 min) and (b) terpinen-4-ol ( $P = 50$  W,  $p = 5$  mTorr, 5 min) films.



**Figure 7.5.**  $C_{1s}$  XPS spectra showing PC-TE treated with (a) Ar only at  $P = 40$  W and  $p = 150$  mTorr and (b) Ar followed by 1 h terpinen-4-ol flow with no applied power.



environments corresponding to (1) C–C/C–H at 285.0 eV; (2) C–O at 285.3 eV; (3) C=O at 286.3 eV; and (4) O–C=O at 288.4 eV. After terpinen-4-ol flow, however, a small peak corresponding to %O=C(–O)<sub>2</sub> appears at 291.0 eV. Note, however, that this peak is also present in as-received PC-TE.

The binding environment composition for ppCin and ppT-4-ol coated PC-TE is shown in Table 7.2. Here, we present the O/C ratios for each sample. PC-TE as received as O/C = 0.39 ± 0.01. Argon plasma treatment increase the O/C to 0.40 ± 0.01 and flowing terpinen-4-ol over Argon activated PC-TE increases O/C further to 0.47 ± 0.02. ppCin coatings on PC-TE, however, greatly increase the O/C for PC-TE membranes.

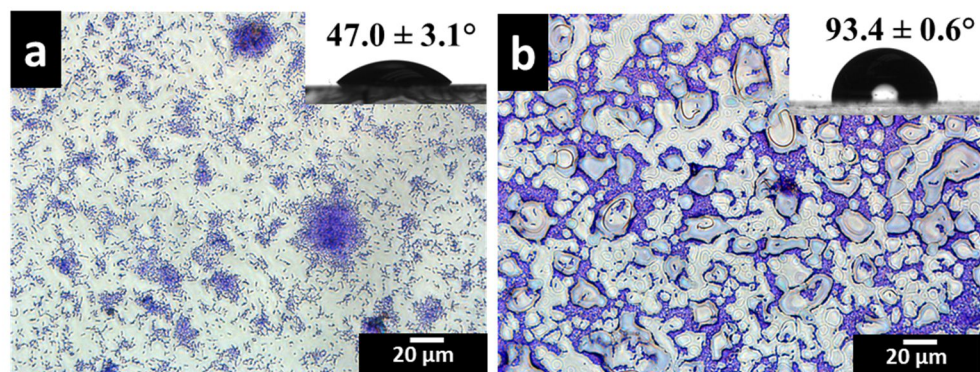
Figure 7.6 shows representative bright field microscopy images depicting *E. coli* biofilm growth on ppT-4-ol and ppTer films, Fig. 7.6a and b, respectively. Glass slides and ppOct films were once again used as controls in this assay (see Fig. 6.9 for these images). ppT-4-ol films in general, exhibit a similar surface coverage to that discussed in Chapter 6 for ppCin films. ppTer films, in contrast, exhibit both a substantial amount of biofilm coverage as well as indications of films instability (e.g., bubbling and partial delamination).

Notably, zone of inhibition assays (Chapter 2.5 and Chapter 4) were also completed for ppCin coated PC-TE membranes, and no zone of inhibition was observed for any films. For SEM analysis of attached bacteria, both PC-TE membranes and PCL scaffolds were coated with ppCin (high *P*, *p*). Figure 7.7 shows SEM images of *E. coli* attached to both scaffolds and membranes. After PC-TE membranes are coated with the ppCin film, *E. coli* attachment is reduced by 63 ± 31%. For coated PCL scaffolds, attachment is reduced by 75 ± 11%.

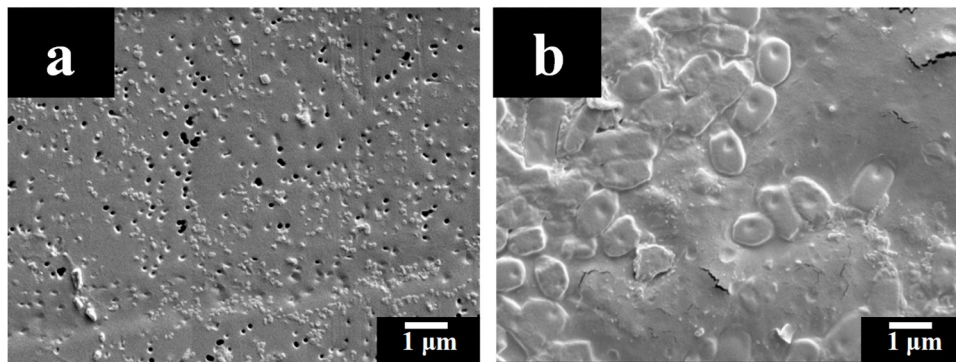
**Table 7.2.** O/C, N/C, and C<sub>1s</sub> XPS binding environments for PC-TE membranes.

Treatment type on PC-TE membrane	Binding environments							
	O/C	N/C	%C-C/C-H	%C-O	%C=O	%O-C=O	%O=C(-O) <sub>2</sub>	$\pi \rightarrow \pi^*$
PC-TE as-received	0.39 ± 0.01	--	61.1 ± 1.0	15.0 ± 0.3	--	--	5.4 ± 0.5	3.6 ± 0.3
ppCin (high <i>p,P</i> )	0.13 ± <0.01	--	69.8 ± 7.0	14.2 ± 3.1	1.8 ± 0.8	--	--	--
ppT-4-ol	0.47 ± 0.02	~0.1	42.3 ± 0.4	23.3 ± 0.2	8.1 ± 0.5	1.7 ± 0.4	1.3 ± 0.1	--
Ar only	0.40 ± 0.01	~0.1	27.4 ± 2.0	25.2 ± 0.7	6.8 ± 0.5	15.4 ± 2.0	--	--

<sup>a</sup>(no terpinen-4-ol)



**Figure 7.6.** Bright field microscopy images of *E. coli* biofilm growth after 5 day incubation on glass slides with films of a) ppT-4-ol [50 W, 7 mTorr, 10 min]; and (b) ppTer [25 W, 60 mTorr, 10 min]. Bacteria were stained with crystal violet. Images are representative of  $n \geq 9$  samples examined.



**Figure 7.7.** Representative SEM images depicting *E. coli* attached to (a) PC-TE membrane (b) PCL porogen-leached scaffold. Magnification is 5000×. Samples were coated with 10 nm of Au to reduce surface charging.

Initial flux studies for H<sub>2</sub>O<sub>(v)</sub> treated ppCin (high  $p, P$ ) on PC-TE membranes reveal a similar flux for coated membranes compared to as-received PC-TE (data not shown). Fouling results are depicted in Table 7.3 in mass of BSA adsorbed per unit surface area of PC-TE membranes as-received, ppCin coated, and ppCin coated and water plasma treated. As-received PC-TE membranes are most easily fouled by BSA, with  $60 \pm 9 \mu\text{g cm}^{-2}$ . ppCin coating slightly lowers the propensity for fouling, but when ppCin coating is followed by H<sub>2</sub>O<sub>(v)</sub> plasma treatment, fouling is cut in half from that of as-received PC-TE.

PC-TE membranes coated with ppCin (high  $p, P$ ) before and after plasma treatment were fouled with BSA. XPS analysis was done on fouled membranes to determine relative amounts of nitrogen adsorbed, a method often used to ascertain extent of protein fouling on surfaces (Chapter 2.4 and Chapter 5). Here, PC-TE membranes coated with ppCin were more susceptible to fouling in that the N/C ratio was higher ( $\sim 0.3$ ) than untreated ppCin-coated PC-TE ( $\sim 0.2$ ).

### 7.3. Discussion

*Monomer and film biocidal activity.* The first metric for determining potential candidates for antibacterial PECVD precursors was comparing their kill rate for bacteria in bulk solution. Comparing our kill rate results to the MIC values listed in Table 7.1, we see that general trends in biocidal activity hold, with terpinen-4-ol effective at lower concentrations than 1,8-cineole. Using both values from the literature and our kill rate data, it was apparent that terpinen-4-ol is biocidal at relatively low concentrations. As such, our interest lies in determining what characteristics of the monomer may lead to improved biocidal activity and whether that chemistry could be retained upon plasma polymerization of the essential oil-derived precursor.

**Table 7.3.** Amount of protein adsorbed per unit membrane area.

<b>Membrane</b>	<b>Protein adsorbed (<math>\mu\text{g}/\text{cm}^2</math>)</b>
Untreated PC-TE	$60 \pm 9$
ppCin on PC-TE	$50 \pm 9$
H <sub>2</sub> O <sub>(v)</sub> treated ppCin on PC-TE	$29 \pm 13$

Observing the bright field images of bacteria attached to ppT-4-ol and ppTer on glass, we observe more extensive biofilm formation for  $\alpha$ -terpinene films. Because the concentration of bacteria was unchanged between precursors, it follows that we would expect less antibacterial activity for  $\alpha$ -terpinene, as it takes 20 times the concentration of terpinen-4-ol to kill the same number of bacteria.<sup>10, 13</sup> Note, however, that much work remains to improve adhesion of these films on glass substrates to allow for further elucidation of film properties and biocidal performance.

*Film composition.* C<sub>1s</sub> XPS spectra reveal that the composition of ppT-4-ol and ppTer films on glass are roughly similar to ppCin, comprising primary hydrocarbon functionality with some contributions from alcohol and aldehyde binding environments. Although  $\alpha$ -terpinene contains no oxygen, oxygen incorporation is often seen in plasma processed materials, as long-lived free radicals on the material surface induced by the plasma participate in oxidation reactions upon exposure to atmosphere.<sup>34-35</sup> Compared to ppCin and ppTer, ppT-4-ol contains substantially more oxygen in the form of C–OH and C=O functionality. This is unsurprising given the phenolic functionality of terpinen-4-ol, and it is likely this increased surface oxygen content that leads to the slightly increased wettability of ppT-4-ol films when compared to ppCin (low  $p,P$ ), as discussed extensively in previous chapters. Interestingly, C=C components are unique to ppT-4-ol films. This may be explained by the abstraction of H or removal of OH from the precursor during PECVD, also evidenced by the greater density of OH radicals in terpinen-4-ol plasmas, that results in the formation of a double bond.<sup>29, 36</sup> Because these double bonds are unconjugated, it follows that we would expect to see an increase in C=C functionality versus  $\pi \rightarrow \pi^*$  binding environments.

ppTer films are hydrophobic, unsurprising given their purely hydrocarbon structure. Only in ppTer films do we observe contributions from the  $\pi \rightarrow \pi^*$  shake up satellite region, indicating a small degree of aromaticity is likely introduced during PECVD of ppTer. This is unsurprising given that cyclic polymerizable precursors, such as  $\alpha$ -terpinene, likely polymerize via scission of the double bonds, and are not expected to retain their ring structure. Nevertheless, it is known that intact monomers adsorb to the surface during PECVD, where cross-linking and propagation reactions are initiated by the plasma to bind intact monomer molecules to the growing film.<sup>29-30,</sup>  
<sup>37</sup> Indeed, we hypothesize it is incorporation of intact monomer that may be responsible in part for the biocidal behavior of the films investigated in Chapters 6 and 7.

*Film wettability and stability.* Unsurprisingly, ppT-4-ol films are significantly more wettable than ppTer films. The phenolic functionality of the terpinen-4-ol monomer likely results in significantly more oxygen-containing functionalities (as evidenced by XPS data) than the hydrocarbon monomer. Jacob and coworkers plasma polymerized several aromatic plant-derived compounds, including terpinen-4-ol and cis- $\beta$ -ocimene, a hydrocarbon similar to  $\alpha$ -terpinene, but non-cyclic. Their results agree with our WCA data; they found films fabricated from terpinen-4-ol had  $\theta_{\text{static}} = 68.5^\circ$ , and the hydrocarbon films had  $\theta_{\text{static}} = 94^\circ$ .<sup>38</sup> Ahmad and coworkers plasma polymerized  $\gamma$ -terpinene, an isomer of  $\alpha$ -terpinene, and found  $\theta_{\text{static}} \sim 80$  degrees).<sup>39-40</sup> In short, the range of WCA values achieved through depositing essential oil constituents here and in Chapter 6 demonstrate that films from essential oils are suitable for biological settings as they have wettabilities that are tunable and customizable chemistry to optimize antibacterial properties and promote favorable mammalian cell outcomes.

Film stability and adhesion are critical for the success of a biomaterials coating that will be deployed *in vivo*. In contrast, films that dissolve or delaminate from substrates upon immersion



in media are often desirable for sacrificial coatings for drug delivery.<sup>41</sup> Thus, it is critical to investigate film stability regardless of the desired outcome. Because numerous factors contribute to film quality, it is difficult to ascertain precisely how plasma parameters may affect film stability. Several studies have found that increased carboxyl functionality may contribute to film instability by promoting the interaction of water with the films, rendering them instable in aqueous environments. Likewise, some studies correlate film hydrophobicity and stability, with films deposited at higher powers being more hydrophobic and thus more stable.<sup>32</sup>

In one example, Easton and coworkers create polyLA films plasma polymerized from lavender, or *Lavandula angustifolia* (LA), oil and find CO functionality retention in the polyLA films depended on plasma parameters and seemed to directly influence film adhesion.<sup>42</sup> As RF power was increased, the authors observed a greater loss of functional groups (as evidenced by FTIR). Moreover, a clear trend existed in the WCA values for the polyLA films. All films were nominally hydrophobic, yet films deposited at a very low RF power (~10 W) were significantly less hydrophobic than films deposited at high power (75 W), ~82° vs 92° (error is approximately ±1°).<sup>42</sup>

In a related work, Easton and Jacob investigated the adhesion and solubility of polyLA films in several solvents, an important step towards creating both stable films for coatings or sacrificial layers for drug delivery.<sup>41</sup> They found adhesion increased with RF power, with no delamination from the substrates [glass, poly(ethylene terephthalate), and polystyrene].<sup>41</sup>

Ahmad and coworkers also found their  $\gamma$ -terpinene plasma polymers (pp-GT) were stable for all deposition conditions.<sup>32</sup> As RF power (and  $\theta_{\text{static}}$ ) increased, the authors observed increasing stability for pp-GT films, and they attributed this to increasing cross linking density under these conditions.<sup>32, 41</sup>

We observed instable films for several conditions (although the parameter space was limited) for both  $\alpha$ -terpinene and terpinen-4-ol systems. Others have observed this for similar films, and for films fabricated early in the optimization of the system discussed in Chapter 6. ppTer films exhibited bubbling similar to ppOct films deposited in Chapter 6 and other literature<sup>27</sup>, yet did not fully delaminate. In contrast, ppT-4-ol films exhibited no bubbling, but partially or completely delaminated in many cases. The delamination of ppT-4-ol films may be explained by their increased alcohol, ether, or carboxyl content.

We propose there may be some important interplay between achieving increased stability through increased cross-linking density (sometimes achieved by increasing power), without simultaneously introducing pinholes to the polymer film. Some instability may arise from possible pinholes (as hypothesized in Chapter 6 and observed in Fig. 6.3).

It is possible that the increased wettability and C–OH functionality of the ppT-4-ol film increases the difficulty of obtaining films stable in biological settings. Deposition of ppT-4-ol and ppCin on polymer membrane and scaffolds appears to result in a conformal film that largely retains the bulk properties (i.e., porous morphology, roughness) of the biomaterial. Nevertheless, more work remains to create ppT-4-ol films stable and adherent enough for a more complete quantification of bacterial surface coverage.

*Film biological performance.* Results from our preliminary analysis of bacterial attachment on coated polymeric constructs reveal promising signs of reduced propensity to fouling. Considering the best practices recommended in Chapter 4, it may appear that a ~60-70% reduction in bacterial attachment is negligible; however, Chapter 4 studies focused on the analysis of planktonic bacteria, whereas reductions on the order of 1-log are a significant feat in the mitigation of surface fouling. Note this reduction in attachment is on par with that observed

for ppCin films in Chapter 6. We also wish to point out that, although the values are within statistical error, a larger reduction in bacterial attachment for the PCL scaffolds may be explained by their substantially larger surface area compared to PC-TE membranes, providing a larger amount of coating to expose to the same population of bacteria.

Also promising are our results from static protein fouling experiments, wherein the adsorptive fouling of BSA was found to decrease upon ppCin coating of the PC-TE membranes. The implications here are not only important to the reduction of fouling by protein; the prevention or slowing of conditioning protein layer formation may directly influence the attachment of bacteria to that same surface.<sup>43-44</sup> Preliminary flux studies reveal we can apply ppCin films to PC-TE membranes, H<sub>2</sub>O<sub>(v)</sub> plasma surface modify them and see no decrease in membrane permeability. For practical use of such coated materials, further stability studies as a function of pH and ionic strength, as well as assessing storage stability (via aging studies, as discussed in Chapter 3 and 6) are required.

In the context of biomaterials, we not only care about optimizing chemical functionality retention to maximize antibacterial behavior, but, in some cases, also optimizing the attachment and proliferation of mammalian cells.<sup>28, 45-47</sup> As such, ongoing work should seek to optimize favorable cell interactions, by tuning nitrogen content or oxygen-containing functionalities.<sup>24, 45-47</sup> Moreover, by combining antifouling surfaces with active biocidal agents (e.g., loading an amine plasma polymer with metal oxide nanoparticles), a dual-approach to mitigate biofouling on materials may be achieved, further advancing attractive biomaterial properties. Some strategies to further enhance retention of essential oil monomer chemistry may include lowering substrate temperature to encourage monomer adsorption on the substrate surface during PECVD or using pulsed plasma systems to minimize monomer fragmentation.<sup>30, 37, 48-49</sup>

Another key area of ongoing work should center around understanding the dependence of gas-phase species densities on monomer functionality. To further elucidate the dependence of film properties on plasma parameters, spectroscopic studies, including further OES to relate species density to power and pressure, as well as *in situ* mass spectrometry (MS) to probe fragmented, monomeric, oligomeric and excited state species during PECVD processes.<sup>40</sup> Using time-of-flight secondary ion MS (ToF-SIMS) or near edge X-ray absorption fine structure (NEXAFS) spectroscopy to probe the film-substrate interface before and after biological immersion to understand interactions of bacteria with the film, as well as the adhesion and stability of the film on biomedically-relevant substrates.<sup>49-51</sup>

#### **7.4. Summary and Conclusions**

The ability to create conformal, well-adhering thin films is critical to advance low-fouling coatings for biomaterials. Understanding how such films can be created through PECVD processes using antibacterial, naturally-derived essential oil compounds is a unique approach to the field, and comprehensive characterization of the gas phase, material surface, and biological outcomes is necessary to understand the mechanisms by which such materials act against bacteria. Herein, we demonstrate monomer chemistry drives film properties, such as wettability and surface functionality, yet also has clear effects on film stability and adhesion. Coated membrane permeability does not suffer, whereas protein fouling is reduced. By understanding approaches to tune film chemistry, we can determine which essential oil constituents make excellent candidates for plasma polymerization systems and how to maximize adhesion to 3D biomaterials.

## REFERENCES

1. Burt, S., Essential oils: their antibacterial properties and potential applications in foods--a review. *Int J Food Microbiol* **2004**, *94* (3), 223-253.
2. Burt, S. A.; Reinders, R. D., Antibacterial activity of selected plant essential oils against *Escherichia coli* O157:H7. *Lett. Appl. Microbiol.* **2003**, *36*.
3. Carson, C. F.; Hammer, K. A.; Riley, T. V., *Melaleuca alternifolia* (tea tree) oil: a review of antimicrobial and other medicinal properties. *Clin Microbiol Rev* **2006**, *19* (1), 50-62.
4. Carson, C. F.; Mee, B. J.; Riley, T. V., Mechanism of action of *Melaleuca alternifolia* (tea tree) oil on *Staphylococcus aureus* determined by time-kill, lysis, leakage, and salt tolerance assays and electron microscopy. *Antimicrob. Agents Chemother.* **2002**, *46* (6), 1914-1920.
5. Carson, C. F.; Riley, T. V.; Cookson, B. D., Efficacy and safety of tea tree oil as a topical antimicrobial agent. *J Hosp Infect* **1998**, *40*, 175-178.
6. Cox, S. D.; Mann, C. M.; Markham, J. L.; Bell, H. C.; Gustafson, J. E.; Warmington, J. R.; Wyllie, S. G., The mode of antimicrobial action of the essential oil of *Melaleuca alternifolia* (tea tree oil). *J. Appl. Microbiol.* **2000**, *88*, 170-175.
7. Dalleau, S.; Cateau, E.; Berges, T.; Berjeaud, J. M.; Imbert, C., *In vitro* activity of terpenes against *Candida* biofilms. *Int J Antimicrob Agents* **2008**, *31* (6), 572-576.
8. Dorman, H. J. D.; Deans, S. G., Antimicrobial agents from plants: antibacterial activity of plant volatile oils. *J. Appl. Microbiol.* **2000**, *88*, 308-316.
9. Hendry, E. R.; Worthington, T.; Conway, B. R.; Lambert, P. A., Antimicrobial efficacy of eucalyptus oil and 1,8-cineole alone and in combination with chlorhexidine digluconate against microorganisms grown in planktonic and biofilm cultures. *J. Antimicrob. Chemother.* **2009**, *64* (6), 1219-1225.
10. May, J. C., C.H.; King, A.; Williams, L.; French, G.L., Time-kill studies of tea tree oils on clinical isolates. *J. Antimicrob. Chemother.* **2000**, *45*, 639-643.
11. Bakry, A. M.; Abbas, S.; Ali, B.; Majeed, H.; Abouelwafa, M. Y.; Mousa, A.; Liang, L., Microencapsulation of oils: A comprehensive review of benefits, techniques, and applications. *Compr. Rev. Food. Sci. Food Saf.* **2016**, *15* (1), 143-182.
12. Al-Jumaili, A.; Kumar, A.; Bazaka, K.; Jacob, M. V., Plant secondary metabolite-derived polymers: A potential approach to develop antimicrobial films. *Polymers* **2018**, *10* (5), 515.
13. Loughlin, R.; Gilmore, B.; McCarron, P.; Tunney, M., Comparison of the cidal activity of tea tree oil and terpinen-4-ol against clinical bacterial skin isolates and human fibroblast cells. *Lett. Appl. Microbiol.* **2008**, *46* (4), 428-433.
14. Kalemba, D.; Kunicka, A., Antibacterial and antifungal properties of essential oils. *Curr. Med. Chem.* **2003**, *10* (10), 813-829.
15. Edmondson, M.; Newall, N.; Carville, K.; Smith, J.; Riley, T. V.; Carson, C. F., Uncontrolled, open-label, pilot study of tea tree (*Melaleuca alternifolia*) oil solution in the decolonisation of methicillin-resistant *Staphylococcus aureus* positive wounds and its influence on wound healing. *Int. Wound J.* **2011**, *8* (4), 375-384.
16. Swamy, M. K.; Akhtar, M. S.; Sinniah, U. R., Antimicrobial properties of plant essential oils against human pathogens and their mode of action: an updated review. *Evid. Based Complement. Alternat. Med.* **2016**, *2016*.
17. Ozkan, A.; Erdogan, A., Membrane and DNA damaging/protective effects of eugenol, eucalyptol, terpinen-4-ol, and camphor at various concentrations on parental and drug-resistant H1299 cells. *Turk. J. Biol.* **2013**, *37* (4), 405-413.
18. Christaki, E.; Bonos, E.; Giannenas, I.; Florou-Paneri, P., Aromatic plants as a source of bioactive compounds. *Agriculture* **2012**, *2* (3), 228-243.

19. Trombetta, D.; Castelli, F.; Sarpietro, M. G.; Venuti, V.; Cristani, M.; Daniele, C.; Saija, A.; Mazzanti, G.; Bisignano, G., Mechanisms of antibacterial action of three monoterpenes. *Antimicrob. Agents Chemother.* **2005**, *49* (6), 2474-2478.
20. Li, L.; Li, Z.-W.; Yin, Z.-Q.; Wei, Q.; Jia, R.-Y.; Zhou, L.-J.; Xu, J.; Song, X.; Zhou, Y.; Du, Y.-H.; Peng, L.-C.; Kang, S.; Yu, W., Antibacterial activity of leaf essential oil and its constituents from *Cinnamomum longepaniculatum*. *Int J Clin Exp Med* **2014**, *7* (7), 1721-1727.
21. Bazaka, K.; Jacob, M. V.; Ostrikov, K., Sustainable life cycles of natural-precursor-derived nanocarbons. *Chem. Rev.* **2016**, *116* (1), 163-214.
22. Wilbon, P. A.; Chu, F.; Tang, C., Progress in renewable polymers from natural terpenes, terpenoids, and rosin. *Macromol. Rapid Commun.* **2013**, *34* (1), 8-37.
23. Hawker, M. J.; Pegalajar-Jurado, A.; Fisher, E. R., Conformal encapsulation of three-dimensional, bioresorbable polymeric scaffolds using plasma-enhanced chemical vapor deposition. *Langmuir* **2014**, *30* (41), 12328-12336.
24. Hawker, M. J.; Pegalajar-Jurado, A.; Hicks, K. I.; Shearer, J. C.; Fisher, E. R., Allylamine and allyl alcohol plasma copolymerization: Synthesis of customizable biologically-reactive three-dimensional scaffolds. *Plasma Proc. Polym.* **2015**, *12* (12), 1435-1450.
25. Abrigo, M.; Kingshott, P.; McArthur, S. L., Bacterial response to different surface chemistries fabricated by plasma polymerization on electrospun nanofibers. *Biointerphases* **2015**, *10* (4), 9.
26. Bazaka, K.; Jacob, M. V.; Truong, V. K.; Wang, F.; Pushpamali, W. A. A.; Wang, J. Y.; Ellis, A. V.; Berndt, C. C.; Crawford, R. J.; Ivanova, E. P., Plasma-enhanced synthesis of bioactive polymeric coatings from monoterpene alcohols: A combined experimental and theoretical study. *Biomacromolecules* **2010**, *11* (8), 2016-2026.
27. Pegalajar-Jurado, A.; Easton, C. D.; Styan, K. E.; McArthur, S. L., Antibacterial activity studies of plasma polymerised cineole films. *J. Mater. Chem. B* **2014**.
28. Pegalajar-Jurado, A.; Easton, C. D.; Crawford, R. J.; McArthur, S. L., Fabrication of a platform to isolate the influences of surface nanotopography from chemistry on bacterial attachment and growth. *Biointerphases* **2015**, *10* (1), 10.
29. Flamm, D. L.; Auciello, O., *Plasma deposition, treatment, and etching of polymers: the treatment and etching of polymers*. Elsevier: 2012.
30. Grill, A., *Cold Plasmas in Materials Fabrications: from fundamentals to applications*. IEEE: New York, 1994.
31. Sun, L.-m.; Zhang, C.-l.; Li, P., Characterization, antibiofilm, and mechanism of action of novel PEG-stabilized lipid nanoparticles loaded with terpinen-4-ol. *J. Agric. Food Chem.* **2012**, *60* (24), 6150-6156.
32. Ahmad, J.; Bazaka, K.; Oelgemoller, M.; Jacob, M. V., Wetting, solubility and chemical characteristics of plasma-polymerized 1-isopropyl-4-methyl-1,4-cyclohexadiene thin films. *Coatings* **2014**, *4* (3), 527-552.
33. Bazaka, K.; Jacob, M. V.; Ivanova, E. P., A study of a retention of antimicrobial activity by plasma polymerized terpinen-4-ol thin films. In *Mater. Sci. Forum*, Nie, J. F.; Morton, A., Eds. Trans Tech Publications Ltd: Stafa-Zurich, 2010; Vol. 654, pp 2261-2264.
34. Salim, M.; Wright, P. C.; McArthur, S. L., Studies of electroosmotic flow and the effects of protein adsorption in plasma-polymerized microchannel surfaces. *Electrophoresis* **2009**, *30* (11), 1877-1887.
35. Whittle, J. D.; Short, R.; Douglas, C.; Davies, J., Differences in the aging of allyl alcohol, acrylic acid, allylamine, and octa-1, 7-diene plasma polymers as studied by x-ray photoelectron spectroscopy. *Chem. Mater.* **2000**, *12* (9), 2664-2671.
36. Friedrich, J., Mechanisms of plasma polymerization - Reviewed from a chemical point of view. *Plasma Proc. Polym.* **2011**, *8* (9), 783-802.
37. López, G. P.; Ratner, B. D., Substrate temperature effects on film chemistry in plasma depositions of organics. II. Polymerizable precursors. *J. Polym. Sci., Part A: Polym. Chem.* **1992**, *30* (11), 2415-2425.

38. Jacob, M. V.; Easton, C. D.; Anderson, L. J.; Bazaka, K., RF plasma polymerised thin films from natural resources. *Int. J. Mod. Phys.* **2014**, *32*, 1460319.
39. Ahmad, J.; Bazaka, K.; Vasilev, K.; Jacob, M. V., Electrical conduction in plasma polymerized thin films of  $\gamma$ -terpinene. *J. Appl. Polym. Sci.* **2015**, *132* (30).
40. Ahmad, J.; Bazaka, K.; Whittle, J. D.; Michelmore, A.; Jacob, M. V., Structural characterization of gamma-terpinene thin films using mass spectroscopy and x-ray photoelectron spectroscopy. *Plasma Proc. Polym.* **2015**, *12* (10), 1085-1094.
41. Easton, C. D.; Jacob, M. V., Solubility and adhesion characteristics of plasma polymerized thin films derived from *Lavandula angustifolia* essential oil. *J. Appl. Polym. Sci.* **2010**, *115* (1), 404-415.
42. Easton, C. D.; Jacob, M. V.; Shanks, R. A.; Bowden, B. F., Surface and chemical characterization of polyLA thin films fabricated using plasma polymerization. *Chem. Vap. Deposition* **2009**, *15* (7-9), 179-185.
43. Bryers, J. D., Medical biofilms. *Biotechnol. Bioeng.* **2008**, *100* (1), 1-18.
44. Costerton, J. W.; Lewandowski, Z.; Caldwell, D. E.; Korber, D. R.; Lappin-Scott, H. M., Microbial biofilms. *Annu. Rev. Microbiol.* **1995**, *49* (1), 711-745.
45. Detomaso, L.; Gristina, R.; Senesi, G. S.; d'Agostino, R.; Favia, P., Stable plasma-deposited acrylic acid surfaces for cell culture applications. *Biomaterials* **2005**, *26* (18), 3831-3841.
46. Ertel, S. I.; Ratner, B. D.; Horbett, T. A., Radiofrequency plasma deposition of oxygen-containing films on polystyrene and poly (ethylene terephthalate) substrates improves endothelial cell growth. *J. Biomed. Mater. Res.* **1990**, *24* (12), 1637-1659.
47. Babaei, S.; Girard-Lauriault, P.-L., Tuning the surface properties of oxygen-rich and nitrogen-rich plasma polymers: functional groups and surface charge. *Plasma Chem. Plasma Process.* **2016**, *36* (2), 651-666.
48. Swaraj, S.; Oran, U.; Lippitz, A.; Friedrich, J. F.; Unger, W. E., Aging of plasma-deposited films prepared from organic monomers. *Plasma Proc. Polym.* **2007**, *4* (S1), S784-S789.
49. Oran, U.; Swaraj, S.; Friedrich, J. F.; Unger, W. E., Surface analysis of plasma deposited polymer films, 5. *Plasma Proc. Polym.* **2005**, *2* (7), 563-571.
50. Swaraj, S.; Oran, U.; Lippitz, A.; Schulze, R. D.; Friedrich, J. F.; Unger, W. E., Surface analysis of plasma-deposited polymer films, 4. *Plasma Proc. Polym.* **2005**, *2* (4), 310-318.
51. Swaraj, S.; Oran, U.; Lippitz, A.; Friedrich, J. F.; Unger, W. E., Surface analysis of plasma-deposited polymer films, 6. *Plasma Proc. Polym.* **2005**, *2* (7), 572-580.

## CHAPTER 8

# INVESTIGATION OF THE EFFECT OF SOLVENT CLEANING AND H<sub>2</sub>O<sub>(v)</sub> PLASMA TREATMENT ON ULTRAFILTRATION MEMBRANE WETTABILITY AND PERFORMANCE

This chapter builds on the H<sub>2</sub>O<sub>(v)</sub> plasma surface modification of UF membranes discussed in Chapter 3, with the goal of extending such a modification platform to current commercially-available UF membranes. Here, we note several challenges to achieving a translatable plasma processing methodology and lay out how these challenges were addressed using our suite of surface characterization techniques and membrane performance metrics. This research was supported by the National Science Foundation (CHE-1152963) and the Camille and Henry Dreyfus Foundation. A large portion of this chapter arose from a collaboration with two undergraduate researchers. Ms. Zoe Austermann completed all cleaning, H<sub>2</sub>O<sub>(v)</sub> plasma treatment, WCA analysis, and gravimetric studies for PVDF membranes. I collected and analyzed PVDF XPS spectra. Mr. Matthew R. Maynard completed gravimetric and WCA analysis for PES membranes and I performed the H<sub>2</sub>O<sub>(v)</sub> plasma treatment, flux studies, and XPS analysis for the same membranes.

### 8.1. Introduction

Biomedical, dairy, and water treatment industries rely on efficient separation processes – namely, filtration membranes that are highly permeable and selective. Ultrafiltration membranes, with typical MWCO of 10-100 kDa, are particularly suitable for the removal of bacteria and protein found in blood and wastewater. PES and PVDF are common materials for



UF membrane, due in part to their thermal stability, chemical inertness, and mechanical strength. These surface chemistries, however, are especially susceptible to adsorptive protein fouling and colonization by attached bacteria. As fouling proceeds, flux can rapidly decline and membrane lifetime suffers. Overall, this results in wasted energy and materials; improving membrane performance via reduced surface fouling is a route to more environmentally responsible separation processes.

Surface modification has been explored as both a route to improve overall membrane hydrodynamic performance by increasing hydrophilicity and as a way to introduce alternate surface chemistries. Previous studies have shown increasing surface wettability, by wet chemical grafting methods or plasma processing, can also mitigate adsorptive fouling, as it is primarily initiated by unfavorable interactions between bacteria or protein and the hydrophobic polymer surface. In Chapter 3, we demonstrated low temperature  $\text{H}_2\text{O}_{(v)}$  plasma surface modification of PSf membranes led to increased wettability, such that the membrane no longer had to be preconditioned before use. It follows that this technique could be extended to commercial UF membranes. The effect of  $\text{H}_2\text{O}_{(v)}$  plasma treatment on the performance of commercial UF membranes, however, can be somewhat difficult to interpret because they are often fabricated with a hydrophilic additive to increase performance in industrial applications. Thus, the addition of a wetting agent can pose a challenge, not only because its proprietary identity complicates analysis of wettability and compositional data, but also because it is unknown if the wetting agent is homogeneously incorporated into the membrane. To mitigate this challenge, effective methodologies for distinguishing the effect of plasma treatment on the polymer from any chemical or physical change to the wetting agent is critical. One way to accomplish this is to remove the additive (e.g., dissolution by rinsing) prior to plasma treatment.

As discussed in Chapters 2 and 3, various solvents (e.g., MeOH) are commonly used to remove low-molecule-weight oxidized material (LMWOM) from filtration membranes, but little research has gone into how these solvents may affect commercial membranes containing hydrophilic additives. The ultimate goal is to develop a universal plasma treatment platform that could be translated from research laboratories to commercially available membranes used on an industrial scale.

Herein, we aim to investigate the use of solvents to clean commercial PES and PVDF membranes to determine their effect on membrane composition and wettability. These data provide insight into the presence and amount of additive in the membranes.  $\text{H}_2\text{O}_{(v)}$  plasma treatment is performed on as-received and treated membranes to determine whether the removal of an additive affects membrane performance. Specifically, methanol, ethanol, hexanes, water, and a 1% SDS solution were used as solvents to identify the presence of additives and ultimately remove them from the membranes. The resultant membranes were analyzed using gravimetric analyses, WCA goniometry, and XPS. Elucidating changes in mass and surface properties after membrane cleaning can help determine the presence of an additive and the extent of its removal. Consequently, any changes in surface composition or wettability can be more easily attributed to the result of plasma treatment and not incorporated additives.

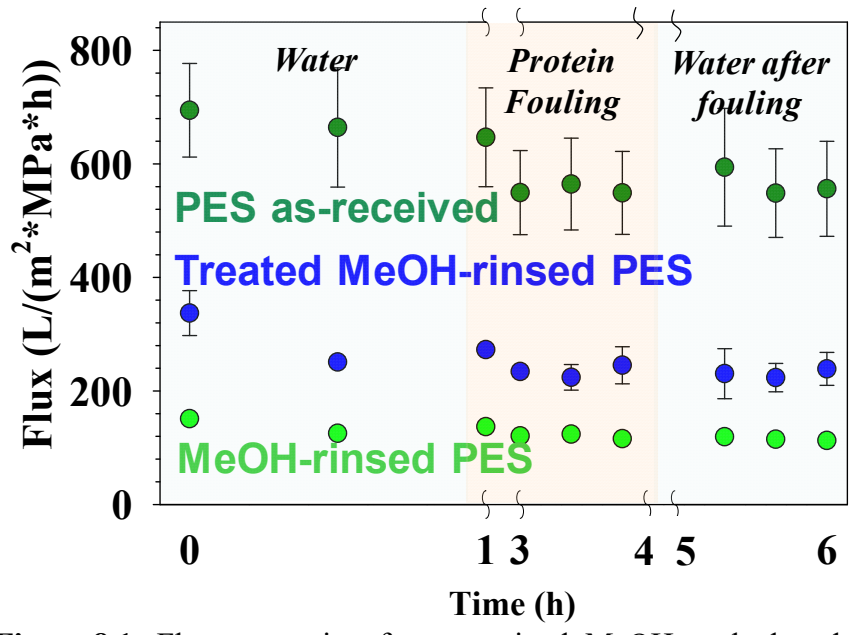
## **8.2. Results**

Here,  $\text{H}_2\text{O}_{(v)}$  plasma modification was explored for the enhancement of UF membrane performance, specifically on whether this treatment can be extended from PSf materials in Chapter 3 to industrial chemically-treated UF membranes. Both PES and PVDF were employed for this study, as they make excellent candidates for comparison to PSf membranes (Chapter 3).

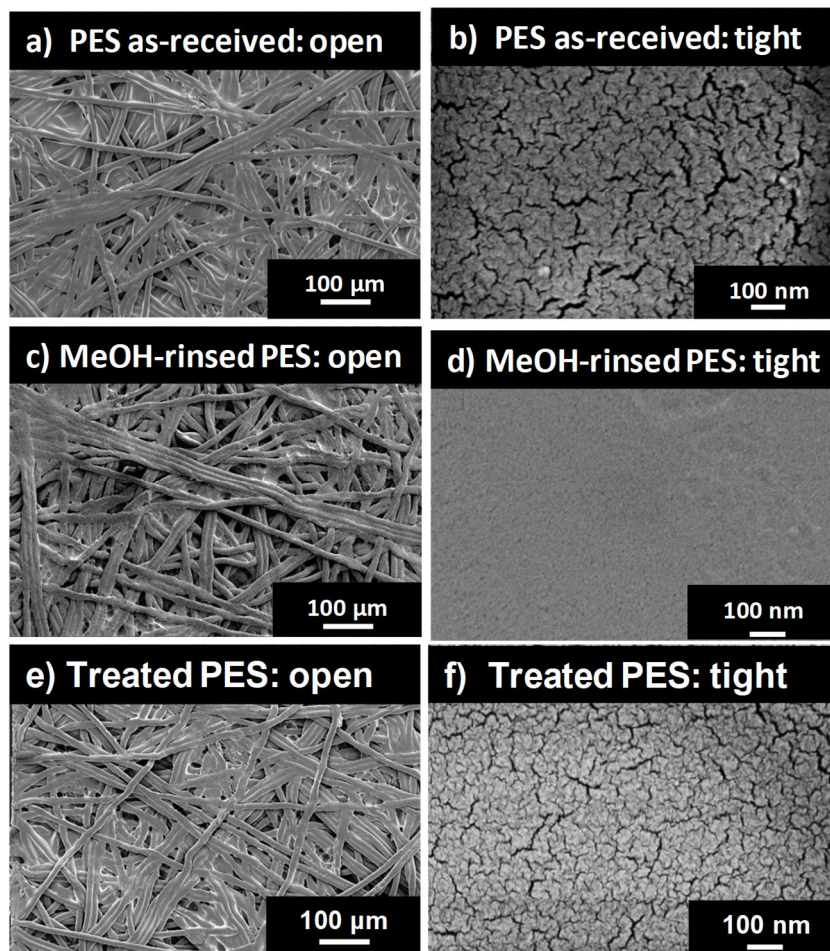
We employed our standard washing procedure (Chapter 2.1.2) by immersing membranes in MeOH prior to plasma treatment and flux experiments. Figure 8.1 depicts flux over time for PES membranes as-received, after MeOH washing, and after plasma treating washed membranes. Commercial PES membranes have relatively high permeabilities, with flux values  $\sim 700 \text{ L m}^{-2} \text{ MPa}^{-1} \text{ h}^{-1}$ , that remain over the course of a 6 h flux experiment, only declining to  $\sim 600 \text{ L m}^{-2} \text{ MPa}^{-1} \text{ h}^{-1}$  even after protein fouling. After MeOH washing, membrane performance drops drastically, with starting flux values of  $>200 \text{ L m}^{-2} \text{ MPa}^{-1} \text{ h}^{-1}$ , and declining to  $\sim 100 \text{ L m}^{-2} \text{ MPa}^{-1} \text{ h}^{-1}$  after protein fouling. Plasma treatment increases flux of the washed membranes, with starting flux of  $\sim 350 \text{ L m}^{-2} \text{ MPa}^{-1} \text{ h}^{-1}$ , though it does not reach that of the membranes as-received, with fluxes of  $\sim 200 \text{ L m}^{-2} \text{ MPa}^{-1} \text{ h}^{-1}$  after protein fouling.

*Membrane morphology and damage.* Because membrane flux suffered after MeOH rinsing, it was critical to assess membrane morphology for any pore damage. Figure 8.2 shows SEM images of both the open (Fig. 8.2a) and tight (Fig. 8.2b) sides of PES membranes. The morphology of the open side is that of a fibrous support, whereas the tight side has a cracked morphology typical of UF membranes. Although the open side morphology is unchanged by either MeOH cleaning or plasma surface modification, the tight side morphology is significantly changed after MeOH rinsing, with membrane pores appearing shrunken. Indeed, macroscopically, the tight side was visibly cracked after MeOH cleaning.

Gravimetric analyses were completed to assess any mass lost from the membrane via solvent cleaning (Table 8.1). Cleaning times were 5, 15, and 30 min, and mass loss from PVDF was independent of cleaning time. Water, MeOH, EtOH, and SDS each result in an approximate percent mass loss of 24% for PVDF membranes. Similarly, a 15 min cleaning of PES with H<sub>2</sub>O,



**Figure 8.1.** Flux versus time for as-received, MeOH washed, and H<sub>2</sub>O<sub>(v)</sub> plasma treated MeOH washed PES membranes.



**Figure 8.2.** SEM images showing PES membrane tight and open sides (a-b) as-received; (c-d) after MeOH rinsing; and (e-f) after H<sub>2</sub>O<sub>(v)</sub> plasma exposure.

**Table 8.1.** Average % mass loss for PES and PVDF membranes following different cleaning techniques.

	Cleaning Time (min)	water	methanol	ethanol	hexane	SDS (1%)
<b>PES</b>	15	23 ± 3	--	25 ± 5	1 ± ≤1	30 ± 5
	5	24 ± 5	24 ± 5	20 ± 3	0	24 ± 5
<b>PVDF</b>	15	24 ± 5	24 ± 5	24 ± 5	0	24 ± 5
	30	24 ± 5	24 ± 5	24 ± 5	0	24 ± 5

EtOH, or SDS results in a similar mass loss (20-30%). Interestingly, hexanes removed no mass from either PES or PVDF membranes.

*Membrane wettability.* The flux decline could arise in part from a change in membrane morphology, yet change in membrane wettability may also influence performance. As such, WCA measurements were made on membrane tight sides as-received, after MeOH washing, and after plasma treatment. Both sides of PES and PVDF as-received are nominally hydrophilic. The open side of the membranes completely absorbed the water droplet in <3 s. Water droplets deposited on the tight sides of PES membranes as received stabilized after ~5 s; thus,  $\theta_{\text{static}} = 63 \pm 7^\circ$  could be obtained.  $\theta_{\text{static}}$  for PVDF membrane tight sides as-received is  $61 \pm 10^\circ$ .

Table 8.2 contains  $\theta_{\text{static}}$  values for PVDF membranes after cleaning with several solvents for various lengths of time. At first glance,  $\theta_{\text{static}}$  values for cleaned materials appear generally larger than that for the membrane as-received membranes. Upon closer inspection, however, the WCA values corresponding to each soaked membrane at all cleaning times are not statistically different. Regardless of solvent used,  $\theta_{\text{static}}$  for cleaned membranes are similar to one another, ranging from  $\sim 60^\circ$  to  $\sim 70^\circ$ . Thus, MeOH rinsing does not affect the wettability of PES membranes ( $\theta_{\text{static}} = 62 \pm 3^\circ$ ), but does moderately improve the reproducibility of the measurement. Note that the error on  $\theta_{\text{static}}$  for membranes washed in hexanes is significantly larger, especially at longer cleaning times.

$\text{H}_2\text{O}_{(\text{v})}$  plasma treatment was completed on select membranes to determine its effectiveness after membrane cleaning. In short, plasma treatment is effective at improving the wettability of membranes when treated as-received (Table 8.3), yet largely ineffective at improving cleaned membrane hydrophilicity. Compared to PVDF membranes when received ( $\theta_{\text{static}} = 61 \pm 10^\circ$ ), those that have been  $\text{H}_2\text{O}_{(\text{v})}$  plasma treated have a  $\theta_{\text{static}}$  of  $15 \pm <1^\circ$ . Likewise, the WCA for

**Table 8.2.**  $\theta_{\text{static}}$  (°) for PVDF membrane tight sides after different cleaning techniques.<sup>a</sup>

<b>Cleaning Time (min)</b>	water	methanol	ethanol	hexane	SDS (1%)
<b>5</b>	67 ± 5	67 ± 1	68 ± 3	62 ± 4	69 ± 4
<b>15</b>	71 ± 4	70 ± 3	68 ± 1	71 ± 10	70 ± 2
<b>30</b>	73 ± 4	70 ± 2	66 ± 3	75 ± 11	71 ± 2

<sup>a</sup>mean ± standard deviation of n = 9.



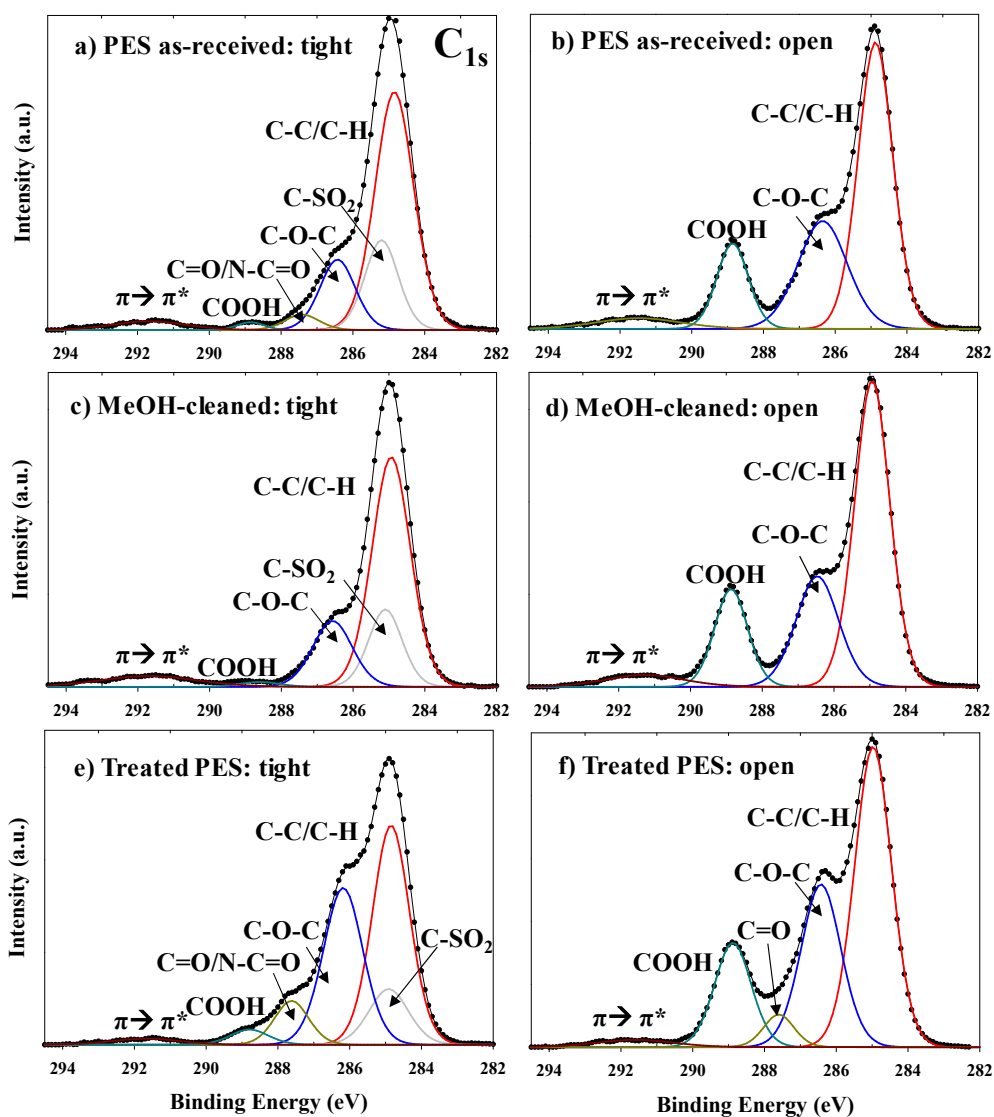
**Table 8.3.** WCA values for membrane tight sides as-received and following H<sub>2</sub>O<sub>(v)</sub> plasma treatment. <sup>a</sup>

<b>Membrane Type</b>		<b>Contact Angle (°)</b>
PES	As-received	61 ± 10
	H <sub>2</sub> O <sub>(v)</sub> plasma treated	14 ± 2
PVDF	As-received	63 ± 7
	H <sub>2</sub> O <sub>(v)</sub> plasma treated	15 ± 1

plasma treated PES membranes that have not been washed is  $14 \pm 2^\circ$ . Clearly, when as-received membranes are modified with no prior cleaning treatment, wettability is greatly enhanced. For MeOH cleaned membranes after plasma treatment, however,  $\theta_{\text{static}}$  is  $56 \pm <1^\circ$ , whereas  $\theta_{\text{static}}$  is substantially higher after plasma treatment for those PVDF membranes cleaned in 1% SDS ( $72 \pm <1^\circ$ ). For membranes with greater mass loss upon cleaning, plasma treatment performs less effectively at improving membrane wettability.

*Membrane composition.* Determining the surface composition of membranes before and after cleaning elucidates whether any additives are present, how homogeneously they may be incorporated, and if cleaning removed additives from the membranes. PVDF membranes rinsed with ethanol and SDS were chosen to undergo XPS analysis as they had the most consistent mass after cleaning. The tight sides of the as-received membranes had compositions consistent with the structure of PVDF.<sup>1-8</sup> High-resolution scans show two distinct peaks, the first at a binding energy of 286.4 eV and the second at 290.9 eV. These energies correspond to  $\underline{\text{C}}\text{H}_2\text{-CF}_2$  and  $\text{CH}_2\text{-}\underline{\text{C}}\text{F}_2$ , respectively. The  $\text{F}_{1s}$  spectra show a single peak at 689.3 eV, consistent with a  $\underline{\text{C}}\text{F}_2$  bond.  $\text{N}_{1s}$  and  $\text{O}_{1s}$  high-resolution scans were also obtained, and although a distinct peak occurred for each element, neither are indicative of the PVDF polymer backbone. Oxygen and nitrogen could arise from an additive, a contaminant, or, in the case of plasma treated membranes, we often observe O and N arising from the reaction of activated surface sites with atmospheric oxygen and nitrogen.

Figure 8.3 contains  $\text{C}_{1s}$  XPS spectra for PES membranes. As received, PES membrane tight sides have six unique  $\text{C}_{1s}$  binding environments: (1) C-C/C-H at 285.0 eV; (2) C-SO<sub>2</sub> at ~285.3 eV; (3) C-O-C at ~286.3 eV; (4) C=O/N-C=O at ~287.5 eV; (5) COOH at 289.5 eV; and (6)  $\pi \rightarrow \pi^*$  at ~291.6 eV. The open sides of both as-received PVDF and PES membranes are



**Figure 8.3.**  $C_{1s}$  XPS spectra for tight and open sides of PES membranes (a-b) as-received; (c-d) after MeOH cleaning; and (e-f) after plasma treatment (no MeOH cleaning).

markedly different in composition compared to the tight side. PES membrane open sides contain only components 1, 3, 5, and 6 above, indicative of a polyester-like supportive backing. PVDF scans showed three peaks for carbon, 285.0 eV, 286.2 eV, and 288.8 eV. Each one corresponds to  $\underline{\text{C}}\text{H}_2\text{-CH}_2$ ,  $\underline{\text{C}}\text{-O-C}$ , and  $\text{O-}\underline{\text{C}}=\text{O}$ , respectively. The  $\text{O}_{1s}$  region contained two peaks, one at 533.1 eV for  $\underline{\text{O}}\text{-(C=O)-C}$  and the other at 531.8 eV for  $\text{O-(C=}\underline{\text{O}}\text{)-C}$ .

After MeOH cleaning, component 4 disappears from PES tight side spectra, whereas open side spectra are largely unchanged.  $\text{H}_2\text{O}_{(v)}$  plasma treatment increases the oxygen content of both the open and tight sides of the PES membranes. For treated tight sides, there is no change in the components present, yet the amounts of components 3 (C-O-C functionality) and 5 (COOH functionality) increase substantially. Plasma treatment introduces a new component to PES membrane open sides at  $\sim 287.5$  eV representing C=O functionality and increases the area of C-O-C and COOH binding environments.  $\text{N}_{1s}$  spectra also revealed a loss of nitrogen-containing species upon MeOH washing. N/C for as-received PES was  $0.05 \pm <0.01$  whereas after MeOH washing, the N/C decreased to  $0.03 \pm <0.01$ .

Notably, oxygen content also decreases from  $6.7 \pm 0.4$  to  $3.6 \pm 0.6$  after MeOH cleaning of PVDF membranes. The atomic composition results (Table 8.4) also reveal concomitant loss of nitrogen upon solvent cleaning. With MeOH cleaning, the loss of nitrogen is not statistically significant, whereas 1% SDS cleaning results in a decrease in N content from  $1.6 \pm 0.4$  % to  $0.8 \pm <0.1$  % resulting in a membrane with an amount of nitrogen below the detection limit of the instrument. The composition of the open side is largely unchanged by cleaning with the notable exception of a disappearance of nitrogen ( $1.5 \pm <0.1$  % in the as-received membrane) upon cleaning with either MeOH or SDS.

**Table 8.4.** Atomic compositions for PVDF membranes as received and after select cleaning treatments.<sup>a</sup>

<b>XPS Atomic Composition</b>					
<b>Membrane</b>	<b>Side</b>	<b>%C</b>	<b>%O</b>	<b>%N</b>	<b>%F</b>
As-received	Tight	51.9 ± 0.2	6.7 ± 0.4	1.6 ± 0.4	38.7 ± 0.2
	Open	69.1 ± 0.2	27.4 ± 0.3	1.5 ± <0.1	---
MeOH cleaned	Tight	49.2 ± 0.3	3.6 ± 0.6	1.1 ± 0.4	46.1 ± 0.3
	Open	70.7 ± 0.1	28.8 ± 0.1	---	---
SDS cleaned	Tight	52.3 ± 1.5	4.4 ± 1.5	0.8 ± 0.3	43.5 ± 1.7
	Open	71.8 ± 0.3	27.4 ± 0.3	---	---

<sup>a</sup>All cleaning times were 30 min.

### 8.3. Discussion

Gravimetric analysis clearly shows a significant mass loss during the cleaning process; however, this alone does not yield information on the composition of any material removed from the membranes. Membrane compositional data can help determine if an additive is present on the surface, and variability between trials on the same membrane can confirm that an additive was not homogeneously incorporated on the surface of a membrane. As expected, the membrane tight sides are primarily composed of carbon and fluorine (Table 8.4). Although a 100% PVDF membrane should only include carbon, fluorine, and hydrogen, the tight sides as received are also composed of  $6.5 \pm 0.5\%$  oxygen and  $>2\%$  nitrogen.

The open sides of PVDF and PES membranes strongly indicate polyester is the support backing, with carbon and oxygen peaks characteristic of polyethylene terephthalate, a common commercial polyester.<sup>8-9</sup> This conclusion is supported by many patents using polyester as support for filtration membranes and another study showing that polyester as a membrane support material showed good rejection properties to foulants without decreasing flux through the membrane, making it an obvious choice for commercial filtration purposes.<sup>10</sup>

After cleaning, the open side composition does not change appreciably, indicating that the polyester support is unaffected by cleaning. This is important in light of the gravimetric analysis, as it signifies any wetting agent mass lost is likely from the tight side and not the polyester backing. Looking at the data for the tight side, we note the amount of oxygen present is likely too great to be contamination alone. Moreover, we see a decrease in both oxygen and nitrogen content upon cleaning, causing the cleaned membrane composition to more closely resemble spectra for 100% PVDF. We hypothesize this is likely because of removal of a wetting agent, as oxygen and nitrogen are often components of polar hydrophilic additives. For example,

many commercial membranes manufacturers use PVP as a wetting agent because of its high solubility in water and organic solvents, low toxicity, and good biocompatibility.<sup>11</sup> PVP has been incorporated into commercial polymer membranes in numerous ways, including cross-linking and creating spun membranes.<sup>12</sup> We hypothesize our standard membrane cleaning procedures remove proprietary compounds from commercial membranes, resulting in a severe loss of performance and complicating our characterization of plasma surface modified materials.

To further support this, we observe increased hydrophobicity after cleaning, as expected if a hydrophilic additive were removed. Indeed, we see increased hydrophilicity for membranes cleaned in all solvent except hexanes, unsurprising given polar additives are insoluble in nonpolar solvents. As previously discussed, PVDF is known to have a slightly hydrophobic surface, which corresponds to the plasma treated membranes that were cleaned beforehand. If a hydrophilic additive were removed, the WCA would be expected to increase between the as-received membranes and the cleaned membranes. Specifically, membranes cleaned in SDS were most hydrophobic and had the most reproducible  $\theta_{\text{static}}$ , suggesting SDS may be the most effective solution for removing additives from these commercial membranes.

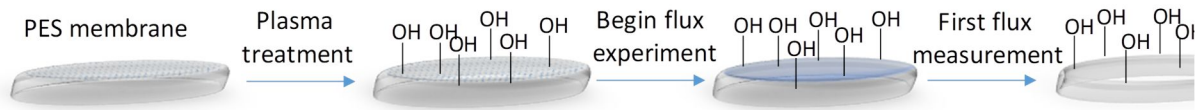
Overall, wettability and compositional analyses provide insight into the drastic decline in flux we observe after membrane cleaning. We further investigated to determine if our  $\text{H}_2\text{O}_{(\text{v})}$  plasma treatment can improve membrane wettability such that flux could be recovered. Plasma treatment was very successful on as-received membranes (suggesting materials can be modified even with additives), whereas those that had been cleaned were not made significantly more hydrophilic by plasma treatment. It may appear that plasma treatment was ineffective for cleaned membranes; however, we believe similar processes likely occur during plasma treatment of both as-received and clean membranes. Competitive processes, however, such as washing

away of additives, may counteract any wettability increase resulting from surface modification. A conceptual depiction of this is shown in Figure 8.4. Because the wetting agent may make up to 25% of total membrane mass, we believe this loss of wetting agent is likely significant to cause such a decline. Moreover, this relatively large composition of wetting agent in the membrane provides insight to the amount of wetting agent required to increase membrane flux, demonstrating the need to develop an effective plasma surface modification platform for quick, facile implementation of desired surface properties.

#### **8.4. Summary and conclusions**

This study investigated the removal of proprietary wetting agents from commercial PES and PVDF filtration membranes. The results suggest that several cleaning processes removed the wetting agent and left a membrane with composition more closely resembling that of the nominal polymer. XPS data revealed a concomitant decrease in nitrogen and oxygen content upon cleaning, suggesting the likely removal of a polar N- and O-containing additive (e.g., PVP). The additive appeared to be present only in the tight side, whereas the open side of PES and PVDF membranes was polyester in composition. Confirming the presence of an additive and assessing the best methodologies for its removal allows us to characterize the plasma treatment of membranes with and without additives. Distinguishing chemical changes occurring in the polymer backbone from those occurring with a removable additive is an important step towards developing improved surface modification platforms in the research laboratory that can be translated to industrial settings for the modification of commercial membranes.





**Figure 8.4.** Conceptual depiction of possible loss of wetting agent from plasma treated membrane, resulting in overall flux decline.

## REFERENCES

1. Briggs, D.; Beamson, G., Primary and secondary oxygen-induced C1s binding energy shifts in X-ray photoelectron spectroscopy of polymers. *Anal. Chem.* **1992**, *64* (15), 1729-1736.
2. Griesser, H. J.; Da, Y.; Hughes, A. E.; Gengenbach, T. R.; Mau, A. W., Shallow reorientation in the surface dynamics of plasma-treated fluorinated ethylene-propylene polymer. *Langmuir* **1991**, *7* (11), 2484-2491.
3. Hoffmann, E. A.; Körtvélyesi, T.; Wilusz, E.; Korugic-Karasz, L. S.; Karasz, F. E.; Fekete, Z. A., Relation between C1s XPS binding energy and calculated partial charge of carbon atoms in polymers. *J. Mol. Struct.* **2005**, *725* (1-3), 5-8.
4. Le Moel, A.; Duraud, J.; Balanzat, E., Modifications of polyvinylidene fluoride (PVDF) under high energy heavy ion, X-ray and electron irradiation studied by X-ray photoelectron spectroscopy. *Nucl. Instrum. Methods Phys. Res., Sect. B* **1986**, *18* (1-6), 59-63.
5. Pal S áBadyal, J., Surface modification of poly (vinylidene difluoride)(PVDF) by LiOH. *J. Chem. Soc., Chem. Commun.* **1991**, (14), 958-959.
6. Perruchot, C.; Abel, M. L.; Watts, J. F.; Lowe, C.; Maxted, J. T.; White, R. G., High-resolution XPS study of crosslinking and segregation phenomena in hexamethoxymethyl melamine–polyester resins. *Surf. Interface Anal.* **2002**, *34* (1), 570-574.
7. Vandencastele, N.; Reniers, F., Plasma-modified polymer surfaces: Characterization using XPS. *J. Electron. Spectrosc. Relat. Phenom.* **2010**, *178*, 394-408.
8. Arendt, M. F.; Beamson, G.; Briggs, D., High resolution XPS of organic polymers: The Scienta ESCA300 database. *J. Am. Chem. Soc.* **1993**, *115* (25), 12229-12229.
9. Tompkins, B. D.; Dennison, J. M.; Fisher, E. R., H<sub>2</sub>O plasma modification of track-etched polymer membranes for increased wettability and improved performance. *J. Membr. Sci.* **2013**, *428*, 576-588.
10. Lohokare, H.; Bhole, Y.; Kharul, U., Effect of support material on ultrafiltration membrane performance. *J Appl Polym Sci* **2006**, *99* (6), 3389-3395.
11. Yan, L.; Li, Y. S.; Xiang, C. B., Preparation of poly (vinylidene fluoride)(PVDF) ultrafiltration membrane modified by nano-sized alumina (Al<sub>2</sub>O<sub>3</sub>) and its antifouling research. *Polymer* **2005**, *46* (18), 7701-7706.
12. Teella, A.; Zydney, A. L.; Zhou, H.; Olsen, C.; Robinson, C., Effects of chemical sanitization using NaOH on the properties of polysulfone and polyethersulfone ultrafiltration membranes. *Biotechnol. Progr.* **2015**, *31* (1), 90-96.

## CHAPTER 9

### RESEARCH SUMMARY AND PERSPECTIVES

#### 9.1 Research summary

In past decades, plasma processing has become a prevalent technique for the modification of biomaterials. Nevertheless, little is understood about the fundamental processes that govern film deposition of antibiotic precursors or how plasmas may modify drug-loaded constructs. The research in this dissertation contributes to these areas by offering insight to the influence of parameters of modified materials' properties. Importantly, gas-phase data offer clues to the energetics involved in material modification process. Moreover, the direct implications of material surface properties are discussed in the context of the biological performance of the materials. Recommendations are made for the analysis of the antibacterial performance of the materials in the context of clinical applications. The overarching goal of this dissertation is to understand how materials can be plasma processed to implement and/or tune antibacterial properties.

Chapter 3 began by discussing routes to enhance the biocompatibility of polymeric membranes routinely used in medical separations. Chapter 8 further elaborated on this by discussing some of the challenges faced when modifying commercial filtration materials.

Chapter 4 introduced the incorporation of antibacterial characteristics into the polymeric materials. The primary theme of this chapter focused on the importance of considering and reporting material performance in the context of the standards of the biomaterials community. Chapter 5 offered an example of high-performing antibacterial Tygon® films and the delayed,

yet effective, release of biocidal nitric oxide that occurred upon H<sub>2</sub>O<sub>(v)</sub> plasma surface modification.

In Chapter 6, plasma polymerized thin films fabricated from 1,8-cineole (denoted ppCin films) were successfully fabricated on flat non-polymeric substrates (e.g., glass).<sup>1</sup> We found stable adherent ppCin films can be deposited under a range of plasma parameters. Wettability was assessed by WCA goniometry, and the resulting coatings were hydrophobic to varying degrees with largely hydrocarbon composition (as revealed via surface analysis). WCA values strongly correlated with  $p$ , with hydrophobicity increasing linearly as deposition pressure increased, yet are relatively independent of  $P$ . Compared to control hydrophilic glass and hydrophobic plasma polymerized 1,7-octadiene films, ppCin films were low-fouling (4-7% compared to 40% for controls). We further enhanced film wettability via plasma surface modification to assess the effect of film hydrophilicity on film quality (i.e., adhesion) and antibacterial performance. When deposited films were H<sub>2</sub>O<sub>(v)</sub> plasma treated, antibacterial activity largely remained (15% *E. coli* surface coverage). Thus, we concluded film antibacterial performance could likely be attributed to a combination of both the antibacterial properties of the monomer as well as the hydrophobicity of the film.<sup>2</sup> This result emphasizes the importance of elucidating the effect of film properties, which are largely determined by plasma species energetics, on film-bacteria interactions. Chapter 7 expanded on these ideas by introducing some preliminary data for the deposition of three essential-oil based precursors onto select biomaterials.

The ability to reduce morbidity and mortality associated with HAIs that arise from fouling of biomaterials and the prominence of antibacterial resistance is a major focus of new biomaterial development. Reduction of bacterial attachment on surfaces will diminish the risk of infection,

and achieving such a reduction without the use of synthetic antibiotics eliminates the occurrence of antibiotic resistance and environmental pollution. The key lies in understanding the fundamental influence of plasma processing conditions on material properties and performance. Through exploiting the multi-pronged approach described herein to comprehensively analyze material surface and bulk properties and plasma species in the gas phase, we can fabricate advanced biomaterials with attractive properties to achieve desirable outcomes. This knowledge can improve materials performance and lifetime by fundamentally understanding how materials are made and modified by these techniques. Moreover, our suite of bacterial assays and *in vitro* performance studies are translatable to clinical situations and will provide insight to factors influencing biological interactions with plasma processed materials, thus guiding development of advanced, high performing antibacterial biomedical devices.

## **9.2 Future directions**

The work presented in this dissertation lays a foundation for understanding how low-fouling biomaterials can be engineered. Plasma processing has utility in both tuning the release of drug from polymeric materials and in depositing adherent, antifouling coatings. Clearly, there remains much work left to fully understand the surface properties that drive desired biological reactions. Moreover, there are several avenues for further development and optimization of PECVD systems for antibacterial, low-fouling films.

*Further development of essential oil-based PECVD systems.* A broad potential direction for the future of this work involves approaches that synergistically reduce biofilm formation. For example, essential oil based coatings can be loaded with drugs (metal nanoparticles, NO) and designed to dissolve or otherwise release the agent in a controlled manner. Moreover, low-

fouling plasma polymerized films could be tuned to have functionality that promotes the tethering of small biocidal agents (AgNPs, AMPs).

Additionally, there remain numerous essential oil-derived molecules with potential use in antibacterial surface fabrication, thus, further advancement of PECVD systems using these compounds is of great interest. ppTer and ppT-4-ol films described in Chapter 7 show promise in use as low-fouling coatings, yet much work remains to determine how to maximize adhesion on 2D and 3D substrates. Additional insight into film formation and its dependence on substrate chemistry and morphology would advance the development of films with superior adhesion and stability in biological matrices. Moreover, H<sub>2</sub>O<sub>(v)</sub> plasma surface modification should be explored to further enhance the biocompatibility of the films, especially ppTer films. Ultimately, a promising route to fabricate high-performing, low-fouling surfaces may be to develop copolymerization systems, as has been done successfully with PECVD for biomaterials.<sup>3</sup> Isolating a few promising antibacterial constituents will likely provide films with superior antibacterial performance than films fabricated from a single molecule or from whole tea tree (*Melaleuca alternifolia*) oil.

*Further biocompatibility studies and advanced biofilm analysis.* Another major area of focus to further advance the fundamental studies discussed here should entail development of quantitative methods for *in vivo* and *in vitro* assessment of biofilm formation and film stability. Understanding how films behave in more representative physiological environments is imperative to developing these coatings for biomaterials. Mammalian cell (e.g., HDFs and osteoblasts) studies combined with further blood coagulation studies, using human blood plasma and whole blood, will provide critical information about any potential foreign body reaction that could be caused by deploying the coated device *in vivo*. Investigation of additional material

properties that drive bacterial attachment (e.g., material hardness<sup>4-5</sup>) is necessary to begin to comprehensively elucidate the effect of material properties on bacterial proliferation.

Coated membranes should undergo protein flux and fouling studies like those described in Chapter 3, with the addition of more complex bacterial-protein filtration mixtures. Our imaging and colony counting assays could be further optimized to better understand the formation of biofilm on the modified materials. For example, we have had success in imaging biofilm on coated transparent glass substrates, yet this imaging is difficult on opaque polymeric constructs like those used herein. To overcome this, thin films could be deposited onto transparent polymeric membranes for staining and semi-quantitative imaging assays.

*Advanced gas-phase and surface analysis.* To best tune film properties resulting from plasma processing, it is imperative to assess gas-phase species. As discussed previously, OES allows us to gather quantitative information about excited state gas-phase species. The addition of our broadband absorption spectroscopy (BAS) technique to future studies could elucidate information about ground state species relevant to surface modification and film formation. Finally, data from mass spectrometry (MS) could provide further information needed to understand the effect of plasma parameters on film chemistry, as it can probe gas-phase fragmented and oligomeric species that are critical to PECVD film deposition.

A major limitation to developing advanced low-fouling surfaces is the difficulty in assessing what occurs at the bacteria-material interface and, for coated materials, at the film-substrate interface. Advanced surface analytical techniques have found utility in understanding fundamental bacterial-surface interactions with modified biomaterials. Time-of-flight secondary ion MS (ToF-SIMS) and other surface sensitive techniques have been used by others to identify components present throughout the film before and after exposure to biological environments.<sup>6-10</sup>

Tyler and coworkers have employed ToF-SIMS to film-substrate characteristics, providing valuable information about causes of film delamination.<sup>10</sup> Understanding the causes of delamination at the film-substrate interfaces, as well as how bacteria may metabolize the film, is an important steps towards overcoming challenges with biomaterials coatings.<sup>10</sup> The promising platforms developed herein suggest the future of advanced, low-fouling biomaterials may aid in alleviating chronic, drug-resistant infections.



## REFERENCES

1. Mann, M. N.; Fisher, E. R., Investigation of antibacterial 1, 8-cineole-derived thin films formed via plasma-enhanced chemical vapor deposition. *ACS Appl. Mater. Interfaces* **2017**, *9* (42), 36548-36560.
2. Pegalajar-Jurado, A.; Easton, C. D.; Styan, K. E.; McArthur, S. L., Antibacterial activity studies of plasma polymerised cineole films. *J. Mater. Chem. B* **2014**.
3. Hawker, M. J.; Pegalajar-Jurado, A.; Hicks, K. I.; Shearer, J. C.; Fisher, E. R., Allylamine and allyl alcohol plasma copolymerization: Synthesis of customizable biologically-reactive three-dimensional scaffolds. *Plasma Process. Polym.* **2015**, *12* (12), 1435-1450.
4. Aguayo, S.; Donos, N.; Spratt, D.; Bozec, L., Single-bacterium nanomechanics in biomedicine: unravelling the dynamics of bacterial cells. *Nanotechnology* **2015**, *26* (6), 062001.
5. Song, F.; Koo, H.; Ren, D., Effects of material properties on bacterial adhesion and biofilm formation. *J. Dent. Res.* **2015**, *94* (8), 1027-1034.
6. Ahmad, J.; Bazaka, K.; Oelgemoller, M.; Jacob, M. V., Wetting, solubility and chemical characteristics of plasma-polymerized 1-isopropyl-4-methyl-1,4-cyclohexadiene thin films. *Coatings* **2014**, *4* (3), 527-552.
7. Ahmad, J.; Bazaka, K.; Whittle, J. D.; Michelmore, A.; Jacob, M. V., Structural characterization of gamma-terpinene thin films using mass spectroscopy and x-ray photoelectron spectroscopy. *Plasma Process. Polym.* **2015**, *12* (10), 1085-1094.
8. Swaraj, S.; Oran, U.; Lippitz, A.; Friedrich, J. F.; Unger, W. E., Surface analysis of plasma-deposited polymer films, 6. *Plasma Process. Polym.* **2005**, *2* (7), 572-580.
9. Swaraj, S.; Oran, U.; Lippitz, A.; Schulze, R. D.; Friedrich, J. F.; Unger, W. E., Surface analysis of plasma-deposited polymer films, 4. *Plasma Process. Polym.* **2005**, *2* (4), 310-318.
10. Tyler, B. J.; Hook, A.; Pelster, A.; Williams, P.; Alexander, M.; Arlinghaus, H. F., Development and characterization of a stable adhesive bond between a poly (dimethylsiloxane) catheter material and a bacterial biofilm resistant acrylate polymer coating. *Biointerphases* **2017**, *12* (2), 02C412.

## LIST OF ABBREVIATIONS

2D	Two-dimensional
3D	Three-dimensional
AAS	Atomic absorption spectroscopy
ABS	Acrylonitrile butadiene styrene
ACS	American Chemical Society
AFM	Atomic force microscopy
Ag	Silver
Ag <sub>3d</sub>	Silver 3d (XPS spectrum)
AgNO <sub>3</sub>	Silver nitrate
AgNP(s)	Silver nanoparticle(s)
allylNH	Allylamine
allylOH	Allyl alcohol
AMP	Antimicrobial peptide
ANOVA	Analysis of variance
ASTM	American Society for Testing and Materials
ATCC	American Type Culture Collection
AWG	American wire gauge
BE	Binding energy
BSA	Bovine serum albumin
C/N (or N/C)	Carbon-to-nitrogen (or nitrogen-to-carbon) ratio
C/O (or O/C)	Carbon-to-oxygen (or oxygen-to-carbon) ratio
C <sub>1s</sub>	Carbon 1s (XPS Spectrum)
CaCl <sub>2</sub>	Calcium chloride
CFU	Colony forming unit
CHCl <sub>3</sub>	Chloroform
CLSI	Clinical and Laboratory Standards Institute
CO	Carbon monoxide
CO <sub>2</sub>	Carbon dioxide
CVD	Chemical vapor deposition
DCM	Dichloromethane
DI	Deionized
DMF	Dimethylformamide
DNA	Deoxyribonucleic acid
<i>E. coli</i>	<i>Escherichia coli</i>
ECC	Extracorporeal circuit
ECM	Extracellular matrix
EDS	Energy dispersive spectroscopy
EPS	Extracellular polymeric substances
EtOH	Ethanol
F/C	Fluorine-to-carbon ratio
FC	Fluorocarbon
fps	Frames per second

FRR	Flux recovery ratio
FTIR	Fourier transform infrared spectroscopy
FWHM	Full width at half maximum
GSNO	<i>S</i> -nitrosoglutathione
GSNO20	Tygon® film with 20% <i>S</i> -nitrosoglutathione (w/w)
h	Hour
GSNO5	Tygon® film with 5% <i>S</i> -nitrosoglutathione (w/w)
H <sub>2</sub>	Diatomic hydrogen
H <sub>2</sub> O	Water
HAI	Hospital-acquired infection
HDF	Human dermal fibroblast
HEMA	Hydroxyethyl methacrylate
ICP	Inductively couple plasma
i.d.	Internal diameter
<i>J</i>	Flux
LA	<i>Lavandula angustifolia</i>
LMWOM	Low-molecular-weight oxidized material
LOD	Limit of detection
LOQ	Limit of quantification
LTP	Low-temperature plasma
MA	Maximum amplitude (TEG)
M <sub>n</sub>	Number average molecular weight
MeOH	Methanol
min	Minute
MH	Mueller-Hinton
MIC	Minimum inhibitory concentration
MRSA	Methicillin-resistant <i>S. aureus</i>
MRTG	Maximum rate of thrombus generation (TEG)
MWCO	Molecular weight cut off
N <sub>2</sub>	Diatomic nitrogen
N/C	Nitrogen-to-oxygen ratio
NA	Nutrient agar
NaCl	Sodium chloride
NaOH	Sodium hydroxide
NBM	Nutrient broth media
NH <sub>3</sub>	Ammonia
NO	Nitric oxide
NOA	Nitric oxide analyzer
NTC	Non-tissue culture (polystyrene)
O <sub>1s</sub>	Oxygen 1s (XPS Spectrum)
O/C	Oxygen-to-carbon ratio
OD	1,7-octadiene
O.D. <sub>600nm</sub>	Optical density at 600 nm
OES	Optical emission spectroscopy
OV	Overnight (culture)
<i>P</i>	Applied plasma power

<i>p</i>	Pressure
<i>P. aeruginosa</i>	<i>Pseudomonas aeruginosa</i>
PBS	Phosphate buffered saline
PC	Polycarbonate
PC-TE	Track-etched polycarbonate (membrane)
PCL	Polycaprolactone
PE	Polyethylene
PECVD	Plasma-enhanced chemical vapor deposition
PEG	Polyethylene glycol
PES	Polyethersulfone
PET	Polyethylene terephthalate
PGA	Polyglycolic acid
PI	Propidium iodide
PLA	Poly(lactic acid)
PLGA	Poly(lactic-co-glycolic acid)
PLGH	Carboxyl-functionalized polymer prepared from L-lactide, glycolide, and 2,2-bis(hydroxymethyl propionic acid)
polyLA	Plasma polymerized <i>Lavandula angustifolia</i>
<i>pp</i>	Plasma polymerized
ppCin	Plasma polymerized 1,8-cineole
ppCin (high <i>p,P</i> )	1,8-cineole plasma polymerized at $p = 100$ mTorr, $P = 100$ W
ppCin (low <i>p,P</i> )	1,8-cineole plasma polymerized at $p = 15$ mTorr, $P = 50$ W
ppOct	Plasma polymerized 1,7-octadiene
ppT-4-ol	Plasma polymerized terpinene-4-ol
ppTer	Plasma polymerized $\alpha$ -terpinene
PSf	Polysulfone
PTFE	Polytetrafluoroethylene
PVC	Polyvinyl chloride
PVDF	Polyvinylidene fluoride
PVP	Polyvinylpyrrolidone
R	Reaction time (TEG)
$R_a$	arithmetic average roughness
rf	Radio frequency
RFR	Relative flux reduction
RMS	Root mean squared
RO	Reverse osmosis
$R_q$	Root mean square roughness
RSNO	<i>S</i> -nitrosothiol
s	Second
<i>S. aureus</i>	<i>Staphylococcus aureus</i>
S <sub>2p</sub>	Sulfur 2p (XPS Spectrum)
SDS	Sodium dodecyl sulfate
SEM	Scanning electron microscopy
SEM-EDS	Scanning electron microscopy-energy dispersive spectroscopy
SF	Survival fraction
SSD	Silver sulfadiazine

SSI	Surgical site infection
TC	Tissue culture (polystyrene)
TEG	Thromboelastography
THF	Tetrahydrofuran
TMA	Time to maximum amplitude (TEG)
TMRTG	Time to maximum rate of thrombus generation (TEG)
ToF-SIMS	Time-of-flight secondary ion mass spectrometry
TTG	Total thrombus generation (TEG)
UF	Ultrafiltration
UHP	Ultrahigh purity
UPS	Ultrafiltration polysulfone
UV-vis	ultraviolet visible spectroscopy
WCA	Water contact angle
XPS	X-ray photoelectron spectroscopy
$\theta$	Water contact angle value ( $^{\circ}$ )
$\theta_{\text{static}}$	Static water contact angle